APPLICATIONS OF FIELD-EVAPORATION THEORY

BY

KHALED CHIBANE

Submitted for the

Degree of Doctor of Philosophy

at the

University of Aston in Birmingham

NOVEMBER 1985

THE UNIVERSITY OF ASTON IN BIRMINGHAM

APPLICATIONS OF FIELD-EVAPORATION THEORY

by

Khaled Chibane

Submitted for the
Degree of Doctor of Philosophy
at the
University of Aston in Birmingham
November 1985

Summary

This thesis is concerned with the application of the theory of the evaporation of metal atoms from a surface under the influence of a strong electric field. The theory of field evaporation under discussion, put forward by Forbes, assumes that the shape of the atomic bonding-well is parabolic and also that a Gomer-type mechanism operates. When this theory is combined with a standard Arrhenius-type emission equation, we predict linear relationships between $T^{\frac{1}{2}}$ and $1/F$ and also between x^{cr} and $Q^{\frac{1}{2}}$, where T is the temperature, F the electric field necessary for evaporation, x^{cr} the crossing point of the atomic and ionic curves and Q the activation energy.

Experimental results obtained by various workers using Tungsten, Molybdenum and Rhodium tips in an electric field, are compared with this theory over a limited temperature range. The employment of other forms for the atomic bonding-well has also been investigated, in order to improve the performance of the theory at high temperatures.

In the case of Rhodium, values have been derived for some surface atomic parameters, namely, the electrical bonding distance of a surface atom nucleus and the vibrational force-constant and frequency of a typical surface atom.

Keywords

FIELD-ION EMISSION, FIELD-EVAPORATION, SURFACE ATOMIC PARAMETERS

ACKNOWLEDGEMENTS

The supervisor of this project was Dr. R. G. Forbes, and I thank him for his guidance and keen interest; I am specially grateful for his efforts to maintain close contact with me after he had left Aston University to take up another appointment.

I also thank Professor Mulvey for his continued interest in the subject, and also for being my supervisor during the last few months of this project.

In the department, I have benefited from discussions with Dr. G. L. R. Mair.

I thank my parents, and my family in general, for their moral support throughout my education.

I thank Mrs. H. M. Turner for typing this project.

I thank the Ministry of Higher Education and Scientific Research of the Republic of Algeria, for providing me with a grant during my post-graduate education.

Finally, I thank the Nuffield trust foundation for their financial help and the Department of Electronic and Electrical Engineering of the University of Surrey for their hospitality during the last months of this work.

CONTENTS

LIST OF TABLES

Table Number

LIST OF FIGURES

Figure Number

Figure Number

LIST OF SYMBOLS

a	Surface atom bonding distance measured from the metal's electrical surface in the absence of an applied field.
a^*	Dimensionless scaled length used in the Universal binding energy function.
a^e	Bonding distance defined by Q=0 in the charge-draining mechanism.
a_n	Bonding distance (for an n-fold ion) measured from the metal's electrical surface in the absence of an applied field.
A	Pre-exponential factor.
$A^{onset}_{\alpha nr}$	Onset appearance energy for an ion initially bound in a partially ionic state α .
$A^{stand}_{\alpha nr}$	Standard appearance energy.
$b(orb)$	Proper SI polarizability due to orbital polarization.
b_s	Gaussian polarisability .
$b(eff)$	Effective polarisability .

c_α The F^2-energy-term coefficient for a surface atom participating in field evaporation from a kink-site.

c_n The F^2-energy term coefficient for an n-fold ion.

c_δ The F^2-energy-term coefficient for a diffusing atom.

D_j Probability of potential barrier penetration from a vibrational state j, in ion-tunnelling.

e Elementary (proton) charge.

E Universal binding energy.

E* Universal binding energy function.

E^{cr} Standardised energy of an ion at the crossing point.

E_t Total energy of a tunnelling ion.

F External electric field.

F^c Critical evaporation field defined by a fixed rate-constant.

F^e Zero-activation energy evaporation field.

F^o Onset evaporation field defined by a fixed evaporation flux.

F_n^{HD} Hump-disappearance field for an n-fold ion.

F_α^{loc} Self-consistent local field.

G Constant in t^{th} power repulsive law (between atom or ion and surface).

h "Pivot height" as defined by Forbes (1982d).

h^e "Standard pivot height" at the field $F=F^e$.

H_n Energy needed to form an n-fold ion, from corresponding neutral, in remote field-free space.

I_s s^{th} free-space ionization energy.

J Evaporation flux.

J^o Constant evaporation flux.

k Total evaporation rate-constant in ion-tunnelling.

k_j Rate-constant for escape by tunnelling from state j.

k^d Evaporation rate-constant for a thermally activated process.

k^d_{hr} Evaporation rate-constant for "high risk" sites surface atoms.

K^o_n Thermodynamic quantity called "configurational term".

ℓ Scaling length as defined in the Universal binding energy function.

n Charge-state of an ion at escape.

n_{hr} Number of surface atoms at "high risk" of field evaporation.

Q Activation energy.

S_n "Variable part" of the standard potential energy of an n-fold ion.

t Exponent in repulsive power law.

T Evaporation temperature.

T^c Critical temperature at which escape by thermal activation and escape by direct ground state tunnelling become equally important.

U_α Potential energy of a surface atom in its initial bonding state α .

U_n Standard potential energy of an n-fold ion.

U_α^B Potential energy of a "neutral" surface atom at its bonding point.

ΔU Difference between the level of the top of the hump and the value of the pure n-fold ionic potential in the charge-draining mechanism.

V Atomic potential energy measured relative to the bottom of the bonding well.

W_n Standard potential energy for an n-fold ion measured relative to the potential energy of the atom in the initial bonding state.

W_n^* Energy difference between the level of the plateau in the ionic curve and the bottom of the atomic curve.

x Distance of the evaporating atom nucleus measured from the electrical surface.

x^p Position of the point of escape.

x^{sh} Position of the Schottky hump.

x^{cr} Position of the crossing of the atomic and ionic curves.

z Number used in a temperature dependent correction term related to appearance energies.

α Subscript used to describe the initial bonding state of a surface atom.

β Universal binding energy constant.

Γ Half-width broadening in the Gurney model of chemisorption.

ε_o Electric constant (or permittivity of free space).

$\Delta\varepsilon$ Energy shift.

η_n Term relating to the "purely chemical" ion-surface interaction.

Θ Temperature at which the onset evaporation field becomes equal to half the zero-Q evaporation field.

Θ_c Debye temperature.

κ Force-constant.

λ_1, λ_2 Parameters related to flux field sensitivity.

Λ^o Zero-field binding energy.

Λ^F Total binding energy in the presence of a field.

$\Delta\Lambda$ Field-induced increase in binding energy.

μ_1, μ_2 Partial energies.

ν Vibration frequency.

ξ Proportionality number between image-potential and repulsive terms.

π^e Correction due to field-induced effects (polarization and partial ionization).

ρ Morse constant.

ρ_o Neutral atom radius.

σ_n Constant used in the energetics based F^e formula.

ϕ^E Local work-function of emitter.

Ω Quantity defined in the O-F formula.

CHAPTER 1

FIELD EVAPORATION THEORY:

INTRODUCTION AND BASIC DEFINITIONS

1.1 BACKGROUND

The term field-ion emission applies today to solid and liquid metals. Both techniques use sharply pointed specimens as emitters, and ion beams are produced by application of very strong positive electric fields (up to 60 V/nm).

Two main emission processes can occur at or above the highly charged emitter surface, field-ionization and field evaporation.

Field-ionization of neutral atoms by electron tunnelling was first predicted by Oppenheimer (1928) more than 50 years ago. Above a field-ion emitter surface, the neutral atom (usually a gas atom) is first attracted towards the surface by polarization forces due to the field gradient. It is ionized slightly above the emitter surface, normally after a sequence of hops, and then the resulting ion is repelled away from the surface. Field-ionization takes place preferentially above the most protruding kink site atoms, where the local field is enhanced. However, the ionization rate-constant goes to zero inside the critical surface where the highest occupied level of the incoming atom sinks below the emitter Fermi level.

On the experimental side, field-ionization was first used by Müller (1951) when he observed the first blurred field-ion microscope image, due to the ionization of Hydrogen in free space, for fields exceeding 30 V/nm.

Alternatively, if now the atom is adsorbed on a charged surface, then its field-induced removal as an ion is known as field-desorption. If the ion is formed from the field-induced detachment of a surface atom itself, then the process is known as field-evaporation.

Field-desorption was discovered by Müller (1941) when he studied surface migration of Barium on Tungsten, and tried to use the field desorbed ions to image their sites.

In field-ion microscopy (FIM), field evaporation is important in that it is used to prepare perfectly clean surfaces. Also, a specimen tip could be observed in atomic detail and its depth could be explored in a layer by layer evaporation process (e.g. Müller; 1960). With the invention of the atom-probe field-ion microscope (Müller: 1968), this layer by layer dissection could also be used to provide the chemical composition of emitters.

Today, field evaporation is discussed as a possible emission process in liquid-metal field-ion sources. These have considerable technological potential in the context (for example) of scanning-ion beam instruments and micro-circuit fabrication (Cleaver et al.: 1983).

The applications of field evaporation are well established. But, as in other areas of Physics relating to the interaction of ions with surfaces, important theoretical aspects are far from being properly understood. Nevertheless, some basic aspects of the theory are well

established and we continue by summarising a little of the basic physics.

Prior to emission by field evaporation, surface metal atoms are bound to the charged emitter surface, and are in thermodynamic equilibrium with the emitter. At the temperatures near 80 K conventionally used in FIM, ion formation is a thermally activated process with an atomic evaporation rate-constant k^d obeying the Arrhenius equation:

$$k^d = A \exp(-Q/kT) \qquad (1.1)$$

where: k is the Boltzmann constant, T is the thermodynamic temperature, Q is the activation energy necessary for escape, and A is the field evaporation pre-exponential. (At very low temperature, however, ion tunnelling is the dominant process: this is discussed in Section 1.8).

In general, it is supposed that only a limited number of surface atoms n_{hr} are at "high risk" of field evaporation; these are assumed to have the same rate-constant k^d_{hr} (Forbes: 1977a), and hence the flux J of evaporating atoms is given by:

$$J = n_{hr}\, k^d_{hr} \qquad (1.2)$$

where J has the dimensions amount-of-substance/time and is measured in layers/s (or atoms/s), n_{hr} has the dimensions amount-of-substance and is measured in "layers" or "atoms", and k^d_{hr} is measured in s^{-1}. Equation (1.2) is termed the "emission equation".

Field evaporation was originally envisaged as a single-stage process, that is, it was implicitly assumed that the observed charge state of an ion would be the same as that immediately after escape. However, the discovery of multiply-charged ions led eventually to the conclusion that field evaporation is often a two-stage process: thermally-activated escape into a singly or possibly doubly-charged state, followed by one or more post-ionization events (as discussed in Section 1.6).

Much past work in field evaporation theory has concentrated on the nature of the escape mechanism. This is normally discussed at a classical level and in terms of potential energy curves.

As regards the escape mechanism, two main possibilities are commonly considered: The Müller (image-hump) mechanism, and Gomer-type (surface charge-exchange) mechanisms.

The Müller mechanism (Müller: 1956, 1960) assumes that ionization precedes escape and that escape of the ion occurs over a Schottky hump. This mechanism has often been analysed in terms of simple "image-hump" mathematical formalisms, where the mathematics are simple and roughly predict the evaporation field.

The Gomer-type mechanisms (Gomer: 1959, Gomer and Swanson: 1963) assume simultaneous ionization and escape in a surface charge-exchange process. However, Forbes (1981) and Kingham (1981) remind us that several variants of surface

charge-exchange process can in fact be distinguished, the two extreme cases being:

(1) "charge-hopping" in which the motion of the ion is relatively fast, and the electron transfer occurs in a sharp hopping transition.

(2) "charge-draining" in which the ion motion is relatively slow and electron transfer is best described as a slow draining of charge out of the escaping atom.

In this thesis the mathematical formalisms associated with the charge-hopping mechanism are called "curve-intersection formalisms". In the past, the Gomer-type mechanisms have often been discussed in terms of a "constant intersection distance" version of a curve intersection formalism; it was in effect assumed that change in the field produced no significant change in the position of the intersection of the atomic and ionic potential-energy curves. This treatment, now known to be invalid, led to erroneous formulae for the field dependence of activation energy.

A new formula for activation energy was worked out by Forbes (1982d) (see Appendix A); this has the form:

$$Q = \Omega(F^e/F-1)^2 \qquad (1.3)$$

where F denotes the electric field, F^e is the field at which the activation energy becomes zero, and Ω is a quantity that is nearly constant if F is sufficiently close to F^e. This formula forms the basis for part of the work in this thesis.

1.2 AIMS AND STRUCTURES OF THE THESIS

The initial objective of the work is to examine the evidence that simple image-hump formalisms do not adequately describe the available experimental data. In consequence, the possibility of evaporation via the Müller mechanism is put aside.

The next part of the work utilises a simple model of the charge-hopping mechanism, based on formula (1.3) above. The main objective has been to show that this model fits experimental data adequately, gives plausible explanations whenever discrepancies are found, and can be used to extract some surface atomic information. This work is then extended to deal with more detailed bonding well shapes.

Many simplifications obviously lie behind the use of classical models. A further part of the work has been to identify the principal assumptions made. These assumptions include the validity of the image-law very near the surface, the use of flat surfaces and the disregard of local field variations. But perhaps the most serious objection to the classical models is that we might reasonably expect field evaporation to be a charge-draining rather than a charge-hopping process. This implies that activation energy calculations really need to be quantum mechanical in nature. Another part of this work has thus been to look at the difficulties likely to be involved in a charge-draining calculation.

The structure of the thesis is as follows: This first chapter introduces the basic energetics of field evaporation, reviews some background material and describes various escape mechanisms with potential-energy diagrams.

In Chapter 2, we carry out some tests on the Müller mechanism using, first some evaporation-flux field sensitivity data for six materials, and second an "extended" formalism. This chapter establishes that the simple formalisms are not compatible with the Müller mechanism and indicates why a Gomer-type mechanism is assumed in the remaining work.

Chapter 3 points out the main assumptions and limitations of our model and also indicates the complications of treating the charge-draining mechanism quantum-mechanically.

Chapter 4 then uses formula (1.3) and confirms a predicted temperature dependence of evaporation field for some Tungsten and Molybdenum data, over a limited temperature range.

In Chapter 5, we show how the F^2-energy term coefficient c_α can be derived from experimental measurements of activation and appearance energies, taken as a function of evaporation field, in the case of Rhodium. This chapter also discusses the effect of including c_α in formula (1.3).

Chapter 6 is an extension of Chatper 5 since it uses similar experimental data to make estimates of bonding distance a, vibrational frequency ν and force-constant κ.

This is also done in the context of formula (1.3) and the physical assumptions behind it.

In Chapter 7, a Morse-potential shape for the atomic curve is used, following an apparent "failure" of the parabolic approximation, at high temperatures. Theoretical Q-F plots are produced for both bonding-well shapes, and are compared with experimental plots in the cases of W, Mo and Rh. This work is compatible with Kellogg's experimental results on the field-dependence of the pre-exponential factor.

Chapter 8 draws things together and looks again at the issue of whether the curve-intersection formalism is adequate as a representation of the charge-draining mechanism.

1.3 THE ENERGETICS OF FIELD EVAPORATION

This section examines the basic energetics and behaviour of atoms at neutral and charged surfaces, and during the field evaporation process. Simple equations for binding, ionic potential and activation energies will be derived, and the shape of the neutral bonding potential will be discussed in a more general context.

1.3.1 Atoms At Surfaces

In general, the surface of a solid can be thought of as its top few atomic layers, with different properties from the bulk material and where many kinds of processes can occur. But in the context of field ion emission, we are concerned with atoms at the topmost layer only. For a perfect flat surface, these atoms are arranged in two-dimensional structures of different types (e.g. square, rectangular, hexagonal) reflecting the periodicity of the bulk.

But in reality a solid surface is not perfect and contains many "defect structures", i.e. steps, ledges, kink sites. Because of the overall emitter shape, the imaged surface of a field ion emitter contains or can be described in terms of features of this type. There may also be vacancies in a flat plane, or adatoms on it. Fig. (1.1) illustrates some of these features.

Each surface atom is bound to the bulk by being trapped in a well of depth Λ^{o}, called the binding energy (e.g.

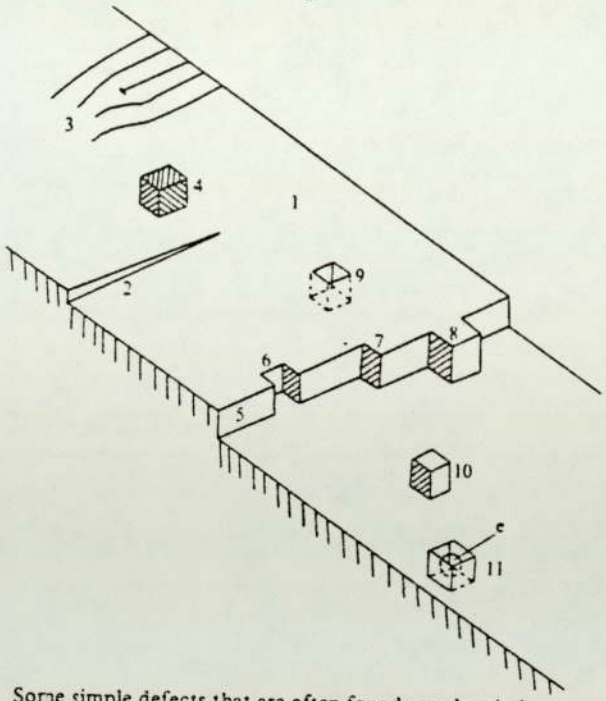

Some simple defects that are often found on a low-index crystal face. 1. The perfect flat face itself – a terrace; 2. an emerging screw dislocation; 3. the intersection of an edge dislocation with the terrace; 4. an impurity adatom (adatoms are discussed in Chapter 6); 5. a monatomic step in the surface – a ledge; 6. a vacancy in the ledge; 7. a step in the ledge – a kink; 8. an adatom of the same kind as the bulk atoms situated upon the ledge; 9. a vacancy in the terrace; 10. an adatom on the terrace; 11. a vacancy in the terrace where an electron is trapped – in an alkali halide this would be an F-centre.

Fig. (1.1) Illustration of some defects on a flat surface.

(from Prutton: 1983).

Λ° = 8.66 eV for Tungsten). In a direction normal to the surface, this potential well has the following general shape:

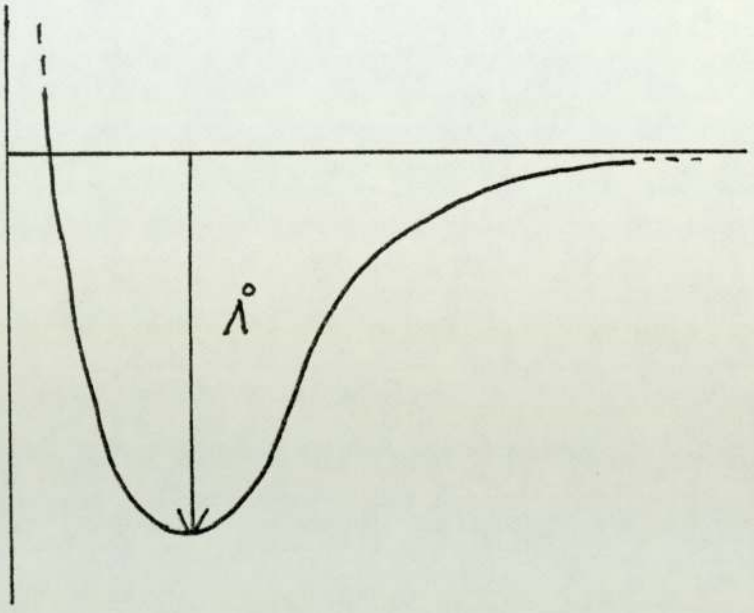

The atom is vibrating around its equilibrium position.

An atom in an exposed position, e.g. at a kink site, will,however,see a "diffusion-type barrier" in some directions parallel to the surface, as shown below:

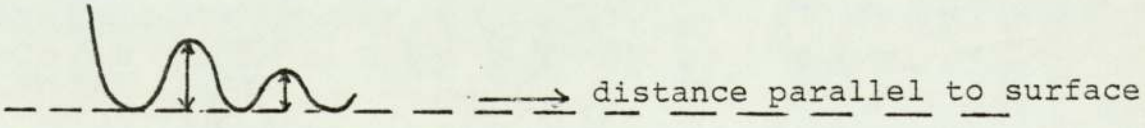

Barriers in different lateral directions will usually be of different heights. An atom may leave a site if enough thermal energy is supplied to overcome the potential barrier due to its neighbouring sites. This process is surface diffusion. Diffusion experiments include observations of the diffusion of single adatoms deposited upon different tips in a field-ion microscope: activation energies for diffusion have been measured and found to vary from one crystal face to another (e.g. Q^{diff} = 0.87, 0.57, 0.84 eV for W on W(011), W(112) and W(321) respectively, by Bassett, 1973).

The atoms that are imaged in a FIM are the most protruding atoms, in particular the kink site atoms as shown in Fig. (1.2) for a ball model. It is also these protruding atoms that are at high risk of field evaporation.

More generally, when an external electric field is applied, many properties of the atoms at the surface are modified. Effects such as orbital polarisation and partial charge transfer into the emitter can occur, and the subject becomes one of charged surfaces.

1.3.2 The Surface Atom Binding Energy

The surface atom binding energy is defined as the work needed to remove the atom as a neutral and place it at a point in remote field-free space. However, the presence of a high electric field induces a modification of the electronic structure of the bound atom. The binding energy

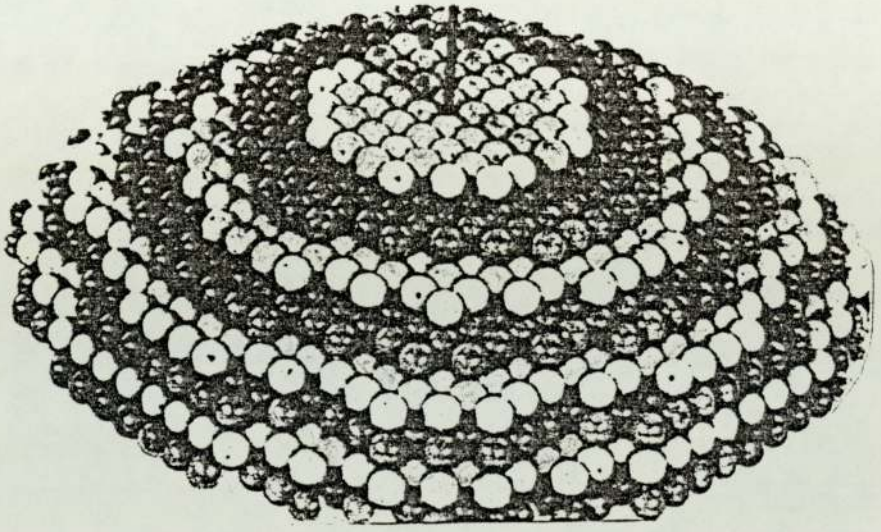

Fig. (1.2) A ball model.

The kink site atoms (balls in white) are the ones that are imaged on a field-ion microscope screen.

Λ^F can be written in the form:

$$\Lambda^F = \Lambda^o + \frac{1}{2} c_\alpha F^2 \qquad (1.4)$$

where Λ^o is the zero-field value for the binding energy, F is the external electric field (i.e. the field somewhat above the surface), c_α is a parameter usually assumed constant and discussed below. The second term - sometimes denoted by $\Delta\Lambda$ - represents the field-induced increase in binding energy.

Historically, Λ^o values were first estimated from thermodynamic experiments based on second and third law procedures (by use of the Clausius-Clapeyron equation, at T = 298 K) by Langmuir (1913); later, values were obtained by many other investigators, using various methods (e.g. Flood:1966). Tsong (1978a) lists values for materials of particular interest to field evaporation theory.

The most protruding surface atoms are the ones participating in the field evaporation process. From a theoretical point of view, they can be treated as chemisorbed atoms; calculations of binding energies involve solving the Schrödinger equation in a one-electron approximation to a N-body problem (see Appendix B, on chemisorption).

The parameter c_α is defined by equation (1.4) above and deserves some comments. It is often called "polarisability" in the literature, but following Forbes (1977c, 1978a) this name is avoided here. The parameter cannot be identified with the parameter conventionally named "polarisability"

because it is not defined in terms of the local field acting on the atom in question, but rather in terms of the external field that exists somewhat above the surface atom. Hence, in order to avoid confusion, c_α is called the "F^2-energy-term coefficient". Also, as will be argued in Chapter 5, the physical origin of this coefficient c_α lies not only in the polarisability of atomic orbitals, but also partly in charge transfer from the surface atom: this charge transfer is necessary in order to sustain the external electric field.

1.3.3 The Neutral Atom Bonding Potential

Although the general shape of an atomic bonding curve is intuitively obvious, detailed energy-distance relations for atoms at solid surfaces have not yet been obtained experimentally. There are two general approaches to the determination of bonding curve shape:

(1) Some empirical form (e.g. a Morse potential) is assumed, and the coefficients involved are obtained by a fitting procedure, via some physical parameter that can be (a) measured, and (b) predicted from the model in terms of the coefficient values.

(2) First-principles computational methods, such as those carried out by Smith et al.:1975; Khan and Ying: 1976; Carlsson et al.: 1980.

Many of the more relevant first-principles calculations have been carried out for bulk solids rather than for the surface atom situation. It is clear that purely theoretical binding energy-distance relationships are very difficult to obtain, even for bulk solids. In principle, one needs to carry out chemisorption-type calculations as a function of the position of the relevant atomic nucleus (see Appendix B).

The approach taken in the main part of this thesis is essentially similar to the empirical approach just mentioned. This empirical approach is often used in simple analyses of the gas physics and solid-state situations. Thus, a kink-site surface atom will be assumed to be in a quasi-neutral state, and simple classical approximations will be used to describe its behaviour prior to field evaporation. A parabolic shape for a bonding curve is the simplest one. Other types of model may include Lennard-Jones, Buckingham or Morse potentials. The latter is used in Chapter 7 in the form;

$$V(x) = \Lambda^{o}\left[1-\exp(-\rho)(x-a)\right]^{2} \qquad (1.5)$$

where x is the distance of the evaporating atom nucleus from the emitter's electrical surface (see Appendix C for a fuller discussion), and V(x) is the atomic potential energy measured relative to the bottom of the bonding well; ρ is a constant and a is the surface atom bonding distance.

These models have simple analytic forms and work well for diatomic molecules. They are not appropriate for solids where volume-dependent forces are involved, but can be used for surface atoms as simple approximations. Recently, it has been shown (Rose et al.:1981; Ferrante et al.: 1983) that a "Universal binding energy" curve fits several different situations, such as adhesion, cohesion, chemisorption and the bonding of diatomic molecules. The curve has the algebraic form:

$$E^*(a^*) = -(1+\beta a^*) \exp(-\beta a^*) \qquad (1.6)$$

where $E^*(a^*)$ is the "Universal binding energy function" which describes the shape of the binding energy curve, a^* is a dimensionless scaled length defined relative to the bottom of the Universal binding energy function, and β is a constant.

Note that for each of the potential wells mentioned, a characteristic frequency is associated with the vibrating atom.

1.3.4 The Standard Ionic Potential Energy

This section deals with the derivation of an expression for the standard potential energy of an ion. The treatment, based on an electrothermodynamic (or Born-Haber type) cycle, is used to calculate the work done in creating an ion outside a charged emitter surface and follows that of Forbes (1982a). The standard potential energy, denoted by $U_n(x)$, where n is

the ion charge number, is defined as the work done in removing the atom from a position in remote field-free space (and in its neutral state) to some position x (in an n-fold ionic state). This work is seen from a classical point of view as an electrothermodynamic cycle achieved by a hypothetical external agent; the following steps are considered:

(1) removal of n electrons from the neutral atom in remote field-free space;

(2) the n electrons are then assumed to be placed at the emitter Fermi level;

(3) the resulting ion is finally moved from the remote field-free space position to a position close to the emitter surface.

Step (1) can easily be seen as being given by the sum of the first n free-space ionization energies $\sum_{s=1}^{n} I_s = H_n$; whilst steps (2) and (3) are regarded as a combination due to a contribution of "chemical" and "electrical" interactions of the electrons and the ion with the surface.

When the electrons are placed at the emitter Fermi level, and the electrostatic component of ion potential energy is taken into account, the electron and electrostatic ionic contributions involved are given (in the usual approximation) by $-n\phi^E - neFx$, where ϕ^E is the local work-function, e the elementary (proton) charge and F is the external field above

the emitter surface (considered to be the same at all distances).

Contributions to the "purely chemical" interactions of the ion with the surface are mainly due to correlation forces given by the image-potential as $-n^2e^2/16\pi\varepsilon_o x$, where ε_o is the permittivity of free-space; and to polarization forces given by $-\frac{1}{2} c_n F^2$ where c_n is the F^2-energy-coefficient for an n-fold ion. Short-range repulsive terms also need to be included, at least in principle, and we approximate these by a term of the form G/x^t, where G and t are constants.

The standard ionic potential energy is thus a field and position dependent quantity, given by:

$$U_n(x) = H_n - n\phi^E - neFx - \frac{n^2e^2}{16\pi\varepsilon_o x} - \frac{1}{2} c_n F^2 + \frac{G}{x^t} \qquad (1.7)$$

The "variable part" of this ionic potential term is denoted $S_n(x,F)$ and given by:

$$S_n(x,F) = -neFx - \frac{n^2e^2}{16\pi\varepsilon_o x} - \frac{1}{2} c_n F^2 + \frac{G}{x^t} \qquad (1.8)$$

1.3.5 The Activation Energy

The activation energy Q_n that appears in equation (1.1) can be defined as the amount of energy a bound surface atom should acquire in order to escape from the surface of a material as an n-fold ion. If this process can be considered as "slow" and thermodynamically reversible, then we may follow the treatment suggested by Forbes (1977b) in terms

of a "desorption virial" and a "subsidiary condition".

The desorption virial W_n is the potential energy for an ion measured relative to the potential energy of the atom in its initial bonding state. W_n is a function of x and F as defined above, and of the charge-state n that the ion has just after it has escaped, and is written $W_n(x,F)$.

The activation energy, Q_n, may be defined as the value of the virial W_n at the point of escape x^p. (Whatever the escape mechanism, the point of escape is located at the top of activation energy hump over which escape occurs.) This Q_n is a function of field F and may be written:

$$Q_n(F) = W_n(x^p,F) \qquad (1.9)$$

Another equation called the "subsidiary condition" is needed to represent the fact that the escape point x^p is both field and charge-state dependent, i.e. $x^p = x_n^p(F)$. The subsidiary condition can be written in a general form as:

$$\mathcal{G}(x_n^p,F) = 0 \qquad (1.10)$$

Combination of equations (1.9) and (1.10) in effect leads to the elimination of x^p, and hence to an explicit expression for the field-dependence of Q_n. Different models of field evaporation are characterised by different subsidiary conditions, as will be seen later, but we need first to look

at basic theory from which an expression for $W_n(x,F)$ can be derived.

From the definition of the virial W, using U_α^B to denote the potential energy of the "neutral" atom at its bonding point, we have:

$$W_n(x,F) = U_n(x,F) - U_\alpha^B \tag{1.11}$$

where

$$U_\alpha^B = -\Lambda^F = -\Lambda^o - \frac{1}{2} c_\alpha F^2 \tag{1.12}$$

From equation (1.7) for $U_n(x,F)$, the virial W_n can now be written explicitly as:

$$W_n(x,F) = (H_n - n\phi^E + \Lambda^o) - neFx - \frac{n^2e^2}{16\pi\varepsilon_o x} + \frac{1}{2}(c_\alpha - c_n)F^2 + \frac{G}{x^t} \tag{1.13}$$

and the activation energy Q_n is given by equation (1.13) taken at $x=x^p$, as:

$$Q_n(F) = (H_n - n\phi^E + \Lambda^o) - neFx^p - \frac{n^2e^2}{16\pi\varepsilon_o x^p} + \frac{1}{2}(c_\alpha - c_n)F^2 + \frac{G}{(x^p)^t} \tag{1.14}$$

This is a one-dimensional classical expression applicable when the departing particle has a well defined charge state.

The term $(H_n - n\phi^E + \Lambda^o)$ is the "constant" part in equation (1.13), and is characteristic of a given material. It is called the "configurational term" and is denoted by K_n^o.

1.4 THE CONCEPT OF EVAPORATION FIELD

1.4.1 Evaporation Field Criteria

When an external electric field F is applied to a material, the first atoms to be detached - when the field is high enough - are those at the "high risk" positions and the rate of evaporation increases as the field is increased. However, for practical and theoretical purposes, one has to define an evaporation field that corresponds to some specific criterion. For this, three different forms have been formulated:

(a) The field F^e defined by the requirement that:

$$Q(F^e) = 0 \qquad (1.15)$$

which is known as the "zero-Q evaporation field". This is a theoretical quantity, constant for a given material and higher than any observed field in low-temperature field evaporation experiments for the material in question.

(b) The field F^c as used by Forbes (1974, 1978b) in his analysis of Tsong's experiments (1971), which is known as the "critical evaporation field" and is defined by the requirement that the rate-constant for evaporation be equal to $1s^{-1}$. This criterion is used in single-atom experiments where the rate-constant is measured directly, and leads to:

$$Q(F^c) = kT\ell n[A/1s^{-1}] \qquad (1.16)$$

(c) Finally, the field F^o defined by the requirement that the evaporation flux has some fixed value, J^o, for example 0.01 layers/s, in experiments involving observation of the evaporation flux, or 10^9 ions/s in atom-probe experiments (e.g. Kellogg: 1981a). This field F^o can be called the "onset evaporation field" and is given by:

$$Q(F^o) = kT\ell n[J^o/n_{hr}A] \qquad (1.17)$$

With liquid metal field-ion sources, where macroscopic electrical measurements are used, a fixed emission current criterion is employed, for example, 1nA (Aitken and Mair: 1980). Note that the value of F^o depends both on the flux level chosen and on temperature.

1.4.2 Prediction of F^e From an Energetic Argument

The zero-Q requirement for the evaporation field was first made by Müller (1960) in the context of a simple image-hump formalism and a simple F^e formula was derived (Chapter 2). Subsequently, Brandon (1964) using different escape charge numbers, found that for most metals the evaporation fields for doubly charged ions are lower than those for singly charged ions. He hypothesised that evaporation charge-state at escape would be that corresponding to the lowest predicted evaporation field. This is known as Brandon's criterion.

Much later, Forbes (1982b) derived an F^e formula based

on energetics only, by making the assumption that at Q=0 the image-potential is some significant fraction of the configurational term K_n^o. This leads to the result:

$$F^e = \sigma_n \left(\frac{16\pi\varepsilon_o}{n^3 e^3}\right) (K_n^o)^2 \qquad (1.18)$$

where σ_n is around 0.2. Formula (1.18) leads to reasonable agreement with observed evaporation fields for most metals employed in low temperature field evaporation.

1.5 EVAPORATION CHARGE-STATE

For both the Müller and Gomer mechanisms, the theoretically predicted evaporation field is a function of the charge-state assumed for the ion immediately after escape. Using a simple image-hump formalism, Müller (1960) assumed that metals field evaporate in a singly-charged state. But Brandon's criterion leads to the conclusion that n is 2 for most metals. Tsong and Müller (1970), using the charge-hopping mechanism, also predicted that the charge-state at escape would be 2 for most metals.

However, with the development of techniques such as the atom-probe field-ion microscope (Müller, Panitz and McLane: 1968) which measures the mass-to-charge ratios, it was found that refractory metals often evaporated in charge-states higher than 2. For example, 3^+ and 4^+ charge-states were commonly observed for Tungsten (e.g. Brenner and McKinney:1968; also Kellogg: 1981a) and even a 6^+ state (Müller and Krishnaswamy: 1976).

There was thus a discrepancy between experiment and theory, which persisted for most of the 1970's.

1.6 POST-IONIZATION

It is strongly improbable that the high observed charge-states are formed in a single-stage process at the moment of escape. It is much more likely that escape of the ion occurs into singly or doubly-charged states, and that further ionization then takes place as the ion is moving away from the emitter, with the resulting electron(s) tunnelling back into empty states at or above the emitter's Fermi level. This process is termed "post-ionization".

The theoretical work of Taylor (1970) and Chambers (1970, 1975) originally suggested that post-ionization is an unlikely event. However, Ernst (1979), in his experiments on the field evaporation of Rhodium, measured the activation energies of both Rh^{+} and Rh^{++} as a function of evaporation field. One important result was that Rh^{+} and Rh^{++} had the same activation energy, within experimental errors. This strongly suggested that escape of a Rhodium ion is initially into a singly-charged state, and then formation of Rh^{++} is due to post-ionization. Ernst then used a simple one-dimensional model to predict ionization probability, and the theoretical curve was found to be a good fit to his experimental results, within experimental errors.

Ernst's one-dimensional theoretical model was, however, regarded as insufficiently accurate by Haydock and Kingham (1980). They developed a method of calculating the total probability of post-ionization based on a three-dimensional

version of the WKB approximation for the field-ionization of imaging-gas atoms, and applied it to metal ions. Their conclusion was that post-ionization is a likely process and that the final charge-state is field-dependent. Increasing the field - i.e. decreasing the temperature if one would like to keep the rate of evaporation constant - would certainly enhance the probability of post-ionization and explain the high charge-state cases.

Ernst and Jentsch (1982) in their work on measurements of differential energy distributions of Rh^{+} and Rh^{++}, found that the Haydock and Kingham model contained some errors. They went on to construct a three-dimensional model, again using the WKB approximation, and found it in good agreement with their experimental results, as well as with Ernst's previous work. Subsequently, Kingham (1982a) revised his model in the light of their criticisms, and calculated post-ionization probabilities for a large number of materials.

The above arguments also find support in the work of Kellogg (1981b; 1982) on the relative abundance of W^{+}, W^{2+}, W^{3+} and W^{4+} measured as a function of field using a Pulsed Laser Atom Probe (PLAP), and Andrén et al. (1984) on the charge-state of W using an Atom Probe Field-Ion Microscope (APFIM).

1.7 ESCAPE MECHANISMS

Having established the basic energetics of field evaporation, we now return to describe the escape process for the Müller and Gomer mechanisms. This is done with the use of potential energy diagrams, and the relevant subsidiary conditions are given.

Figure (1.3) shows schematic standard potential energy curves for (a) a bound neutral atom, and (b) an ion, near a solid metal surface in the absence of an external electric field. For the atomic curve U_α, the bonding is metallic with short-range repulsive forces due to the overlapping of electron clouds (Pauli's exclusion principle), whereas in the ionic curve U_n, the image-potential is the main attractive force at long distance.

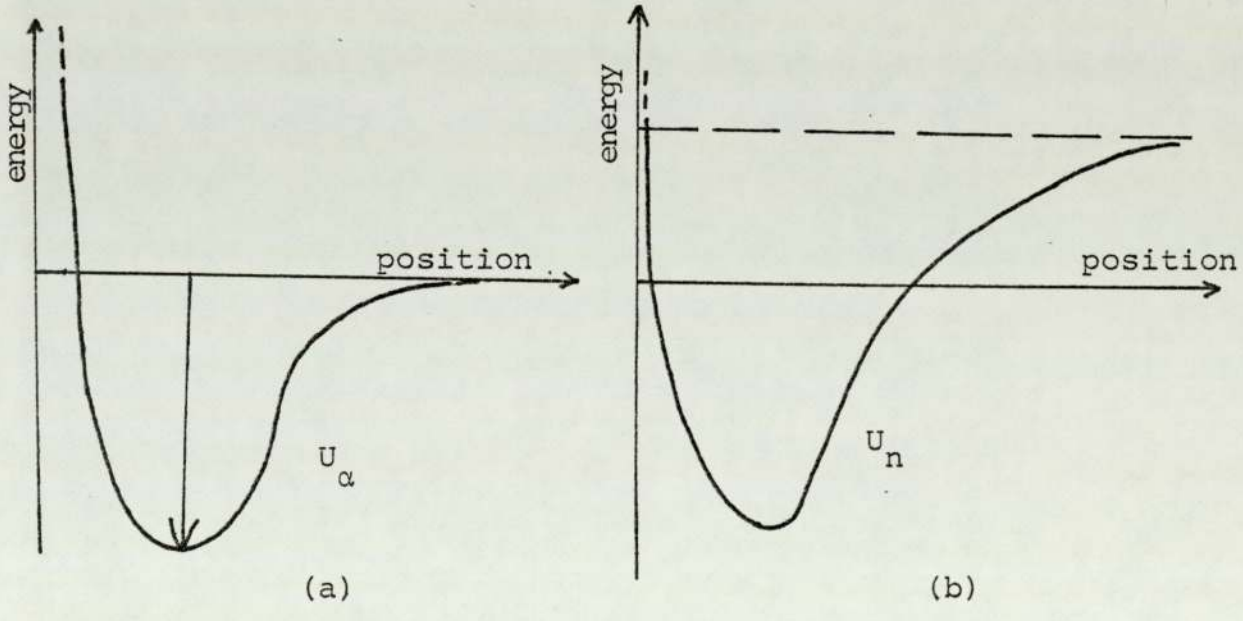

Fig. (1.3): Potential energy curves for a bound neutral atom and an ion near an emitter surface in the absence of any external field.

Now consider the effect of field on the ionic potential energy curve. For low-to-medium fields, there is a hump - The Schottky hump - in the curve; at higher fields the hump disappears, as shown in Fig. (1.4a). Figure (1.4b) illustrates the case where the hump has just disappeared (at $F=F^{HD}$).

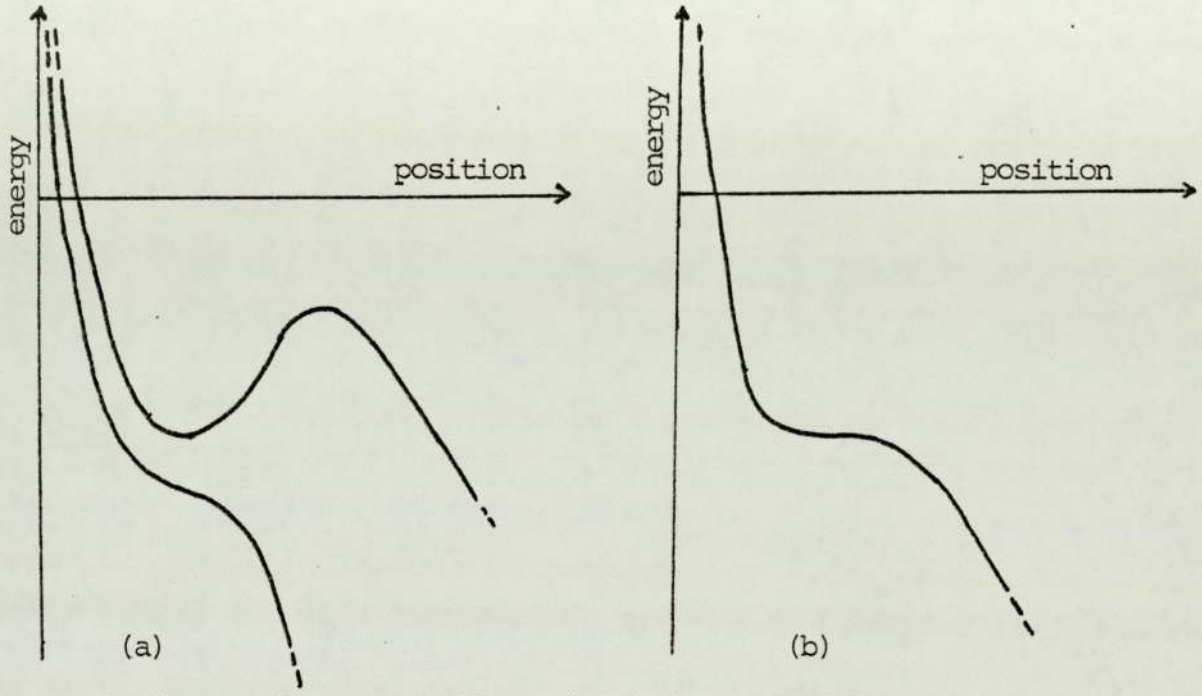

Fig. (1.4) : Effect of field on the ionic potential energy curve.

The different mechanisms of field evaporation are obtained for different configurations of the atomic and ionic curves above.

(a) The Müller Mechanism

Taking the low-to-medium fields ionic curve, assuming a low $(H_n-n\phi^E)$ value and combining with the atomic curve U_α, we obtain Fig. (1.5). This represents the Müller mechanism.

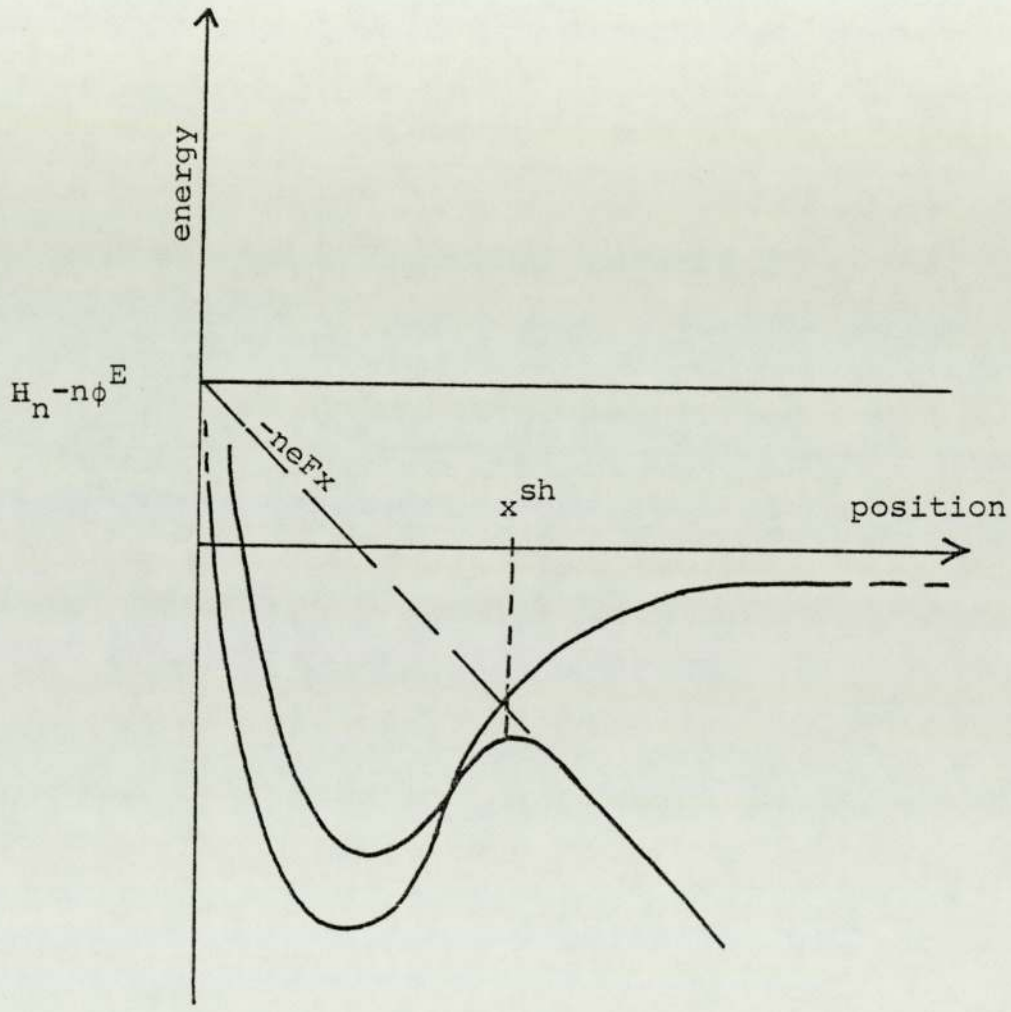

Fig. (1.5) The Müller mechanism

It illustrates that ionization occurs before escape and that escape occurs over the Schottky-hump at $x^p = x^{sh}$. From the definition of the virial, the subsidiary condition is given by:

$$\left.\frac{\partial W_n}{\partial x}\right|_{x=x^{sh}} = 0 \qquad (1.19)$$

In the so-called "basic image-hump formalism", where the F^2-energy terms and the repulsive term in the classical expression for W_n are neglected, this condition leads to:

$$x^{sh} = \frac{1}{2}\left(\frac{ne}{4\pi\varepsilon_o F}\right)^{\frac{1}{2}} \qquad (1.20)$$

This relation is now known to be invalid, as will be seen in Chapter 2.

(b) <u>The Charge-Hopping Mechanism</u>

Taking the high fields version of the ionic curve, assuming a high $(H_n - n\phi^E)$ value and combining with the atomic curve, we obtain Fig. (1.6), which represents the charge-hopping mechanism. Ionization and escape occur simultaneously at the crossing point of the atomic and ionic curves, denoted here by x^{cr}, and the subsidiary condition is given from:

$$U_n(x^{cr},F) - U_\alpha(x^{cr},F) = 0 \qquad (1.21)$$

The distance x^{cr} is, of course, a function of external field. Much of the older work in the literature, however, assumes that the variation of x^{cr} with F may be neglected

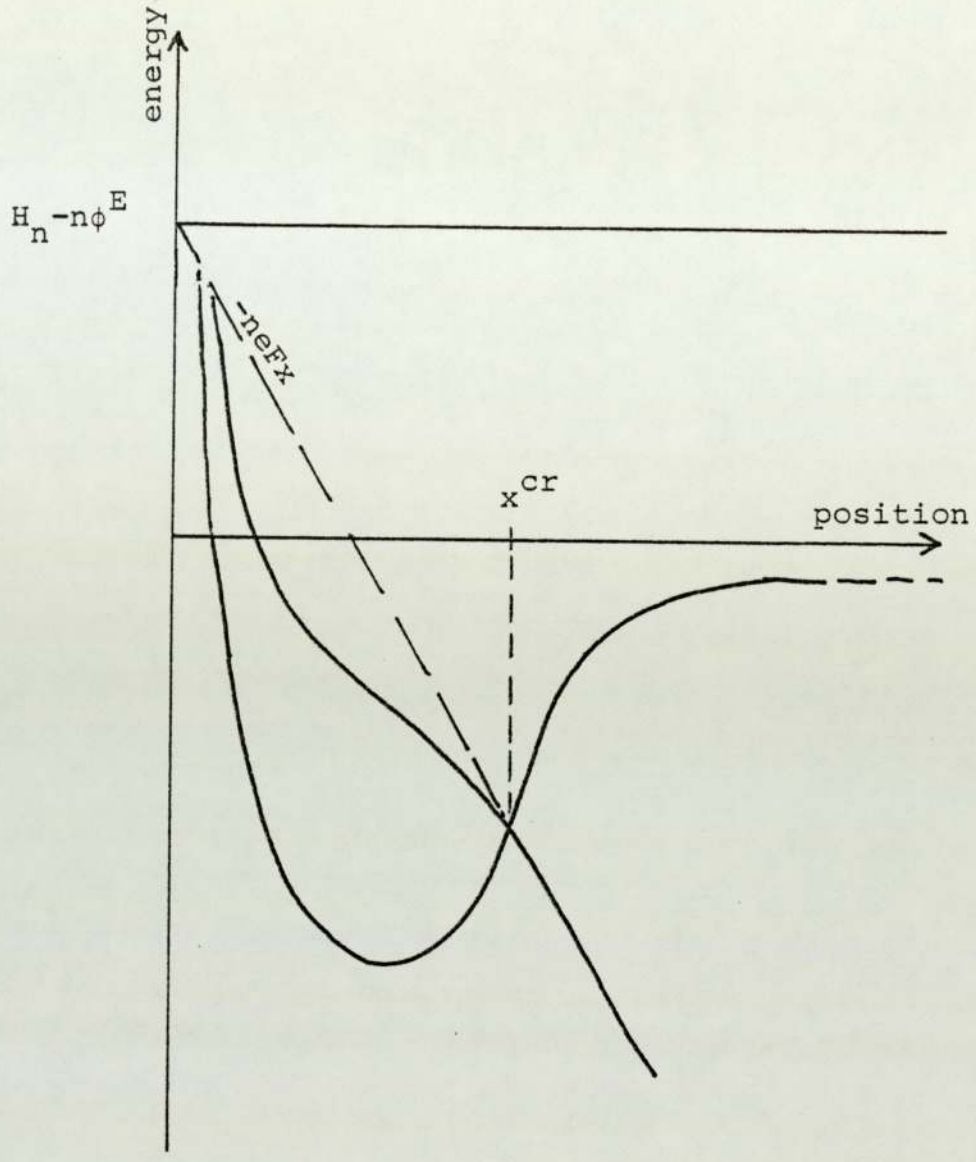

Fig. (1.6) The charge-hopping mechanism.

in a first approximation, and thus in effect uses the simplified subsidiary condition:

$$x^p = x^{cr} = \text{const} \simeq \rho_o$$

where ρ_o is the neutral atom radius.

The mathematically unsatisfactory nature of this "constant intersection distance" approximation has been pointed out by McKinstry (1972) and by Forbes (1978b). The latter in effect subtracted Λ^F from each side of equation (1.21) to give the subsidiary condition form:

$$W_n(x^{cr},F) - V(x^{cr},F) = 0 \qquad (1.22)$$

where $V(x,F)$ is the potential energy of the bound atom measured relative to the level of the potential minimum. Forbes then used a parabolic well approximation for $V(x,F)$ but in principle other shapes might be used, as discussed in section 1.3.3 earlier. (also see Chapter 7).

(c) <u>The Charge-Draining Mechanism</u>

If field evaporation occurs in such a fashion that electron(s) are draining out slowly, the departing atom has a non-integral charge-state at the moment of escape, and the atomic and ionic curves are drawn as "repelled" in the crossing region. This is shown in Fig. (1.7) and represents the charge-draining mechanism.

In this case, the potential energy at x^p (relative to the bottom of the atomic curve) is related to the virial

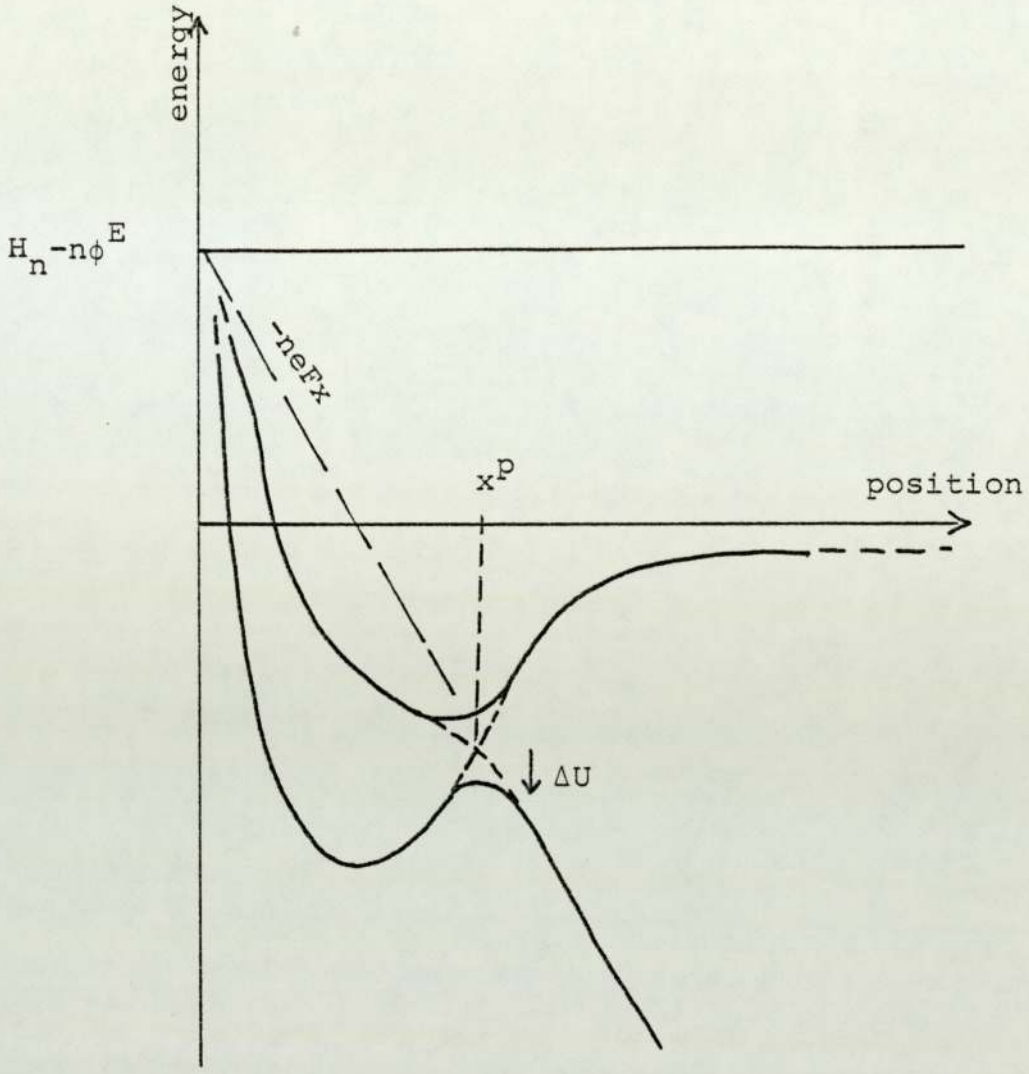

Fig. (1.7) The charge-draining mechanism.

$W_n(x^p,F)$ by:

$$W_n(C.D) = W_n(x^p,F) - \Delta U \tag{1.23}$$

where ΔU is due to the curve "repulsion effect" (see Chapter 3), and C.D stands for charge-draining.

A formal subsidiary condition for charge-draining is derived by assuming escape to occur at the top of the hump shown in Fig. (1.7), which leads to:

$$\left.\frac{\partial W_n(x,F)}{\partial x}\right|_{x^p} - \left.\frac{\partial \Delta U}{\partial x}\right|_{x^p} = 0 \tag{1.24}$$

Unfortunately, no well-established analytical expression for ΔU is available yet.

1.8 TUNNELLING IN FIELD EVAPORATION

As already indicated, the phenomenon of tunnelling was first predicted by Oppenheimer (1928) in the case of ionization of a Hydrogen atom under an applied electric field. It is a purely quantum-mechanical effect and, for example, constitutes the escape process in field electron emission from metals.

In the context of field evaporation, the probability for escape by tunnelling of an ion from a given vibrational state j, below the top of the activation energy barrier, is given in the WKB approximation by:

$$D_j = \exp\left[-2\left(\frac{2m}{\hbar^2}\right)^{\frac{1}{2}} \int_{x_1}^{x_2} (V(x) - E_t)^{\frac{1}{2}} dx\right] \qquad (1.25)$$

where m is the mass of the ion, $\hbar$ is Planck's constant divided by 2π, V(x) the potential describing the shape of the barrier, E_t the energy of the tunnelling ion, and (x_2-x_1) is the width of the barrier. D_j is the probability of barrier penetration, so the rate-constant k_j for escape from state j is obtained by multiplying this by the atomic vibration frequency ν_t, giving:

$$k_j = \nu_t D_j \qquad (1.26)$$

In some circumstances it is necessary to include in equation (1.26) an electronic transition probability (see, for example, Gomer and Swanson: 1963), but we do not consider this case here.

If the probability that state j is occupied is P_j, then the probability per unit time that escape will occur from state j, which we denote by z_j is

$$z_j = \nu_t P_j D_j \qquad (1.27)$$

Assuming occupation of the states according to Boltzmann statistics, we have:

$$P_j = \exp(-jh\nu/kT)\left[1-\exp(-h\nu/kT)\right] \qquad (1.28)$$

And, because the total probability of finding the atom in some one of its vibrational states is unity, we have:

$$\left[1-\exp(-h\nu/kT)\right] \sum_{j=0}^{\infty} \exp(-jh\nu/kT) = 1 \qquad (1.29)$$

Tunnelling occurs from all vibrational states below the level of the activation energy hump , and the total probability per unit time of escape by tunnelling is obtained by summing over all the states below the top of the hump.

The contribution due to escape from states above the level of the hump should be added, and the corresponding evaporation rate-constant is given by putting $D_j=1$ in equation (1.26) above.

Thus, the total evaporation rate-constant k is given by:

$$k = \nu_t\left[1-\exp(-h\nu/kT)\right] \sum_{j}^{\infty} D_j \exp(-j\, h\nu/kT) \qquad (1.30)$$

where D_j is given by equation (1.25) below $j=Q/h\nu$ and is equal to 1 above $j=Q/h\nu$.

It is now important to investigate what the dominant escape process (i.e. thermally activated or tunnelling) is. Two limiting cases are considered:

(1) <u>At High Temperatures</u>, only those states above the level of the activation energy hump are considered to contribute significantly, i.e. the excited states such that $jh\nu \geq Q$ and $D_j=1$. In this case the rate-constant for evaporation reduces to:

$$k = \nu_t [1-\exp(-h\nu/kT)] \sum_{j \gtrsim \frac{Q}{h\nu}} \exp(-j \frac{h\nu}{kT}) \qquad (1.31)$$

Using equation (1.29), it can be shown that:

$$\sum_{j \gtrsim \frac{Q}{h\nu}} \exp(-j \frac{h\nu}{kT}) \simeq \frac{\exp(-Q/kT)}{1-\exp(-h\nu/kT)} \qquad (1.32)$$

and equation (1.30) becomes:

$$k \simeq \nu_t \exp(-Q/kT) \qquad (1.33)$$

This corresponds to a thermal activation and indicates that at high temperatures, the thermally activated process is the dominant effect.

(2) At Low Temperatures, the excited states such that $jh\nu<Q$ are considered. D_j is now given by equation (1.25) and the rate-constant for evaporation is given by equation (1.30) summed for j=0 to $j< \frac{Q}{h\nu}$. The summation is not easy to carry out and depends on the shape assumed for the activation energy barrier. However, the result would be different from a thermally activated one and tunnelling is expected to be the dominant process.

At Very Low Temperatures, however, only the ground state (j=0) is considered, and the rate-constant can be shown to be:

$$k = k_{j=0} \simeq \nu_t D_o \qquad (1.34)$$

Many authors have considered a critical temperature T^c at which escape by thermal activation and escape by direct ground state tunnelling become equally important. T^c is calculated by putting k as given by equation (1.33) equal to $k_{j=0}$ as given by equation (1.34). It has been investigated in the context of the Müller mechanism (Ehrlich and Kirk: 1968), the charge-hopping mechanism (Gomer and Swanson: 1963; Brandon: 1966) and "an ionic bonding" (Tsong: 1968). Kingham (1981) considered different surface barrier models for different escape mechanisms (triangular for charge-hopping, parabolic for image-hump and charge-draining) and found that T^c is model dependent. He derived a value of T^c = 40 K for W using the image-hump formalism (in accordance "with Ehrlich and Kirk estimate" of 41 K), and a value of $T^c \lesssim 35$ K using the charge-draining mechanism. We return to the question of the critical temperature in Chapter 4.

CHAPTER 2

ARGUMENTS AGAINST THE IMAGE-HUMP FORMALISMS

2.1 INTRODUCTION

In order to extract useful information from field evaporation data, it is necessary to understand which field evaporation mechanism is operating. The aim of this chapter is to summarise the evidence that (in so far as simple one-dimensional classical arguments are valid) experimental field evaporation data are incompatible with the Müller mechanism.

The first part of the author's research work, carried out early in the project jointly with R. K. Biswas and R. G. Forbes, was an attempt to discriminate between the Müller and Gomer-type mechanisms by investigating the field sensitivity of evaporation flux (J). The method was a theoretical extension/application of one developed by Forbes (1978b), and we applied it to field evaporation data reported by Tsong (1978b) for six metals. The results (reported in Forbes, Biswas and Chibane: 1982) tended to suggest that the Müller mechanism was not compatible with data but a Gomer mechanism was. In consequence, the author investigated a Gomer-type mechanism in more detail, as described in Chapters 4 to 7.

The above early work used numerical values given in Tsong (1978b). Subsequently, when the present

author carried out a proper regression analysis of Tsong's raw data, it was realised that the error limits assumed in the earlier work were incorrect. And, as a consequence, the field-sensitivity based tests were less convincing than previously thought. By this time, however, the author was achieving good agreement between experimental results and an analysis of Gomer-type mechanisms using a curve-intersection formalism, and Biswas and Forbes were devising additional tests that indicated more convincingly against the Müller mechanism.

We therefore present here a summary both of the original arguments against the Müller mechanism (but using the revised data), and of the better arguments subsequently put forward.

2.2 FIELD SENSITIVITY AND PARTIAL ENERGIES

A change in the voltage applied to a field-evaporating field-ion emitter causes a change in the mean field at the evaporation sites, and a change in the evaporation rate-constant and flux. Measurements of the field sensitivity of rate-constants and/or fluxes have been made by various workers, in particular Brandon (1965, 1966), Taylor (1970), Tsong (1971, 1978b); theoretical discussions are to be found in

these papers and in the work of McKinstry (1972), Vesely and Ehrlich (1973), Patel (1974) and Forbes (1974, 1978b).

The raw data concerning flux field sensitivity are often presented in the form of a plot of ℓgJ (or ℓnJ) against (V/V_o) or (F/F^o), where V_o is some reference voltage (corresponding approximately to evaporation at a given flux level J^o) and F^o is the corresponding field at the high-risk sites. Tsong's (1978b) data are shown in Fig. (2.1). Fitting a quadratic curve to the data provides regression coefficients, and the values of these could in principle be compared with theoretical values derived from field evaporation models. However, it may be argued (Forbes, Biswas and Chibane: 1982), that it is better to derive from the data the parameters:

$$\lambda_1 = kT.\partial \ell n(J)/\partial(F/F^o)\Big|_{F=F^o} \qquad (2.1a)$$

$$\lambda_2 = kT.\partial^2 \ell n(J)/\partial^2(F/F^o)\Big|_{F=F^o} \qquad (2.1b)$$

From the emission equation (Equation (1.2)), if field dependence in the quantity n_{hr} may be ignored, then λ_1 and λ_2 may be identified with the partial energies μ_1 and μ_2 introduced by Forbes (1974). Thus

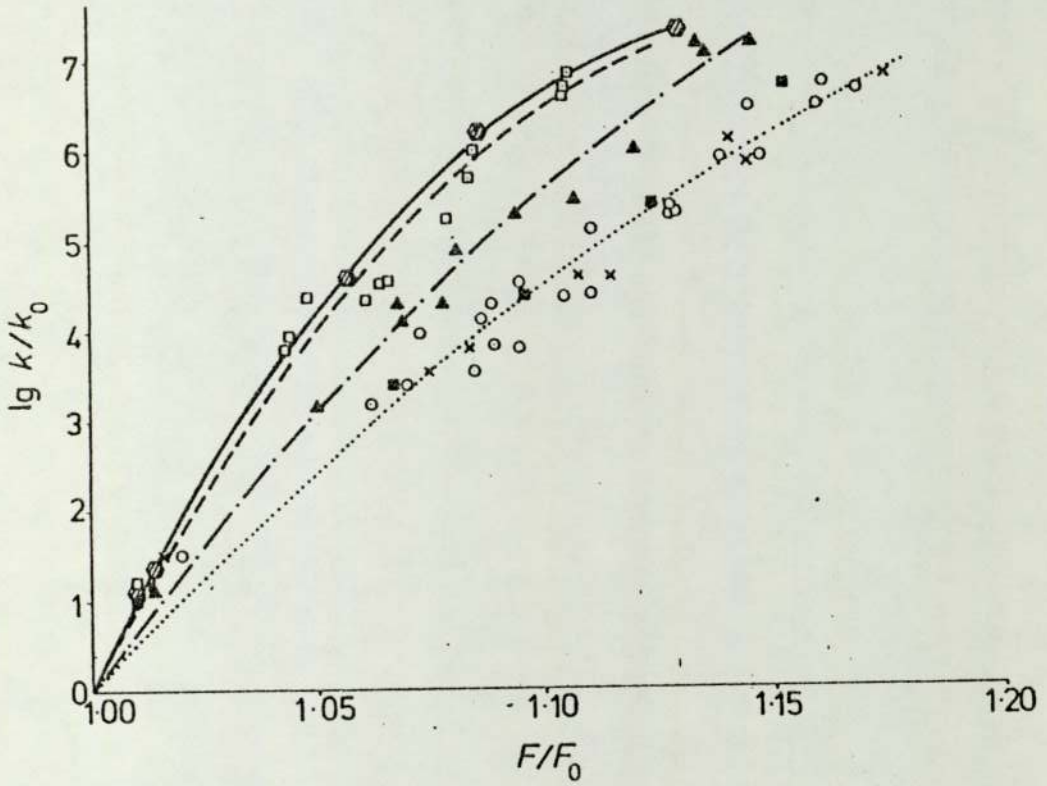

Figure 2.1. The field dependence of the field evaporation rate of tungsten, molybdenum hafnium, ruthenium, iridium and platinum ($k_0 \equiv 10^{-2}$ layer s^{-1}). The Ru, Ir and Pt data fit into the same dotted curve. ▨ W(110); □ Mo(110); ▲ Hf(10$\bar{1}$0); ■ Ru(11$\bar{2}$1); O Ir(100); × Pt(100).

$$\lambda_1 \simeq \mu_1 = kT.\partial \ell n(k_{hr})/\partial(F/F^o)\Big|_{F=F^o} \qquad (2.2a)$$

$$\lambda_2 \simeq \mu_2 = kT.\partial^2 \ell n(k_{hr})/\partial^2(F/F^o)\Big|_{F=F^o} \qquad (2.2b)$$

And from the Arrhenius equation (Equation (1.1)), if variation in the pre-exponential A with field may be ignored we obtain:

$$\mu_1 \simeq -F^o \frac{dQ}{dF}\Big|_{F=F^o} \qquad (2.3a)$$

$$\mu_2 \simeq -(F^o)^2 \frac{d^2Q}{dF^2}\Big|_{F=F^o} \qquad (2.3b)$$

(Details on the derivation of the above equations are given in Appendix D).

The theoretically predicted values of $\frac{dQ}{dF}$ and $\frac{d^2Q}{dF^2}$ depend on the field evaporation model used, so comparison of theory and experiment is possible.

The assumed constancy of the pre-exponential A, at least for temperatures near 80 K, deserves comment. The arguments for assuming this have in the past been as follows. First, the pre-exponential A involves a factor relating to the vibrational frequency of the bound atom. This frequency depends on the shape of the atomic potential well, which (in comparison with the activation energy) is unlikely to be sensitively

affected by a small field variation. Second, the pre-exponential involves a factor that relates to the possibility of ion tunnelling (Gomer and Swanson: 1963; Müller and Tsong: 1969) and is in principle field dependent for this reason. It has always been supposed that, at temperatures near 80 K and above, any field dependence due to this cause is insignificant. However, very recently, Kellog (1984) reported experiments on Tungsten in which some field dependence in A was detected (particularly for fields below about 52 V/nm). We discuss this point further in Chapter 7. We think that it does not significantly affect the interpretation of results presented in Section (2.5) below.

2.3 THE IMAGE-HUMP FORMALISMS

To begin with, a distinction has to be made between a mechanism and a formalism. A mechanism is a physical process which depends on the relative configurations of the potential-energy curves for the evaporating atom in its atomic and ionic states. A formalism is a mathematical procedure with a precise choice of algebraic expressions used to describe the associated mechanism. There may be several formalisms corresponding to a given mechanism. In particular, in connection with the Müller mechanism, several different

classical formalisms can be distinguished.

In the "basic image-hump" formalism, the activation energy Q_n for escape over the hump is obtained by neglecting the F^2 and repulsive terms in equation (1.14) and evaluating the resulting expression with $x^p = x^{sh}$, giving:

$$Q_n(F) = (\Lambda^o + H_n - n\phi^E) - neFx^{sh} - \frac{n^2e^2}{16\pi\varepsilon_o x^{sh}} \qquad (2.4)$$

A relationship between x^{sh} and F is obtained by similarly neglecting the F^2 and repulsive terms in equation (1.13) and applying subsidiary condition (1.19). This gives:

$$neF = \frac{n^2e^2}{16\pi\varepsilon_o (x^{sh})^2} \qquad (2.5)$$

substituting back into equation (2.4) gives:

$$Q_n(F) = (\Lambda^o + H_n - n\phi^E) - \left(\frac{n^3e^3F}{4\pi\varepsilon_o}\right)^{\frac{1}{2}} \qquad (2.6)$$

It is then easy to derive an expression for F^e from the requirement $Q_n(F^e)=0$, which gives:

$$F^e = \frac{4\pi\varepsilon_o}{n^3e^3} (\Lambda^o + H_n - n\phi^E)^2 \qquad (2.7)$$

And from equations (2.3) and (2.6) we obtain:

$$\mu_1 = + \frac{1}{2} \left(\frac{n^3 e^3 F^o}{4\pi\varepsilon_o} \right)^{\frac{1}{2}} \qquad (2.8a)$$

$$\mu_2 = - \frac{1}{4} \left(\frac{n^3 e^3 F^o}{4\pi\varepsilon_o} \right)^{\frac{1}{2}} \qquad (2.8b)$$

If the F^2 terms are kept in equations (1.13) and (1.14), but the repulsive term is still excluded, then equation (2.5) remains valid but for the activation energy formula we obtain:

$$Q_n(F) = (\Lambda^o + H_n - n\phi^E) - \left(\frac{n^3 e^3 F}{4\pi\varepsilon_o} \right)^{\frac{1}{2}} + \frac{1}{2}(c_\alpha - c_n)F^2 \qquad (2.9)$$

and for the partial energies, it can be shown that:

$$\mu_1 = \frac{1}{2} \left(\frac{n^3 e^3}{4\pi\varepsilon_o}\right)^{\frac{1}{2}} (F^o)^{\frac{1}{2}} - (c_\alpha - c_n)(F^o)^2 \qquad (2.10)$$

$$\mu_2 = - \frac{1}{4} \left(\frac{n^3 e^3}{4\pi\varepsilon_o} \right)^{\frac{1}{2}} (F^o)^{\frac{1}{2}} - (c_\alpha - c_n)(F^o)^2 \qquad (2.11)$$

These two formalisms, in which the repulsive term is neglected, are called <u>simple</u> image-hump formalisms.

Formalisms in which the repulsive term is taken into account are called <u>extended</u> image-hump formalisms. The work of Biswas and Forbes, described

later, is based on the use of extended formalisms.

2.4 EVAPORATION FIELD VALUES

Values of F^e predicted from equation (2.7), using an appropriate escape charge-state, are found to be in good numerical agreement with values of onset evaporation field as observed in field-ion microscopy (Müller: 1960; Brandon: 1964; Müller and Tsong: 1969; Tsong and Müller: 1970; Tsong: 1978a). There are, however, certain objections that can be raised against the basic image-hump formalism, in particular that values of x^{sh} from equation (1.20) were found to be too small to be plausible (Brandon: 1964; Tsong: 1971), and that when the repulsion term is taken into account, the Schottky hump may not exist (e.g. Brandon: 1963). There is also the point, coming from the experimental work of Wada et al. (1980), that the value of the zero-Q evaporation field F^e might be expected to be somewhat higher than observed evaporation fields near 80 K.

This dilemma can be solved by considering the energetics based F^e formula given in Chapter 1. This formula is valid irrespective of the mechanism, and showed good agreement with observed evaporation fields.

2.5 TESTS BASED ON PARTIAL ENERGIES

As indicated earlier, Tsong's (1978b) original data (Fig. 2.1) were re-analysed, and new regression coefficients were derived by fitting a quadratic form. The regression calculations were performed using a well-tested computer program provided by Dr. D. R. Weaver at the Birmingham University Radiation Centre. The standard deviations on each regressed coefficient, and covariance matrices, were found and have been used to calculate a correlation coefficient ρ in each case. The latter has been used to obtain the error limits on the final results, by means of the standard error propagation formula. Table (2.1) shows the derived "experimental" partial energies μ_1, μ_2 and their ratio. Also shown is the value of the correlation coefficient $\rho(\mu_1, \mu_2)$.

2.5.1 A Basic Test on Partial Energy Ratios

The basic image-hump formalism predicts that $\mu_2/\mu_1 \simeq -\frac{1}{2}$, as can be seen from equation (2.8). This theoretical prediction is now to be compared with experimental partial energy ratios, shown in Table (2.1).

The ratio values lie between -2 and -6.7. For Ru,

Hf, Ir and Pt, the error limits on μ_2/μ_1 are very large, so no conclusion is possible. However, with this test, Mo and W are certainly incompatible with the basic image-hump formalism. Further, because the basic formalism, without F^2 terms, makes a prediction that is independent of species and of charge-state at escape, the six ratio values in Table (2.1) can be taken as six independent estimates of a quantity whose value is known. Hence, we may deduce that $\mu_2/\mu_1 = -3.7\pm0.8$. There is no agreement between this average value and the predicted one of $-\frac{1}{2}$. So we may conclude that the basic image-hump formalism cannot generally represent the field evaporation of metals.

TABLE 2.1

Species	μ_1(eV)	μ_2(eV)	$\rho(\mu_1,\mu_2)$	μ_2/μ_1
Mo(110)	1.39±0.13	-8.2±2.2	-0.956	-5.9±2.1
Ru(11$\bar{2}$1)	0.76±0.11	-1.5±1.5	-0.962	-1.97±2.8
Hf(10$\bar{1}$0)	1.05±0.18	-3.6±2.2	-0.959	-3.43±2.7
W(110)	1.55±0.05	-10.3±0.7	-0.963	-6.65±0.7
Ir(100)	0.73±0.08	-1.6±0.8	-0.957	-2.19±1.3
Pt(100)	0.71±0.10	-1.5±1.1	-0.955	-2.11±1.8

Experimental partial energies μ_1 and μ_2, and their ratio, derived from regression of Tsong's (1978b) original data.

2.5.2 Tests on the Simple Image-Hump Formalism (including F^2 Terms)

The simple image-hump formalism (including F^2 terms) is next to be tested. The first test concerns comparison of derived and observed evaporation field values, and is achieved as follows.

Further manipulations of equations (2.10) and (2.11) lead to the relations:

$$\left(\frac{n^3 e^3 F^o}{4\pi\varepsilon_o} \right) = \frac{4}{3} (\mu_1 - \mu_2) \qquad (2.12)$$

and

$$\frac{1}{2} (c_\alpha - c_n) F^{o^2} = - \frac{1}{6} (\mu_1 + 2\mu_2) \qquad (2.13)$$

Equation (2.12) enables values of F^o to be calculated from data in Table (2.1), for different values of charge-state n. These derived evaporation field values may be compared with observed field values given by Tsong (1978b), as shown in Table (2.2), for n=1,2.

For n=2, derived evaporation field values and observed fields are certainly not in agreement. In the n=1 case, for Ru, Ir and Pt we may conclude that derived and observed field values are not compatible in spite of error limits that are large in comparison with the derived value, and for W the incompatibility is

TABLE (2.2)

Species	$K' = \frac{4}{3}(\mu_1 - \mu_2)$ (eV)	Derived field (V/nm)		$\sigma(K')$	$\sigma(K')/K'$	$\sigma(F_1)$	$\sigma(F_2)$	F^{obs} (V/nm)
		n=1	n=2					
Mo	12.8	113.5	14.2	3.1	0.2	55.0	6.9	46
Ru	3.0	6.3	0.8	2.1	0.7	9.0	1.1	42
Hf	6.2	26.7	3.3	3.2	0.5	27.2	3.4	40
W	15.8	173.4	21.7	1.0	0.1	21.7	2.7	55
Ir	3.1	6.7	0.8	1.2	0.4	5.0	0.6	52
Pt	2.95	6.0	0.75	1.6	0.5	6.6	0.8	48

Values of evaporation field F^o, as derived from equation (2.12), using data in Table (2.1) for n=1,2. The r.h.s. of equation (2.12) is denoted by K'. The last column gives the experimental field F^{obs}, at liquid-nitrogen temperature, made by Tsong (1978b).

evident. However, for Mo and Hf no conclusion is possible, when the error limits are taken into account.

A further test for this simple image-hump formalism can be carried out. It is a test of self-consistency and is obtained by substituting, at $F=F^{o}$, equations (2.12) and (2.13) back into equation (2.9), to give:

$$(\Lambda^{o}+H_{n} - n\phi^{E}) - Q(F^{o}) = \frac{3}{2}\mu_{1}-\mu_{2} \qquad (2.14)$$

i.e.

$$K_{n}^{o} - Q(F^{o}) = \frac{3}{2}\mu_{1}-\mu_{2} \qquad (2.15)$$

Equation (2.15) enables a comparison between an expression whose value is known (l.h.s.), and an expression derived from experimental data (r.h.s.). $Q(F^{o})$ is set equal to 0.2 eV; this value is derived by combining the emission and Arrhenius equations, to give:

$$Q = kT\ell n(n_{hr}A/J) \qquad (2.16)$$

and putting J=0.01 layers/s, n_{hr}=0.01 layers, $A=10^{12}s^{-1}$, and T=77.3 K (the temperature value employed by Tsong:1978b).

Values of the l.h.s. and r.h.s. of equation (2.15)

are summarised in Table (2.3), for n=1 and 2. Values of ϕ^E have been taken from J. C. Riviere (1969) and Z. Knor (1977), whilst values of Λ^o and ionization potentials I_n have been taken from Tsong (1978a).

The immediate conclusion is that for n=2 (and certainly for n>2) it is very improbable that the two sides of equation (2.15) can be considered equal. For the n=1 case if we use the criterion that the two sides must be considered different if $\Delta/\sigma > 2.5$, then for three elements (Ru, Ir and Pt) there is no consistency between the two sides of equation (2.15); the Hf case is indecisive, though consistency is not very likely. However, for W and Mo, there is no significant difference between the two sides of equation (2.15).

In general terms, we can conclude that the simple image-hump formalisms have not been found to be in agreement with Tsong's experimental data when the latter are converted into partial energies. Hence, it follows either that the Müller mechanism is not operating, or that these simple image-hump formalisms do not properly represent the Müller mechanism (or both).

In our argument here, it is necessary to proceed on the assumption that the second interpretation may be

TABLE (2.3)

Species	ϕ^E (eV)	r.h.s.* (eV)	σ (eV)	$K^O_{n=1}$	$-Q(F^O)$ (eV) n=2	Δ/σ
Mo(110)	5.12	10.3	2.4	9.5	21.5	0.3
Ru(11$\bar{2}$1)	4.86	2.6	1.7	9.3	21.6	4.0
Hf(10$\bar{1}$0)	3.65	5.2	2.5	9.7	21.1	1.8
W(110)	5.14	12.6	0.8	11.9	25.4	0.9
Ir(100)	5.27	2.7	0.9	10.5	22.2	8.7
Pt(100)	5.84	2.6	1.2	9.4	22.6	5.7

* r.h.s. = $(\frac{3}{2})\mu_1 - \mu_2$.

Test on the simple image-hump formalism (including F^2 terms), based on equation (2.15). Values of the r.h.s. of equation (2.15) have been derived from data in Table (2.1). [σ is the error limit on the r.h.s. and Δ is the difference between the l.h.s. and r.h.s. values.]

true. One possible way to remedy to the supposed invalidity of the simple formalisms is to include a term relating to a repulsive interaction. This approach has been examined by Biswas and Forbes (1982), Biswas (unpublished work) and Forbes (1982c) on the basis of an "extended" image-hump formalism.

2.6 TESTS USING THE EXTENDED FORMALISM

2.6.1 Tests Based on Hump-Disappearance Field

As just indicated, one objection to the simple image-hump formalisms is the absence of a repulsion term. This may be significant at positions close to the metal's surface. Biswas and Forbes (1982) thus developed an extended formalism by including a repulsive ion-interaction term G/x^t, and calculated the field F_n^{HD} at which the Schottky hump disappears. This is found to be given by:

$$F_n^{HD} = \Gamma \left(\frac{ne}{16\pi\varepsilon_o a_n^2} \right) \qquad (2.17)$$

where a_n is the distance of the ionic bonding point (for an n-fold ion) from the electrical surface, and Γ is a function of the assumed repulsive exponent, t.

In their analysis Biswas and Forbes then approximated a_n by the neutral atom radius, to derive approximate values of F^{HD} for all the materials commonly used in field evaporation experiments. Further analysis gave the results:

A. For most of the elements commonly used in field-ion experiments, the values of F^e predicted by the basic image-hump formalism (formula 2.7) were found higher than the field at which the hump disappears. This result strongly suggests that the basic image-hump formalism is inadequate to describe the Müller mechanism.

B. Observed evaporation fields were, in most cases, higher than the hump-disappearance field. This result suggests that a hump does not in fact exist at real operating fields, and that - if the extended formalism is realistic - the Müller mechanism is not operating.

2.6.2 Test Based on Field-Sensitivity

Still within an extended formalism treatment, Biswas (unpublished work) has carried out some further field-sensitivity calculations using the data of Table (2.1). By solving a set of simultaneous equations, he

has been able to use "experimental" μ_1, μ_2 and Q values to derive values for the parameters a_n and F that appear in the theory. But his derived evaporation field values are found to be incompatible with the observed field values of Table (2.2) and hence the theory is inconsistent. This test lends further support to conclusion B above - that the Müller mechanism is not operating - for the six materials examined.

2.7 THE A-PRIORI PREDICTION OF ESCAPE MECHANISM

The final argument against the Müller mechanism comes from an a-priori prediction of field evaporation mechanism made by Forbes (1982c).

At the field F_n^{HD}, there is a plateau in the ionic curve. Biswas and Forbes showed that the level U_n^* of this plateau in the ionic potential, measured relative to a zero of potential corresponding to the potential of the neutral atom in remote field-free space, is given by:

$$U_n^* = H_n - n\phi^E + \Theta \frac{n^2 e^2}{16\pi\varepsilon_o a_n} - \frac{1}{2} c_n (F_n^{HD})^2 \qquad (2.18)$$

where Θ is a constant of value depending on the exponent in the repulsive term but roughly of value

1.6, and the other symbols have their previous meanings.

Relative to the same zero-level, the potential-energy of the bound atom, at F_n^{HD} is:

$$U_\alpha^B = -\Lambda^o - \frac{1}{2} c_\alpha (F_n^{HD})^2 \qquad (2.19)$$

Hence, the energy difference W_n^* between the level of the plateau and the bonding potential-energy is:

$$W_n^* = (\Lambda^o + H_n - n\phi^E) + \Theta \frac{n^2 e^2}{16\pi\varepsilon_o a_n} + \frac{1}{2} (c_\alpha - c_n)(F_n^{HD})^2 \qquad (2.20)$$

This is illustrated in Fig. (2.2) where three different situations are presented: (A) $W_n^* >> 0$; (B) $W_n^* \tilde{>} 0$; (C) $W_n^* << 0$. Q^{exp} is the activation energy as given from the emission equation, which is 0.2 eV at temperatures near 80 K.

If the Müller mechanism is operating then the situation must be as in Fig. (2.3) curve A_1; the activation energy must be greater than W_n^*. But if Q^{exp} is taken as a working value, and it can be shown that $Q^{exp} \lesssim W_n^*$, then the configuration must actually be as in Fig. (2.3) curve A_3, which corresponds to a Gomer-type mechanism.

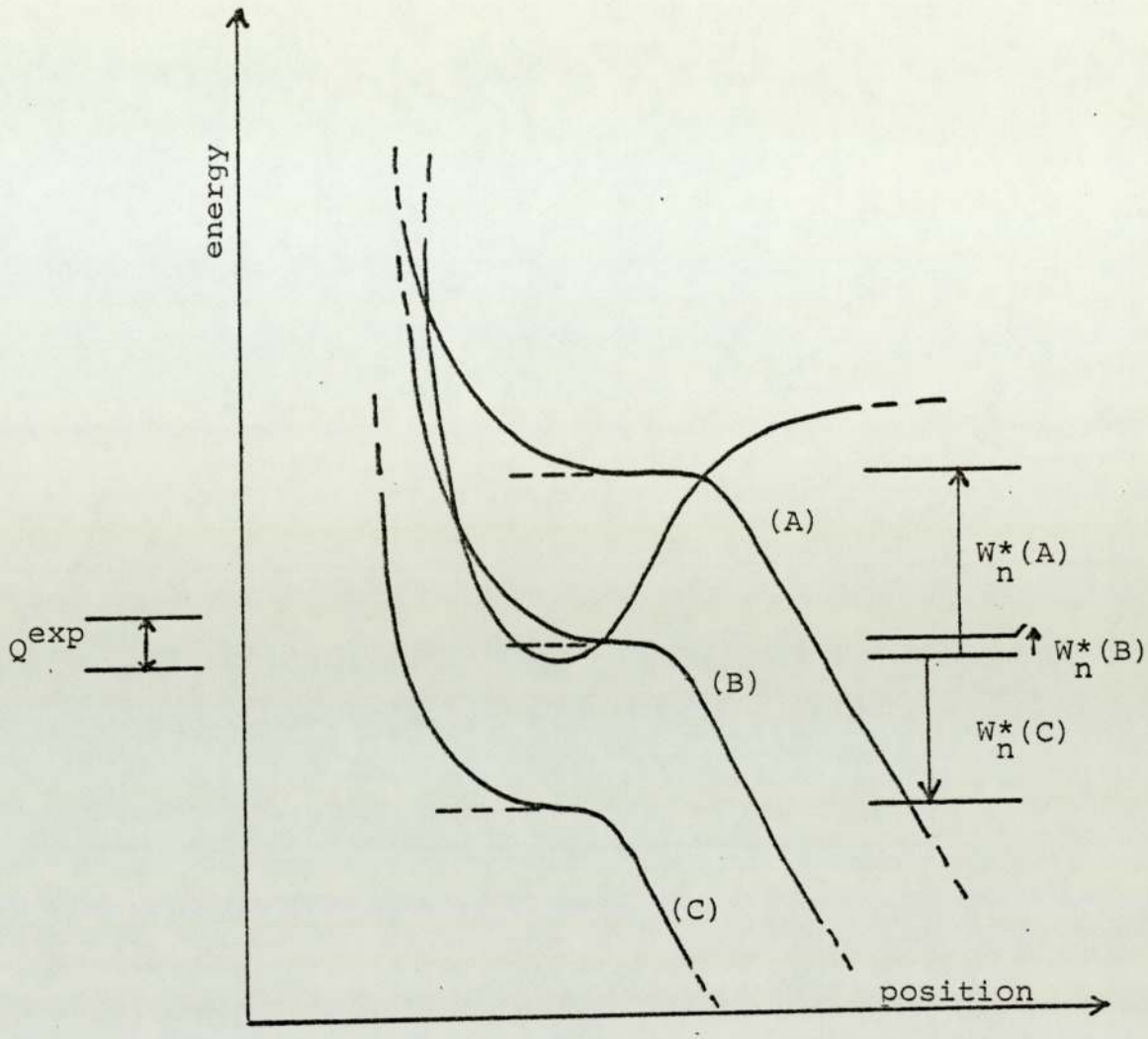

Fig. (2.2) : The a-priori prediction of escape mechanism: Possible configurations of the ionic potential curve, relative to the atomic potential curve. (A): $W_n^* >> 0$; (B): $W_n^* \gtrsim 0$; (C): $W_n^* << 0$. Q^{exp} represents an activation energy, as given from the emission equation, of a size to illustrate the argument in the text.

(from Forbes, 1982c)

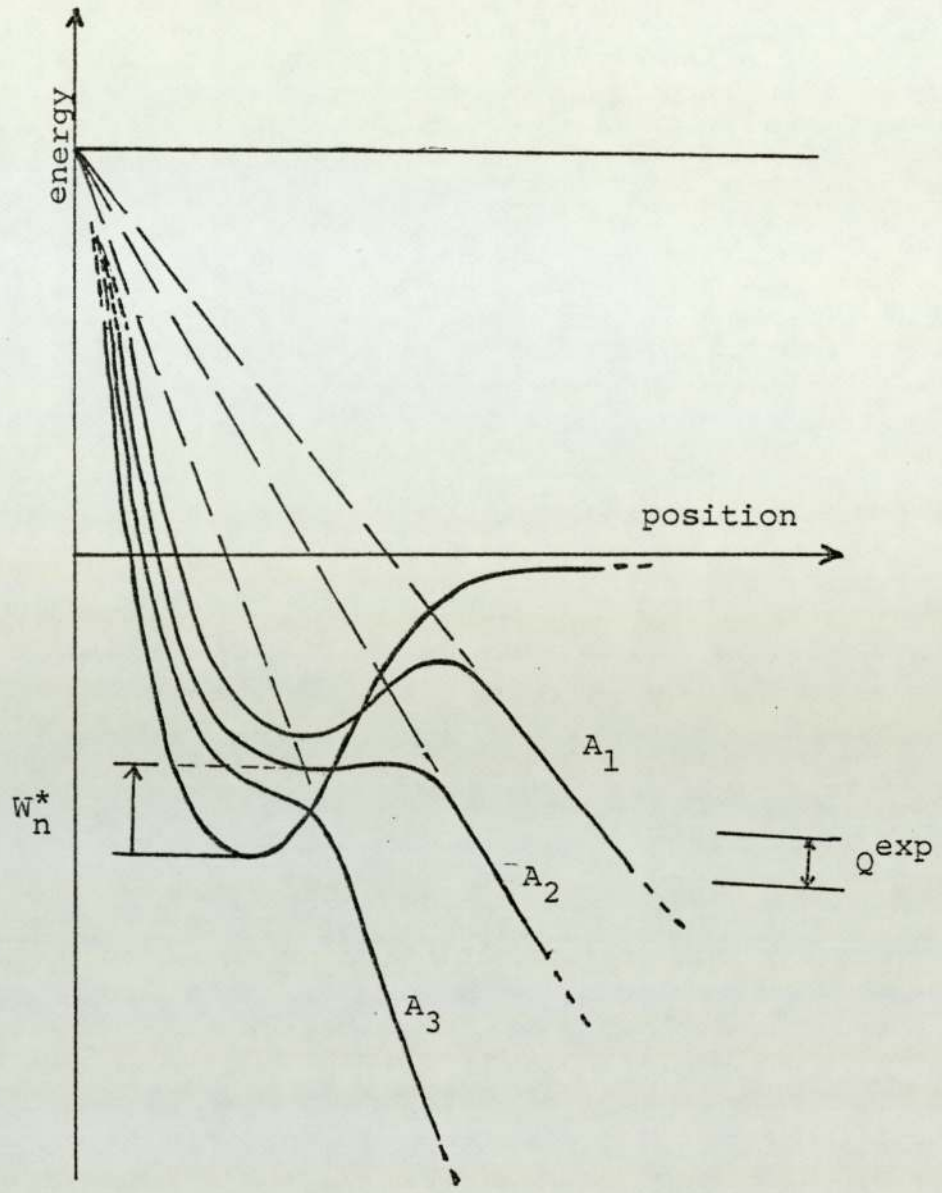

Fig. (2.3): The a-priori prediction of escape mechanism: Positions of the ionic curve relative to the atomic curve, with increasing field strengths. A_2 corresponds to the field F_n^{HD} at which the Schottky hump disappears.

A_3 corresponds to the situation where field evaporation is taking place with an activation energy Q^{exp}.

(From Forbes: 1982c)

In summary, the condition $W_n^* >> Q^{exp}$ implies that a charge-exchange mechanism is operating. This is the basis of the Forbe's criterion. Cases where $W_n^* \simeq Q^{exp}$, or $W_n^* < 0$, are difficult to decide.

Since the F^2 energy-term coefficients c_α and c_n in equation (2.20) are not well known, W_n^* (NP) - where (NP) stands for no-polarisation terms - is used instead of W_n^* to provide a numerical criteria, where $W_n^*(NP)$ is given by:

$$W_n^*(NP) = (\Lambda^o + H_n - n\phi^E) + \theta \frac{n^2 e^2}{16\pi\varepsilon_o a_n} \qquad (2.21)$$

Following Brandon (1964), it is now widely accepted that $c_\alpha >> c_n$, hence the F^2 term in equation (2.20) is certainly positive. Hence, for the criterion to work, it is sufficient to show that $W_n^*(NP) >> Q^{exp}$.

Forbes carried out the calculations for all metals normally employed in low-temperature field evaporation or in liquid metal ion sources. Table (2.4) shows the results for n=1 and n=2; ρ_o, the neutral atom radius for the species in question, is taken as an approximation for a_n in equation (2.21).

From Table (2.4), if we use the requirement

TABLE (2.4)

Species	ρ_o (pm)	W_n^*(NP) (eV) n=1	W_n^*(NP) (eV) n=2
W	137	8.1	9.4
Ta	143	7.9	8.0
Re	137	6.8	6.5
Ir	135.5	6.6	6.0
Hf	156.5	6.3	7.0
MO	136	5.6	5.3
Pt	139	5.5	6.8
Ru	132.5	5.3	4.9
AU	144	4.8	9.4
Rh	134.5	4.3	5.2
La	186.5	4.0	2.8
Ti	144.5	3.8	1.8
Si*	117.5	3.8	0.8
Co	125	3.4	2.7
Fe	124	3.3	1.6
Ni	124.5	2.6	2.4
Ge*	122.5	2.5	0.0
CU	128	2.3	4.9
Pb	175	2.2	3.6
Sn*	140	2.1	0.4
Ag	144.5	2.1	7.4
Cr	125	1.8	0.4
AP	143	1.3	4.4
Cs*	266	0.3	3.7
Ga*	122	0.1	2.8

Results for W_n^*(NP); n=1,2 concerning most elements of relevance to field-ion emission. ρ_o is the neutral-atom radius. Species for which W_1^*(NP) or W_2^*(NP) is less than 1 eV, are marked with an asterisk.

(from Forbes: 1982c)

that $W_n^*(NP)-Q^{exp} > 1$ eV, it can be concluded that for all metals conventionally used in low temperature field evaporation, escape will occur via a charge-exchange mechanism. (With elements for which either $W_1^*(NP)$ or $W_2^*(NP)$ is less than 1 eV, the situation is still unclear.)

2.8 CONCLUSION

The main conclusions of this chapter can be summarised as follows:

(1) The simple image-hump formalisms are not adequate to describe the Müller mechanism.

(2) If the extended formalism is reaslistic, then for most metals used in field-ion experiments, the Müller mechanism does not operate.

These conclusions are, of course, based on classical arguments. They should be in principle checked by quantum-mechanical calculations, and until then it is not possible to completely reject the Müller mechanism.

Nevertheless, the conclusions provide a reasonable justification for a decision to proceed with the analysis of field evaporation data on the basis of a

Gomer-type mechanism. This will be the subject of Chapters 4 to 7. However, prior to this, Chapter 3 examines the main assumptions assumed in our model.

CHAPTER 3

MODEL ASSUMPTIONS AND LIMITATIONS, AND THE CHARGE-DRAINING MECHANISM

The first part of this chapter identifies the main assumptions and limitations made behind our field evaporation model (Chapters 4 to 7), and in the literature in general. These include the use of classical potential energy terms in the context of flat surface models, and the assumption of an escape path perpendicular to the surface. Each term will be introduced and discussed separately.

In the second part, an account of the charge-draining mechanism will be given and some of its complications will be pointed out.

3.1 CLASSICAL POTENTIAL ENERGY TERMS

In the following discussion, the definition of each potential energy term is essentially made in the context of flat surfaces. In particular, in discussing the electrostatic potential energy term, two flat surface models are considered: a "smooth-flat" surface (e.g. the Jellium surface discussed in Appendix C), and an "atomically-flat" surface, incorporating the atomic structure of a real flat surface (e.g. Wafi: 1981). However, a real surface model - which is not discussed in detail here - should fully include the geometrical and electronic structure of an emitter tip. It is of course assumed that all the models mentioned above are

positively charged by an applied voltage.

A comment on the location of the electrical surface should first be made. It is argued in Appendix C that in flat surface models, the electrical surface must be considered to lie outside the plane of the surface nuclei, but inside the substrate charge cloud. In the case of an atomically-flat emitter surface, the position of the electrical surface is shown schematically in Fig. (3.1).

3.1.1 The Electrostatic Term

For both the "smooth-flat" and "atomically-flat" models the electric field is uniform and constant, at sufficient distance from the surface. This field is known as the "external field", and it is this quantity that is denoted by F.

Consider the flat-surface models. The electrostatic potential is taken as zero inside the metal. For simplicity, we wish to have the electrostatic potential energy of an ion of charge (ne) at a distance x given by -neFx. This distance x is said to be measured from the model's electrical surface. The latter is defined by extrapolating the electrostatic potential (as calculated from some more

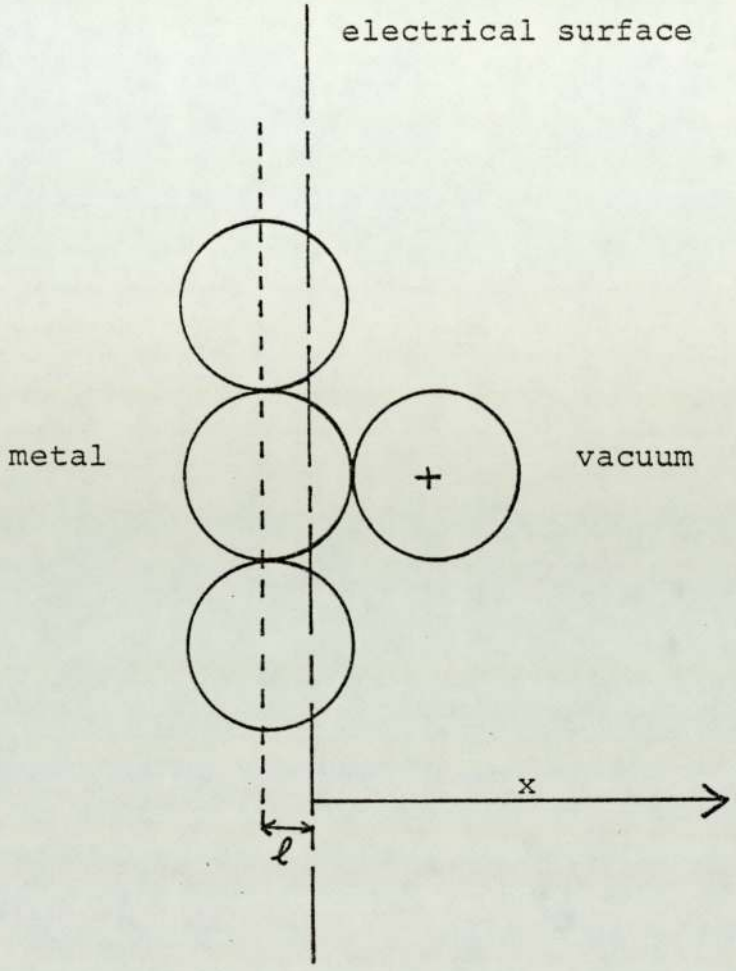

Fig. (3.1) Position of the electrical surface for an atomically-flat emitter surface. The external atom is assumed to be directly above a substrate atom.

detailed model) back towards the metal; the intersection with the distance axis defines the origin of x. This is illustrated in Fig. (3.2) for a Jellium-type model as developed by Lang and Kohn (1973). This extrapolation process is also valid for the "atomically-flat" case and the electrostatic potential energy is still given by -neFx. Since the ionic nucleus is of necessity outside the substrate charge cloud, with the "smooth-flat" models, the nucleus is always in a region of uniform field. With the "atomically-flat" models, however, there are field variations close to the surface and the ion does "see" these variations.

The source of these local field variations is the local crystallographic structure of the plane in question. This problem has never been examined in detail, but we can discuss as an analogous example the work of Wafi (1981). He used a structured model for the W(111) surface, namely an array of monopoles and dipoles, with a distant array of negative charges for electrostatic self-consistency. Fields and potentials were calculated for two cases:

(1) above a surface atom;
(2) above a point midway between two surface atoms.

The above-atom potential due to monopoles tends to

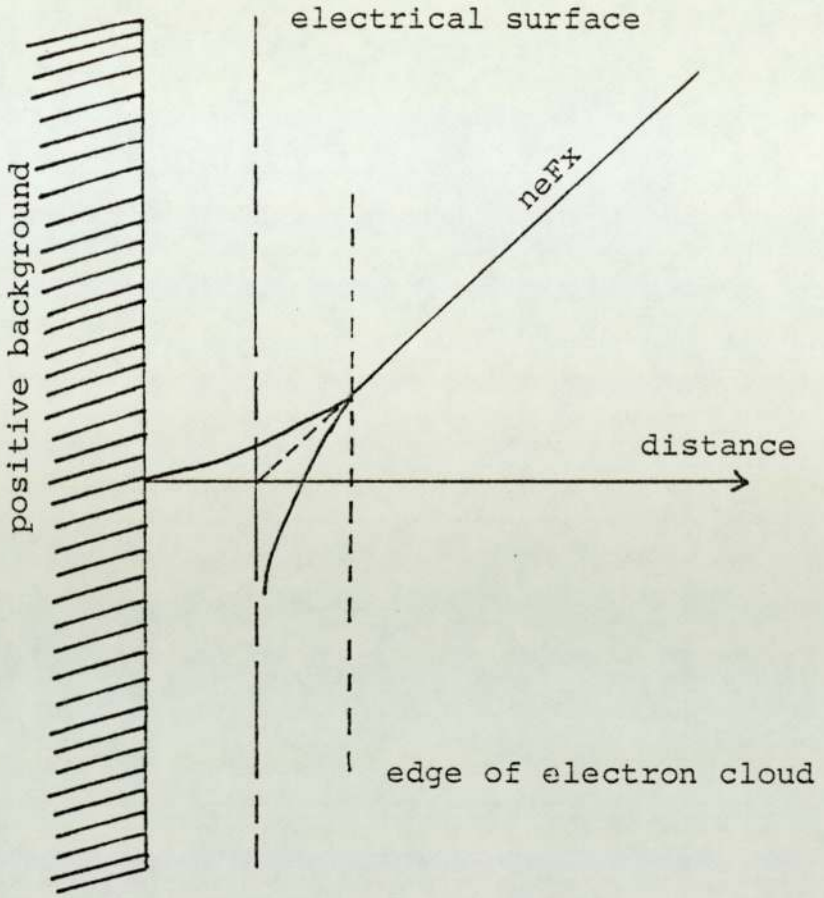

Fig. (3.2) Definition of the electrical surface for a Jellium-type model.
(illustrates the case of negative charges)

minus infinity as the plane of the surface nuclei is approached, whereas the between-atom potential tails off towards zero as the interior of the emitter is approached (Fig. 3.3a). Both curves tend to the same straight line, that represents the electrostatic term neFx, as distance is increased. The main effect of including the dipoles contribution is to move the electrical surface outwards, as shown in Fig. (3.3b).

The field variations as a function of distance R_z, due to the joint contribution of monopoles and dipoles is shown in Fig. (3.4), for two values of surface atom polarisability. The above-atom field approaches infinity as the plane of the surface nuclei is approached, whereas the between-atom field has in this plane a finite value. At large distances, both curves converge to the external field. Wafi notes that the size of these field variations across the surface will depend on the crystallographic structure of the array but mainly on the area per lattice point of the array.

It is useful to give some indication of the size of local field variations at distances likely to be of interest in field evaporation. We use W(111), for which Wafi carried out calculations as shown in Fig. (3.4). Two situations are considered:

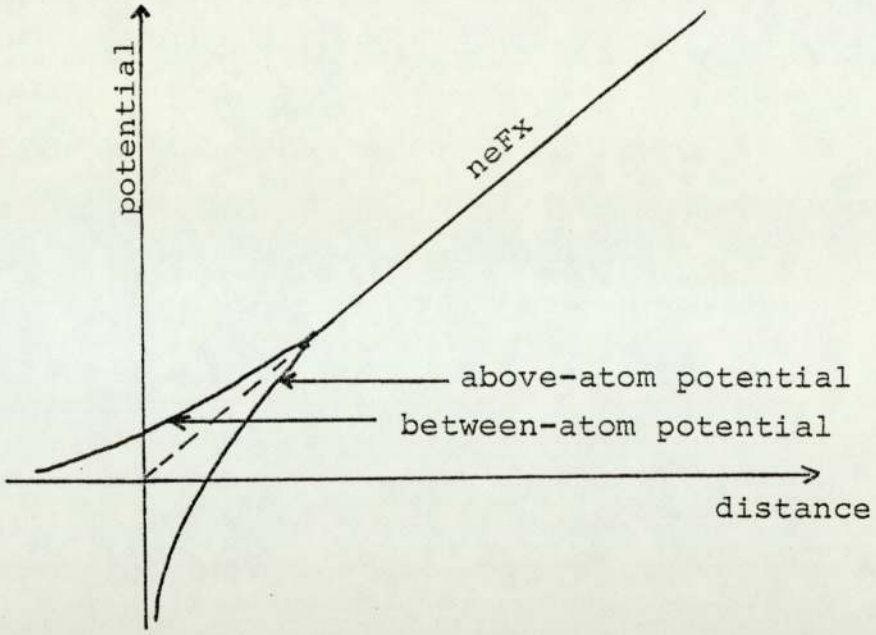

(a)

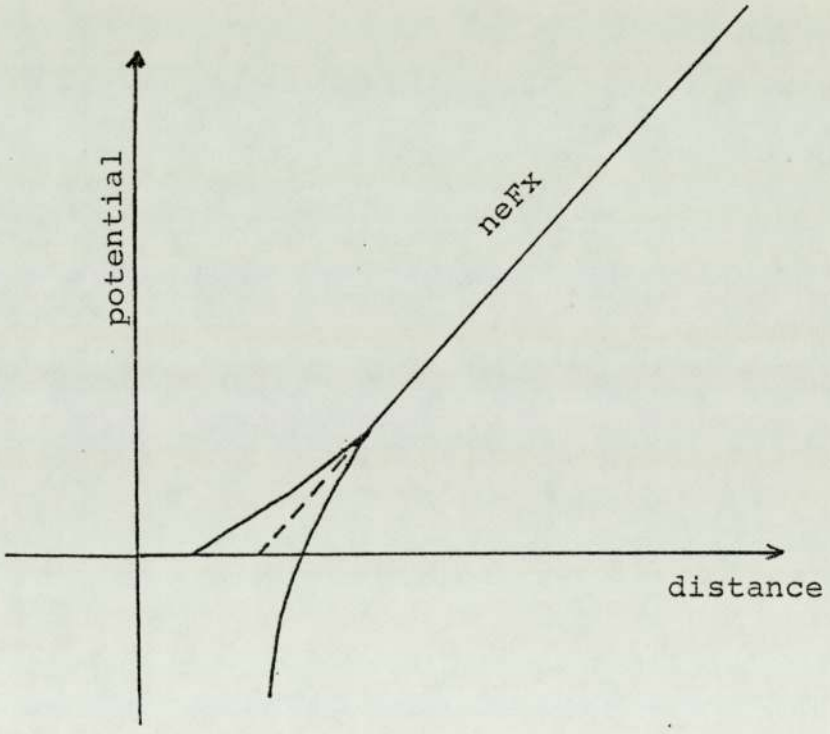

(b)

Fig. (3.3) (a) potential variations due to monopoles.

(b) potential variations due to monopoles and dipoles.

(illustrates the case of negative charges)

(from Wafi: 1981)

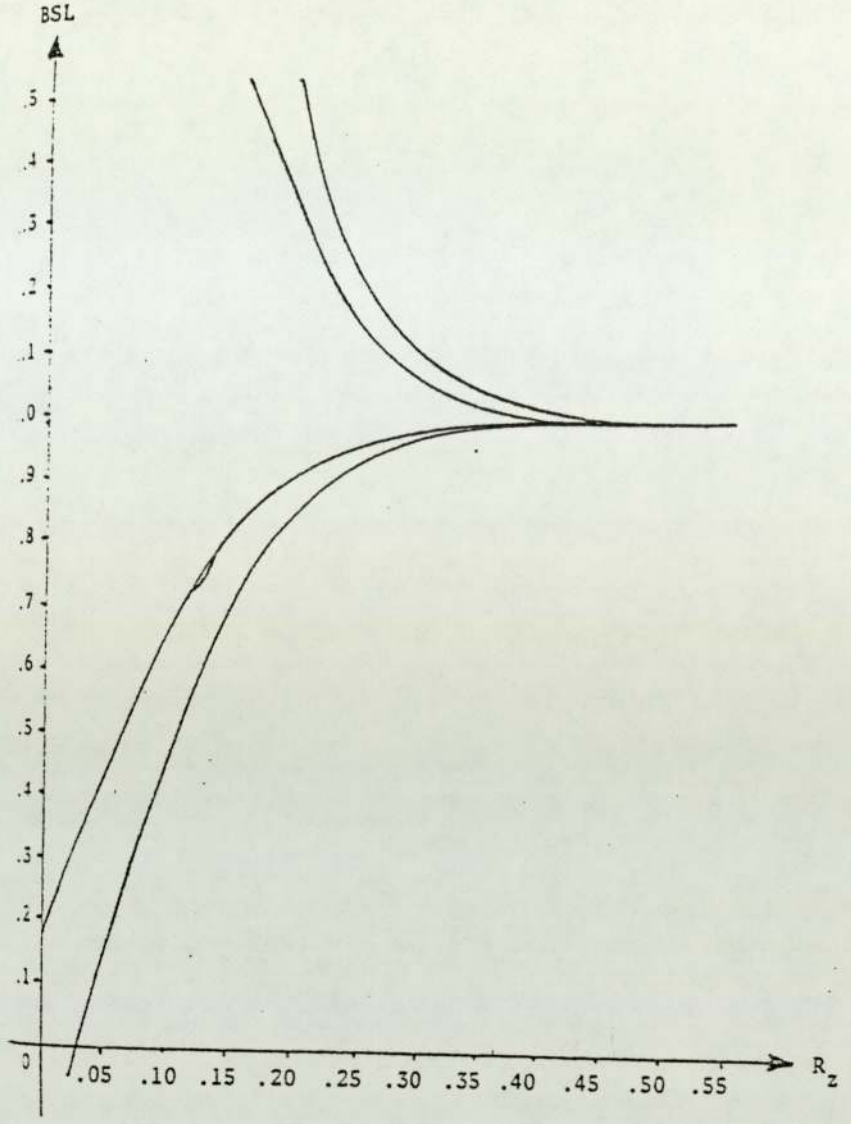

Variation of the field ratio above a single layer β_{SL} with the distance R_z, for $b_E = 2b^{\theta}$ and $b_E = 7b^{\theta}$

Fig. (3.4) Field variations due to monopoles and dipoles.

(from Wafi: 1981)

First, consider the position where a W atom would be "field-adsorbed" on the W(111) plane at the above-atom position. This would be at a distance $R_z = 2\rho_o = 0.274$ nm from the plane of the nuclei, where ρ_o is the neutral W radius (of value 0.137 nm). It is seen from Fig. (3.4) that at this position the local field has increased by nearly 10% from the external field value.

In the second case, consider the position where a W atom would be adsorbed on the W(111) plane but above the between-atom (i.e. between closest neighbours) position. If the atom were in direct contact with the underlying atoms, then its nucleus would be at $R_z \simeq 0.16$ nm. From Fig. (3.4) it can be seen that at this position the local field is less than the external field value by about 15%.

In principle we ought to consider the situation where a W atom would be adsorbed on the W(111) plane in the "symmetrical" position, so that it is in contact with three underlying atoms. Its nucleus would be at a distance R_z of approximately 0.09 nm. Wafi's calculations do not consider this case but it is clear that the predicted difference between the external field and the local field variations would be higher than 15%. At such small distances, on the other hand, one may wonder whether the Wafi model is an accurate

prediction of field values.

Work-Function Related Effects. The discussion so far has been concerned with flat models and the induced effects in the presence of an applied electric field. However, other sources of local field variations exist even in the absence of an applied field. They originate from the "smoothing" and "spreading" of electron clouds across the surface, as discussed by Smoluchowski (1941) to account for the surface double layer. These effects are of short range and give rise to "surface fields".

Also, each double layer is characterised by its own electric dipole moment (per unit area), and differences in work-function from one plane to another are attributed to different moments. Hence, between two adjacent planes on a real emitter, there are local fields due to these different work-functions, and their effects can extend well away from the surface. These fields are called "patch fields".

Tip Geometry Effects. In general terms the local field variations for flat models can be seen as "microscopic" field variations. In the real situation of a field-ion emitter, different atomic planes are exposed to the external applied field. The latter has

an average value over the entire cap and is calculated roughly from the applied voltage assuming some hemispherical or paraboidal shape for the end of the emitter.

The field normally has different average values over different areas of an emitter end form. These variations in "average regional external field" are of "macroscopic" origin and they depend on various factors such as the cone angle of the shank, the angular distance from the apex, the local radius of curvature, the degree of protrusion and the size of the plane from which evaporation is occurring. The variation is of the order of 10 to 20%; however, this variation is frequently ignored in the literature of field evaporation. These macroscopic fields fall off with distance away from the surface, but so slowly that the linear approximation is negligibly affected.

Finally, we must also note smaller scale field variations due to tip geometry, such as those over steps at the edges of atomic planes, and at kink sites. These variations have for example been investigated by Birdseye (1972) in the context of a classical conductor model; she found that the variations had effectively vanished at about 1Å away from the step edges.

In summary, we should distinguish between microscopic fields due to the presence of atoms with their electronic structure, and macroscopic fields directly related to the shape of a field emitter endform. In field evaporation all these effects should in principle be taken into account. As a result, as we have seen above, the "mean field" acting on an atom during the field evaporation process may be somewhat different from the external field somewhat above the atom (which is what is measured in experiments of the type performed by Sakurai and Müller: 1973). And the assumption of a linear form for the potential variation with distance may not be particularly good. Nevertheless, the linear form has always been used in field evaporation theory; we will continue with this tradition in the main part of this thesis. Really there is no practical alternative because no well-based theoretical models of charged structured surfaces exist. We return to this point again in Chapter 8.

3.1.2 The Image-Potential Term

In the standard ionic potential energy, the correlation interaction of the ion with the surface has been given by the classical image-potential $-n^2e^2/16\pi\varepsilon_o x$, where (as before) x is distance

measured from the electrical surface. It has been shown by Lang and Kohn (1973) that this form is correct in the limit of large distance from the surface. However, very near the surface this approximation is expected to break down, as shown for example by Smith et al. (1973) for Hydrogen chemisorption on metals. The latter authors found that the image term was valid to describe the interaction energy between the Hydrogen ion and the metal, down to a distance about 1 to 1.5 Å away from the electrical surface. As the H^+ approached the surface, at distances less than 1 Å, the interaction energy began to deviate significantly from the image-potential approximation.

Knowing that the radius of a metal atom is greater than 1 Å (see Table 2.4 for example), the work of Smith et al. may be thought to justify to a certain extent the use of the classical image term for metal field evaporation, at least as a first approximation.

3.1.3 The Repulsive Term

In Chapter 2, the main objection to the simple image-hump formalisms has been their neglect of any repulsive term that may be important at very small distances from the metal's surface. We have mentioned in this context that Biswas and Forbes have developed

an extended model that includes a repulsive ion-surface interaction term. In their work, the form G/x^t has been assumed, where t and G are adjustable constants. This form will also be assumed in Chapters 4, 6 and 7.

In the case of two isolated atoms or molecules, the repulsive interaction is always given as a function of the distance between the centres of the two nuclei. Hence, according to Fig. (3.1), for an external ion adsorbed on a flat plane above one substrate atom, the distance between the two nuclei is $(x+\ell)$, and it might be thought that the repulsive term should have the form $G/(x+\ell)^t$. However, since our convention is that any distance is measured from the electrical surface, the form G/x^t is used instead, due to its simplicity and mathematical convenience (the parameters G and t would, of course, be different in the two forms). Another alternative would be to use an exponential form as is done in the Buckingham potential.

One might also expect the repulsive term to be expressed as a sum of pairwise interactions, summed over all the surface atoms, but this may not be valid at a metal surface.

In general, the size and behaviour of the

repulsive term is not very important in our work (see Chapter 6), so the use of the form G/x^t to model the repulsive interaction is probably satisfactory.

3.1.4 The F^2-energy Term in the Atomic Bonding Potential

This term has already been introduced in Chapter 1 in the form $\frac{1}{2} c_\alpha F^2$, for a surface atom in its bonding state. The F^2-energy coefficient c_α is discussed in more detail in Chapter 5. It is, however, important to note that the F^2-energy term assumes the surface atom to be in a constant field, normally taken to be the external field. But for the many reasons that have been cited in Section (3.1.1), the atom in question sees different local fields depending on various factors. Hence, in principle, we expect the coefficient c_α to be variable and it should be defined relative to the site and/or position concerned. In practice, since realistic charged-surface models do not yet exist, in our numerical work the form $\frac{1}{2} c_\alpha F^2$ is assumed and c_α is taken as constant. In particular, in Chapter 5 a value of c_α for Rhodium will be estimated using these assumptions.

3.2 ONE-DIMENSIONALITY AND TOPOLOGY OF THE ESCAPE PATH

Simple discussions also assume field evaporation to be taking place perpendicular to the surface, as in the model of an adatom on a smooth-flat plane. The continued use of this one-dimensional structure is mainly due to its simplicity, and the question is: Can the nucleus of the evaporating atom be moving sideways prior to evaporation as discussed by Waugh et al. (1976), and shown in Fig. (3.5).

Waugh et al. suggest that as the electric field is raised, it eventually becomes energetically favourable for a kink-site atom on a low-index plane to leave its lattice site and move to a position more exposed to the field. They extend this idea by suggesting that all atoms are likely to move on the specimen surface before evaporation, rather than evaporate perpendicularly from their original sites. This movement is governed by interactions between the evaporating atom and its former near neighbours. This movement sideways prior to evaporation seems not an unlikely possibility, and rises a further question of how ionization is taking place, whether on the "lateral" or "perpendicular" portions of the path. In either case if escape is via a Gomer-type mechanism, a curve-intersection-type formalism might be expected to work as a first

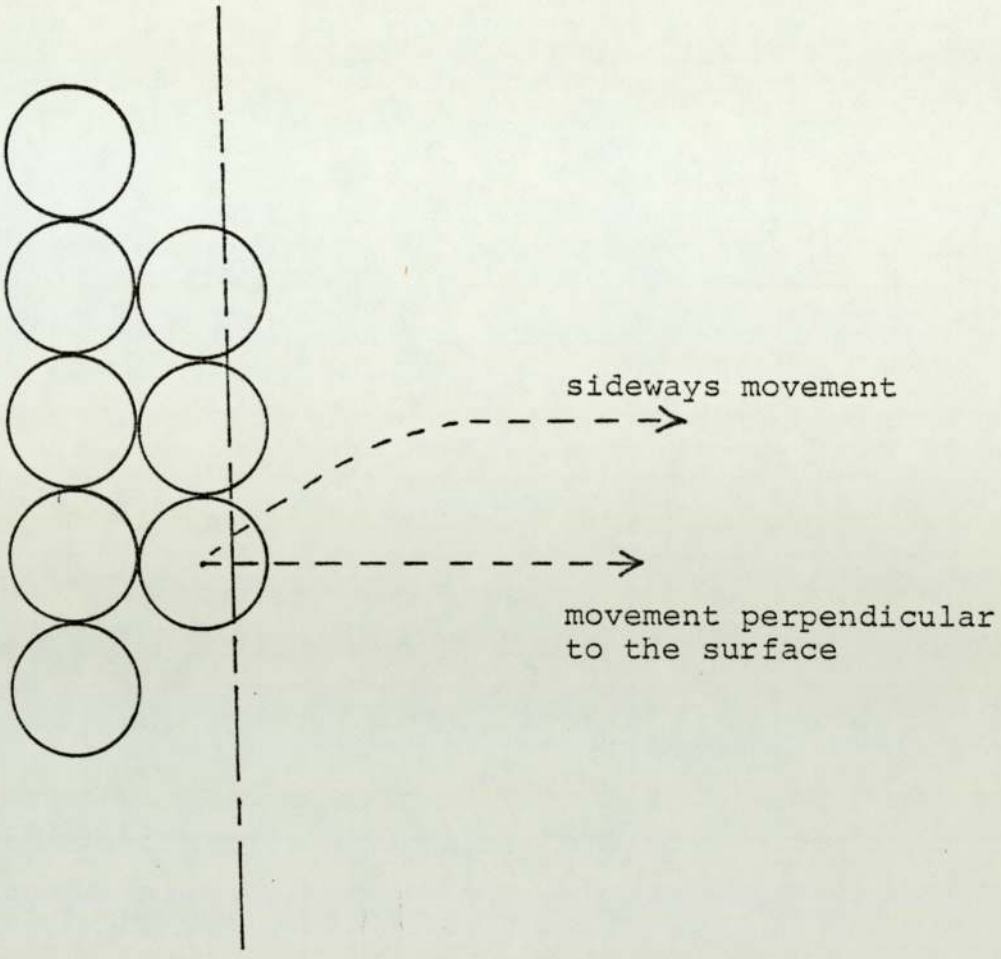

Fig. (3.5) Topology of the escape path.
Illustrates the argument suggested by
Waugh et al. (1976).

approximation, though really is should work better if ionization takes place on the perpendicular part of the path. We also return to this point in Chapter 8.

3.3 THE CHARGE-DRAINING MECHANISM

In Chapter 1, the charge-draining mechanism was briefly introduced. We must now look at this mechanism in more detail, since it could be considered the most likely mechanism of field evaporation.

There are two approaches to discussion of charge-draining. Gomer and Swanson (1963) were the first to discuss field evaporation (and field desorption in general) in terms of both bonding-potential curves and electron energy levels. The relationship between the two approaches has also been discussed by Forbes (1982a). Kingham (1982b) re-introduced the electron energy level method of discussing the initial evaporation process and concluded that charge-hopping is unlikely to be the evaporation mechanism. He found it appropriate only when the atom or ion is a few Angstroms away from the surface, as is the case of field-ionization in field-ion microscopy.

3.3.1 The Two Pictures of Charge-Draining

3.3.1.1 The Electron-Level Picture

Consider an external atom A at some distance away from the surface of a metal M, in the absence of any electric field. As long as the interaction between A and M is negligible, the electron valence level in the external atom remains sharp and well defined. As the atom A approaches the metal surface, its energy level broadens due to correlation and exchange interactions with the metal. At a very small distance the valence electrons are shared between the metal and the external atom, and its level is fully broadened.

Consider now the atom A in free space but in the presence of an electric field. The barrier for tunnelling of the valence electron is reduced. The electron energy level has a finite life-time and is broadened. Near to the metal surface, the barrier is further reduced and the broadening is greater, as above.

A second effect occurring in the presence of the field is that the (mean) energy of the level (relative to the Fermi level) becomes a function of position. The consequences are illustrated in Fig. (3.6) taken from Kingham (1982b).

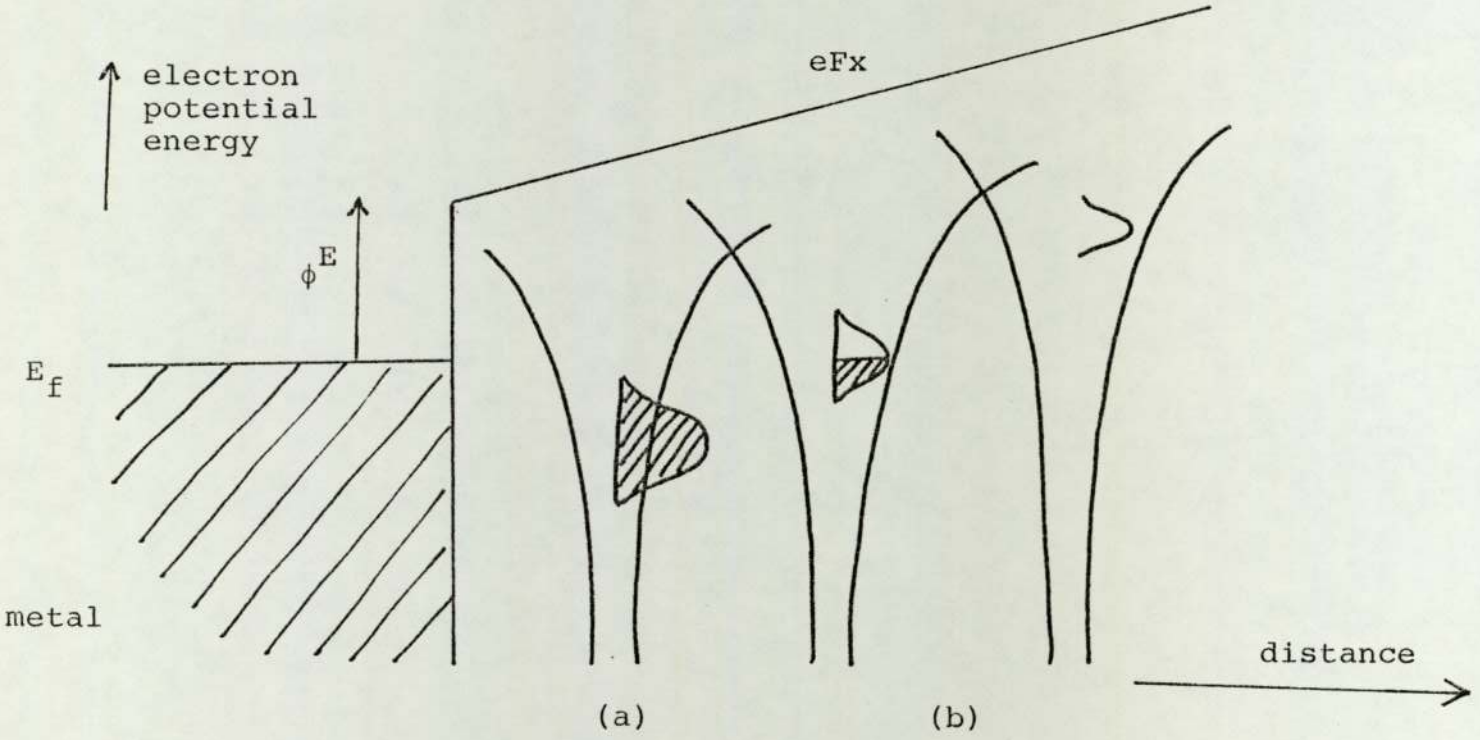

Fig. (3.6) The electron-level picture of charge-draining.

(From Kingham: 1982b)

In position (a), the topmost electron energy level is shown as broadened. It falls below the metal Fermi level E_f and so is fully filled. As the evaporating atom moves to position (b), the broadened energy level comes partly above the Fermi level: electrons drain out, and partial occupation of the level occurs. With further movement outwards, the broadened level comes completely above the Fermi level and ionization is complete. Finally, all the energy levels become narrower as the ion moves away from the surface.

Thus, in this picture we see that the external atom is "partially charged" at some positions in space, and ionization takes place over a range of distances. This picture, however, does not provide us with a means of representing Q as a function of F.

In the literature the escape mechanism is commonly discussed with the use of potential energy diagrams. So we now look at charge-draining from this point of view.

3.3.1.2 The Bonding-Curve Picture

For the charge-draining mechanism, the most commonly used bonding-curve picture is that employed by

Müller and Tsong (1973). This picture seems to have been developed from the "localised bonding" model of field evaporation described in Müller and Tsong (1969), which is in turn an adaptation of the original work of Gomer and Swanson (1963). An atom A is initially bound to a metal M. The evaporation mechanism in the presence of an electric field is pictured by modifying the crossing region of two distinct "atomic" (M+A) and "ionic" (M^-+A^+) curves, as shown in Fig. (3.7a).

In the vicinity of the original crossing point, in the region where ionization is occurring, the evaporating entity is partially charged, as discussed in the previous section. Energetically, the partially charged object has lower energy than either the system (M+A) or the system (M^-+A^+), so the true system is given by the full curve in Fig. (3.7b). This curve is sometimes called the "adiabatic curve". It falls below the so-called "non-adiabatic curve" (shown dotted) and the top of the hump lies below the crossing point of the non-adiabatic curve by an energy ΔU. In the literaure ΔU is often written in the form:

$$\Delta U = -\Delta\varepsilon - \Gamma/2 \qquad (3.1)$$

where $\Gamma/2$ is the half-width of the level broadening and $\Delta\varepsilon$ is an energy shift. This form seems to have

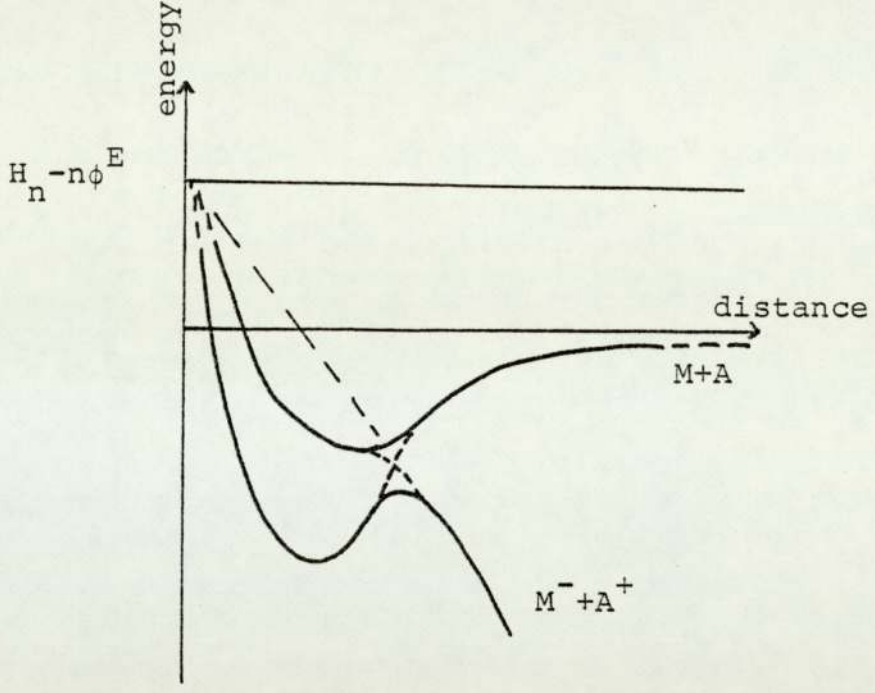

(a)

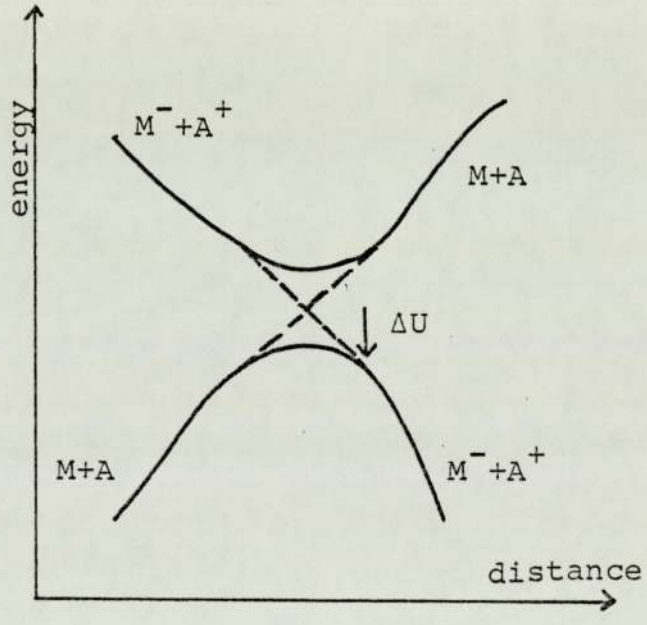

(b)

Fig. (3.7) The bonding-curve picture of charge-draining.

(a) The "common" bonding curve.

(b) The crossing region of the atomic and ionic curves.

(c) The total "adiabatic" curve.

been introduced into field evaporation theory by Müller and Tsong (1969, 1973).

Figure (3.7c) shows the total adiabatic curve for the charge-draining mechanism, at a fixed evaporation field value. The corresponding activation energy Q(C.D) has been introduced in Chapter 1. Using equation (3.1) for ΔU, Q(C.D) is now written:

$$Q(C.D) = Q(C.H) - \Delta U = Q(C.H) - \Gamma/2 - \Delta\varepsilon \qquad (3.2)$$

As before, the initials C.D and C.H stand for "charge-draining" and "charge-hopping". The names were first used by Forbes (1981) when he re-examined the initial field evaporation mechanism. However, Forbes associates the quantity ΔU with a "curve repulsion" effect, by making analogies with a phenomenon that occurs in diatomic molecules band spectra (e.g. Landau and Lifshitz: 1958).

One of the major tasks in field evaporation theory is to determine an explicit field dependence for activation energy. Figure (3.8) shows schematically the expected variation of the total adiabatic curve for charge-draining when the electric field strength is gradually increased. In this case a field dependence of Q(C.D) is given formally from equation (3.2), but

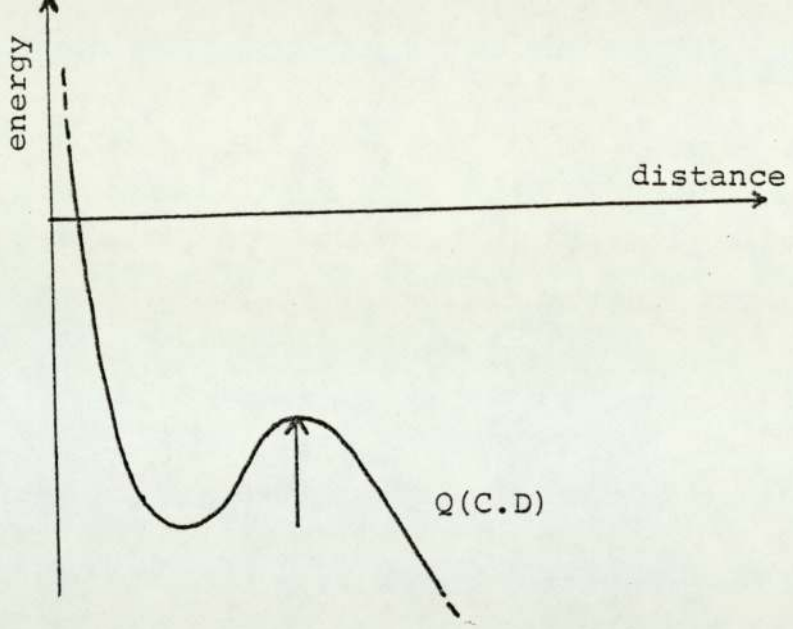

Fig. (3.7c) The total "adiabatic" curve.

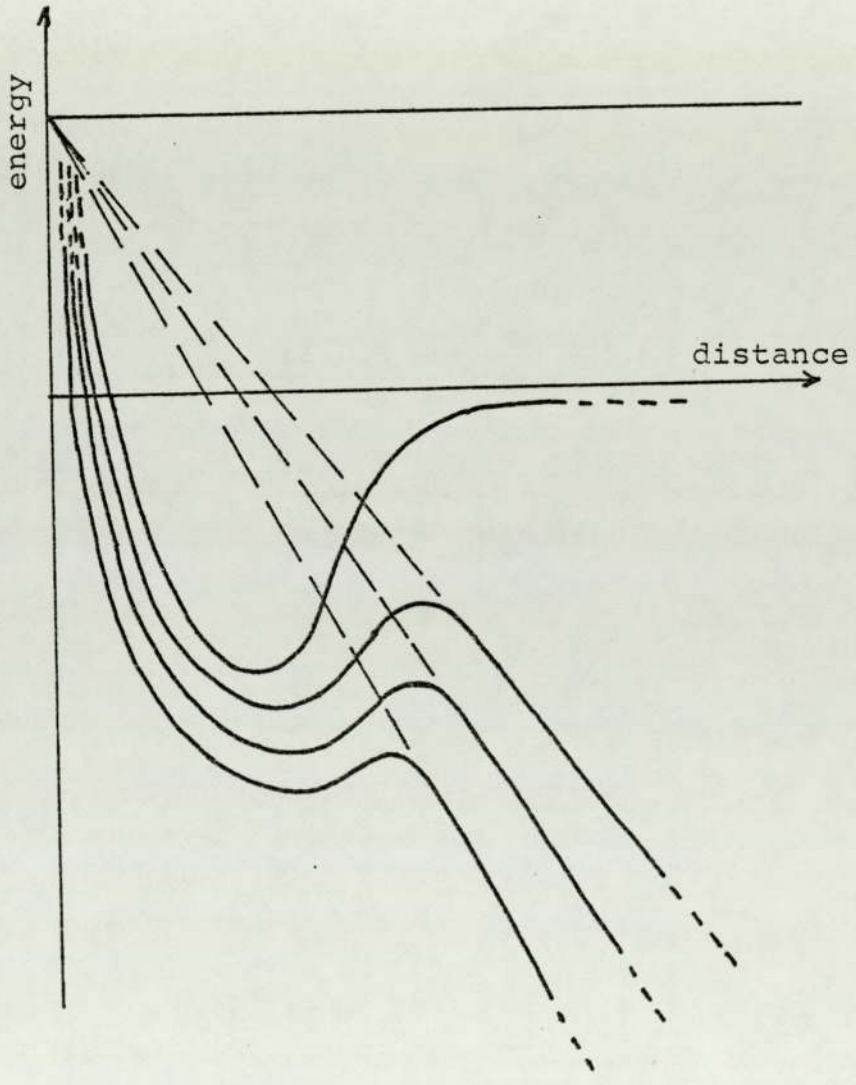

Fig. (3.8) The variation of the adiabatic curve for charge-draining, when the electric field is gradually increased.

the actual determination requires not only a knowledge of the field dependence of Q(C.H) but also of ΔU. Currently, there are no satisfactory calculations of ΔU as a function of x and F. Hence a determination of the field dependence of Q(C.D) from equation (3.2) seems impossible at the present time.

An alternative approach would be to derive the potential-energy curves from first principles calculations, as a function of field and distance, and to evaluate the corresponding activation energies.

3.3.2 A Cluster Model for Charge-Draining

The first quantum-mechanical attempt to treat charge-draining comes from Kingham (1982c) and was constructed for Rhodium. The treatment is based on calculations of the Local Density of Electronic States (LDOS) on an atom field evaporating from a cluster of Rh atoms. The cluster contains 171 Rh atoms with one extra Rh atom above the centre of the top face. The extra atom is allowed to move, but all other atoms are fixed. The LDOS and total charge of the extra atom are calculated as a function of its position (away from the cluster) and the applied electric field. The method of determining the local density of states on the extra atom uses a recursive procedure developed by Haydock et

al. (1972; 1975).

In this way, Kingham produced a set of theoretical curves (Fig. 3.9), that show the variation of the LDOS and the total valence charge. In particular, the LDOS distribution for a field evaporating atom was found to narrow as the ion is moved away from the cluster (to ~3.5 Å); and there was a gradual decrease in the total valence electron charge near the evaporating atom. This indicates that a charge-draining mechanism is operating. The process was found to be taking place over a distance of about 1 Å from the initial atom position.

Kingham's calculated diagrams thus clearly support the occurrence of charge-draining, but it is difficult to check on the details of his calculations. For example, he does not give any indication about the position of the electrical surface, or the various numbers he used. Also, Kingham's calculations do not include any information about ΔU or Q(C.D). Nevertheless, his cluster model is, so far, the only published numerical quantum-mechanical treatment of the charge-draining mechanism.

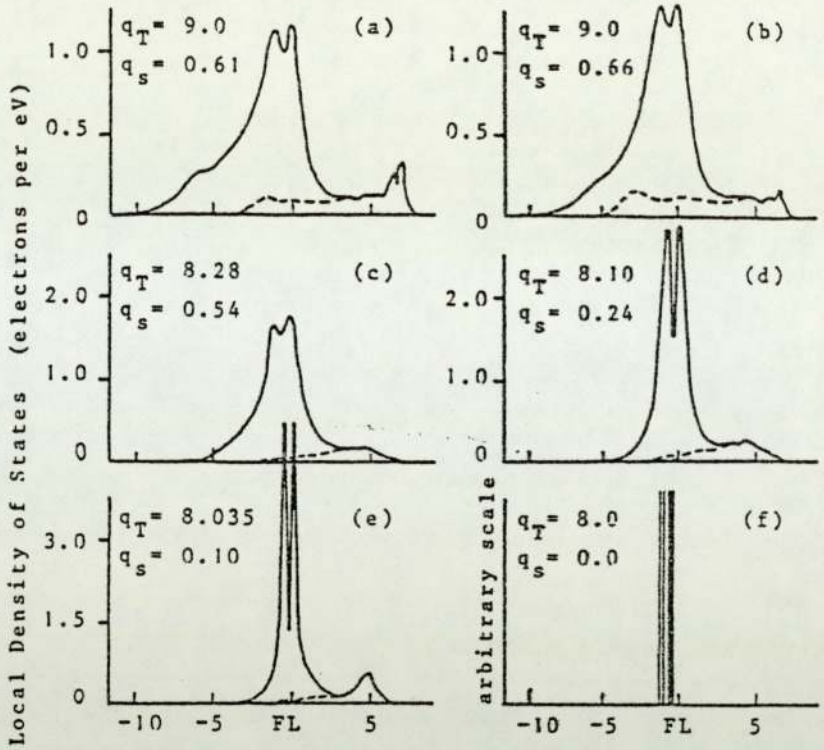

The Local Density of States of valence electrons on (a) a bulk atom, (b) a surface atom and (c) to (f) a field evaporating atom. q_T is the total valence electron charge and q_s is the s electron charge. The s electron contribution to the LDOS is shown dashed.

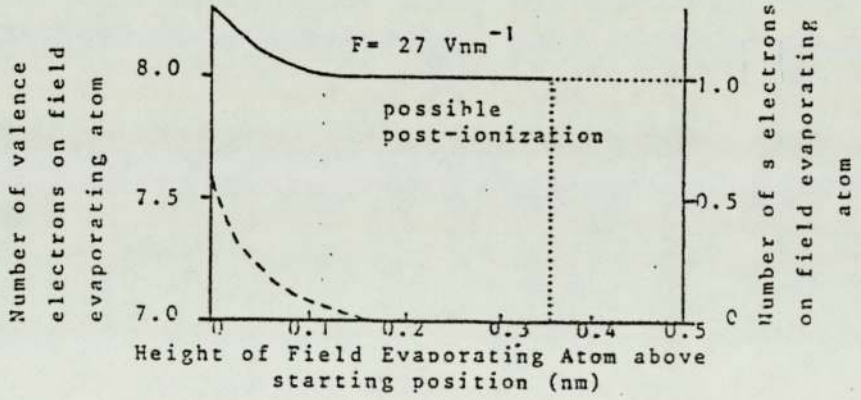

Total valence electron charge and s electron charge on a field evaporating rhodium atom.

Fig. (3.9) The cluster model results.

(From Kingham: 1982c)

3.4 SUMMARY AND CONCLUSIONS

The objective of this chapter has first been to identify and discuss the principal assumptions, and hence limitations, of a simple field evaporation model. Amongst the main limitations we may cite the use of a linear approximation for the ion electrostatic potential, use of the image-potential form and the use of flat surface models.

Second, the charge-draining mechanism has been reviewed in terms of electron energy levels and potential energy curves.

The next objective is to analyse some field evaporation experimental data, where temperature dependence of evaporation field and field dependence of activation energy, are involved. Taking into account the field evaporation process that a partially charged surface atom undergoes, one should expect this objective to be carried out in the context of a charge-draining mechanism. However, as already noted, no explicit activation energy dependence of field is available yet. Hence, our analysis will be carried out in terms of a Q(C.H)-type formula, that is in terms of a curve-intersection formalism. The latter is first derived with the use of an additional simple

approximation, namely that the field evaporating atom is initially assumed to be vibrating in a parabolic well around its bonding point. The next chapter introduces the corresponding formulae, and shows how some experimental data due to Wada et al. (1980) can be analysed in this context. We shall come back in Chapter 8 to the question of the validity of using a curve-intersection formalism to represent the field evaporation process.

CHAPTER 4

THE TEMPERATURE DEPENDENCE OF EVAPORATION FIELD AND THE Q-F FORMULA

4.1 INTRODUCTION TO A NEW THEORY

In 1980, in the course of studies on the bonding behaviour of Gallium (Ga) and Tin (Sn) on Tungsten (W) and Molybdenum (Mo) substrates, Wada et al. reported some new results concerning the temperature dependence of onset evaporation field for W and Mo (which are two of the most field-resistant metals conventionally used in field-ion techniques). Figure(4.1)shows the observed temperature dependence of evaporation field for W(011), Mo (011), Ga on W and Sn on W taken from the Wada et al. experiments.

Their theoretical analysis however, both in the 1980 paper and in a subsequent paper (Konishi et al: 1981), used the "constant-intersection-distance" version of the charge-hopping mechanism (i.e. they supposed that the intersection point of the atomic and ionic curves was constant, independent of field strength). The results derived from this theory were thought unsatisfactory. An alternative approach is presented here, based on an approximate formula recently derived by Forbes (1982d), that is introduced in the next section.

4.1.1 New Activation-Energy Formula for Gomer-Type Mechanisms

In investigating the temperature dependence of evaporation field, Forbes (1982d) derived an expression for the activation energy using the parabolic approximation for the pre-evaporating atom, as given by equation (A12) in Appendix A.

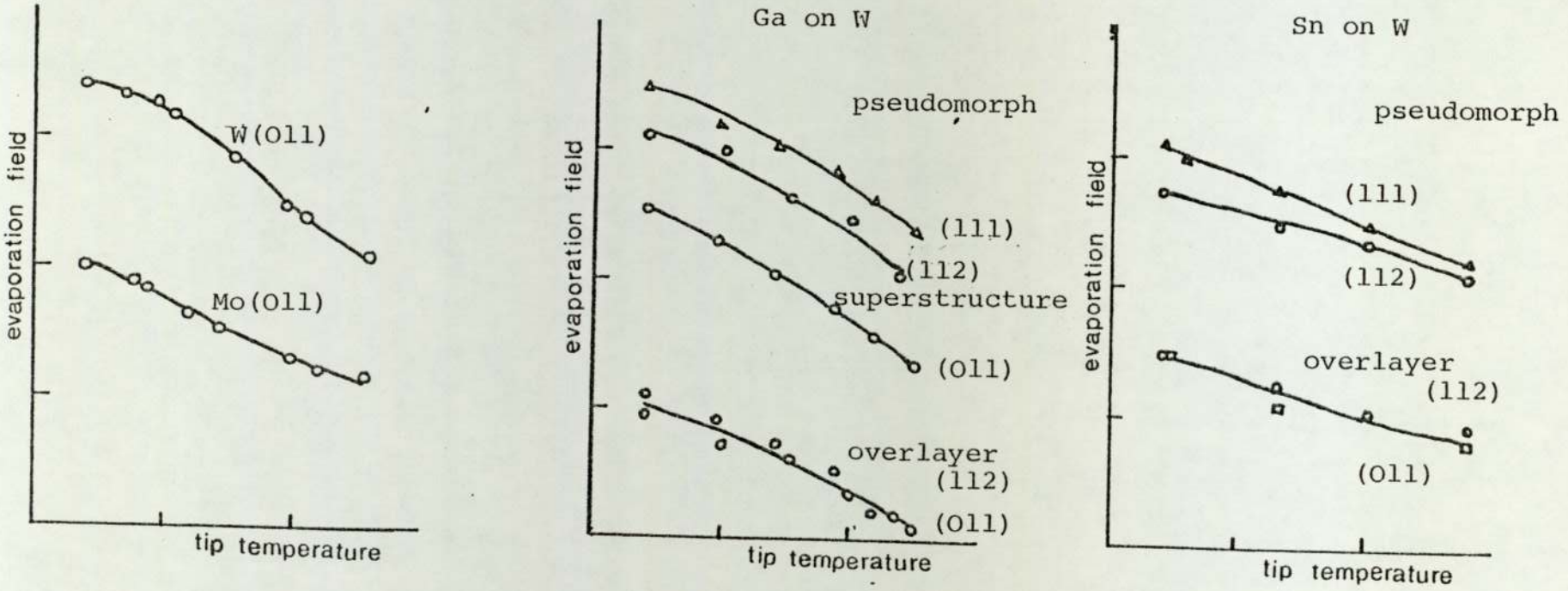

Fig. (4.1): Experimental temperature dependence of evaporation field for W, Mo, Ga on W and Sn on W.

The approximation is supposed to be valid around the bottom of the parabolic well, where it can be assumed that the activation energy Q is small enough to be neglected in comparison with the configurational term K_n^F and other terms relating to the ion-surface interactions, namely the image-potential plus the repulsive and polarisation terms. This new activation-energy expression has the form:

$$Q = \Omega\left[\left(F^e/_F\right)-1\right]^2 \qquad (4.1)$$

where F is the field value and F^e the zero-Q evaporation field, and Ω is a quantity with the dimension of energy defined by this equation. In a first approximation, Ω can be regarded as a constant given by:

$$\Omega = \tfrac{1}{2}\,\kappa a^2 \qquad \text{(first approx.)} \qquad (4.2)$$

where κ is the force-constant for the vibrating atom and a the distance of the well bottom from the emitter's electrical surface.

A better approximation for Ω is:

$$\Omega = \tfrac{1}{2}\kappa a^2\left(1-\frac{\pi^e}{nea}\right)^2\left(1-\frac{\eta_n'}{neF^o}\right)^{-2} \qquad (4.3)$$

where π^e is a parameter with the dimensions of S.I. dipole moment, and η_n' the partial derivative with respect to distance, taken at the bottom of the well a and at $F=F^e$ of

a quantity η_n representing the "purely chemical" component of the ion-surface interaction. This interaction is usually approximated by image-potential, repulsion and F^2-energy terms.

Physically, the first bracket in equation (4.3) is a correction due to field-induced effects (polarisation and partial ionisation in the bonding state) and is in fact given by:

$$(1 - \frac{\pi^e}{nea}) \equiv (1- \frac{(c_\alpha - c_n)F^e}{nea}) \qquad (4.4)$$

where c_α and c_n have their usual meaning.

The second bracket is a correction due to the correlation and repulsion interactions between the ion and the surface. Taking all these effects into account, the new activation energy formula can be written as:

$$Q = \tfrac{1}{2}\kappa a^2(1- \frac{\pi^e}{nea})^2 (1- \frac{\eta_n'}{neF^o})^{-2} (\frac{F^e}{F^o} -1)^2 \qquad (4.5)$$

Details on the above discussion, in particular the derivations of equations (4.1) and (4.3), the parameters π^e and η_n together with the different assumptions made are to be found in Appendix A.

4.1.2 The Temperature-Dependence of Evaporation Field

The emission equation can be written in the form:

$$\ell n\left(\frac{n_{hr}A}{J}\right) = \frac{Q}{kT} \tag{4.6}$$

where as before, n_{hr} stands for the count of atoms at "high risk" evaporation sites, J is the evaporation flux, A the field evaporation pre-exponential and k the Boltzmann constant. Combining equations (4.6) and (4.1) and eliminating Q, leads to:

$$kT\ell n\left(\frac{n_{hr}A}{J^{o}}\right) = \Omega\left[\left(\frac{F^{e}}{F}\right)-1\right]^{2} \tag{4.7}$$

or

$$\frac{k\ell n\left(\frac{n_{hr}A}{J^{o}}\right)T}{\Omega} = \left[\left(\frac{F^{e}}{F}\right)-1\right]^{2} \tag{4.8}$$

Here, the evaporation flux takes the specific value J^{o} corresponding to the onset evaporation field F at the temperature T. Formula (4.8) is then written in two reciprocal forms:

$$T^{\frac{1}{2}} = \theta^{\frac{1}{2}}\left[\left(\frac{F^{e}}{F}\right)-1\right] \tag{4.9a}$$

and

$$\frac{1}{F} = \left[1+\left(\frac{T}{\theta}\right)^{\frac{1}{2}}\right]\left(\frac{1}{F^{e}}\right) \tag{4.9b}$$

where

$$\theta = \frac{\Omega}{k\ell n\left(\frac{n_{hr}A}{J^{o}}\right)} \tag{4.10}$$

and has the dimensions of temperature. θ can be interpreted as the temperature at which the onset evaporation field F

becomes equal to half the zero-Q evaporation field F^e.

Formula (4.9) expresses the temperature dependence of evaporation field, and a plot of $T^{\frac{1}{2}}$ versus $\frac{1}{F}$ would be linear over a certain temperature range. However, certain conditions are to be met for this to be so.

First, the various arguments behind the derivation of equation (4.1) are assumed to be valid (as discussed in Appendix A).

Second, in order to preserve the linearity of $T^{\frac{1}{2}}$ versus $\frac{1}{F}$, the quantities Ω and θ have to be constants. This is valid when Ω is given by equation (4.2) and A is taken as constant. This last supposition works over a range of temperatures where field evaporation is a thermally-activated process defined by the Arrhenius equation. At very low temperatures, however, ion-tunnelling effects become important, the Arrhenius equation fails, and A is a field-dependent quantity. But, it has conventionally been assumed that these ion-tunnelling effects are not important at temperatures near 80 K and above. Therefore, one expects a theoretical plot of $T^{\frac{1}{2}}$ versus $\frac{1}{F}$ to be linear at temperatures around 80 K and above, with ion-tunnelling effects causing deviations at very low temperatures. This last effect has actually been observed in experimental F versus T plots by Wada et al (1980), Kellogg (1981a) and recently again by Wada at al (1983).

Finally, if a better approximation for Ω as given by equation (4.3) is used, then we have:

$$\theta^{\frac{1}{2}} = \frac{(\frac{1}{2}\kappa)^{\frac{1}{2}}(a-{}^{\pi}e/ne)(1-\frac{\eta_n'}{neF})^{-1}}{\left[k\ell n(\frac{n_{hr}A}{J^o})\right]^{\frac{1}{2}}} \tag{4.11}$$

and

$$T^{\frac{1}{2}} = \frac{(\kappa/2)^{\frac{1}{2}}(a-{}^{\pi}e/ne)(1-\frac{\eta_n'}{neF})^{-1}}{\left[k\ell n(\frac{n_{hr}A}{J^o})\right]^{\frac{1}{2}}} \cdot \left[(\frac{F}{F}^{e})-1\right] \tag{4.12}$$

A condition here would be that $\frac{\eta_n'}{neF}$ is small and slowly varying with field F. Following the definition of η_n', one has:

$$\eta_n' = \left.\frac{\partial \eta_n}{\partial x^p}\right|_a \equiv \frac{n^2e^2}{16\pi\varepsilon_o a^2} - \frac{tG}{a^{t+1}} \tag{4.13}$$

Hence, correlation and repulsion contributions to η_n' are of opposite sign and tend to cancel. One therefore expects $\frac{\eta_n'}{neF}$ to be small. In this case, $\frac{\eta_n'}{neF} << 1$. The following approximation - in the first order - can then be made:

$$(1 - \frac{\eta'}{neF^o})^{-1} \simeq 1 + \frac{\eta_n'}{neF} \tag{4.14}$$

and leads to:

$$\theta^{\frac{1}{2}} = \frac{(\frac{1}{2}\kappa)^{\frac{1}{2}}(a - \pi^{e}/ne)(1 + \eta_n'/neF)}{[k\ \ell n(n_{hr}\ A/J^{o})]^{\frac{1}{2}}} \qquad (4.15)$$

and

$$T^{\frac{1}{2}} = \frac{(\frac{1}{2}\kappa)^{\frac{1}{2}}(a - \pi^{e}/ne)(1 + \eta_n'/neF)}{[k\ \ell n(n_{hr}A/J^{o})]^{\frac{1}{2}}} \left(\frac{F^{e}}{F} - 1\right) \qquad (4.16)$$

The final requirement would then be that A, η_n'/neF and n_{hr} are all constants. A plot of $T^{\frac{1}{2}}$ versus $\frac{1}{F}$ will again be linear over a limited range of temperature. Fitting of experimental data to the above theory would tell where linearity stops at high temperatures.

4.2 ANALYSIS OF WADA ET AL. EXPERIMENTAL RESULTS

In the case of Tungsten and Molybdenum, the points of Fig. (4.1) have been measured up and replotted in the form $T^{\frac{1}{2}}$ versus $\frac{1}{F}$ as shown in Fig. (4.2). It is clearly shown that in the range from about 60 K to 150 K, the relationship is linear, as predicted by equation (4.9). Deviations from linearity occur at low temperatures below 60 K, and may well be an indication that ion-tunnelling effects are taking over. This is because formula (4.9) has been derived from equation (4.1) using the emission equation (4.6), that we know fails at sufficiently low temperatures. Therefore, the failure of the emission equation at low temperatures due to the predominance of ion-tunnelling effects would certainly induce the failure of formula (4.9) and this would manifest itself as a

deviation from linearity. In principle, ion tunnelling is not the only possible explanation of the deviation and we return to this point in Chapter 8. However, we can conclude that, over the range of temperature used, these experimental results are certainly compatible with a Gomer-type mechanism where the evaporating atom is supposed to be vibrating in a parabolic well.

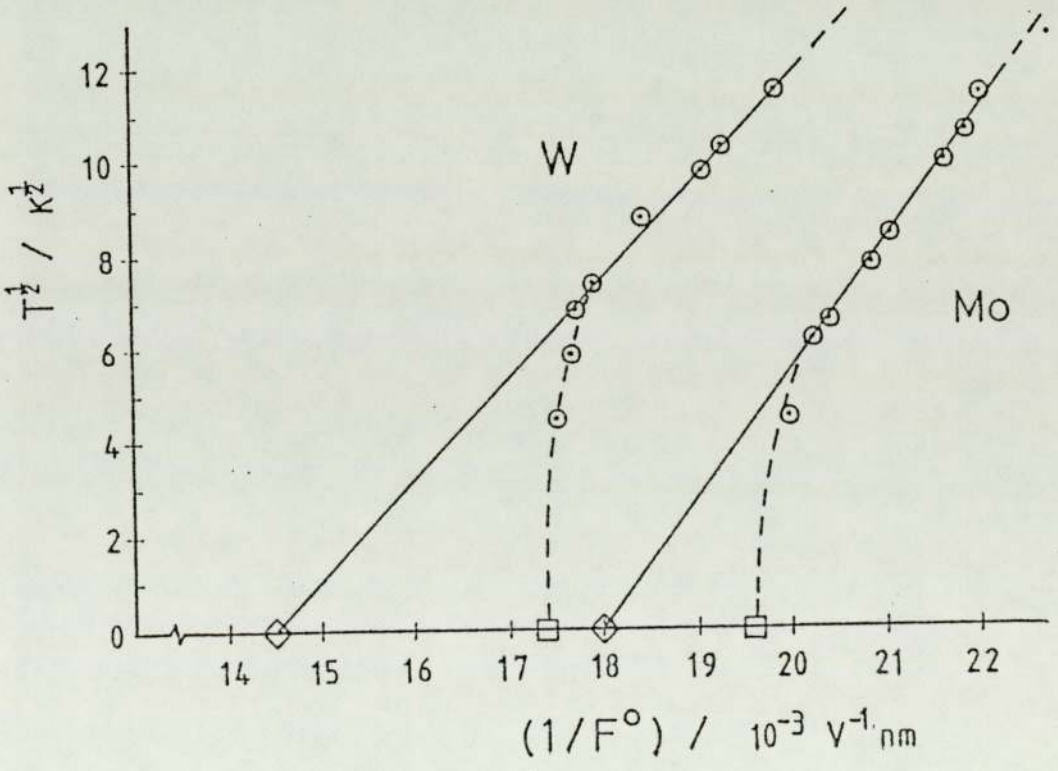

Fig. (4.2) : $T^{\frac{1}{2}}$ vs $\frac{1}{F}$ for W and Mo. The diamonds are the as-regressed values for zero-Q field. The squares are values of experimental zero-T field.

4.2.1 Results and Standardization Procedures

Regression calculations on data points of Fig. (4.2) have been carried out in the form $\frac{1}{F}$ versus $T^{\frac{1}{2}}$, excluding the lowest-temperature point in the case of Molybdenum and the two lowest points in the case of Tungsten. The fitting was of first order in conformity with equation (4.9b). Values of $\frac{1}{F^e}$ (the intercept) and $\frac{1}{F^e \theta^{\frac{1}{2}}}$ (the slope) were subsequently found, together with the error limits. Results are shown in Table (4.1) below, and known as the "regressed" F^e and θ values.

TABLE (4.1)

Species	θ (K)	F^e (V/nm)
W	940 ± 120	69.1 ± 1.0
Mo	2430 ± 190	55.5 ± 0.3

Values of θ and F^e as derived from regression on the data in Fig. (4.2) in the form $\frac{1}{F} = \left[1 + \left(\frac{T}{\theta}\right)^{\frac{1}{2}} \right] \frac{1}{F^e}$, with error limits.

Substituting T = 78K, with "regressed" F^e and θ values into equation (4.9b) leads to F = 53.6 V/nm for Tungsten, which is lower than the usual 78K value of 57 V/nm.

Wada et al did their measurements of onset evaporation fields using an onset flux of 0.1 layers/s. However, we would follow Müller and Tsong (1973) and take somewhat arbitrarily a working "standard condition" corresponding to a situation where field evaporation occurs at a rate of 0.01 layers/s, at a temperature assumed to be 78K exactly and at a field strength of 57.0 V/nm for Tungsten. The Wada et al results can then be "re-standardised". The procedure is as follows:

Equation (4.9b) can also be written as:

$$F = \frac{F^e}{1+(T/\theta_J)^{\frac{1}{2}}} = F(T,J) \qquad (4.17)$$

where θ_J is function only of the chosen onset flux J.

At T=78K

$$F(78,J) = \frac{F^e}{1+(78/\theta_J)^{\frac{1}{2}}} \qquad (4.18)$$

At the same evaporation flux J, F^e can be eliminated from equation (4.18), so that the general form is now:

$$F(T,J) = F(78,J) \cdot \frac{1+(78/\theta_J)^{\frac{1}{2}}}{1+(T/\theta_J)^{\frac{1}{2}}} \qquad (4.19)$$

For a given flux J, this formula enables us to derive the value of evaporation field at any temperature T, as long as F(78,J) is known. In the case of Wada et al, where a different flux criterion is used (J=0.1 ℓ/s), one would have:

$$F(T,0.1) = F(78,0.1)\ \frac{1+(78/\theta_{0.1})^{\frac{1}{2}}}{1+(T/\theta_{0.1})^{\frac{1}{2}}} \qquad (4.20)$$

where F(78,0.1) is required. Using flux field-sensitivity measurements such as those of Tsong (1978b), Forbes (private communication) derived the value: F(78,0.1)=57.59 V/nm. Therefore, in order to "re-standardise" the "regressed" F^e value, equation (4.20) is used at T=0K and $\theta_{0.1}$=940 K, i.e.

$$F^e = F(0,0.1) = F(78,0.1).\left[1+(78/\theta_{0.1})\right]^{\frac{1}{2}} \qquad (4.21)$$

and gives F^e=74.18 V/nm. The same treatment, when applied to Molybdenum leads to: F^e= 60 V/nm.

Hence, after re-standardisation of the Wada et al results, the different parameters are now summarised in Table (4.2) below:

TABLE (4.2)

Species	θ(K)	F^e(V/nm) as regressed	F^e(V/nm) Re-standardised
W	940±120	69.1±1.0	74.2
Mo	2430±190	55.5±0.3	60.0

values of the regressed and"re-standardised"evaporation field F^e for W and Mo.

These re-standardized values of F^e are higher than the "normal" values of evaporation field discussed in the literature: 57 V/nm for Tungsten and 43 V/nm for Molybdenum. This point is discussed further in the next section.

4.3 THE VALUE OF ZERO-Q EVAPORATION FIELD

In the case of Tungsten, the Müller formula for the zero-Q evaporation field is as given by equation (2.7) for n=2 and leads to $F^e(W) = 57$ V/nm.

With the energetics-based formula derived by Forbes (1982e), where it is assumed that the image-potential is some fraction of the configurational term K_n^o, the value of zero-Q evaporation field is given by equation (1.18) with n=2 and $\sigma_2 = 0.24$, and leads to $F^e(W) \simeq 55$ V/nm. Therefore, there exists a discrepancy between the re-standardised F^e value (74.2 V/nm) and the above values.

One solution to this discrepancy would be to include the repulsion and F^2-energy terms into the activation energy expression appropriate to the charge-hopping mechanism. The ion is assumed to escape at the bonding distance a from the metal's electrical surface, so that the requirement that activation energy be zero leads to:

$$neF_n^e a = K_n^o - \frac{n^2e^2}{16\pi\varepsilon_o a} + \frac{G}{a^t} + \frac{1}{2}(c_\alpha - c_n)F_n^{e\,2} \qquad (4.22)$$

Taking a=140 pm and K_2=25.6 eV for Tungsten, and disregarding the last two terms in equation (4.22) (which gives the image-potential energy as -10.3 eV) would also lead to $F^e(W) \simeq 55$ V/nm. But equation (4.22) shows clearly that taking into account the repulsion and F^2 terms would increase the value of F_n^e.

It is a reasonable assumption that the repulsive term should be taken as about one tenth the image-potential term in magnitude, i.e. 1 eV, and that the F^2 term should be taken as about 2 eV. This would give a new estimate of $F^e(W)$ as 65.5 V/nm. This value is higher than the previous ones and closer to the re-standardised value 74 V/nm. An even higher estimate of F^e could be obtained if the F^2 term were greater than 2 eV, or if the strength of the correlation interaction between the departing ion and the surface were less than the 10 eV assumed. This possibility is shown in some modern surface theories (S.C. Ying: 1980 for example). Thus, there is no real difficulty about giving a plausible explanation for the high F^e values obtained from the Wada et al experiments.

4.4 EFFECTS AT HIGH AND LOW TEMPERATURES

Figure (4.2)showed that deviation from linearity occurs at low temperatures. Because the highest temperature in the Wada et al experiments was only 150 K, some results

obtained by Nakamura and Kuroda (1969), which cover temperatures from near 20 K to near 300 K, will be discussed.

4.4.1 Low-Temperatures and Evidence for Ion-Tunnelling

Many authors in the past have postulated theoretically that the Arrhenius equation would fail at low temperatures; for example Gomer and Swanson (1963), Ehrlich and Kirk (1968). Others, Brandon (1966a), Tsong (1968) and Kingham (1981)) have attempted to calculate the "critical temperature" T^c at which the tunelling effect and the thermal activation effect become equally important. Figure(4.2)however, provides an experimental indication that ion-tunnelling at low temperatures is a plausible hypothesis. Table (4.3) compares the experimental "deviation temperature" T^{dev} with the "critical temperature " T^c as obtained by the above authors.

TABLE (4.3)

Tungsten		Molybdenum		Details of Calculation	
T^{dev}(K)	T^c(K)	T^{dev}(K)	T^c(K)	Authors	Barrier Type or Method
50±10		35±10		Present Paper	Experimental value
	705			Brandon	Field Emission analogy
	70		130	Tsong	Triangular barrier
	41			Ehrlich & Kirk	Schottky barrier
	73		91	Kingham	Triangular barrier
	53		69	Kingham	Rectangular barrier
	66		82	Kingham	Parabolic barrier
	40		45	Kingham	Parabolic approx. to Schottky barrier

values of T^{dev}(experimental) and T^c(theoretical) for Tungsten and Molybdenum.

T^c has been obtained by using the WKB approximation with different types of potential barriers.

The value of (50±10)K for Tungsten is in good agreement with most theoretical estimates of T^c, but the value of (35±10)K for Molybdenum agrees less with the "critical temperature". Kingham suggests that this critical temperature is in fact significantly dependent on model and assumptions employed. On the other hand, the question arises of whether the critical temperature T^c can be identified with the deviation temperature T^{dev}. The general degree of agreement between theory and experiment must be considered satisfactory.

More important, the experimental deviation temperature has been found to be less than 80 K for both Tungsten and Molybdenum. This confirms that in past work it has been legitimate to treat field evaporation as a thermally-activated process obeying the Arrhenius equation.

4.4.2 The Higher Temperatures Case: The Nakamura and Kuroda Results

Nakamura and Kuroda (1969) carried out measurements of temperature dependence of evaporation field ranging from 20 K to about 300 K, for Tungsten, Molybdenum and Tantalum. Their suggestion was: "field evaporation voltage decreased with the nearly square of the emitter temperature", for temperatures between 180 K to 300 K. This can be

theoretically translated into a relationship of the form:

$$F = \gamma_1(1 - \gamma_2 T)^2 \qquad (4.23)$$

where γ_1 and γ_2 are positive constants.

If $(T/\theta)^{\frac{1}{2}}<1$ in equation (4.9b), it follows that:

$$F \simeq F^e(1-\theta^{-\frac{1}{2}}T^{\frac{1}{2}}) \qquad (4.24)$$

Even though the above formulae have analogous forms, the temperature dependence of evaporation field is different. This seems to indicate a regime change at around 180 K. A possible explanation may be as follows:

Increasing the temperature (i.e. decreasing F) might produce a change in regime if the curve-intersection point approached an inflection point in the bonding potential curve and moved into a region where the bonding potential is convex upwards. This possibility is illustrated in Fig.(4.3). Since for steady field evaporation the activation energy Q has to be about 25 kT, a regime change near 180 K might imply an inflection point about 0.4 eV above the bottom of the bonding well. This value is not compatible with a simple bonding well of depth 9 eV or so (the zero-field binding energy for Tungsten is 8.66 eV); but it could be compatible with a localised bonding well of depth about 1 eV, as shown in Fig.(4.3). And the existence of localised bonding wells of about 1 eV is entirely

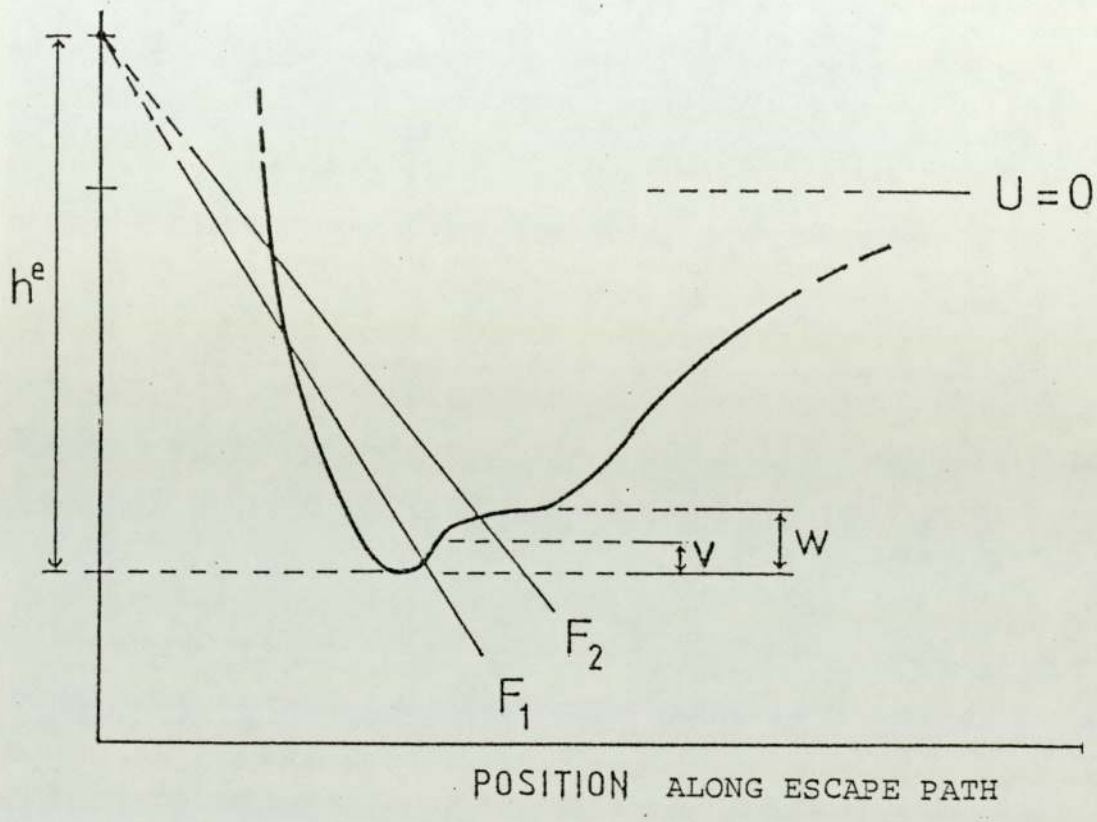

Fig. (4.3) : Illustration of a localised bonding-well in the bonding potential. h^e is the "standard pivot height" as defined in Appendix A. A regime change near 180K might imply an inflection point about 0.4 eV(v) above the bottom of the well. The localised bonding well (w) is about 1 eV. (The "position"axis in this context could be partly parallel to the surface.)

compatible with listed diffusion activation energies for Tungsten, which are of order 1 eV at a field-free surface (Ehrlich and Kirk: 1968).

An alternative explanation has been suggested by Kellogg (private communication; also 1981a). The field-adsorbed layer of imaging-gas, that would have been present at temperatures near 80 K in the Nakamura and Kuroda experiments, would become vacant at higher temperature. The field-adsorbed helium would affect the Tungsten-atom binding energy slightly and a regime change in the field evaporation behaviour could be associated with a change from a high-coverage to a low-coverage situation. Such a coverage change would conceivably occur arround 180 K. Different interpretations can therefore be given to the Nakamura and Kuroda results.

4.5 THE Ga ON W AND Sn ON W SITUATIONS

It appears from Wada at al results that the temperature dependences of evaporation field for Ga on W and Sn on W differ from the Tungsten and Molybdenum cases; this is shown in the F versus T curves.

When redrawn in the form $T^{\frac{1}{2}}$ versus $\frac{1}{F}$, the data points do not follow a straight line. The Ga on W case is illustrated in Fig. (4.4). Gallium is known to be one of the less field evaporation resistant metals, and the escape

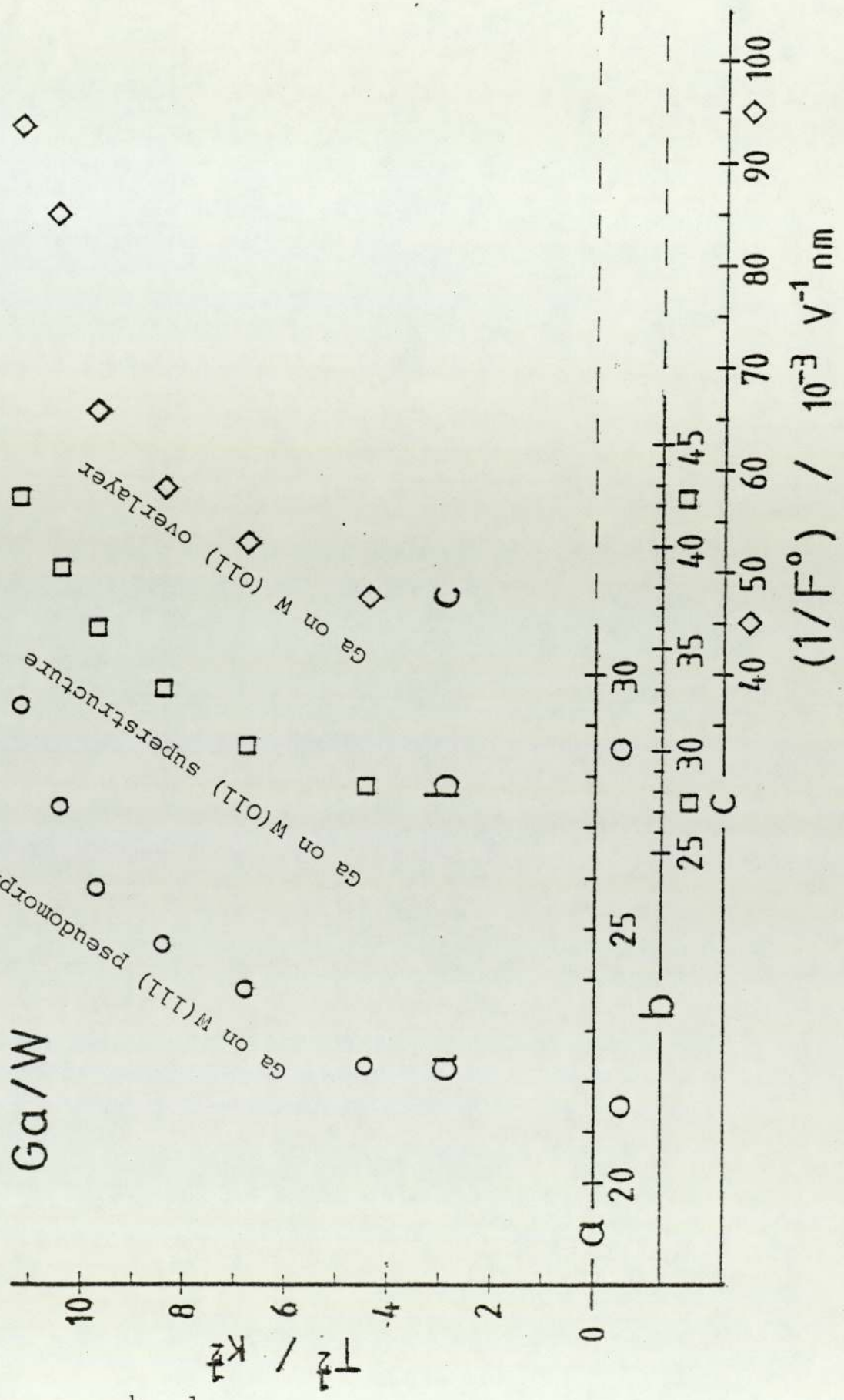

Fig. (4.4) : $T^{\frac{1}{2}}$ vs $\frac{1}{F}$ plots for three bonding situations of Ga on W.

mechanism is not yet fully established. Thus, this failure to conform to equation (4.9) is not entirely surprising.

4.6 SOME CRITICISMS OF THE WADA ET AL THEORETICAL ANALYSIS

Several flaws have been detected in the Wada et al. analysis:

(1) In their theoretical analysis of the experimental results, Wadā et al. used a quantity denoted by k for the evaporation flux measured in 'layers/s' together with a quantity denoted by k_o for the pre-exponential constant - or frequency factor - measured in 's^{-1}', within the equation:

$$k = k_o \exp(-Q/kT) \qquad (4.25)$$

This expression is dimensionally inconsistent.

(2) They used an expression for the activation energy as given by the simple image-hump formalism. This model has been - as already cited - seen to be mathematically invalid in the context of low-temperature field evaporation (Biswas and Forbes; 1982, Forbes: 1982c).

(3) They went on to use the intersection model assuming the intersection distance to be constant.

(4) Finally, they used a parameter α corresponding to

$(c_\alpha - c_n)$ in equation (4.22) for example, calling it polarisability. This point has already been mentioned in Chapter 1.

It is thus not surprising that they achieved poor agreement between theory and experiment.

4.7 CONCLUSIONS AND COMMENTS

This chapter has mainly been concerned with the introduction of new simple formulae and their application to the temperature dependence of evaporation field, as evidenced by the experiments of Wada et al. First an expression for the activation energy function of field has been given for a Gomer-type mechanism, based on a parabolic assumption for the well bottom, valid for small values of Q. Then a general relationship between evaporation field and temperature has been derived and is given by equations (4.9) in the simple case. The fitting of the experimental data in the form $T^{\frac{1}{2}}$ versus $\frac{1}{F}$ was reasonably conclusive as far as Tungsten and Molybdenum were concerned, over a certain range of temperatures (60 K to 150 K). Below 50 K for W and 35 K for Mo, deviations from linearity occur, and are compatible with ion-tunnelling effects. The Ga on W and Sn on W results do not follow the theory. Another possible explanation is discussed in Chapter 8.

This work thus seemed to show clearly that for Tungsten and Molybdenum, which are two of the most field evaporation resistant metals, escape is taking place via a Gomer-type surface charge-exchange process, and that a curve intersection formalism is adequate to describe the escape process.

We will come back in Chapter 7 to the Q-F and T-F formulae. They will be applied to further (temperature dependence of field and field-dependence of activation energy) measurements made by Kellogg (1981a, 1984), in the case of W, Mo and Rh. The noted deviations at high temperatures will be reported and discussed. Before that, the next chapter will concentrate on the analysis of Ernst's (1979) experimental data for Rh, to derive an estimate of the F^2-energy term coefficient c_α.

The results described in this chapter have been published as: "The temperature dependence of evaporation field for Gomer-type field-evaporation mechanisms", by K. Chibane and Richard G. Forbes, Surface Science 122 (1982) pp 191-215.

CHAPTER 5

FIELD DEPENDENCE OF BINDING ENERGY AND DERIVATION OF AN F^2-ENERGY TERM COEFFICIENT FOR Rh

The intention of this chapter is to derive a value for the F^2-energy-term coefficient c_α of Rhodium by using Ernst's (1979) experimental results. This value will be compared with a theoretical one, obtained in a qualitative way. In conclusion, it will be shown that polarisation-type effects in the Q-F formula introduced in the preceding chapter, could influence the interpretation of field-sensitivity data.

Ernst's experiments involved the field-dependence of:

(1) the relative abundance of variously charged Rhodium ions (Rh^+ and Rh^{++});

(2) appearance energies, and

(3) activation energies.

Field strengths were reported to vary between 17 to 41 V/nm at tip temperatures from 100 to 600 K.

The most important result was that activation energies for singly and doubly-charged Rhodium were found to be the same, within experimental error. Ernst concluded that the doubly-charged Rhodium ions were formed by post-ionization. As already noted in Chapter 1, this was the first experimental evidence for post-ionization, and Ernst found reasonable agreement between the experiments and a one-dimensional theory.

Ernst also concluded that the field-dependence of

experimentally determined appearance and activation energies were inconsistent with simple-image hump formalisms, for both ionic species.

5.1 INTRODUCTION TO F^2-ENERGY TERM COEFFICIENTS

Surface atom binding energy has already been discussed in Chapter 1. It was noted that the presence of a high electric field would cause a change $\Delta\Lambda$ in the total binding energy Λ^F given by equation (1.4). This binding energy change can be expressed in several ways, and we now develop the relevant concepts.

5.1.1 Basic Coefficient Definitions

In free-space, the "proper polarizability" b(orb) of an atom is due to polarization of its atomic orbitals. It is defined in terms of the dipole moment p induced by the local field F^{loc} acting on the atom by:

$$p = b(orb)\ F^{loc} \qquad (5.1)$$

The field-induced energy change, due to polarization of the atomic orbitals is then $-\frac{1}{2}b(orb)(F^{loc})^2$. It can easily be seen that the S.I. unit for the polarizability b(orb) is $JV^{-2}m^2$.

In field-ion emission, energy is usually expressed in eV and field in V/nm. A more convenient unit is therefore used and polarisability is expressed in $(eVV^{-2}nm^2)$ or

$(meVV^{-2}nm^2)$. The conversion factor is:
$1meVV^{-2}nm^2 = 1.6o2189\times10^{4O}JV^{-2}m^2$. In the literature, the most commonly used polarizability is the "Gaussian polarizability" b_s expressed in $\mathring{A}^3$. It is related to b(orb) by the relation:

$$b_s = b(orb)/4\pi\varepsilon_o \qquad (5.2)$$

Forbes and Wafi (1980), using their structured surface model, defined an "effective polarizability" b(eff) slightly greater than b(orb), and including a correction due to the zero-field dipole moment.

At a charged surface, as indicated in Chapter 4, we may also define a coefficient c_α due to orbitals polarization and partial-ionization of the atom. The field-induced change in binding energy $\Delta\Lambda$ is:

$$\Delta\Lambda = \tfrac{1}{2}c_\alpha F^2 \qquad (5.3)$$

F is the external field above the surface. A careful distinction must be made between b(orb) and c_α, as will be seen below.

Many attempts have been made to estimate parameters called "surface atom polarizability", both theoretically and experimentally: Müller (1964); Brandon (1964); Tsong and Kellogg (1975); Tsong and Müller (1970, 1971);

Tsong (1971 , 1978a, 1980) and also Forbes (1980a) from experiments of Culbertson et al. (1979). Most methods were invalid, because the formulae used were mathematically or physically invalid.

5.1.2 The α-Situation: Charge-Transfer and Orbitals Polarization

In the context of this chapter, we want to put a stricter interpretation on the meaning of the suffix α. It refers to an atom participating in normal field evaporation from a kink-site. Two physical effects are associated with the coefficient c_α : (1) partial electron transfer to the metal interior, to create the fractional surface atom charge; (2) polarization of the atomic orbitals of the resulting entity. These two effects can be combined, in a first approximation, as:

$$c_\alpha = c_\alpha\,(ct) + c_\alpha(orb) \qquad (5.4)$$

where (ct) and (orb) stand for charge-transfer and orbitals polarization. The total field-induced binding energy $\Delta\Lambda$ could also be split into two components, as:

$$\Delta\Lambda = \Delta\Lambda(orb) + \Delta\Lambda(ct) \qquad (5.5)$$

$\Delta\Lambda(orb)$ and $\Delta\Lambda(ct)$ are respectively the orbital-polarization and charge-transfer components of $\Delta\Lambda$. Like the free-space situation $\Delta\Lambda(orb)$ has an F^2 form given by:

$$\Delta\Lambda(\text{orb}) = \tfrac{1}{2}c_\alpha(\text{orb})F^2 \qquad (5.6)$$

It will be shown in a later section that an F^2 form may also be applied to $\Delta\Lambda(\text{ct})$.

If the self-consistent local field F_α^{loc} at the surface atom site could be defined, the component $\Delta\Lambda(\text{orb})$ would also be given by:

$$\Delta\Lambda(\text{orb}) = \tfrac{1}{2}b_\alpha(\text{orb})\ (F_\alpha^{loc})^2 \qquad (5.7)$$

$b_\alpha(\text{orb})$ is "the proper polarizability" of the surface atom in the α situation. The relationship between $b_\alpha(\text{orb})$ and $c_\alpha(\text{orb})$ is:

$$c_\alpha(\text{orb}) = \beta_\alpha^2\ b_\alpha(\text{orb}) \qquad (5.8)$$

where β_α defines the ratio of local and external fields by:

$$\beta_\alpha = F_\alpha^{loc}/F \qquad (5.9)$$

5.1.3 The δ-Situation

The other possibility that can be considered at a charged surface is an atom diffusing on top of a crystal plane. This defines the δ-situation . The corresponding coefficient is denoted by c_δ. A method of evaluating c_δ has been developed by Tsong and co-workers (1972, 1975, 1980). In particular Tsong and Kellogg (1975) measured c_δ for

an Iridium atom performing a field-induced directional walk on a Tungsten (110) plane. Its value has been estimated to be (2.28± 0.26) meV $V^{-2}nm^2$.

5.2 STANDARD AND ONSET APPEARANCE ENERGIES

The concept of appearance energy was introduced to field ion theory by Goldenfeld et al. (1974). In a retarding field experiment, an ion is brought to rest close to the retarding electrode of work-function ϕ_r. If the ion has charge re on arrival at the retarding electrode and needs a small voltage δ to halt it, then it is said to have an appearance energy A given by:

$$A = r(e\delta + \phi_r) \qquad (5.10)$$

A is in the nature of the electrical work done by the emitter + field system, in order to produce an ion from the corresponding neutral. Its value depends on the details of the ion emission process.

Theoretically, we define the "standard appearance energy" as the energy related to an ion that has just sufficient energy to escape over the top of the activation-energy barrier, and then is slowly moved away from the surface (Forbes: 1976). In the ionization process, the electron(s) must be directly transferred to the emitter Fermi-level. This standard appearance energy is denoted by $A^{stand}_{\alpha nr}$ for an

ion initially bound in a partially ionic state α. The subscript n denotes the charge-state immediately after escape, whilst the subscript r denotes the charge-state on arrival at the collector. r may be different from n as a result of post-ionization. In the same way, the activation energy for escape is denoted by $Q_{\alpha nr}$.

On the experimental side, the measured "onset appearance energy" $A_{\alpha nr}^{onset}$ was found to be less than the standard appearance energy. This has been discussed by Block and co-workers (1978), where the correction (a temperature dependent shift) was seen to be due partly to the statistical distribution of the bound-state vibrational energy, partly to electron transfer (during ionization) intc temporarily-unoccupied states below the emitter Fermi-level. We then have:

$$A_{\alpha nr}^{onset} = A_{\alpha nr}^{stand} - zkT \qquad (5.11)$$

where k is the Boltzmann constant, T the temperature and z a number of the order of 10, or less.

The binding energy Λ^F, is related to the activation energy and the standard appearance energy $A_{\alpha nr}^{stand}$ (Forbes: 1976, 1981; Ernst: 1979) by:

$$\Lambda^F = A_{\alpha nr}^{stand} + Q_{\alpha nr} - H_r \qquad (5.12)$$

where H_r is now given by the sum of the first "r-free-space

ionization potentials". From equation (5.11), it follows that:

$$\Lambda^F = (A_{\alpha nr}^{onset} + Q_{\alpha nr}) - H_r + zkT \qquad (5.13)$$

Relationships (5.12) and (5.13) are illustrated in Fig.(5.1.)

5.3 INTRODUCTION TO ERNST'S DATA

Ernst's results are summarised in Table (5.1). They are given in the form, values of $(A_{\alpha nr}^{onset} + Q_{\alpha nr})$, as field increases. They are compared with $(H_r+\Lambda^o)$ values taken from the literature (Tsong: 1978a). This can be seen from equation (5.12) when neglecting the zkT term, and taking the zero-field value Λ^o, as an approximation for the total binding energy Λ^F. $(A_{\alpha 11}^{onset} + Q_{\alpha 11})$ and $(A_{\alpha 12}^{onset} + Q_{\alpha 12})$ correspond to singly and doubly-charged arriving Rhodium ions respectively.

For singly charged Rhodium, $(A_{\alpha 11}^{onset} + Q_{\alpha 11})$ varies slightly with field and is in broad agreement with $(H_1+\Lambda^o) = (I_1 + \Lambda^o) = 13.21eV$. For doubly-charged Rhodium, $(A_{\alpha 12}^{onset} + Q_{\alpha 12})$ increases by about 1.3 eV when raising the field from 17 to 41V/nm, but is in the vicinity of $(H_2 + \Lambda^o) = (I_1+I_2+\Lambda^o) = 31.29eV$.

Ernst suggested that these deviations with decreasing field may be associated to field-dependent terms and temperature influences (Block and co-workers: 1978).

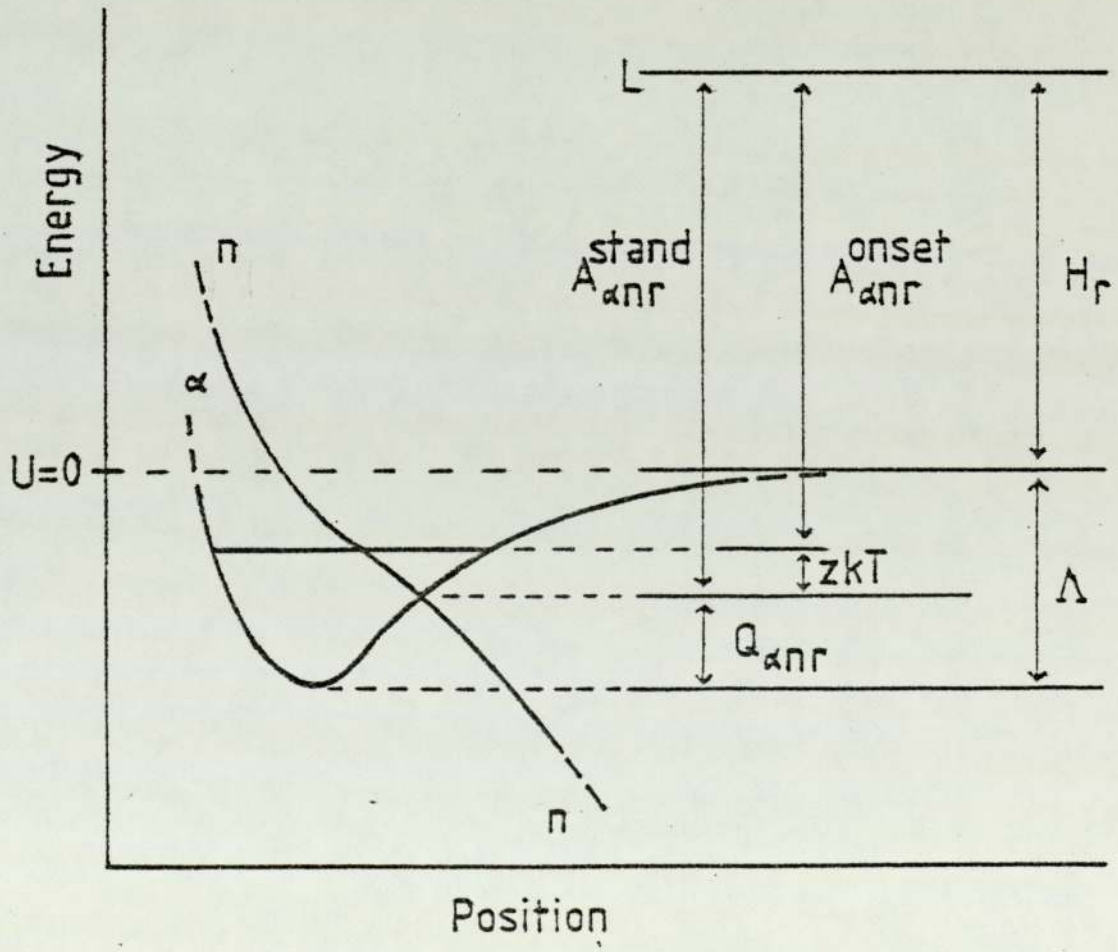

Fig. (5.1) : Schematic diagram illustrating the relationships between binding, activation and appearance energies (Equations (5.12) and (5.13)).

TABLE (5.1)

T(K)	F(V/nm)	$A_{\alpha 11}^{onset}+Q_{\alpha 11}$ (eV)	$A_{\alpha 12}^{onset}+Q_{\alpha 12}$ (eV)	$A_{\alpha 12}^{onset}+Q_{\alpha 11}$ (eV)
600	17.0±2.6	12.7±0.3	30.7±0.7	30.5±0.7
510	21.0±3.2	12.6±0.2	31.3±0.5	31.2±0.4
430	24.0±3.6	12.8±0.2	31.1±0.4	31.1±0.4
350	28.0±4.2	13.0±0.2	31.2±0.4	31.2±0.4
250	33.0±5.0		31.8±0.3	
100	41.0±6.2		32.05±0.22	

Experimentally measured sums of appearance and activation energies ($A_{\alpha nr}^{onset} + Q_{\alpha nr}$) with increasing field and their experimental error limits.

(From Ernst: 1979)

He evaluated the zkT term to be 0.3 eV and neglected it in his discussion. Finally, note that values of ($A_{\alpha 12}^{onset}+Q_{\alpha 12}$) and ($A_{\alpha 12}^{onset}+ Q_{\alpha 11}$) are equal within experimental error, i.e. that the singly and doubly-charged ions have the same activation energy. This set of data represents the main achievement of Ernst's work. It is the first experimental demonstration that the doubly-charged Rhodium ions must in fact be formed by post-ionization (because they derive from the same bonding state).

5.4 ANALYSIS OF ERNST'S DATA

5.4.1 Omission of the zkT Term

Neglecting the zkT term in equation (5.13) leads to:

$$\Lambda^F = (A_{\alpha nr}^{onset} + Q_{\alpha nr}) - H_r \qquad (5.14)$$

Knowing that n=1, r=2, we have:

$$\Lambda^F = (A_{\alpha 12}^{onset} + Q_{\alpha 12}) - H_2 \qquad (5.15)$$

Taking H_2=25.54eV for Rhodium, we get the values of Λ^F shown in Table (5.2):

TABLE (5.2)

T(K)	F(V/nm)	$A_{\alpha 12}^{onset}+Q_{\alpha 12}$(eV)	Λ^F(z=0)
600	17.0±2.6	30.7±0.7	5.16
510	21.0±3.2	31.3±0.5	5.76
430	24.0±3.9	31.1±0.4	5.56
350	28.0±4.2	31.2±0.4	5.66
250	33.0±5.0	31.8±0.3	6.26
100	46.0±6.2	32.05±0.22	6.51

Experimental $(A_{\alpha 12}^{onset} + Q_{\alpha 12})$ and Λ^F values when the zkT term is neglected.

A plot of Λ^F versus the external field F is shown in Fig.(5.2). Each data point is surrounded by a "box of measurement uncertainty" derived from Ernst's error limits, using simple linear formulae from equation (5.15). The zero-field binding energy Λ^o = 5.75eV is also shown.

Considering each "box of uncertainty" surrounding each point, it is difficult, at first sight, to speculate about the form of the field-dependence of Λ^F. Using a weighted linear regression and extrapolating the line back to zero-field leads to: Λ^o = (4.42±0.12)eV, so the value given by the regression results is less than the known one. Inclusion, in the binding energy expression, of a linear term of the form $-\theta F$, as suggested by Ernst following a proposal of Tsong (1971), and a quadratic term, is shown schematically in Fig.(5.2). It looks unconvincing. This hypothesis needs more theoretical justification, and a simple F^2 form will be assumed in what follows.

5.4.2 Inclusion of the zkT Term

The effect of including the zkT term will certainly be significant at high temperatures i.e. at low fields. This is investigated by plotting two sets of Λ^F values against F^2 (Fig. 5.3). The "original" data points (Λ^F, z=0 vs F^2) are shown as circles. The "corrected" data points (Λ^F, $z\neq 0$ vs F^2) were obtained from equation (5.13) by scanning the value of z: for a given z value a new set of Λ values are obtained via equation (5.13).

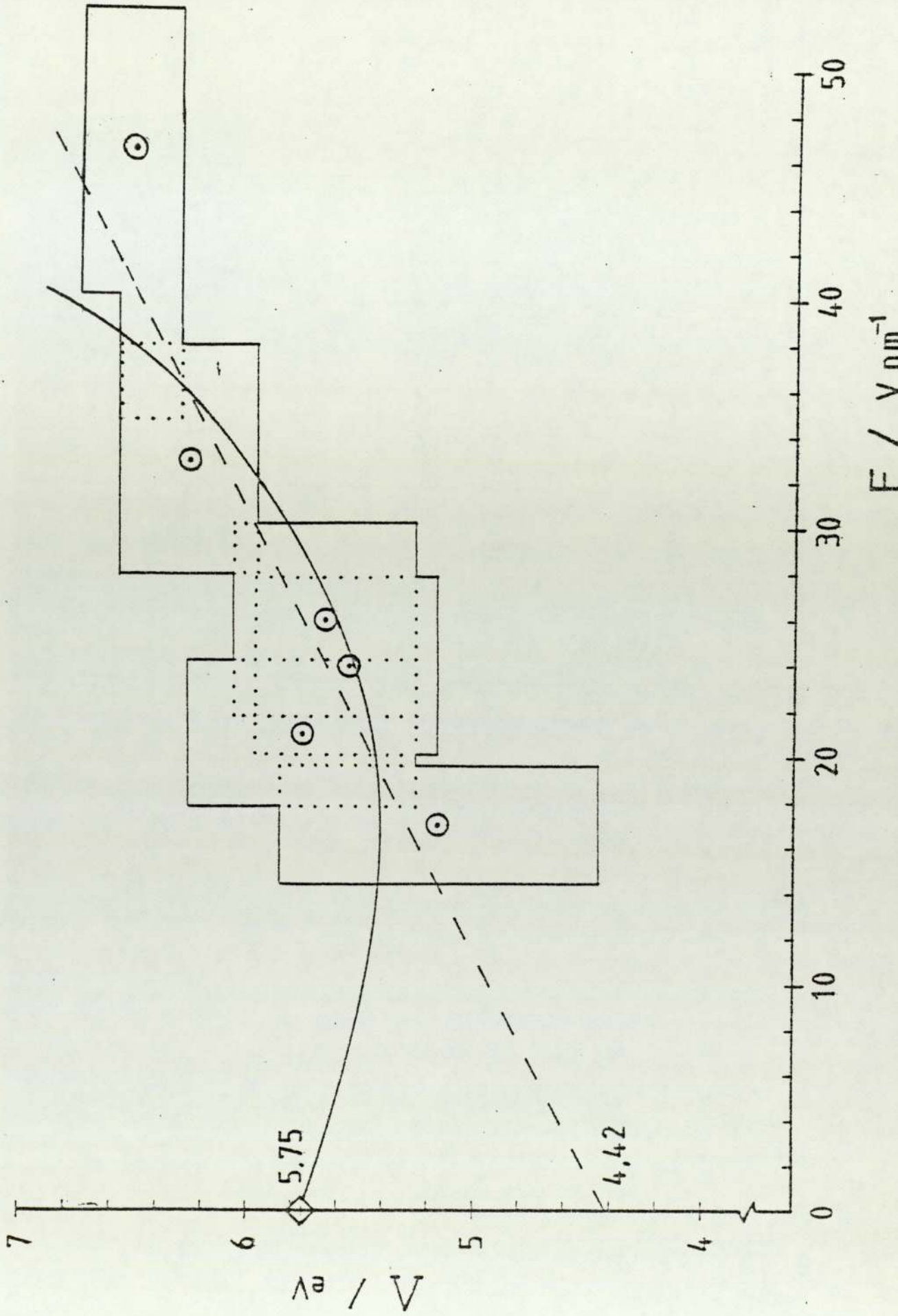

Fig. (5.2) : A plot of Λ^F vs F when z=0 in Equation (5.13)

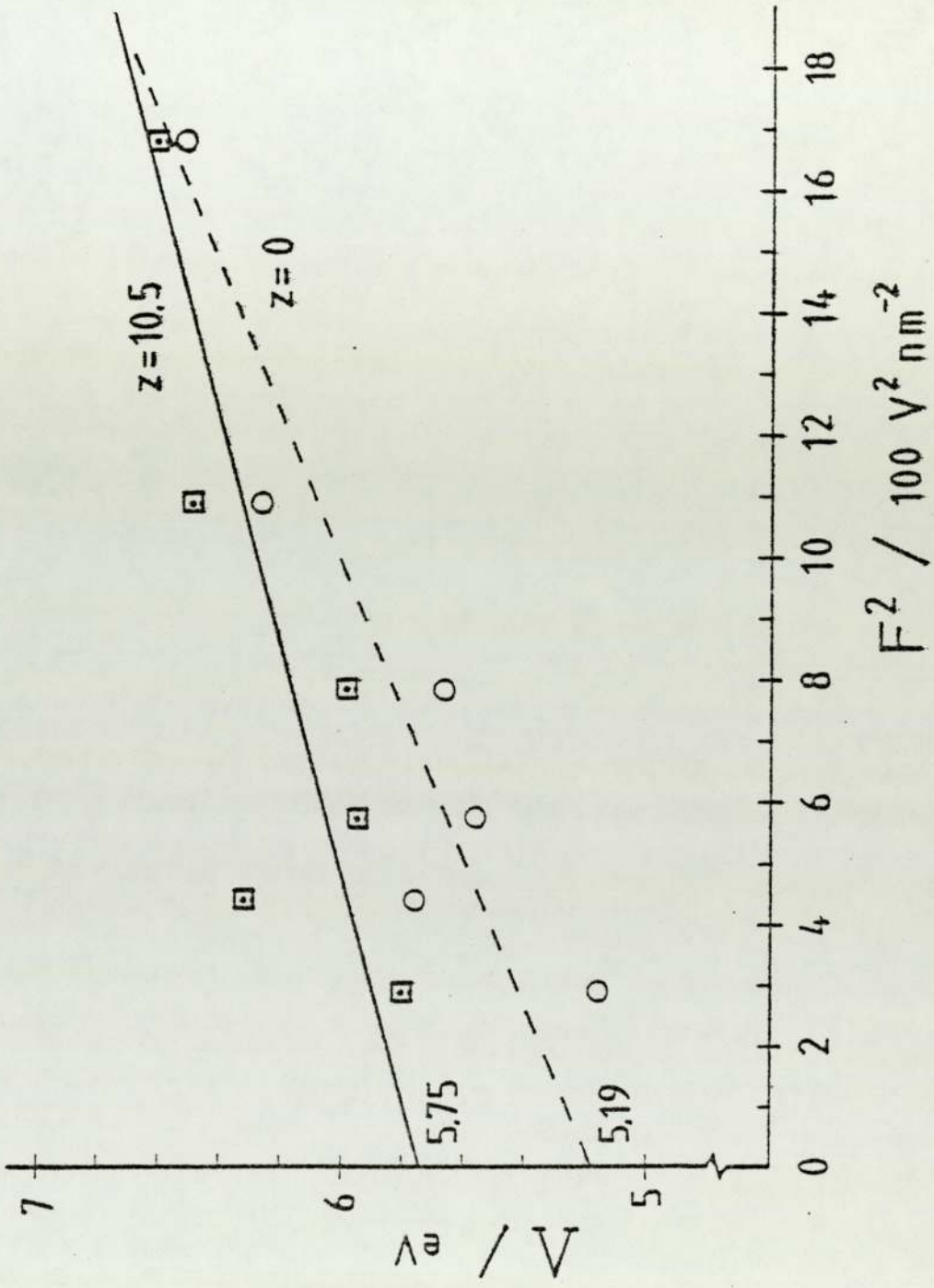

Fig. (5.3) : Plot of Λ^F vs F^2 for z=0 and z=10.5 in equation (5.13). The circles and the dashed regression line are for z=0. The boxed points and the continuous regression line are for z=10.5 which gives an intercept equal to 5.75 eV.

A linear regression in F^2 is then carried out to give a value for Λ^o. The value of z is changed and the process repeated, until the regressed Λ^o value is adequately close to the known zero-field value of 5.75eV. The "corrected" data points in Fig.(5.3)were found to correspond to z=10.5 in equation (5.13).

Regression calculations were performed to fit the form:

$$\Lambda^F = \Lambda^o + \tfrac{1}{2} c_\alpha F^2 \qquad (5.16)$$

and give the intercept (Λ^o_{der}) and the slope ($\frac{1}{2}c_\alpha$) as well as the corresponding standard deviations:

For z = 10.5; Λ^o_{der} = (5.75±0.17)eV.

For z = 0 ; Λ^o_{der} = (5.19±0.18)eV.

In order to make an estimate of the error in z, new regressions were made until a value of z is found for which the intercept is (Λ^o_{der}+0.17)eV. This occurs for z=13.7 and we write:

For z = 13.7 ; Λ^o_{der} = (5.92±0.17)eV.

We then take the difference between this new value of z and the previous one as an estimate of the error in z. Hence:

$$z = 10.5 \pm 3 \qquad (5.17).$$

Table (5.3) displays all the results so far.

TABLE(5.3)

T(K)	F(V/nm)	$(A_{\alpha 12}^{onset}+Q_{\alpha 12})$ (eV)	$\Lambda^F(z=0)$ (eV)	$\Lambda^F(z=10.5)$	3kT(eV)
600	17.0±2.6	30.7±0.7	5.16	5.70	0.16
510	21.0±3.2	31.3±0.5	5.76	6.22	0.13
430	24.0±3.9	31.1±0.4	5.56	5.95	0.11
350	28.0±4.2	31.2±0.4	5.61	5.98	0.09
250	33.0±5.0	31.8±0.3	6.26	6.49	0.06
100	41.0±6.2	32.05±0.22	6.51	6.60	0.03

List of Ernst's results together with Λ^F values for z=0 and z=10.5, derived from equation (5.13). 3kT is the uncertainty over the zkT term, with $\sigma(z)=3$.

5.4.3 Experimental Estimate of c_α

The derived value of z(10.5) is in good agreement with the z-value of approximately 10, derived by Block and co-workers (1978) from their work on the appearance energies of gas-phase ions. At 600K, the zkT value of 0.54eV is higher than the 0.3eV estimated by Ernst. No conclusion can yet be drawn regarding this discrepancy since Ernst made no comments about his value.

Regression procedures were also performed for singly charged ions and lead to : z=14±3. However, the Rh^+ data have only four points, over a limited field range, and are therefore of limited significance.

Finally, values of the slope ($\frac{1}{2}c_\alpha$) and the intercept (Λ^o_{der}) are shown in Table (5.4) below, for the three values of z.

TABLE (5.4)

z	Λ^o_{der}(eV)	$\frac{1}{2}c_\alpha$ ($meVV^{-2}nm^2$)
0	5.19±0.18	0.810±0.14
10.5	5.75±0.17	0.524±0.14
13.7	5.92±0.17	0.438±0.14

Values of the intercept Λ^o_{der} and the slope $\frac{1}{2}c_\alpha$ For z=0, 10.5, 13.7 as given from regressions of "original" and "corrected" data points.

Before giving an estimate of c_α, the total uncertainty in the slope $\frac{1}{2}c_\alpha$ is evaluated as follows. The difference in the value of the z=10.5 and z=13.7 regressions is $0.087meVV^{-2}nm^2$. This is then combined in quadrature with the standard deviation onthe z=10.5 slope, namely 0.14 to give:

$$\sigma(\tfrac{1}{2}c_\alpha) = \left[(0.087)^2 + (0.14)^2\right]^{\frac{1}{2}} \simeq 0.16 \text{meVV}^{-2}\text{nm}^2 \qquad (5.18)$$

Thus the "experimental" value of c_α is:

$$c_\alpha \simeq (1.05 \pm 0.3)\text{meVV}^{-2}\text{nm}^2 \qquad (5.19)$$

The corresponding values of S.I. units, and the corresponding Gaussian coefficient ($c_\alpha/4\pi\varepsilon_o$) are:

c_α (experimental estimate)	
Value in units used here	$(1.05 \pm 0.3)\text{meVV}^{-2}\text{nm}^2$
S.I. unit value	$(1.68 \pm 0.5) \times 10^{-40}\text{JV}^{-2}\text{m}^2$
Gaussian value	$(1.5 \pm 0.5)\ \text{Å}^3$

5.5 THEORETICAL ESTIMATE OF c_α

The field-induced binding energy $\Delta\Lambda$ is known to have an F^2-form as a first correct approximation. This is true for a neutral atom in free-space, where only the orbitals polarization component is considered, and can still be valid at a charged surface, as far as orbitals polarization, for a partially-ionized atom, is concerned.

No F^2 form has yet been demonstrated for the binding energy component $\Delta\Lambda(ct)$. A qualitative approach is hereby presented to show that an F^2-form could be an acceptable

first approximation for $\Delta\Lambda(ct)$. It is based on a simple argument suggested by Forbes (private communication).

As a simple approximation, the work necessary to remove a surface atom, as a neutral, from a charged surface to remote field-free-space may be split into three parts:

(1) The work necessary to depolarize the partially-charged surface atom back into a spherically-symmetric state, is assumed to be $\frac{1}{2}c_{\alpha}(orb)F^2$.

(2) The work necessary to transfer charge back, from the emitter into the atomic orbitals, to make the surface atom neutral; it is identified as $\Delta\Lambda(ct)$.

(3) The work necessary to remove the neutral atom to remote field-free-space. This work is assumed to be the same as Λ^o (even though there could be a small field-dependent correction).

Our interest lies in step (2), and a rough estimate of $\Delta\Lambda(ct)$ can be obtained as follows. The displaced charge (i.e. the charge q necessary to make the surface atom neutral again) has to be moved a distance d, where d is the spacing of the atomic layers normal to the surface. It is also assumed that the "mean" field in which this charge has to move is some fraction $\bar{\beta}$ of the external field F, with $\bar{\beta}$ a dimensionless parameter independent of F. The force acting on the charge is $q\bar{\beta}F$ and the work done on it is:

$$\Delta\Lambda(ct) = q\bar{\beta}Fd \tag{5.20}$$

The charge q is related to the surface charge density σ by: $q = \sigma S$, where S is the surface area per surface atom, and the surface charge density is given by Gauss relationship as: $\sigma=\varepsilon_o F$, where ε_o is the permittivity of free-space. If V_{at} denotes the atomic volume for the lattice in question, being given by: $V_{at} = Sd$, it follows that $\Delta\Lambda(ct)$ would have the F^2 form, which we write:

$$\Delta\Lambda(ct) = \varepsilon_o\bar{\beta}\, V_{at}F^2 \tag{5.21}$$

Hence, $c_\alpha(ct)$ would be given (approximately) by:

$$c_\alpha(ct) \simeq 2\varepsilon_o\bar{\beta}V_{at} \tag{5.22}$$

Using a structured surface model where depolarization effects are considered, Forbes estimated $\bar{\beta}$ as 0.2. The atomic volume for the Rhodium lattice is 0.0138 nm^3. We thus obtain:

$$c_\alpha(ct) \simeq 0.3 \text{ meVV}^{-2}\text{nm}^2.$$

Furthermore, Forbes obtained $c_\alpha(orb)=0.277$ $\text{meVV}^{-2}\text{nm}^2$ applicable to Tungsten, derived from the Culbertson et al experiments (1979). He suggests scaling the Tungsten value by the ratio of the tabulated free-space Gaussian polarizabilities g_s, as given by Miller and Bederson (1977), ignoring the difference in lattice structure. Given that

$g_s(Rh)=7.6$ Å; $g_s(W)=10$ Å^3, then $c_\alpha(orb)\simeq 0.2$ meVV^{-2}nm^2. Knowing that $c_\alpha=c_\alpha(ct)+c_\alpha(orb)$, the (rough) theoretical estimate of c_α is:

$$c_\alpha \simeq 0.5 \text{ meVV}^{-2}\text{nm}^2 \tag{5.23}$$

5.6 "POLARIZATION-TYPE" EFFECTS IN THE ACTIVATION ENERGY FORMULA

For a Gomer-type escape mechanism, the activation energy is given by equation (4.5) i.e.:

$$Q_{\alpha nr} = \tfrac{1}{2}\kappa\left(a-\frac{\pi^e}{ne}\right)^2\left(1-\frac{\eta_n'}{neF}\right)^{-2}\left(\frac{F^e}{F}-1\right)^2 \tag{5.24}$$

where π^e is given by:

$$\pi^e = (c_\alpha - c_n)F^e \tag{5.25}$$

Since it is known that n=1 for Rhodium, an estimate of c_1 can be made using Brandon's discussion (1964); this gives $c_1\simeq 0.15$ meVV^{-2}nm^2.

Using the experimental estimate of c_α as given by equation (5.19) we have $(c_\alpha - c_n)\simeq 0.9$ meVV^{-2}nm^2.

At the lowest temperature (T = 100K), the measured evaporation field for Rhodium is (46±6)V/nm. If we make an arbitrary estimate of F^e as around 50 V/nm, then $\frac{\pi^e}{ne}\simeq 0.045$ nm.

Taking the value of the electrical bonding distance for Rhodium somewhere between the neutral-atom radius (0.134 nm) and its diameter, the term $\frac{\pi^e}{ne}$ in equation (5.24) would be less than a, but not negligible. Hence, for Rhodium a polarization correction (the effect of the first bracket in equation (5.24) would not be insignificant). We shall see confirmation of this in Chapter 6.

5.7 DISCUSSION AND CONCLUSION

Ernst's results have been used to make an experimental estimate of the F^2-energy term coefficient c_α for Rhodium atom. This value is: $c_\alpha \simeq (1.05 \pm 0.3)$ meVV^{-2}nm^2 and agrees with the theoretical estimate to within a factor of about 2. Until a well-formulated quantum-mechanical discussion is established, experiments are for the time being the best way of evaluating c_α. An F^2-form has been assumed for the field-induced binding energy change $\Delta\Lambda$. However, the argument behind the form of $\Delta\Lambda(ct)$ should be taken as a classical first attempt only.

The variations of $(A_{\alpha nr}^{onset} + Q_{\alpha nr})$ with increasing field strength, i.e. decreasing temperature, are attributed to temperature-dependent shift (important at high temperatures). Consequently zkT-type corrections were necessary to Ernst's data and a plausible value for z was derived, namely, $z = 10.5 \pm 3$.

"Polarization-type" corrections could be significant for many materials when the Q-formula (equation (4.5)) is used. They certainly are for Rhodium.

Experiments of the type carried out by Ernst, based on measurements of appearance and activation energies, with increasing field, should be extended to other materials involved in field-ion techniques. It has been shown how a good experimental value of c_α could be derived for Rhodium. It will be shown, next, how surface-atomic parameters, such as κ , a could be derived using such experiments.

The results described in this chapter have been published as "A fresh look at the electric-field dependence of surface-atom binding energy", by R. G. Forbes and K. Chibane, Surface Science, 121, pp. 275-289, (1982).

CHAPTER 6

DERIVATION OF SOME SURFACE ATOMIC PARAMETERS FOR Rh

6.1 INTRODUCTION

In this chapter, we use Ernst's (1979) results again to derive some atomic surface parameters, namely the bonding distance, force-constant and vibration frequency for Rhodium. These are obtained from a weighted linear regression of experimentally measured critical distances x^{cr} against experimental values of activation energy Q. This will be called the "x-Q method". For comparison, a weighted linear regression of $Q^{\frac{1}{2}}$ versus $\frac{1}{F}$ is also carried out. This is known as the "Q-F method".

As an extension to Ernst's calculation, zkT corrections are included using the Chapter 5 value of z, 10.5±3, and values of x^{cr} are calculated from measured evaporation field and onset appearance energy. A repulsive term is also included but has very little effect on the final results.

In addition to his measurements of the field-dependence of appearance and activation energies reported and discussed in the preceding chapter, Ernst and Block (1980) used Ernst's data to determine the vibration frequency ν of Rhodium surface atoms under the influence of the applied electric field, as well as the corresponding Debye temperatures θ_c. His derived θ_c-values were found to be much lower than the θ_c value determined during a LEED experiment on a smooth RH(111) surface by Chan et al (1978).

The frequency values were determined by assumming a parabolic shape for the atomic potential energy curve, as in the "atomic-jug approximation", and values for critical distance x^{cr} were calculated from experimentally measured appearance energies assuming the validity of a simple curve-intersection model associated with a Gomer-type mechanism of field evaporation.

Ernst's data are shown below:

TABLE (6.1)

T	F(V/nm)	Q(eV)	Δx(nm)	$\nu(10^{12}$Hz)	θ_c(K)
100	41.0±6.2	0.05±0.02	0.02±0.04	2.4	120
250	33.0±5.0	0.20±0.10	0.06±0.04	1.6	80
350	28.0±4.2	0.60±0.15	0.07±0.06	2.4	120
430	24.0±3.6	0.70±0.20	0.10±0.06	1.8	90
510	21.0±3.2	0.90±0.20	0.10±0.10	2.1	100
600	17.0±2.6	1.50±0.30	0.17±0.07	1.6	80

Values for the Debye temperature θ_c, the vibrational amplitude Δx and the frequency ν, for Rhodium surface atoms. θ_c is found to be below the value (197±12)K reported by Chan et al.

(Taken from Ernst (1979))

In his calculations, Ernst assumed the equilibrium position to be at 0.15 nm from the electrical surface. The vibrational amplitude Δx is then calculated as the difference between the experimental x^{cr} and the value x_o = 0.15 nm.

6.2 SEMI-EXPERIMENTAL DERIVATION OF x^{cr}

We show in Fig.(6.1) the standard potential-energy U_n of an ion close to an emitter surface and the potential energy U_α of the atom in its initial bonding state α. We first consider the case of an ion that escapes in an n-fold charged state and arrives at a collector in the same charge-state.

The standard potential-energy U_n of this ion, close to the emitter in an external field F, is given from Chapter 1 as:

$$U_n = (H_n - n\phi^E) + S_n(x,F) \qquad (6.1)$$

all the symbols having their usual meaning. At $x=x^{cr}$, the crossing point in Fig.(6.1),we note that the standardised energy E^{cr} (Forbes: 1980b) is equal to the potential-energy U_n^{cr} at the crossing point. It follows that:

$$E^{cr} = (H_n - n\phi^E) + S_n(x^{cr},F) \qquad (6.2)$$

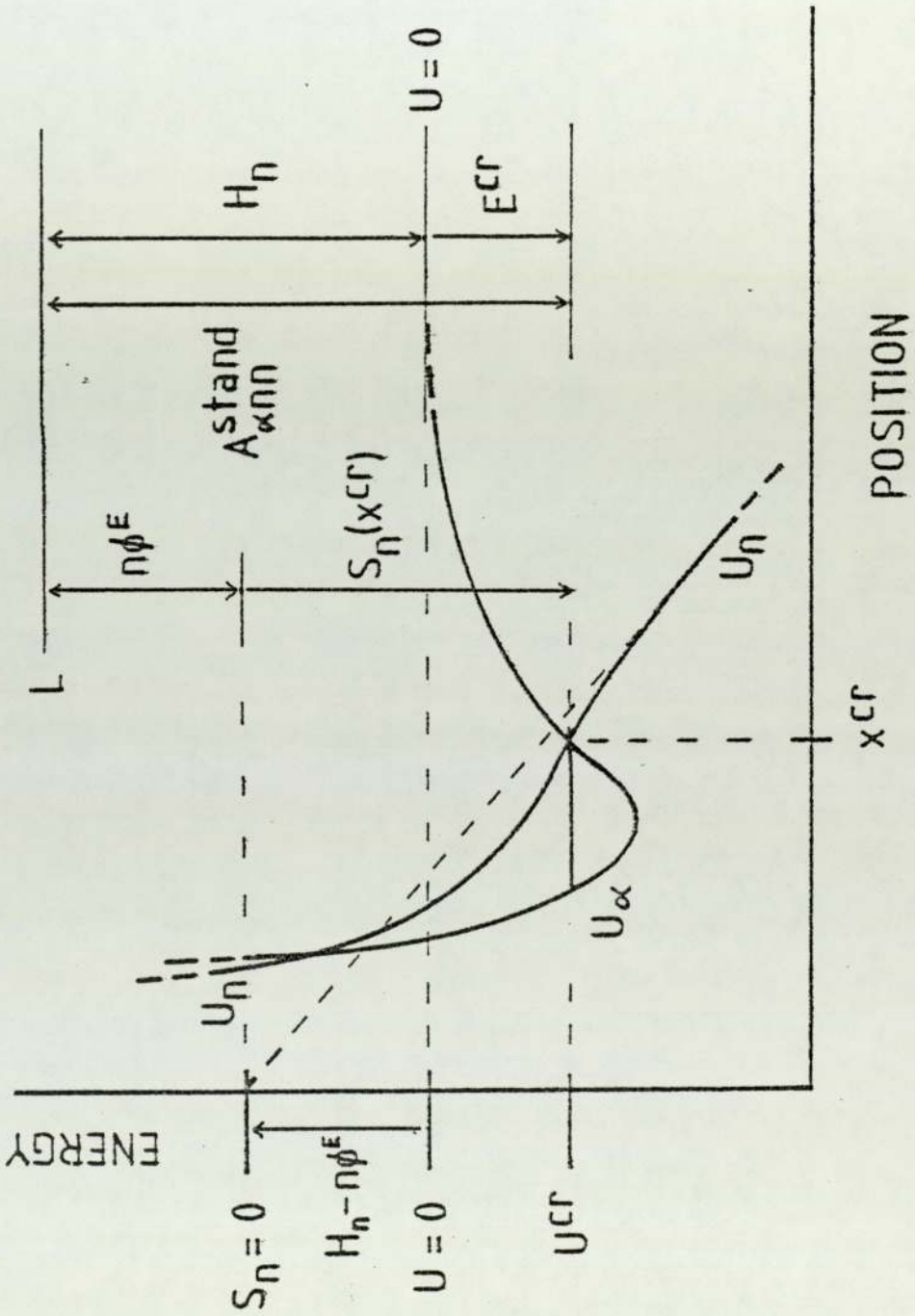

Fig. (6.1) : Standard potential energy curves for an atom and an ion, and illustrates the relationships (6.2) to (6.4).

Also, if the ion exhibits the standard appearance energy $A_{\alpha nn}^{stand}$, Fig.(6.1)shows that:

$$A_{\alpha nn}^{stand} - H_n = -E^{cr} \tag{6.3}$$

Combining equation (6.3) and (6.2) leads to:

$$S_n(x^{cr},F) - n\phi^E + A_{\alpha nn}^{stand} = 0 \tag{6.4}$$

$S_n(x^{cr},F)$ is now represented as a sum of electrostatic, image-potential, repulsion, polarization terms, i.e.:

$$S_n(x^{cr},F) = -neFx^{cr} - \frac{n^2e^2}{16\pi\varepsilon_o x^{cr}} + \frac{G}{(x^{cr})^t} - \frac{1}{2}c_n F^2 \tag{6.5}$$

We now assume that at the crossing point, the repulsive term is a fraction ξ of the image-potential term and write:

$$\frac{G}{(x^{cr})^t} = \xi\frac{n^2e^2}{16\pi\varepsilon_o x^{cr}} \tag{6.6}$$

Relation (6.4) can then be re-arranged and re-written as:

$$neFx^{cr} + \frac{n^2e^2}{16\pi\varepsilon_o x^{cr}}(1-\xi) + \frac{1}{2}c_n F^2 + n\phi^E - A_{\alpha nn}^{stand} = 0 \tag{6.7}$$

or

$$neFx^{cr} - \left[A_{\alpha nn}^{stand} - n\phi^E - \frac{1}{2}c_n F^2\right] + \lambda\frac{n^2e^2}{16\pi\varepsilon_o x^{cr}} = 0 \tag{6.8}$$

where $\lambda=(1-\xi)$

If we consider an ion that arrives at the retarder in a charge-state r different from the charge-state at escape n (as in Ernst's experiments where n=1, r=2), the corresponding appearance energies are related by the relation (Forbes: 1976):

$$A^{stand}_{\alpha nr} = A^{stand}_{\alpha nn} + \sum_{s=n+1}^{r} I_s \qquad (6.9)$$

where I_s is the s-th free-space ionization potential. Thus, equation (6.8) becomes:

$$neFx^{cr} - \left[A^{stand}_{\alpha nr} - n\phi^E - \frac{1}{2} c_n F^2 - \sum_{s=n+1}^{r} I_s\right] + \lambda \frac{n^2e^2}{16\pi\varepsilon_o x^{cr}} = 0 \qquad (6.10)$$

But really, the measured quantity is the onset appearance energy $A^{onset}_{\alpha nr}$, which is related to the corresponding standard appearance energy via equation (5.11). Substituting the latter relation into equation (6.10) leads to:

$$neFx^{cr} - \left[A^{onset}_{\alpha nr} - n\phi^E - \frac{1}{2} c_n F^2 - \sum_{s=n+1}^{r} I_s + zkT\right] + \lambda \frac{n^2e^2}{16\pi\varepsilon_o x^{cr}} = 0 \qquad (6.11)$$

we now put

$$Y = A^{onset}_{\alpha nr} - n\phi^E - \frac{1}{2} c_n F^2 - \sum_{s=n+1}^{r} I_s + zkT \qquad (6.12)$$

Y is a quantity independent of distance. Thus,

$$neFx^{cr} - Y + \lambda \frac{n^2e^2}{16\pi\varepsilon_o x^{cr}} = 0 \qquad (6.13a)$$

$$\text{i.e. } (16\pi\varepsilon_o ne)F(x^{cr})^2 - 16\pi\varepsilon_o Yx^{cr} + \lambda n^2e^2 = 0 \qquad (6.13b)$$

Solving equation (6.13) for x^{cr} gives:

$$x^{cr} = \frac{Y + (Y^2 - \frac{(ne)^3 F\lambda}{4\pi\varepsilon_o})^{\frac{1}{2}}}{2neF} \qquad (6.14)$$

Since Y is a function of parameters that can be determined experimentally, this form leads to "experimental" values of x^{cr}, as a function of measured evaporation field. The effect of λ is not very significant and it will normally be put equal to unity.

6.3 THE x-Q METHOD

Assuming a parabolic-like potential well for the vibrating atom, the activation-energy Q at x^{cr} is:

$$Q = \frac{1}{2}\kappa(x^{cr} - a)^2 \qquad (6.15)$$

where κ is the force-constant and a the electrical bonding distance (i.e. the distance of the well base from the emitter's electrical surface).

Another way of writing equation (6.15) is simply:

$$x^{cr} = a + (2/\kappa)^{\frac{1}{2}} . Q^{\frac{1}{2}} \qquad (6.16)$$

Numerical estimates of x^{cr} can be made from equation (6.14) using experimental appearance energy values at the measured temperature and evaporation field. Other parameters would be taken from literature.

A plot of x^{cr} versus $Q^{\frac{1}{2}}$ should therefore be linear, and average values of a and κ can then be obtained from a weighted linear regression of x^{cr} against $Q^{\frac{1}{2}}$, as long as these parameters (a,κ) are not significant functions of field. This method, based on measurements of appearance and activation energies will be called the "x-Q method".

6.4 THE Q-F METHOD

A new activation-energy formula was introduced in Chapter 4 for Gomer-type mechanisms through equation (4.1), i.e.:

$$Q = \Omega\left(\frac{F^e}{F} - 1\right)^2$$

where F is the external field, F^e the zero-Q evaporation field and Ω is given by equations (4.2) and (4.3).

The above equation is then re-arranged into the form:

$$Q^{\frac{1}{2}} = \Omega F^e\left(\frac{1}{F}\right) - \Omega \qquad (6.17)$$

A $Q^{\frac{1}{2}}$ versus $\frac{1}{F}$ plot would be linear if Ω can be treated approximately as a constant, except that deviations from

linearity are expected at very low temperatures probably due to ion-tunnelling (Chapter 4). A linear regression of $Q^{\frac{1}{2}}$ against $\frac{1}{F}$ would give values for Ω and F^e, hence a value for κ from equation (4.3). This constitutes the method we call the "Q-F method".

6.5 ANALYSIS OF THE x-Q METHOD

For the Rhodium ions in Ernst's experiments, n=1 and r=2, so that Y in equation (6.12) is now given by:

$$Y = A_{\alpha 12}^{onset} - \phi^E - I_2 - \frac{1}{2} c_1 F^2 + zkT \qquad (6.18)$$

where $A_{\alpha 12}^{onset}$ values are obtained from data in Tables (5.1) and (6.1). The values used for other parameters are:

ϕ^E = 5.0 eV (Pierce and Spicer: 1972), but the effect of changing the work-function (±0.5eV) will also be discussed.

I_2 = 18.08eV (Tsong: 1978a)

c_1 = 0.15meVV^{-2}nm^2 (See Chapter 5)

z = 10.5±3 (See Chapter 5)

k = 8.617×10^{-5} eV/K (Boltzmann constant)

Different approximations were used in equation (6.18). They are:

(1) standard case : where ϕ^E = 5eV and λ=1

(2) simple case: where the F^2-energy and zkT terms are omitted, and λ=1.

(3) inclusion of a repulsive term : where the F^2-energy and zkT terms are included, and λ is variable.

(4) different work-function: where ϕ^E = 4.5 and 5.5eV are used.

The final surface parameters (a,κ,ν) values are based on the "standard case" calculations. Cases (2), (3) and (4) will be included for comparisons only.

6.5.1 The Standard Case and the x-Q Plot

The corresponding results are summarised in Table (6.2) below:

TABLE (6.2)

T (K)	F (V/nm)	$Q_{\alpha 12}$ (eV)	$A_{\alpha 12}^{onset}$ (eV)	$\frac{1}{2}c_1F^2$ (eV)	(10.5±3)kT (eV)
100	41.0±6.2	0.05±0.02	32.1±0.2	0.126	0.090±0.026
250	33.0±5.0	0.2±0.1	31.5±0.2	0.082	0.226±0.065
350	28.0±4.2	0.6±0.15	30.6±0.25	0.059	0.317±0.090
430	24.0±3.6	0.7±0.2	30.4±0.2	0.043	0.389±0.111
510	21.0±3.2	0.9±0.2	30.4±0.3	0.033	0.461±0.131
600	17.0±2.6	1.5±0.3	29.2±0.4	0.022	0.542±0.155

Experimental $A_{\alpha 12}^{onset}$ and $Q_{\alpha 12}$ values used for the "standard case". The values for c_1 and z were taken from Chapter 5.

Hence, the values of Y and x^{cr} are:

TABLE (6.3)

T (K)	F (V/nm)	Y (eV)	σ(Y) (eV)	x^{cr} (nm)	$\sigma(x^{cr})$ (nm)
100	41.0±6.2	8.984	0.226	0.166	0.038
250	33.0±5.0	8.564	0.265	0.207	0.043
350	28.0±4.2	7.778	0.340	0.219	0.048
430	24.0±3.6	7.666	0.311	0.262	0.053
510	21.0±3.2	7.748	0.431	0.314	0.063
600	17.0±2.6	6.640	0.555	0.326	0.074

Derived values of Y from equation (6.18) and x^{cr} from equation (6.14) for the "standard case".

The uncertainties on Y are simply given by:

$$\sigma(Y) = \sigma(A_{\alpha 12}^{onset}) + 3kT \qquad (6.19)$$

It is assumed that F^2-energy terms and ionization terms constribute negligibly to σ(Y) and that ϕ^E is known exactly. $\sigma(x^{cr})$ is obtained from σ(Y) and the tabulated σ(F) values, by means of the standard error-propagation formula applied as follows.

x^{cr} can be expressed in a general form as:

$$x^{cr} = f(Y,F) \tag{6.20}$$

hence,

$$\sigma^2(x^{cr}) = \left(\frac{\partial x^{cr}}{\partial Y}\right)\sigma^2(Y) + \left(\frac{\partial x^{cr}}{\partial F}\right)^2 \sigma^2(F) \tag{6.21}$$

Using

$$x^{cr} = \frac{Y + \left[Y^2 - \frac{(ne)^3 F}{4\pi\varepsilon_o}\right]^{\frac{1}{2}}}{2neF} \tag{6.22}$$

we have:

$$\sigma^2(x^{cr}) = \frac{1}{(2neF)^3}\left[1 + \frac{Y}{\left[Y^2 - \frac{(ne)^3 F}{4\pi\varepsilon_o}\right]^{\frac{1}{2}}}\right]^2 \sigma^2(Y) + \tag{6.23}$$

$$\left[\frac{1}{2neF^2}\left[Y + \left(Y^2 - \frac{(ne)^3 F}{4\pi\varepsilon_o}\right)^{\frac{1}{2}}\right] + \frac{1}{4\times 4\pi\varepsilon_o F\left(Y^2 - \frac{(ne)^3 F}{4\pi\varepsilon_o}\right)^{\frac{1}{2}}}\right]^2 \sigma^2(F)$$

Finally, Table (6.4) below shows the "requested" data for the x^{cr} versus $Q^{\frac{1}{2}}$ plot.

TABLE (6.4)

T(K)	F(V/nm)	x^{cr}(nm)	$\sigma(x^{cr})$ (nm)	$Q_{\alpha 12}^{\frac{1}{2}}$ $(eV)^{\frac{1}{2}}$	$\sigma(Q_{\alpha 12}^{\frac{1}{2}})$
100	41.0±6.2	0.166	0.038	0.224	0.045
250	33.0±5.0	0.207	0.043	0.447	0.11
350	28.0±4.2	0.219	0.048	0.775	0.10
430	24.0±3.6	0.262	0.053	0.837	0.12
510	21.0±3.2	0.314	0.063	0.949	0.11
600	17.0±2.6	0.326	0.074	1.225	0.12

Values of x^{cr} and $Q^{\frac{1}{2}}$ on which Fig. (6.2) is based.

The uncertainty on $Q^{\frac{1}{2}}$ is:

$$\sigma(Q^{\frac{1}{2}}) = \frac{\sigma(Q)}{2Q^{\frac{1}{2}}} \qquad (6.24)$$

and is derived from the tabulated $\sigma(Q)$.

The x^{cr} versus $Q^{\frac{1}{2}}$ plot is shown as Fig.(6.2).

Each point is surrounded by its error limits; a weighted linear regression (ignoring the uncertainties in $Q^{\frac{1}{2}}$) gives the straight line shown. The desired parameters are then given from the regression results, i.e.:

$$a = (0.129 \pm 0.020)\ \text{nm}$$

$$\kappa = (80 \pm 30)\ \text{eV/nm}^2$$

$$\tfrac{1}{2}\kappa a^2 = (0.67 \pm 0.06)\ \text{eV} \qquad (6.25)$$

with

$$\phi^E = 5\text{eV}.$$

6.5.2 Different Choice of Work-Function

The value used above for the work-function for Rhodium, namely 5 eV, was derived from photoemission experiments. However, this value may not be entirely applicable, and results (6.25) do not include any effect due to any uncertainty in ϕ^E. Therefore, the calculations were repeated for ϕ^E values of 4.5 eV and 5.5 eV. Since we have

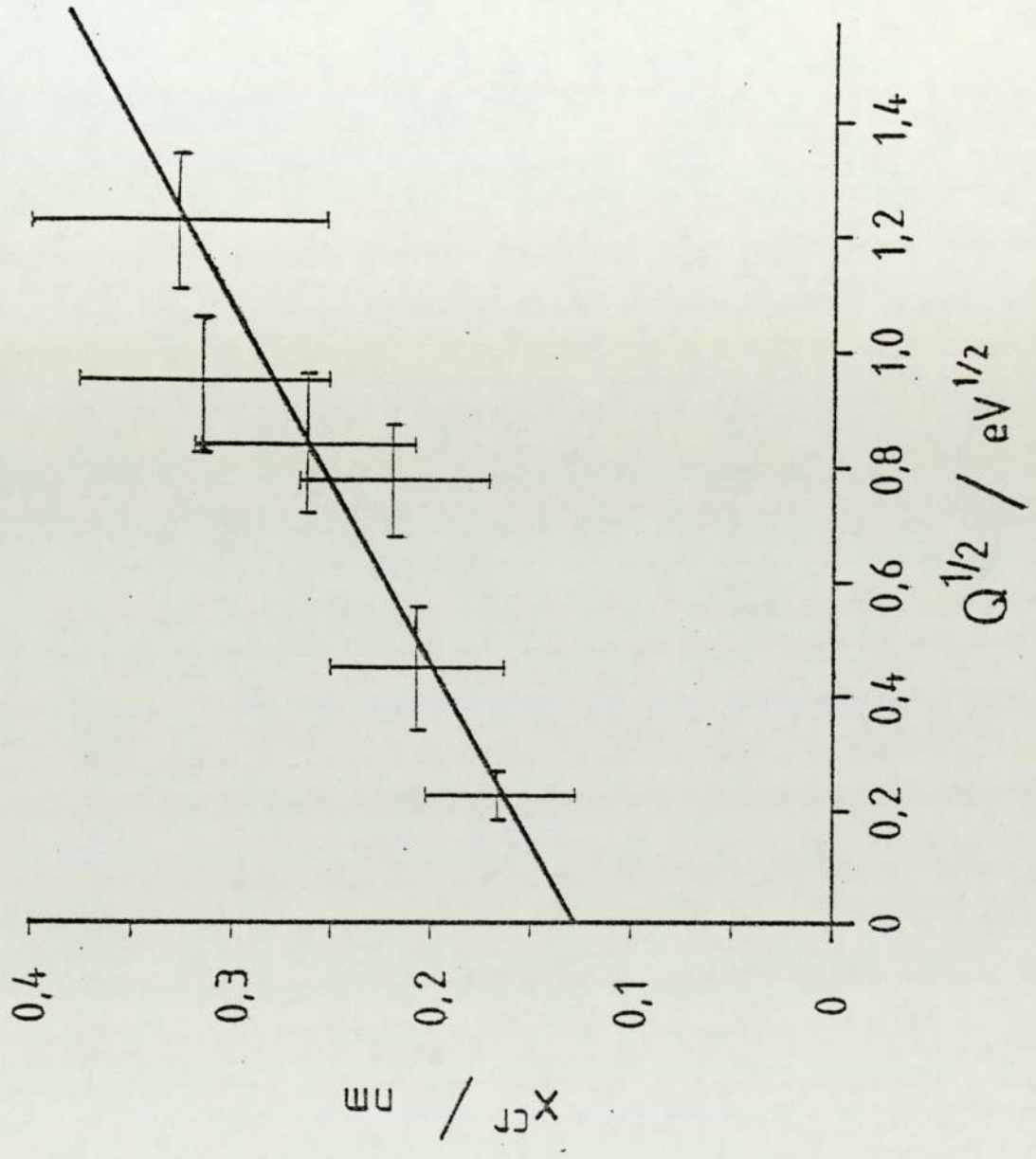

Fig. (6.2) : Plot of x^{cr} vs $Q^{\frac{1}{2}}$, for the data in Table (6.4). The straight line is obtained by weighted linear regression.

no means of estimating the real error limit on ϕ^E, the ±0.5 eV variation has been taken to be a reasonable one.

Table (6.5) shows the x^{cr} results for ϕ^E=4.5 eV and 5.5 eV, whilst Table (6.6) gives the corresponding a and κ values.

TABLE (6.5)

T(K)	F(V/nm)	ϕ^E=4.5eV		ϕ^E=5.5eV	
		x^{cr}(nm)	$\sigma(x^{cr})$	x^{cr}(nm)	$\sigma(x^{cr})$
100	41	0.184	0.038	0.147	0.039
250	33	0.227	0.045	0.186	0.043
350	28	0.243	0.049	0.194	0.048
430	24	0.288	0.055	0.235	0.052
510	21	0.343	0.066	0.285	0.061
600	17	0.361	0.077	0.288	0.074

Effect of choosing different work-functions in equation (6.18). x^{cr} is calculated from equation (6.14).

The above results and Table (6.4) show that varying the work-function by 10%, induces a change in each x^{cr} value (corresponding to ϕ^E = 5eV) by more than 30% (up to 34%) and is not a negligible effect. As for the a and κ values, they are:

TABLE (6.6)

	slope ($nmeV^{-\frac{1}{2}}$)	a (nm)	κ (eV/nm^2)
ϕ^E = 4.5eV	0.173±0.029	0.143±0.02	67±23
ϕ^E = 5.0eV	0.158±0.029	0.129±0.02	80±30
ϕ^E = 5.5eV	0.143±0.028	0.115±0.02	98±39

Regressed values of a and κ for different work-functions.

This shows clearly that choice of ϕ^E value has significant effect on prediction of a and κ values but has little effect on the error limit. For an 0.5eV variation in ϕ^E, a varies by about 14 pm. Given the error limits in equation (6.25) , a 10% variation in ϕ^E would then lead to values of a and κ as:

$$a = 0.129 \pm 0.034 \text{ nm}$$

$$\kappa = 80 \ (-36/+57) \ eV/nm^2 \qquad (6.26)$$

$$\phi^E = 5.0 \pm 0.5 \text{ eV}.$$

6.5.3 The Simple Case

This is the case where F^2-energy and zkT terms are omitted from equation (6.18) which simplifies to:

$$Y = A_{\alpha 12}^{onset} - \phi^E - I_2 \qquad (6.27)$$

The repulsive factor λ is also put equal to 1. New calculated values of Y, $\sigma(Y)$, x^{cr} and $\sigma(x^{cr})$ were obtained and are shown in Table (6.7).

TABLE (6.7)

T(K)	F(V/nm)	Y(eV)	$\sigma(Y)$	x^{cr}(nm)	$\sigma(x^{cr})$
100	41±6.2	9.02	0.20	0.168	0.038
250	33±5.0	8.42	0.20	0.200	0.043
350	28±4.2	7.52	0.25	0.206	0.046
430	24±3.6	7.32	0.20	0.245	0.050
510	21±3.2	7.32	0.30	0.289	0.058
600	17±2.6	6.12	0.40	0.286	0.067

Results for the "simple case", where F^2-energy term and zkT term are omitted in equation (6.18).

Values of a, κ were derived from new regression of x^{cr} against $Q^{\frac{1}{2}}$ and they are:

$$a = 0.140 \pm 0.019 \text{ nm}$$

$$\kappa = 135 \pm 58 \text{ eV/nm} \qquad (6.28)$$

$$\phi^E = 5.0 \text{ eV}.$$

These results show that omitting the F^2-energy term and in particular the zkT terms causes a to increase by about 8.5%, but κ to increase by more than 50%. This variation

is significant and it is important that the above terms - especially the zkT term - be included.

6.5.4 With Repulsion

At the crossing point of the atomic and ionic curves, the constant G of the t-th power repulsive term is given from equation (6.6), by:

$$G = \xi \frac{n^2e^2}{16\pi\varepsilon_o} (x^{cr})^{t-1} \tag{6.29}$$

On the other hand, the potential-energy of an ion outside an emitter surface, in the absence of any external field, is simply given by:

$$U_n = (H_n - n\phi^E) - \frac{n^2e^2}{16\pi\varepsilon_o x} + \frac{G}{(x)^t} \tag{6.30}$$

At the ionic bonding point a_n (i.e. the minimum point in the ionic curve) it follows that:

$$\frac{n^2e^2}{16\pi\varepsilon_o a_n^2} - \frac{tG}{a_n^{t+1}} = 0 \tag{6.31}$$

and hence G is also defined by:

$$G = \frac{n^2e^2}{16\pi\varepsilon_o} \left(\frac{1}{t}\right) . \; a_n^{t-1} \tag{6.32}$$

Identifying equations (6.29) and (6.32) leads to:

$$\xi = \frac{1}{t} \left(\frac{a_n}{x^{cr}}\right)^{t-1} \tag{6.33}$$

For Rhodium, we somewhat arbitrarily take t=9 and $a_n \simeq 0.13$ nm. The resulting values of $\lambda=(1-\xi)$ vary from 0.98 (at F = 41 v/nm) to 0.99 (at F=17 V/nm). Thus we expect inclusion of repulsion to have no significant effect and the use of $\lambda=1$ in the main calculations is justified. Inclusion of the appropriate λ-values leads to the results:

$$a = 0.131 \pm 0.019 \text{ nm}$$

$$\kappa = 82 \pm 30 \text{ eV/nm}^2 \qquad (6.34)$$

$$\phi^E = 5\text{eV}$$

These are not significantly different from those of equation (6.25).

6.6 ANALYSIS ON THE Q-F METHOD

A plot of $Q^{\frac{1}{2}}$ against $\frac{1}{F}$ from data in Table (6.8) below, is shown as Fig. (6.3).

TABLE (6.8)

T(K)	F(V/nm)	$Q_{\alpha 12}$(eV)	$Q_{\alpha 12}^{\frac{1}{2}}(eV^{\frac{1}{2}})$	$\frac{1}{F}$(nm/V)
100	41	0.05±0.02	0.224±0.045	0.0244±0.0037
250	33	0.20±0.10	0.447±0.11	0.0303±0.0046
350	28	0.60±0.15	0.775±0.10	0.0357±0.0054
430	24	0.70±0.20	0.837±0.12	0.0417±0.0063
510	21	0.90±0.20	0.949±0.11	0.0476±0.0073
600	17	1.5 ±0.30	1.225±0.12	0.0588±0.0090

Data on which the $Q^{\frac{1}{2}}$ vs $\frac{1}{F}$ plot of Fig. (6.3) are based.

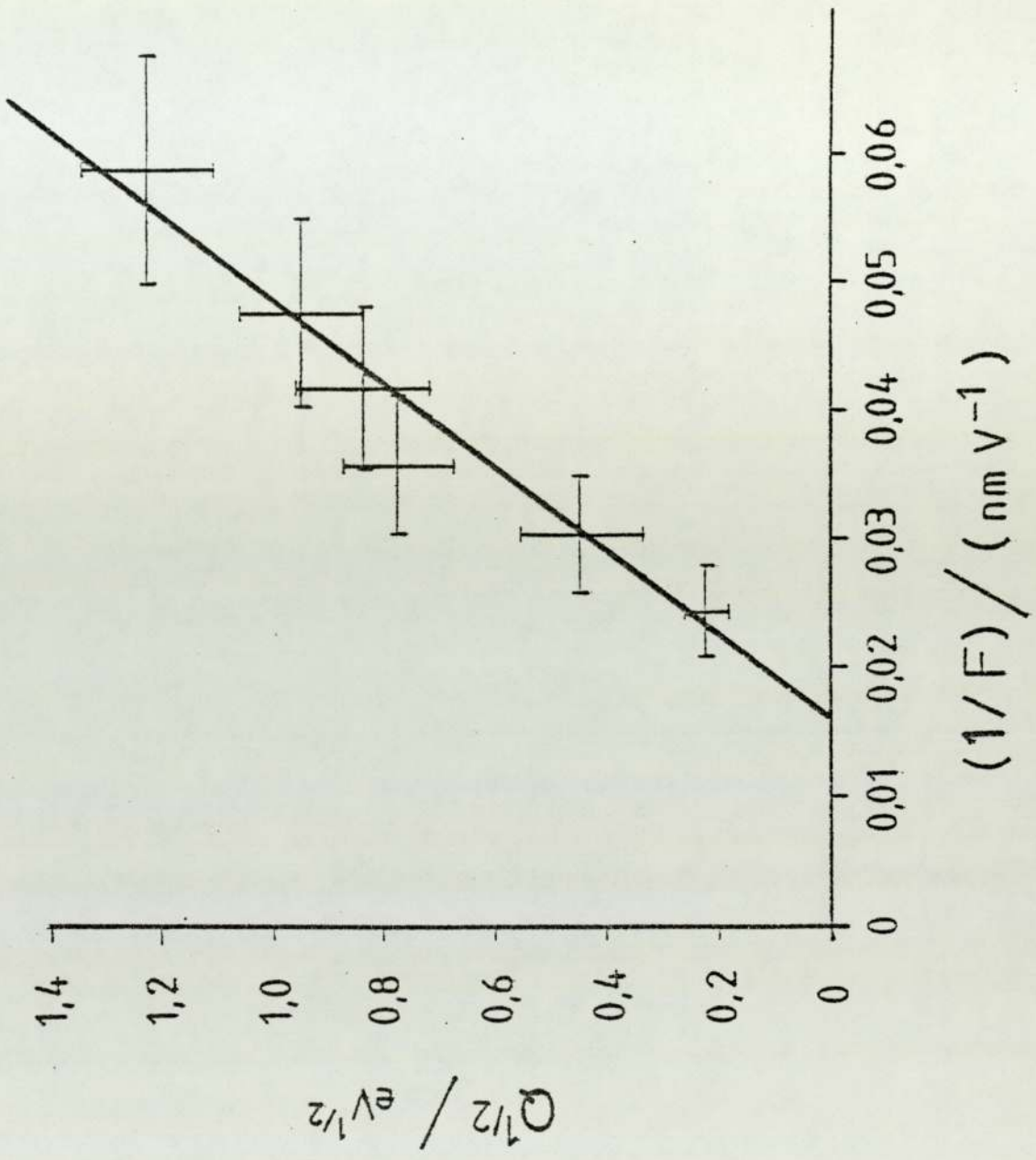

Fig. (6.3) : Plot of $Q^{\frac{1}{2}}$ vs $\frac{1}{F}$, for the data in Table (6.8). The straight line is obtained by weighted linear regression.

The uncertainties on $\frac{1}{F}$ are given by:

$$\sigma(\frac{1}{F}) = \frac{\sigma(F)}{F^2} \tag{6.35}$$

A weighted linear regression on the $Q^{\frac{1}{2}}$ vs $\frac{1}{F}$ plot (ignoring the uncertainties in $\frac{1}{F}$) leads to:

$$\Omega = 0.25 \pm 0.11 \text{ eV}$$
$$F^e = 61 \pm 19 \text{ V/nm} \tag{6.36}$$

6.7 COMPARISON OF THE x-Q AND Q-F PLOTS

The value of the parameter Ω just derived (0.25 eV) from the Q-F plot is certainly not comparable with the product $\frac{1}{2}\kappa a^2$ (0.67eV) as given by the x-Q plot. This experimental finding suggests that equation (4.3) is a better approximation for Ω. In fact, assuming the correlation and repulsion correction bracket equal to unity, we can re-write equation (4.3) into the form:

$$\Omega \simeq \frac{1}{2} \kappa a^2 \left[1 - \frac{(c_\alpha - c_1)}{nea} F^e\right]^2 \tag{6.37}$$

For Rhodium, an estimate of $(c_\alpha - c_1)$ is 0.9 $meVV^{-2}nm^2$ (Chapter 5). Using the 61 V/nm F^e value just derived, estimate equation (6.25) for a and estimate equation (6.36) for Ω, we obtain:

$$\frac{(c_\alpha - c_1)F^e}{ne} = (0.055 + 0.025)\ \text{nm} \tag{6.38}$$

$$\kappa = 91 \pm 89\ \text{eV/nm}^2 \tag{6.39}$$

where

$$\kappa = \frac{2\Omega}{\left[a - \frac{(c_\alpha - c_1)F^e}{ne}\right]^2} \tag{6.40}$$

This estimate of κ is compatible with that derived from the x-Q method but the error limits are wider.

The x-Q method is a direct method for obtaining estimates of a and κ and is better in that respect, whilst the Q-F method needs additional information, namely $(c_\alpha - c_1)$ and a itself to give an estimate of κ. However, the Q-F method gives a far better estimate of Ω showing that polarization and partial ionization-like corrections ought to be included and that equation (4.3) or equation (6.37) are better approximations of Ω than the product $\frac{1}{2}\kappa a^2$.

6.8 VIBRATION FREQUENCY AND DEBYE TEMPERATURE

The vibration frequency ν is related to the force-constant κ by:

$$\nu = \frac{1}{2\pi}\left(\frac{\kappa}{m}\right)^{\frac{1}{2}} \tag{6.41}$$

where m is the mass of the vibrating atom.

For the Rhodium isotope, m = 103 u. Knowing that

$$1u \simeq 1.66\times10^{-27} \text{ kg} \tag{6.42}$$

and using the appropriate units of κ in the S.I. system leads to:

$$\nu \simeq 1.4(-0.3/+0.5)\times10^{12} \text{ Hz} \tag{6.43}$$

This estimate and its error limits is obtained by considering result (6.26) for κ.

The corresponding temperature θ_c is given by:

$$\theta_c = \frac{h}{k}\nu \tag{6.44}$$

where h and k are the Planck and Boltzmann constants taken as:

$$\begin{aligned} h &= 6.62620\times10^{-34} \text{ J/s} \\ k &= 1.38062\times10^{-23} \text{ J/K} \end{aligned} \tag{6.45}$$

Thus an estimate of θ_c is:

$$\theta_c = 67 \ (-14/+24) \text{ K} \tag{6.46}$$

6.9 DISCUSSION: VIBRATION FREQUENCY, CHARACTERISTIC TEMPERATURE AND FORCE-CONSTANT

The presently derived values of vibration frequency ν, force-constant κ and characteristic temperature θ_c are found to be smaller than those obtained by Ernst and Block (Table (6.1)).

First, our results are based on the described x-Q method which assumes a parabolic bonding well where neither κ nor a is a significant function of field, and the subsequently derived value of a (0.13 nm) is smaller than the value they assumed (0.15 nm). The Ernst and Block results are based on each observed temperature and field, which would increase the error limits on their final results. For example, their θ_c values are accurate within a factor of two.

The x-Q method is a more direct method and statistically superior. On the other hand, Ernst and Block suggest that at high temperatures ($\geq$ 350K) anharmonic effects would appear due to deviations from the parabolic shape of the bonding well and hence would lead to lower vibration frequencies. However their results are not accurate enough and such anharmonic effects would certainly appear as major deviations from linearity in the x^{cr} vs $Q^{\frac{1}{2}}$ plot. As with θ_c, the present value (67K) is considerably lower than the value derived from a LEED experiment on a smooth Rh(111)

surface by Chan et al (1978) namely 197±12 K. But in reality, vibration frequency and Debye temperature should be less for kink site atoms.

6.10 DISCUSSION: THE VALUE OF THE ZERO-Q EVAPORATION FIELD F^e

The value of the zero-Q evaporation field F^e=61 V/nm is higher than the observed evaporation field used by Ernst and Block (17 to 41 V/nm). This point has already been taken up in Chapter 4, (section 4.3) in the case of W and Mo and is in line with our expectations. F^e can be seen, as the highest theoretical limit that any observed evaporation field could have. It is defined for Q=0 at the bonding point a, so that equation (4.22) could be written as:

$$(\Lambda^o + H_n - n\phi^E) = neF^e a + \frac{n^2 e^2}{16\pi\varepsilon_o a} - \frac{G}{a^t} - \frac{1}{2}(c_\alpha - c_n)F^{e2} \qquad (6.47)$$

where all the terms have their usual meanings. The left-hand-side term which is of thermodynamic nature should therefore balance the effect of field present in the right-hand-side term.

Taking n=1, we have:

$$(\Lambda^o + H_n - n\phi^E) = 8.4 \text{ eV} \qquad (6.48)$$

Assuming this time, the repulsive term to be one ninth the image-potential term, we have for n=1:

$$\text{nea } F^e = 7.9 \text{ eV}$$

$$\frac{n^2e^2}{16\pi\varepsilon_o a} = 2.8 \text{ eV}$$

$$-\frac{G}{a^t} = -0.3 \text{ eV} \qquad (6.49)$$

$$-\tfrac{1}{2}(c_\alpha - c_n)F^{e2} = -1.7 \text{ eV}$$

$$\text{Total} = 8.7 \text{ eV}$$

The balance between the two sides of equation (6.47) is then good and the value of F^e is justified.

6.11 DISCUSSION : THE VALUE OF THE BONDING DISTANCE a

Our derived value of a (0.13±0.035 nm) is less than the normally accepted definition of a bonding distance to be between the neutral-atom radius (0.1345 nm) and the neutral-atom-diameter.

We will follow here the definition of a bonding distance in a treatment based on the concept of electrical surface as introduced by Lang and Kohn and discussed in Appendix C.

Using the principles of Fig.(3.1), consider a Rhodium atom adsorbed on a Rhodium substrate as follows:

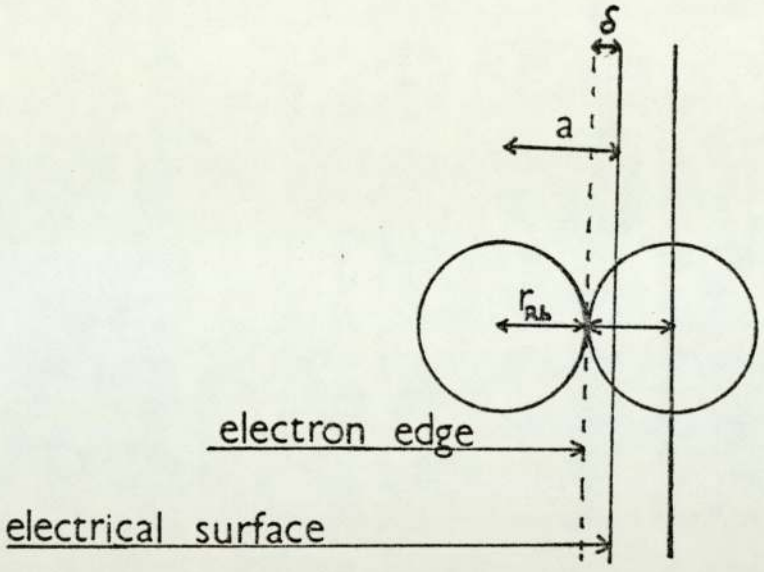

Fig.(6.4a)

We thus expect the bonding distance a to be greater than the neutral atom radius. It is supposed here, that the situation of Rhodium, could be treated as analogous to the case of He adsorbed on W, where δ for tungsten was found to be about 40-60 pm.

Hence, a theoretical estimate of a for Rhodium should be between 175 to 195 pm, a range of values far higher than the experimentally derived 130±35 pm value.

An explanation for this discrepancy suggested here (Forbes: private communication) takes into account the structure of a real metal surface. If, prior to evaporation, the field evaporating atom sits in a bonding site where contact with nearest neighbours is maximised, then the distance of the field evaporating atom from the surface nuclei is reduced and so is the bonding distance a.

This situation is illustrated in Fig. (6.4b)below:

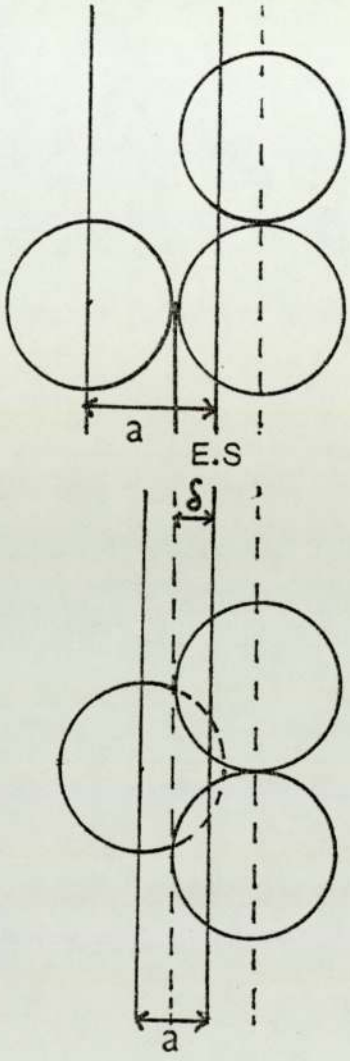

Fig. (6.4b)

6.12 CONCLUSION

The main achievement of this chapter was that we again used Ernst's experimental data, based on joint measurements of field-dependences of activation and appearance energies, to derive some surface atomic parameters (a, κ , ν) for Rh.

The methods employed ("x-Q" and "Q-F"), confirmed that

a Gomer-type mechanism operates for Rh. It was also shown from the Q-F method that "polarization-type" effects should be taken into account in the activation energy formula derived by Forbes.

Chapters 5 and 6 showed how surface atomic parameters could be estimated from experiments. We now return in Chapter 7 to discuss some further T-F and Q-F type measurements.

The results of this chapter have been published as: "Derivation of bonding distance and vibration frequency from field evaporation experiments", by R. G. Forbes, K. Chibane and N. Ernst, Surface Science, 141, pp. 319-340, (1984).

CHAPTER 7

USE OF DIFFERENT BONDING WELL SHAPES

7.1 INTRODUCTION

It has now been established for materials that field evaporate via a Gomer-type escape mechanism, if we assume a parabolic shape for the atomic bonding well, then the field dependence of activation energy Q is given by (see equation (4.1)):

$$Q = \Omega(F^e/F - 1)^2 \tag{7.1}$$

where Ω is the quantity given by equation (4.3) which we now prefer to write as:

$$\Omega = \frac{1}{2}\kappa a^2\left[1 - \frac{(c_\alpha - c_n)F^e}{nea}\right]^2\left[1 - \frac{\eta_n'}{neF}\right]^{-2} \tag{7.2}$$

All the parameters have been defined in Chapter 4. Using the emission equation (equation (1.2)), we then derived a linear relationship between the evaporation field and temperature given by (equation (4.9)):

$$T^{\frac{1}{2}} = \theta^{\frac{1}{2}}[F^e/F - 1] \tag{7.3}$$

where

$$\theta = \Omega/k\ \ell n\ (n_{hr}A/J^o) \tag{7.4}$$

is a temperature-like parameter.

The relation between $T^{\frac{1}{2}}$ and $1/F$ is linear as long as the variation of Ω with evaporation field is negligible.

We have already seen how this result was supported by

the Wada et al. experimental results (Chapter 4) in the case of W and Mo in a temperature range between 60 K to 150 K. Deviations occurring at very low temperatures (around 50 K for W and 35 K for Mo) were attributed to ion-tunnelling effects.

However, experimental measurements of the temperature dependence of evaporation field carried out by Kellogg (1981a) for W, Mo and Rh show $T^{\frac{1}{2}}$ vs $\frac{1}{F}$ plots that deviate at high temperatures (Fig. (7.1)). Among other possibilities, this could be due to the failure of the parabolic approximation at high temperatures. We have therefore investigated the validity of this approximation. Use of a Morse-potential form for the atomic curve has also been investigated. The position of the crossing-point x^P of the atomic and ionic curves was determined and $Q^{\frac{1}{2}}$ vs $\frac{1}{F}$ plots produced theoretically.

We will present our theoretical results and discuss them in relation with some experimental plots.

7.2 THEORETICAL CONSIDERATIONS

7.2.1 Determination of the Crossing-Point

Let $U_n(x,F)$ be the standard potential energy of the escaping ion, at a distance x from the emitter's electrical surface. It is given by (Chapter 1):

$$U_n(x,F) = (H_n - n\phi^E) + S_n(x,F) \qquad (7.5)$$

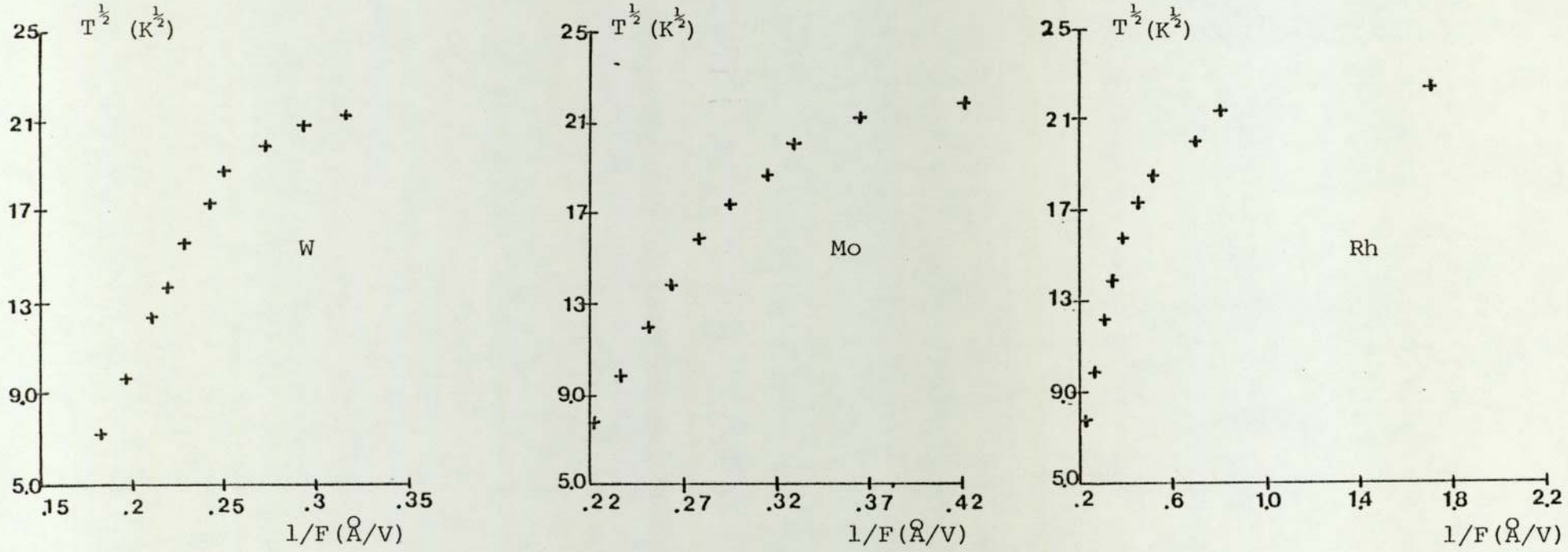

Fig. (7.1) Experimental $T^{\frac{1}{2}}$ vs 1/F plots for W, Mo and Rh.

(From Kellogg; 1981a)

where H_n is the sum of the first n-free space ionization energies, ϕ^E the emitter's work-function, and $S_n(x,F)$ the "variable part" of the ion potential energy.

Consider now an atom vibrating around its bonding point, in an atomic bonding state α. Let V(x) describe the shape of the atomic potential curve, measured relative to the bottom of the well. The total potential energy of the atom, at a distance x is:

$$U_\alpha(x,F) = (-\Lambda^o - \tfrac{1}{2}c_\alpha F^2) + V(x) \qquad (7.6)$$

with Λ^o the zero-field binding energy.

In the context of a curve-intersection formalism, the position of the crossing-point x^p is given by setting $U_n = U_\alpha$. Hence, we obtain:

$$K_n + \tfrac{1}{2}c_\alpha F^2 + S_n(x^p,F) - V(x^p) = 0 \qquad (7.7)$$

where K_n denotes the "configurational " energy term $[H_n - n\phi^E + \Lambda^o]$. This equation can be solved in a variety of approximations, to give a value for x^p. The activation energy Q is then $V(x^p)$.

7.2.2 The Form of the Atomic Potential Curve

For the bonding potential V(x), we have used the two forms:

$$V_1(x) = \tfrac{1}{2}\kappa(x-a)^2 \qquad \text{(parabola)} \tag{7.8a}$$

$$V_2(x) = D\left[1-\exp(-\rho(x-a))\right]^2 \qquad \text{(Morse potential)} \tag{7.8b}$$

D is the Morse well depth, ρ a constant associated with the well width and κ the vibrational force-constant.

For the small vibration amplitudes, ρ is related to κ via:

$$\rho \sim (\kappa/2D)^{\frac{1}{2}} \tag{7.9}$$

7.2.3 The Form of the Ionic Potential $S_n(x,F)$

We have also used different approximations for the ionic term $S_n(x,F)$ as follows:

Primitive case $$S_n = -neFx \tag{7.10a}$$

Simple case $$S_n = -neFx - \frac{n^2e^2}{16\pi\varepsilon_o a} + \frac{G}{a^t} \tag{7.10b}$$

Normal case $$S_n = -neFx - \frac{n^2e^2}{16\pi\varepsilon_o x} \tag{7.10c}$$

For comparisons involving Rhodium, an F^2-energy term was also included.

The simple case (in which the image and repulsive terms are kept constant) can be considered either as an intermediate theoretical approximation between the primitive and normal cases, or as an approximation with some degree of physical

realism, if the initial stage of field evaporation in fact takes place parallel to the surface.

7.3. NUMERICAL VALUES OF THE VARIOUS PARAMETERS

The numerical data were taken from different sources and are summarised in Table (7.1) below:

TABLE (7.1)

	n	Λ^o (eV)	K_n (eV)	a (nm)	κ (eV/nm^2)	ρ (nm^{-1})	$G/10^{-9}$ (eV.nm^9)	t
W	2	8.66	25.6	0.137	90	2.28	19.86	9
Rh	1	5.75	8.41	0.136	76	2.57	4.68	9
Mo	2	6.81	21.66	0.136	80	2.40	18.73	9

Numerical parameter values used in the calculations. The Λ^o, K_n, a(W) and a(Mo) come from Tsong's (1978a) tabulations; κ(W) has been estimated by Forbes (1978b); κ(Rh) and a(Rh) had been estimated in some previous work related to Chapter 6; G is calculated as in Biswas and Forbes (1982). κ(Mo) is derived as explained in the text.

In the case of Mo, the values of κ and ρ have been derived from the experimental $T^{\frac{1}{2}}$ vs $\frac{1}{F}$ of Fig. (7.1). The slope β of the linear part of the graph has been measured to be:

$$\beta \simeq 15.4 \times 10^2 \quad K^{\frac{1}{2}} \text{ V/nm.}$$

According to equation (7.3) we have:

$$\beta = \theta^{\frac{1}{2}} F^e \tag{7.11}$$

i.e.

$$\beta = \left[\Omega / k\ell n\left(\frac{n_n A}{J^o}\right)\right]^{\frac{1}{2}} F^e \tag{7.12}$$

Hence, using the first approximation for Ω(equation (4.2)), we obtain:

$$\kappa = \frac{2k\ell n\left(\frac{nA}{J^o}\right)}{(F^e)^2 a^2} \cdot \beta^2 \tag{7.13}$$

Around the well bottom (and as a first approximation) the zero-Q evaporation field F^e is such that:

$$a \simeq K_n / neF^e \tag{7.14}$$

Substituting back into equation (7.13), κ is given by:

$$\kappa = \frac{2k\ell n(n_{hr} A/J^o)}{K_n^2} (ne)^2 \beta^2 \tag{7.15}$$

Using the data of Fig. (7.1), where J^o=1 layer/s and assuming n_{hr} = 0.01 layers; A = $10^{12} s^{-1}$ leads to κ(Mo)~80 eV/nm^2. Going back to equation (7.9) for ρ, leads to ρ(Mo)~2.40 nm^{-1}. As for the repulsive term constant G, it has been derived by considering the ionic curve, in the absence of any external field, (see Chapter 6). G is given in function of a and t as:

$$G = \frac{n^2 e^2}{16\pi\varepsilon_o} \frac{1}{t} a^{t-1} \tag{7.16}$$

The values of G shown in Table (7.1) are for t=9. Also, the results (when the repulsive term is involved) will be given for t=9 only, since it has been found that the case t=12 was very close to the case t=9.

7.4 THEORETICAL MODELS: RESULTS AND DISCUSSIONS

In this section we look at the results derived from our theoretical models, and at the effects produced by making various different assumptions. In particular, Section 7.4.2 looks at the effects of using different approximations for S_n. Mostly, this is done using the Tungsten data as an example, but we also make reference to the Mclybdenum and Rhodium results, where necessary.

The results are represented in the form of $Q^{\frac{1}{2}}$ vs $\frac{1}{F}$ plots. The evaporation field values were chosen to vary between 167 to 5 V/nm. The extremely high values have no physical meaning, but were used to obtain a theoretical solution over a wide field strength range.

7.4.1 Basic Behaviour

A plot of $Q^{\frac{1}{2}}$ vs $\frac{1}{F}$ for the W data is shown as Fig. (7.2) for the primitive parabola (a) and Morse (b) potentials. Both curves have the same shape and the main features are: (1) each curve intersects the $\frac{1}{F}$ axis at $\frac{1}{F^e}$; (2) there is an initial linear region; (3) then both curves "turn-over" (however, "turn-over" occurs at a higher value of Q (about

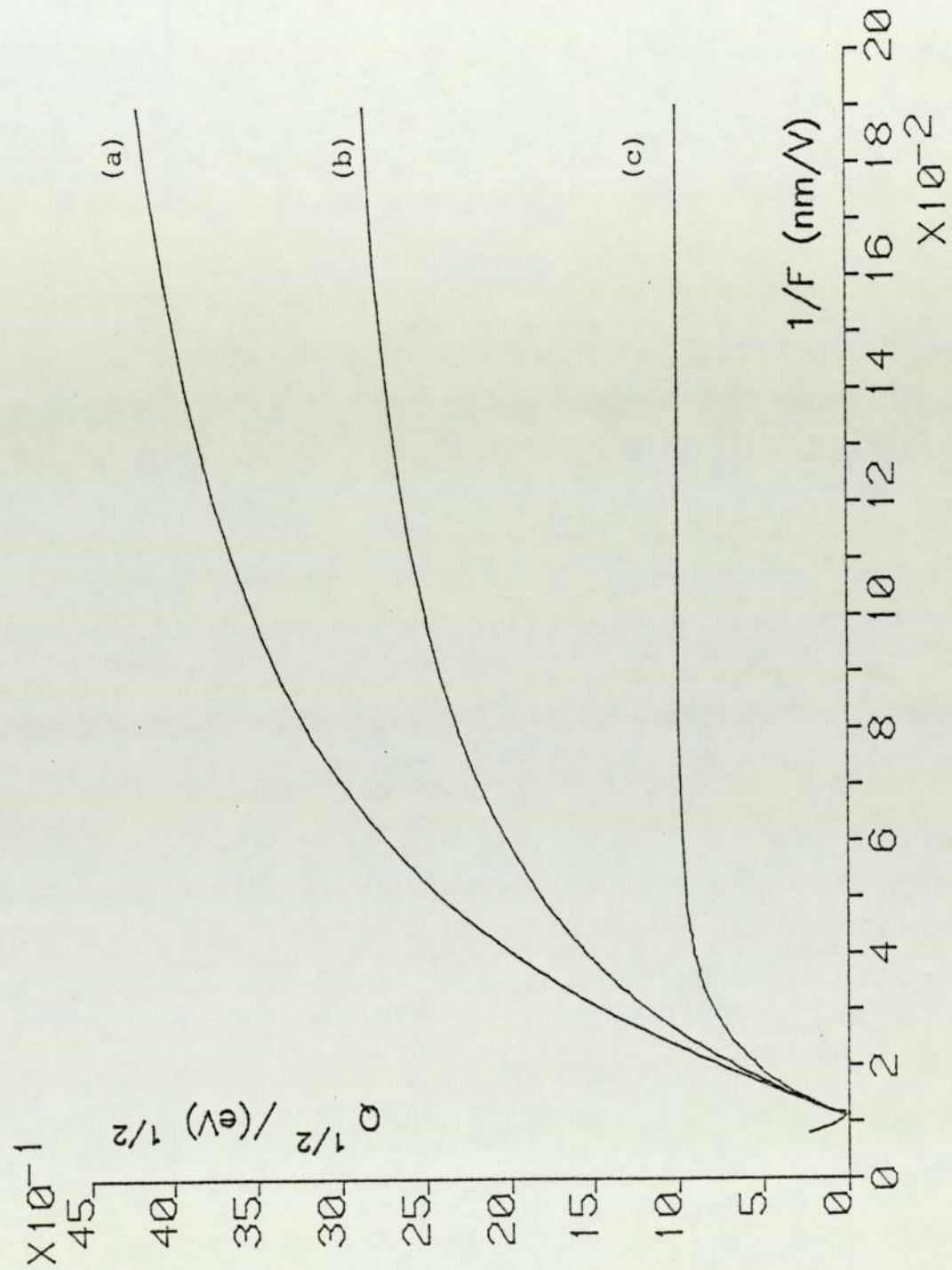

Fig. (7.2) : Theoretical $\Omega^{\frac{1}{2}}$ vs $\frac{1}{F}$ plots using the W data: "primitive case": (a) parabola; (b) Morse; (c) Shallow Morse.

1.8 eV) for the parabola than for the Morse curve (0.5 eV); (4) finally, there is a region where $Q^{\frac{1}{2}}$ increases slowly and non-linearly with $\frac{1}{F}$. On the parabola curve, we show a branch corresponding to high evaporation field (low $\frac{1}{F}$) values. This branch is unphysical and corresponds to an intersection inside the bonding point,e.g. at F = 125 V/nm, x^p = 0.102 nm(<a). The Morse potential curve is plotted for D = 8.66 eV (equal to the Tungsten binding energy). We also show in (c) a Morse curve corresponding to D = 1 eV, where the "turn-over" level is much lower (~0.35 eV). The low D value is used to simulate a Tungsten atom in a local bonding well: such an atom would diffuse across the surface, rather than evaporate, as temperature is increased.

7.4.2 The Effect of Bonding-Well Shape

We have just looked at the effect of bonding-well shape when we use the "primitive" form for S_n. The results are similar when other forms are used.

In the "simple case", we include the electrostatic term as variable, and the image-potential and repulsive terms as constants. The shapes of the $Q^{\frac{1}{2}}$ vs $\frac{1}{F}$ plots for the parabola and Morse-potential curves are much the same, as shown in Fig. (7.3) for the W data. However, compared to the primitive case, the "turn-over" level occurs at lower energies on the parabola curve (a) (0.65 eV) and even lower on the Morse-potential curve (b) (0.3 eV).

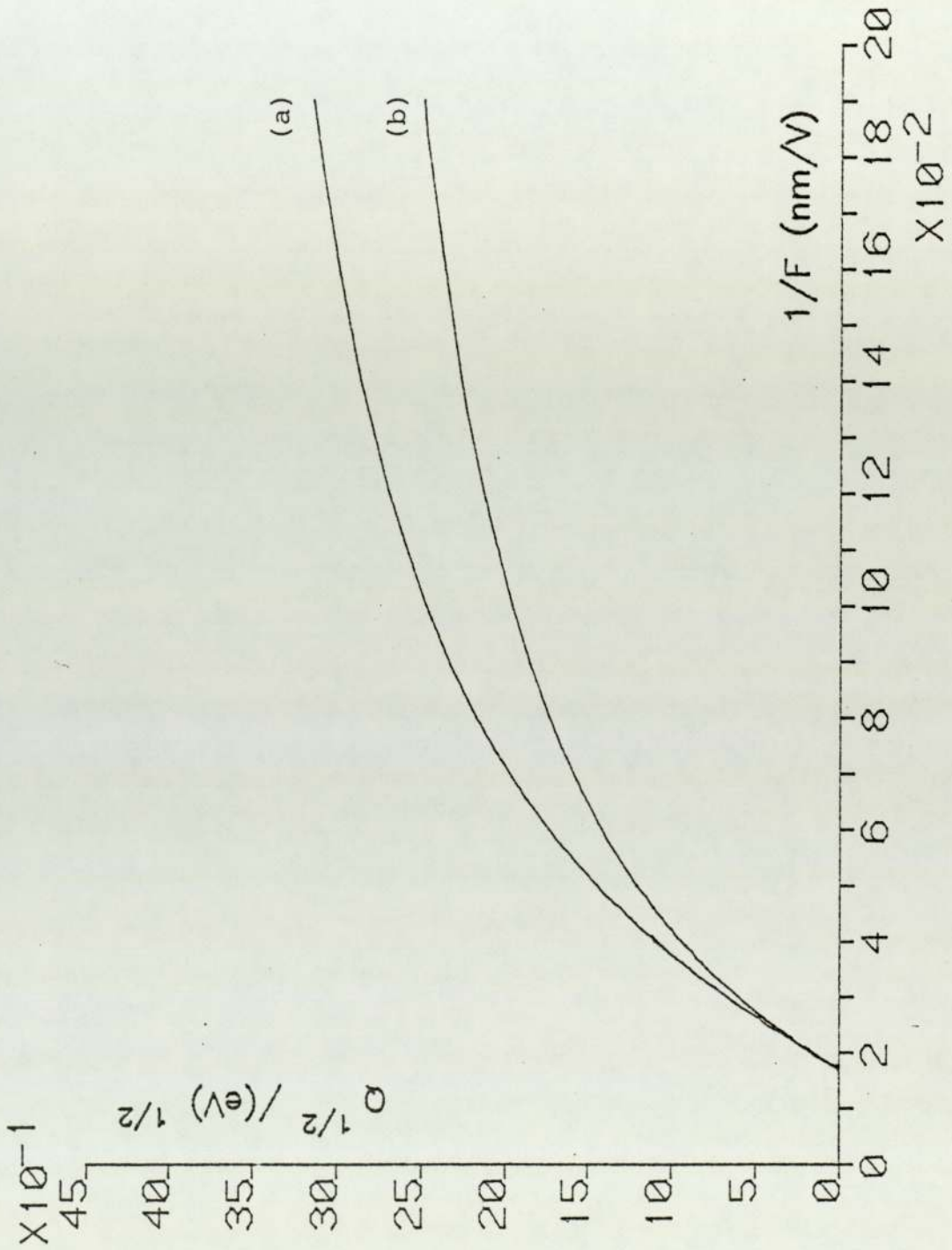

Fig. (7.3) : Theoretical $\Omega^{\frac{1}{2}}$ vs $\frac{1}{F}$ plots using the W data, "simple case" : (a) parabola; (b) Morse-potential curve.

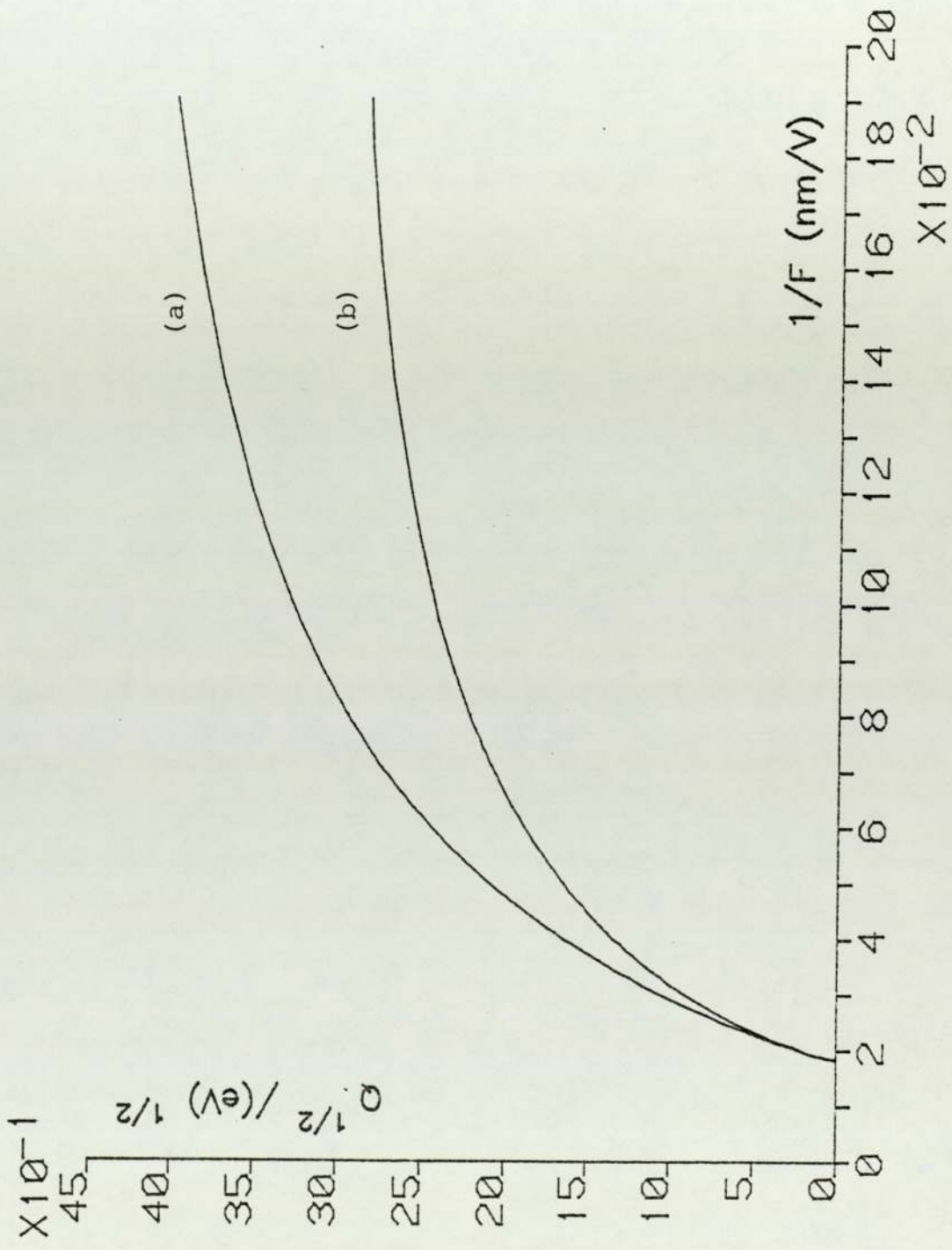

Fig. (7.4) : Theoretical $Q^{\frac{1}{2}}$ vs $\frac{1}{F}$ plots using the W data, "normal case": (a) parabola; (b) Morse-potential curve.

With the "normal case", which corresponds to including the image-potential term as a variable, the general shapes of the curves are again much the same, as shown in Fig. (7.4). The "turn-over" level is also lower than the primitive case, 0.36 eV for the Morse-potential curve (b) and 1.36 eV for the parabola curve (a).

The effect of adding a variable repulsive term (to the normal case) has also been investigated. The results were essentially identical with those of the normal case, so comparisons have been made using the normal case.

7.4.3 Effect of Using Different Approximations for S_n.

We show in Fig. (7.5), for W, the effect of using the different approximations (equation (7.10)) in S_n, for the Morse-potential case (the same discussion applies for the parabolic well, and to Mo and Rh). We see that including the image + repulsive terms (curve b) as constants, causes: (1) a shift to lower F^e; (2) the curve to turn-over at lower energies. Incorporating the constant term corresponds to using a lower value for K_n (16.3 eV as opposed to 25.6 eV).

Including the image term as a variable (curves a) also causes a shift in F^e, but the curve tends towards the primitive case for large Q-values.

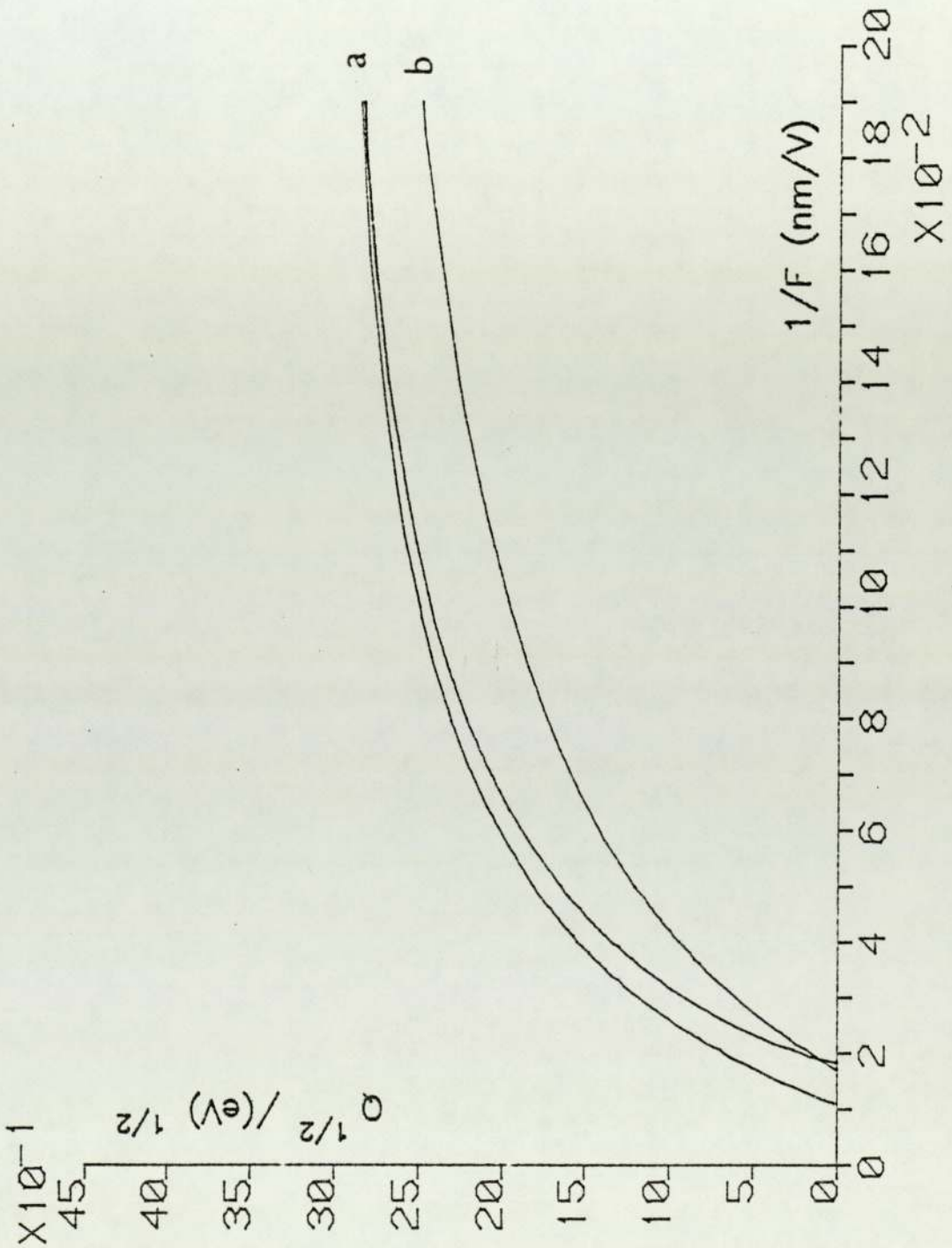

Fig. (7.5) : Effect of using different approximations in S_n for the Morse-potential case (W data).

7.4.4 Inclusion of an F^2-energy Term for Rh

Using the previous estimates of c_α and c_n for Rh (Chapter 5), an F^2-energy term has been included in the form:

$$K_n - neFx^p - \frac{n^2e^2}{16\pi\varepsilon_o x^p} + \frac{G}{(x^p)^t} + \frac{1}{2}(c_\alpha - c_1)F^2 - V(x^p) = 0 \qquad (7.17)$$

where n=1, $c_\alpha \sim 1.05\times10^{-3}$ $eVV^{-2}nm^2$ and $c_1 \sim 0.15\times10^{-3} eVV^{-2}nm^2$ for Rh. A repulsive term is also introduced as a variable.

We show the $Q^{\frac{1}{2}}$ vs $\frac{1}{F}$ plots in Fig. (7.6) for the parabola (a) and Morse (b) potentials. The effect of including the F^2-energy term is compared with the normal case (lower curves in (a) and (b)).

The parabola curve turns-over at Q~0.83 eV whilst the Morse-potential curve turns-over at Q~0.64 eV.

Compared to the normal case, we see that: (1) there is a shift in F^e (increase by about 30%); (2) at high fields, the shifts in Q-values are important, but disappear completely at high temperatures (high Q's).

7.4.5 Summary of Model Behaviour

From the results and the general shape of the theoretical $Q^{\frac{1}{2}}$ vs $\frac{1}{F}$ plots presented in this section, the first important point to be made is that the Forbes prediction of a linear relationship between $Q^{\frac{1}{2}}$ and $\frac{1}{F}$ holds for low Q-values, but

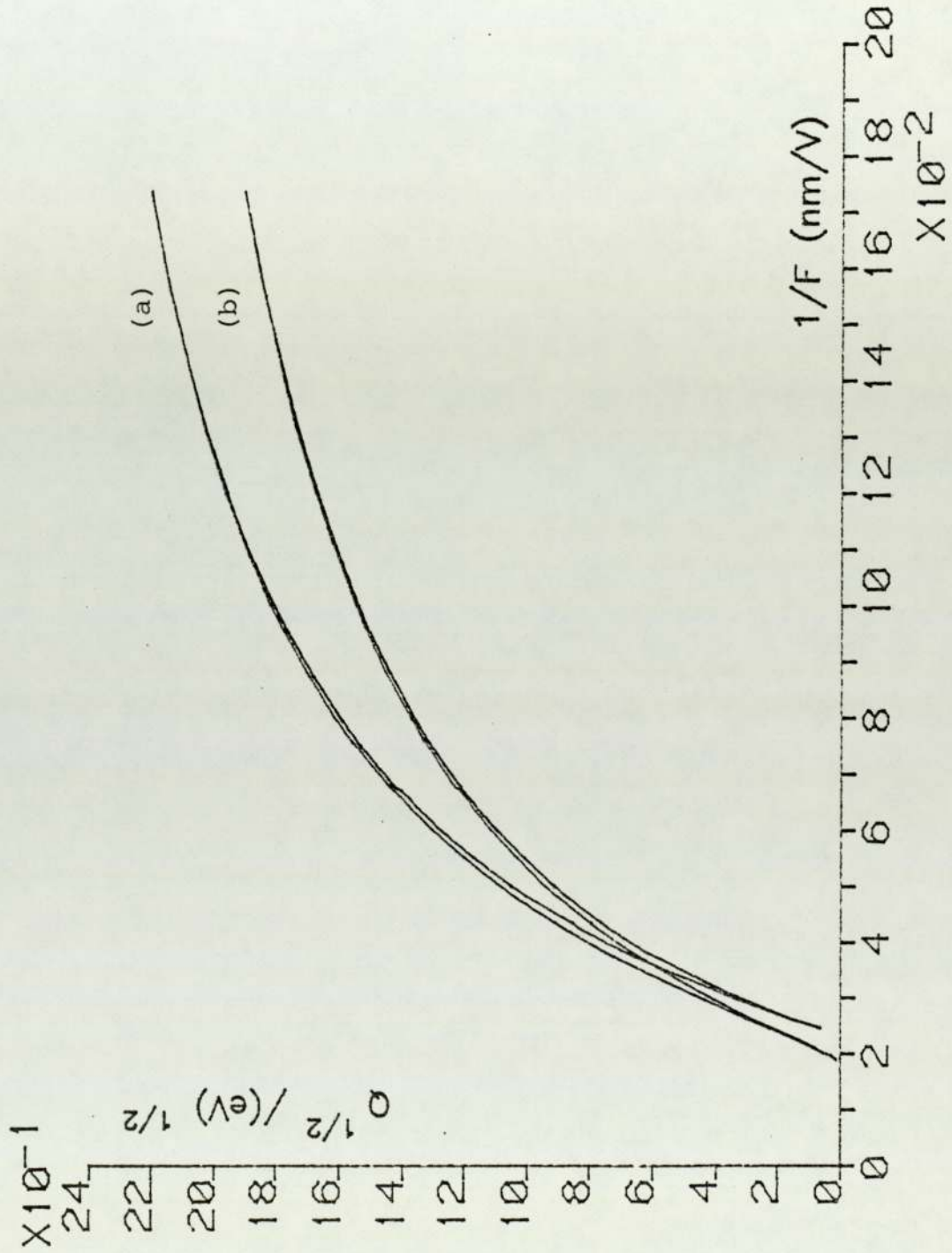

Fig. (7.6) : Effect of including an F^2-energy term using the Rh data

does break down at higher Q-values, even for a parabola.

Going back to Fig. (7.2), we see that:

(1) choosing different forms for V(x) (parabola, Morse, shallow Morse) but keeping κ constant, influence the "turn-over" level;

(2) using the same bonding-well shape but choosing different forms for S_n mainly influence the slope and intercept in the linear region, as shown in Figs. (7.5) and (7.6).

Varying the value of κ would again affect the slope and intercept. But, in general terms, changing materials (i.e. altering the value of κ) but keeping the same bonding well shape, would mainly affect the "turn-over" level.

Results concerning turn-over level, for all three materials investigated are shown in Table (7.2). These turn-over energy level values are all estimated by eye, using what is hopefully a uniform criterion as to the point at which significant departure from linearity occurs.

TABLE (7.2)

Q(eV)

		Parabola	Morse	Shallow Morse
Primitive:	W	1.8	0.5	0.35
	Mo	1.9	0.4	
	Rh	0.53	0.2	
Simple:	W	0.65	0.3	
	Mo	0.8	0.21	
	Rh	0.44	0.1	
Normal:	W	1.36	0.36	
	Mo	0.5	0.18	
	Rh	0.46	0.17	

Q-values at which the "turn-over" level occurs. For W, Mo and Rh(primitive, simple and normal cases). Only the W shallow Morse was carried out for comparison.

7.5 EXPERIMENTAL RESULTS AND COMPARISONS

We may compare our model with the experimental data concerning the temperature dependence of evaporation field (T-F measurements) by Kellogg (1981a, 1984) and Wada et al. (1980), and that concerning the field dependence of activation energy (Q-F measurements) by Kellogg (1984) and Ernst (1979).

As Fig. (7.1) shows, Kellogg's (1981a) and similar results are basically given in the form $T^{\frac{1}{2}}$ vs $\frac{1}{F}$. All T-F measurements were converted into the equivalent $Q^{\frac{1}{2}}$ vs $\frac{1}{F}$ plots, by using the emission equation (Chapter 1):

$$Q = k\ell n \left(\frac{n_{hr}A}{J}\right)T \qquad (7.18)$$

Equation (7.18) is used with the appropriate value of J^{o}. We also suppose that only 1% of the surface atoms, on the cap of the field-ion emitter, were at "high risk" of evaporation (so n_{hr} = 0.01 layers), and that A is constant at $10^{12}s^{-1}$ (Forbes, private communication).

We now present results for each material separately.

7.5.1 Results for Tungsten

In the case of Tungsten, four sets of experimental data were available, of which one concerns the field dependence of activation energy (Kellogg: 1984). Using equation (7.18) and the given evaporation flux J^{o}, we obtain the results in Table (7.3). Note that in the first three sets, different evaporation fluxes J^{o} were used.

The Kellogg (1984) Q-F measurements were performed by fixing the evaporation field (fixed voltage) and varying the temperature and evaporation flux at each measurement; values of Q were then derived from Arrhenius plots. Also note the limited field range of the Wada et al. data.

TABLE (7.3)

Wada et al (1980) T-F data J^o = 0.1 layer/s			Kellogg (1981) T-F data J^o = 1 layer/s		
T(K)	$Q^{\frac{1}{2}}(eV^{\frac{1}{2}})$	$\frac{1}{F}$ (nmV^{-1})	T(K)	$Q^{\frac{1}{2}}(eV^{\frac{1}{2}})$	$\frac{1}{F}$ (nmV^{-1})
20	0.227	0.0175	60	0.345	0.0182
34	0.296	0.0177	104	0.454	0.0194
46	0.344	0.0178	151	0.547	0.0205
54	0.373	0.0179	201	0.632	0.0217
77	0.446	0.0185	252	0.707	0.0225
95	0.495	0.0191	300	0.772	0.0236
105	0.520	0.0193	355	0.839	0.0248
130	0.579	0.0199	398	0.888	0.0262
			448	0.943	0.0284
			504	1.000	0.0317

Kellogg (1984) T-F data J^o = 0.2 layer/s			Kellogg (1984) Q-F data		
T(K)	$Q^{\frac{1}{2}}(eV^{\frac{1}{2}})$	$\frac{1}{F}$ (nmV^{-1})		$Q^{\frac{1}{2}}(eV^{\frac{1}{2}})$	$\frac{1}{F}$ (nmV^{-1})
50	0.326	0.0167		0.346	0.0169
150	0.564	0.0182		0.447	0.0175
200	0.652	0.0192		0.557	0.0183
245	0.721	0.0204		0.592	0.0189
300	0.798	0.0217		0.721	0.0196
350	0.862	0.0233		0.775	0.0203
400	0.921	0.0250		0.949	0.0212
450	0.977	0.0278			
500	1.030	0.0313			
550	1.081	0.0417			

Experimental T-F and Q-F data for W, on which Fig. (7.7) is based.

Figure (7.7) illustrates the various experimental results for Tungsten and includes the normal case (parabola and Morse curves). Only Kellogg's (1984) Q-F measurements represent direct $Q^{\frac{1}{2}}$ vs $\frac{1}{F}$ plots.

We did not attempt to "standardise" these results because our interest lies mainly in the "turn-over" behaviour of the various plots. We see that all experimental plots have a linear region from around 0.35 eV to 0.8 eV. Hence, in this region equation (7.1) must be a good approximation. At low temperatures, the Wada et al. (1980) results diverge from linearity, probably due to ion-tunnelling (Chapter 4). One of the Kellogg (1984) T-F points also lies in this region. The Kellogg (1984) Q-F results give rise to a straight line that seems to be linear up to a level slightly higher than might be expected on the basis of our numerical calculations. The Kellogg (1984) and (1981a) T-F results were taken at different evaporation fluxes, over the same temperature range. They behave similarly and turn-over at about Q~0.9eV.

Although "turn-over" is common to both these results and our theroetical model, the experimental and theoretical results are not really in agreement with each other. Further, except for the Wada et al. (1980) results where the highest temperature is 130 K only, the Kellogg (1981a) and (1984) T-F results "turn-over" but the Q-F results <u>do not</u>.

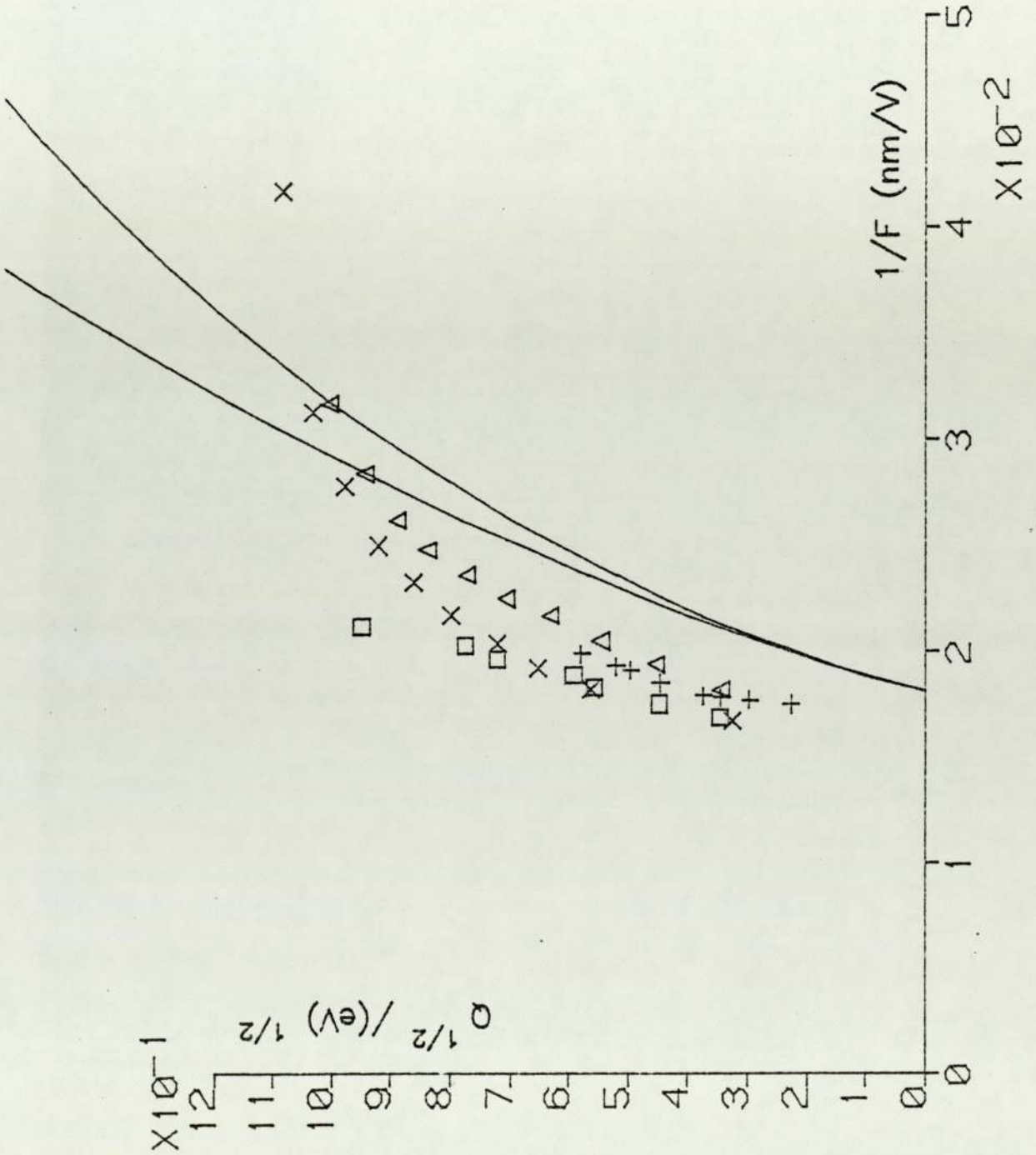

Fig. (7.7) : The W experimental results and the W normal case.
(□) Kellogg's Ω-F (1984); (x) Kellogg's T-F (1984);
(Δ) Kellogg's T-F (1981a); (+) Wada et al (1980).

If the bonding-well parabolic approximation were a prime factor in breakdown of the theory at high temperatures (as suggested by Kellogg: 1984), then both Q-F and T-F plots would have deviated from linearity. The reason for deviation of the T-F plot from linearity must lie somewhere else, and the most obvious hypothesis is that the field dependence in the pre-exponential factor A is responsible for the divergence. This has recently been discovered experimentally by Kellogg (1984) during his Q-F measurements. He found that the pre-exponential factor increases as the evaporation field is decreased, as shown in Table (7.4) below:

TABLE (7.4)

F(V/nm)	Q(eV)	A(s^{-1})
47	0.90±0.04	3×10^{16}
49.3	0.60±0.01	1×10^{13}
51	0.52±0.01	8×10^{12}
53	0.35±0.003	7×10^{11}
54.7	0.31±0.008	7×10^{11}
57.2	0.20±0.004	3×10^{11}
59	0.12±0.012	4×10^{11}

Field variation of the pre-exponential factor A. Taken from Kellogg (1984).

Table (7.4) suggests that the variation in A is mostly important at low fields i.e. high temperatures. This finding

is actually in agreement with formulae (7.3) and (7.4) for the temperature dependence of field: if A increases as F is decreased, then according to these formulae we should expect deviations at high temperatures (as shown in Fig. (7.1) for W, Mo and Rh). Other possibilities could also be explored.

7.5.2 Results for Rhodium

The experimental data were taken from Ernst's (1979) Q-F measurements and from Kellogg's (1981a) T-F measurements. They are as follows:

TABLE (7.5)

Ernst (1979) Q-F data			Kellogg (1981a) T-F data J^o = 1 layer/s		
T(K)	$Q^{\frac{1}{2}}(eV^{\frac{1}{2}})$	$\frac{1}{F}$ (nmV^{-1})	T(K)	$Q^{\frac{1}{2}}(eV^{\frac{1}{2}})$	$\frac{1}{F}$ (nmV^{-1})
100	0.224	0.0244	60	0.345	0.0222
250	0.447	0.0303	105	0.456	0.0246
350	0.775	0.0357	151	0.547	0.0263
430	0.837	0.0417	207	0.641	0.0295
510	0.949	0.0476	247	0.700	0.0322
600	1.225	0.0588	298	0.769	0.0381
			346	0.829	0.0432
			396	0.886	0.0678
			453	0.948	0.0796
			497	0.993	0.1736

Experimental T-F and Q-F data for Rh. The results are illustrated in Fig. (7.8).

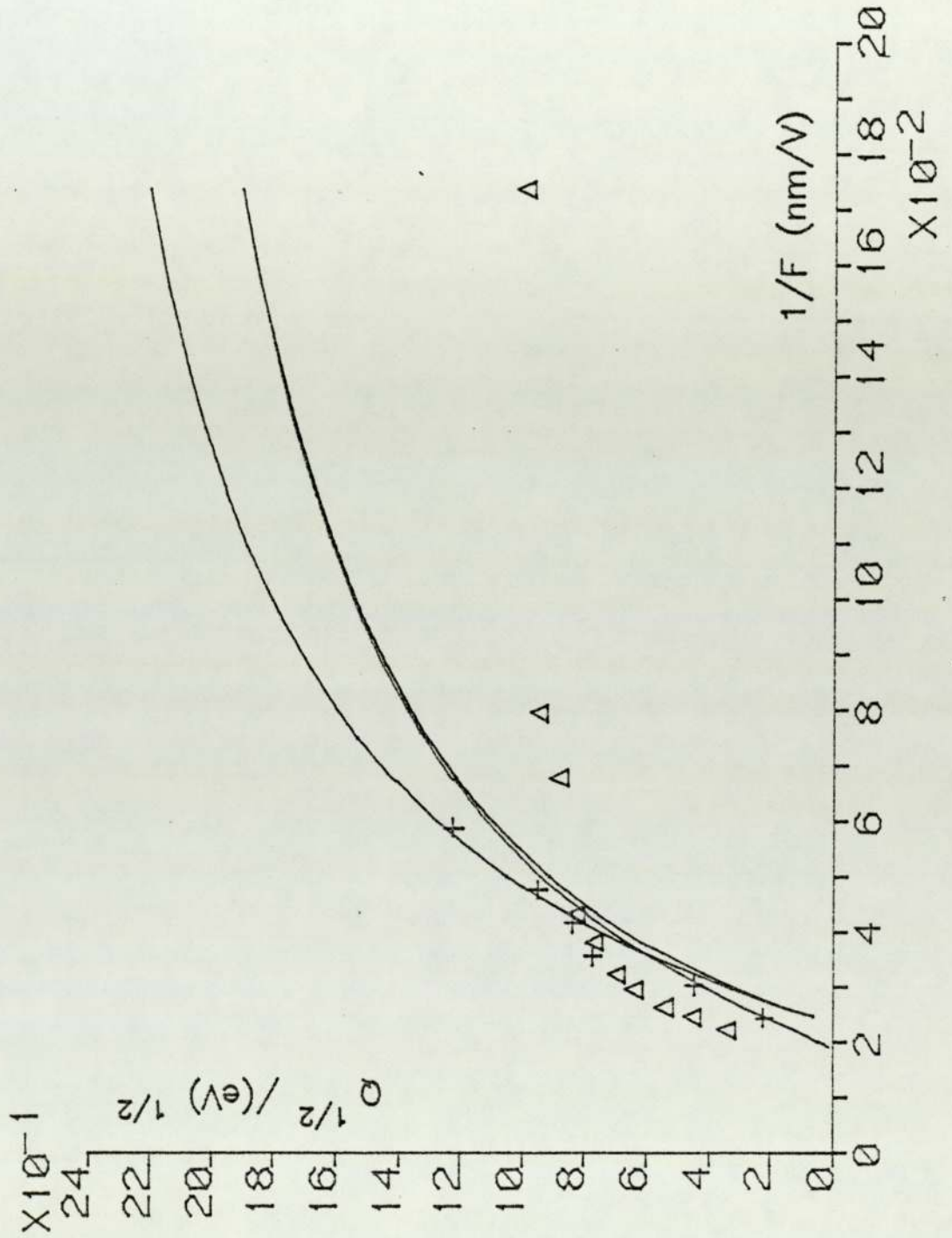

Fig. (7.8) : Experimental and theoretical $Q^{\frac{1}{2}}$ vs $\frac{1}{F}$ plots for Rh. (Δ): Kellogg's (1981a) T-F (1981); (+) Ernst's Q-F (1979).

The corresponding $Q^{\frac{1}{2}}$ vs $\frac{1}{F}$ plots are shown in Fig. (7.8) where we include, the normal case (parabola and Morse curves); the "inclusion of F^2-energy term" Morse curve. The measurements were taken over nearly the same temperature range and Fig. (7.8) shows that Kellogg's T-F measurements turn "faster" than Ernst's Q-F measurements.

The same behaviour is displayed as for Tungsten: Kellogg's T-F points contain a linear region, then turn-over at high temperatures, whilst Ernst's Q-F points lie on a straight line. However, in this case, the Ernst Q-F points are in quite good agreement with our theoretical curves.

Here too, the different behaviour of the Q-F and T-F experimental curves suggests a field dependence in the pre-exponential factor A.

7.5.3 Results for Molybdenum

Only two sets of experimental data were available. The Wada et al. (1980) and Kellogg (1981a) T-F measurements. The results are shown in Table (7.6).

The $Q^{\frac{1}{2}}$ vs $\frac{1}{F}$ plots are shown in Fig. (7.9) where we include the Morse "primitive case" and the Morse "normal case". The Kellogg T-F points deviate at high temperatures, but the Wada et al. T-F data are not sufficient for any "turn-over" to be seen.

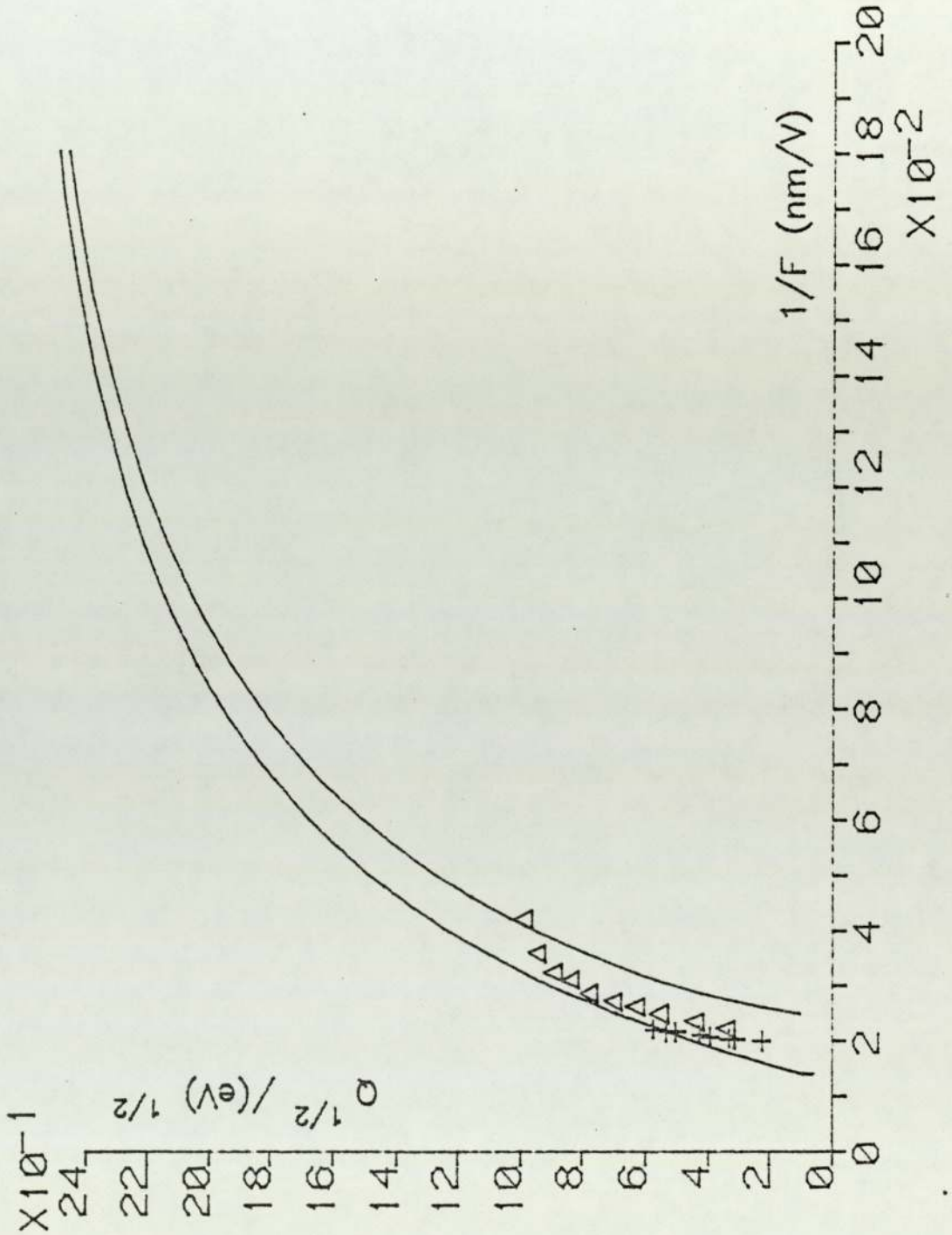

Fig. (7.9) : Experimental and theoretical $Q^{\frac{1}{2}}$ vs $\frac{1}{F}$ plots for Mo. (Δ)Kellogg's T-F (1981a); (+) Wada et al T-F (1980).

TABLE (7.6)

Wada et al. (1980) T-F data J^o = 0.1 layer/s			Kellogg (1981a) T-F data J^o = 1 layer/s		
T(K)	$Q^{\frac{1}{2}}(eV^{\frac{1}{2}})$	$\frac{1}{F}$ $(V^{-1}nm)$	T(K)	$Q^{\frac{1}{2}}(eV^{\frac{1}{2}})$	$\frac{1}{F}$ $(V^{-1}nm)$
20	0.227	0.0200	60	0.345	0.0222
38	0.313	0.0203	100	0.445	0.0236
43	0.333	0.0204	157	0.558	0.0250
60	0.393	0.0208	204	0.636	0.0262
70	0.425	0.0211	250	0.704	0.0272
98	0.503	0.02167	309	0.783	0.0287
110	0.533	0.0217	356	0.840	0.0311
128	0.575	0.0221	406	0.898	0.0324
			452	0.947	0.0359
			497	0.993	0.0420

Experimental T-F data for Mo. The corresponding plots are shown in Fig. (7.9).

The experimental curves fit between the theoretical ones. With the Wada et al. T-F points, deviations at low temperatures are also attributed to ion-tunnelling (Chapter 4), whilst with the Kellogg T-F points deviations at high temperatures could also be due to the variation of A with field.

7.6 THE UNIVERSAL BINDING-ENERGY CASE

For further comparisons it was thought useful to use a Universal bonding form for the atomic bonding well. As mentioned in Chapter 1, a Universal binding-energy function $E^*(a^*)$ was derived by Rose et al. (1981). It was shown to fit different bonding-type cases (e.g. Rose et al.: 1983).

The general algebraic form for $E^*(a^*)$ is as given by equation (1.6), i.e.:

$$E^*(a^*) = -(1+\beta a^*)\exp(-\beta a^*) \qquad (7.19)$$

where a^* is a dimensionless scaled length defined relative to the bottom of the Universal binding energy function, and β a constant (in our calculations β will be put equal to 1).

According to Rose et al., any binding energy-distance relationship $E(x)$ (e.g. adhesion, cohesion, chemisorption etc....) can be scaled by the function E^* (hence its Universal character), by the following relationships:

$$\begin{cases} E(x) = E^*(x^*).\Delta E \\ x^* = \dfrac{x-x_m}{\ell} \end{cases} \qquad (7.20)$$

where ΔE is the binding energy at equilibrium, x_m is the corresponding equilibrium position, and ℓ is a scaling length dependent on the type of bonding under investigation. (Note that for convenience, the parameter previously denoted by "a*" is now replaced by "x*".)

For the purpose of our calculations, and in order to be consistent, it can be seen that ΔE above corresponds to our zero-field binding energy Λ^{o}, $E(x)$ corresponds to the (zero-field) potential energy curve $U(x)$ for a neutral atom, and x_m corresponds to our bonding distance a.

Hence, we may write:

$$\begin{cases} U(x) = E^*(x^*)\Lambda^{o} \\ x^* = \dfrac{x-a}{\ell} \end{cases} \tag{7.21}$$

Using the appropriate forms for $E^*(x^*)$ and x^*, leads to:

$$U(x) = -\Lambda^{o}(1+\frac{x-a}{\ell})\exp(-\frac{x-a}{\ell}) \tag{7.22}$$

It follows that the bonding potential $V(x)$ is now used in the form:

$$V(x) = \Lambda^{o}\left[1-(1+\frac{x-a}{\ell})\exp(-\frac{x-a}{\ell})\right] \tag{7.23}$$

The position of the crossing point x^{p} is given by solving the equation $U_n(x) = U(x)$ and the activation energy is calculated from $Q = V(x^{p})$.

7.6.1 Theoretical Comparisons

The calculations have been carried out for the "primitive" and "normal" cases, for W and Mo, since values of ℓ for these two materials are known. They were taken from Rose et al. (1983), and are: ℓ = 0.053 nm for W and ℓ = 0.055 nm for Mo. The other parameters were taken from data in Table (7.1).

The calculated $Q^{\frac{1}{2}}$ vs 1/F plots are shown in Figs. (7.10) and (7.11) for W, and in Fig. (7.12) for Mo. It can be seen that the Universal $Q^{\frac{1}{2}}$ vs 1/F plots exhibit the same general behaviour as did the parabola and Morse cases. They contain an initial linear region, then turn-over at high Q-values. Also, comparison of Fig. (7.10) with Fig. (7.5) for W, and Fig. (7.12) with Fig. (7.9) for Mo, shows that the "primitive" and "normal" approximations in S_n behave much the same as they did for the Morse-potential.

However, Fig. (7.11) shows that the turn-over behaviour differs significantly when the three bonding wells (parabola, Morse, Universal form) are compared (for the "normal" case). For the Universal bonding well case, the initial linear region covers a wider range of Q-values, but at large 1/F values the plot has much the same level as in the Morse case. In addition, the turn-over for the Universal bonding well is more sharply defined. In general terms, however, we can conclude that the theoretical $Q^{\frac{1}{2}}$ vs 1/F plots - whether parabola, Morse or Universal form - have broadly the same behaviour. So to some extent the expected form of the plots must be independent of the initial bonding well shape.

7.6.2 Comparisons With Experiments

In Fig. (7.13), we show the $Q^{\frac{1}{2}}$ vs 1/F plot for the Universal bonding well in the "normal" W case, and the experimental Q-F results of Kellogg (1984) for W.

The experimental results shown are the only ones for

UNIVERSAL CURVE PLOTS FOR W:

'Primitive and Normal' cases

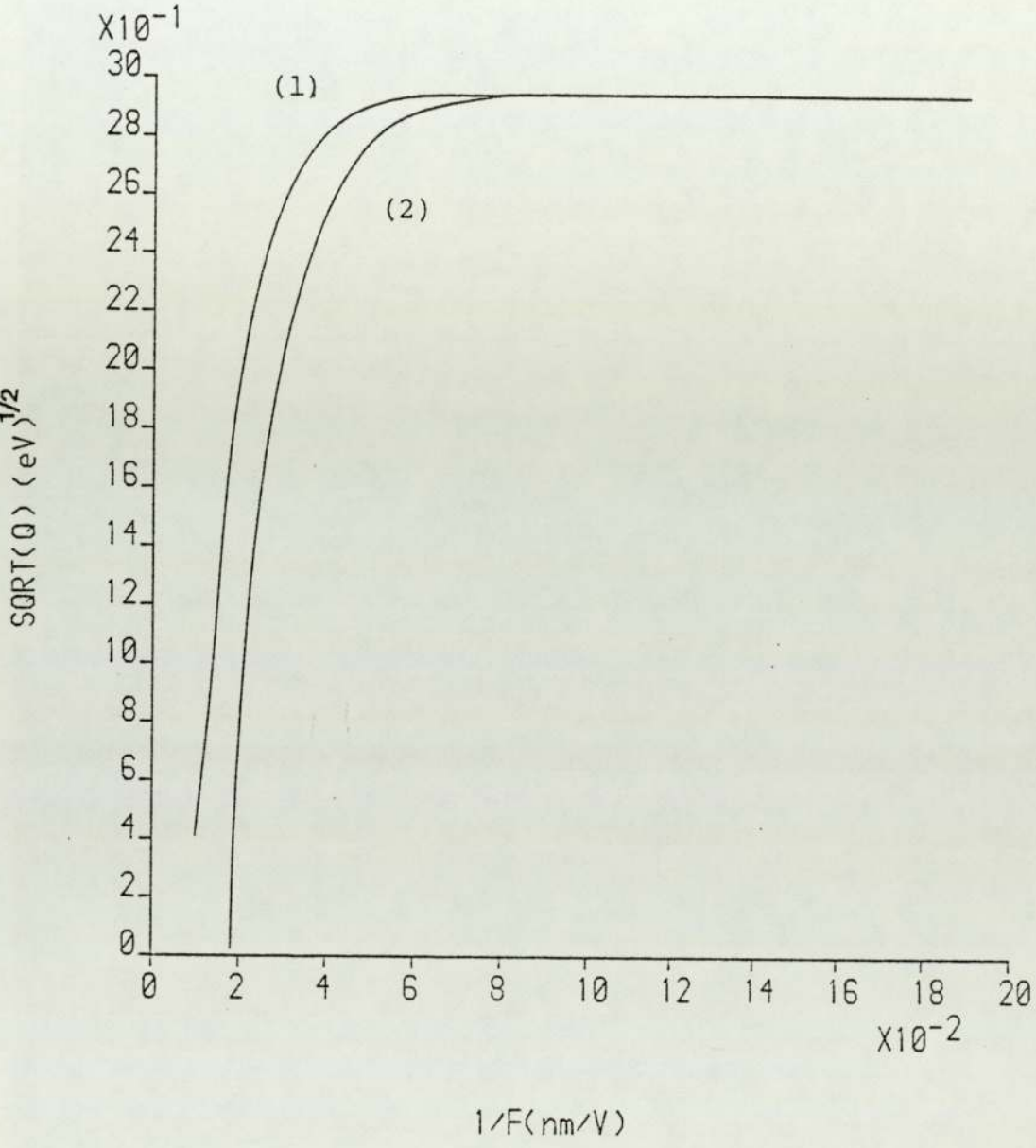

Fig. (7.10) $Q^{\frac{1}{2}}$ vs 1/F plot for W, using the Universal bonding well.

(1) "primitive" case.

(2) "normal" case.

Comparison of the three bonding wells.

(1): Parabola: 'normal' case

(2): Universal: "

(3): Morse : "

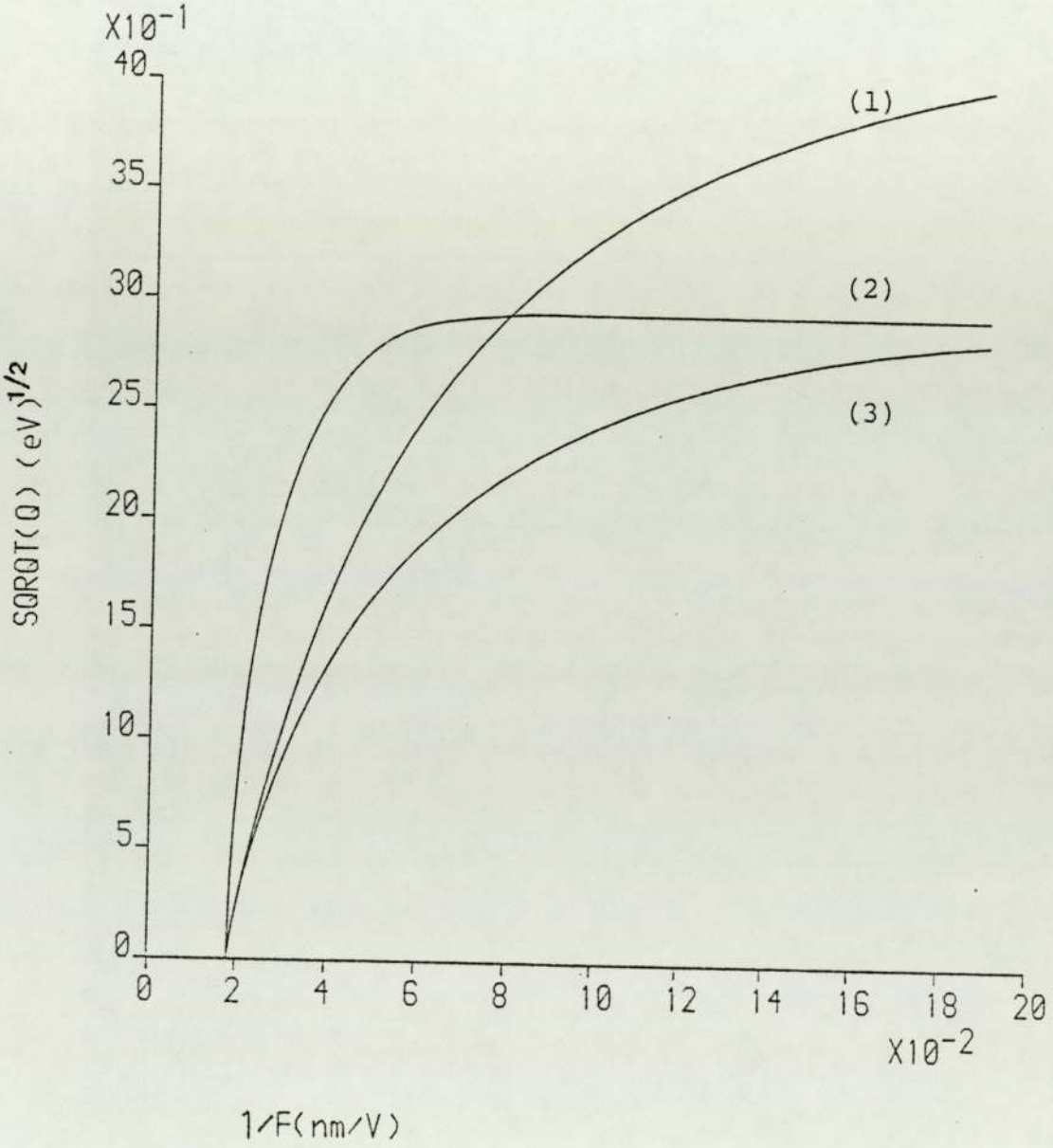

Fig. (7.11) Bonding well behaviour for W.

UNIVERSAL CURVE CALCULATIONS

FOR MO

'PRIMITIVE+NORMAL' CASES

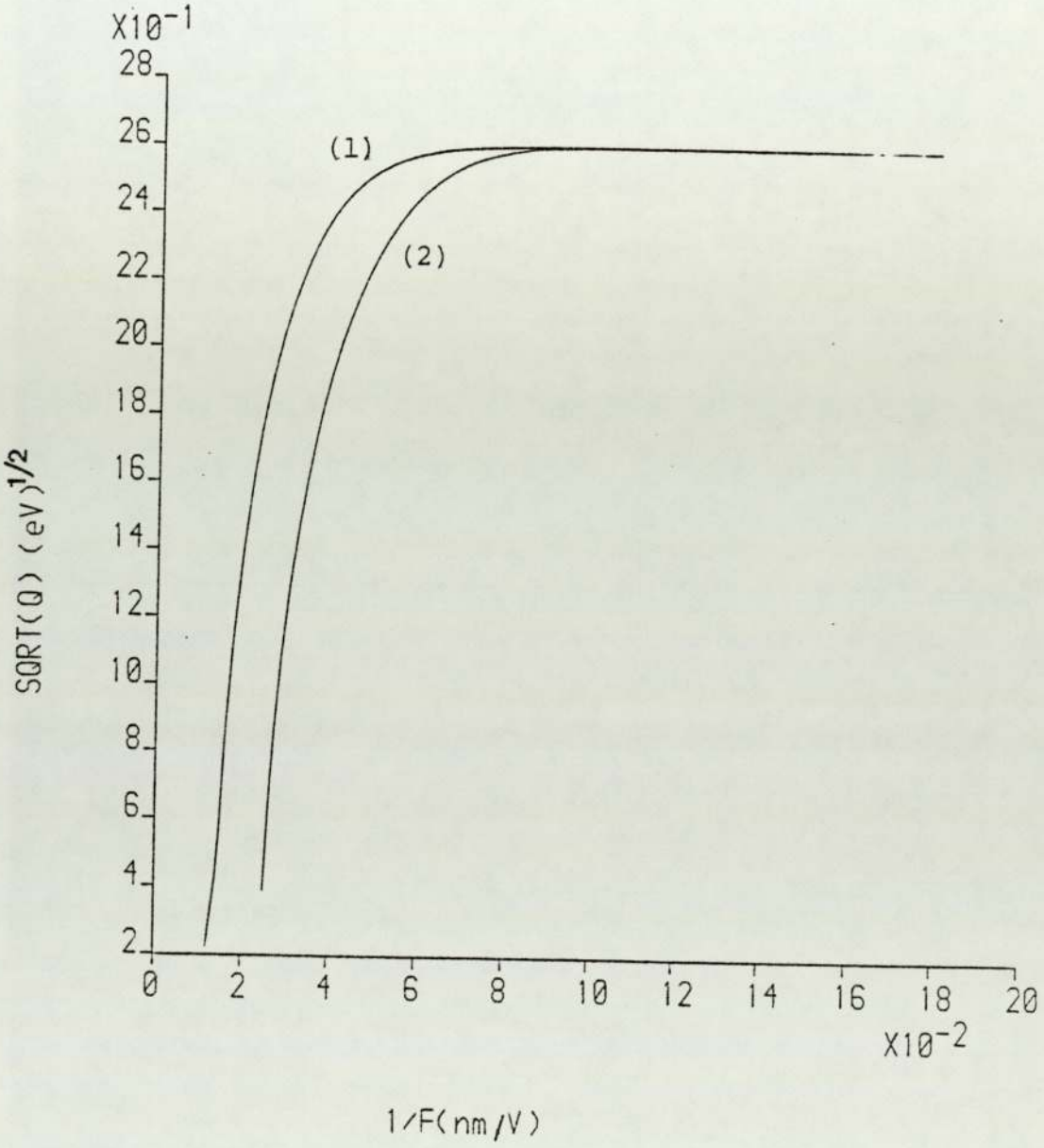

Fig. (7.12) $Q^{\frac{1}{2}}$ vs 1/F plots for Mo, using the Universal bonding well.

(1) "primitive" case.

(2) "normal" case.

Comparison of the Universal bonding well ('normal' case) with experiments:
+: Kellogg's Q-F RESULTS
For W.

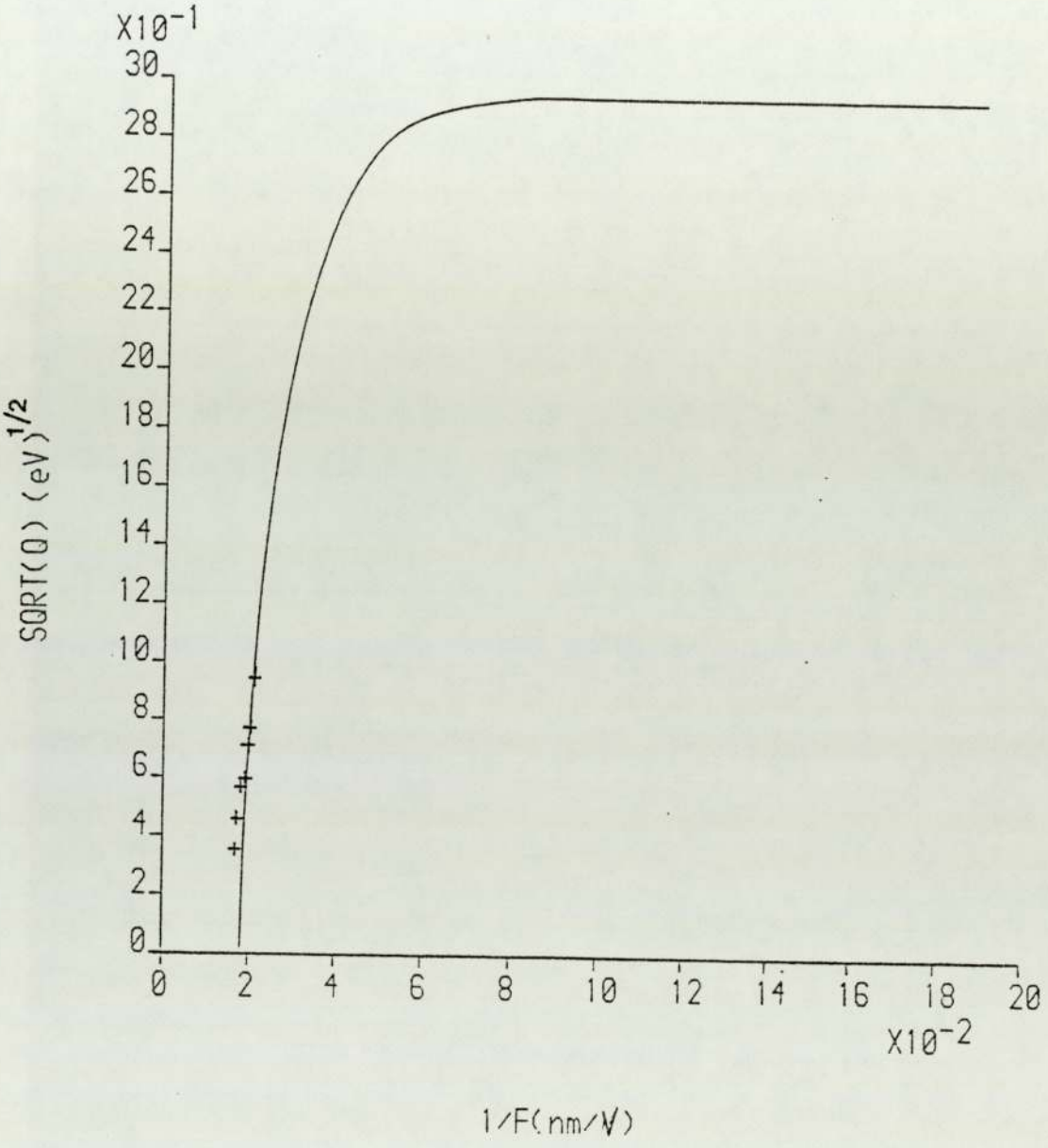

Fig. (7.13)

W that involve a direct measurement of Q. Because of the difficulties discussed earlier with possible breakdown of the assumption that $n_{hr}A$ is constant, we do not here include the results converted from $T^{\frac{1}{2}}$ vs 1/F experimental data.

It can be seen that the experimental results fit very well to the theoretical curve, better than they did in the parabola or Morse cases.

In this Universal bonding curve case, we must note that the slope of the theoretical curve is dependent on the scaling length ℓ. The value of ℓ has been taken from Rose et al. (1983), and we do not know how accurate it is. Also, it is not yet clear if this value of ℓ would really apply to the field evaporation situation. But if ℓ does not vary significantly with field, and the values of ℓ taken from Rose et al. are accurate enough, the agreement between theory and experiments is very good, and it would be encouraging if it could be confirmed for other materials.

7.7 THE OTHER WADA ET AL. RESULTS

Recently, Wada et al. (1983) reported on some measurements of the temperature dependence of evaporation voltage for four less field-resistant materials, namely Fe, Ni, Cu and Pd, in the presence of Neon and in the presence of Hydrogen.

The decrease in the evaporation voltage was particularly significant in the presence of Hydrogen. This effect is

well recognised experimentally, and is known as Hydrogen-promoted chemisorption (e.g. Müller and Tsong: 1973). Since chemisorption of Hydrogen is probably involved, we do not expect the normal theory of field evaporation to apply.

For the experiments conducted in the presence of Neon, the Wada et al. (1983) results were replotted in the form $Q^{\frac{1}{2}}$ vs 1/V, using the relationship given by equation (7.18) with J^{o}=0.1 layers/s, assuming the same values for n_{hr} and A as before. (I thank Dr. Wada for providing me with details of his raw experimental data).

The plots are shown in Figs. (7.14) and (7.15). They show three distinct regions:

(1) A middle region that is reasonably linear.

(2) In the lower region (high fields) deviations are observed as in the case of W and Mo (Chapter 4).

(3) The upper part of the plots diverge from linearity (except in the case of Fe).

The irregularities observed at high 1/V values in the case of Cu and Pd could well be due to experimental difficulties, and it would be useful to have these materials re-investigated by other workers.

In general terms, these results support our previous findings (for W, Mo and Rh), but since no direct estimates of Q or of n_{hr} A are available for the materials discussed

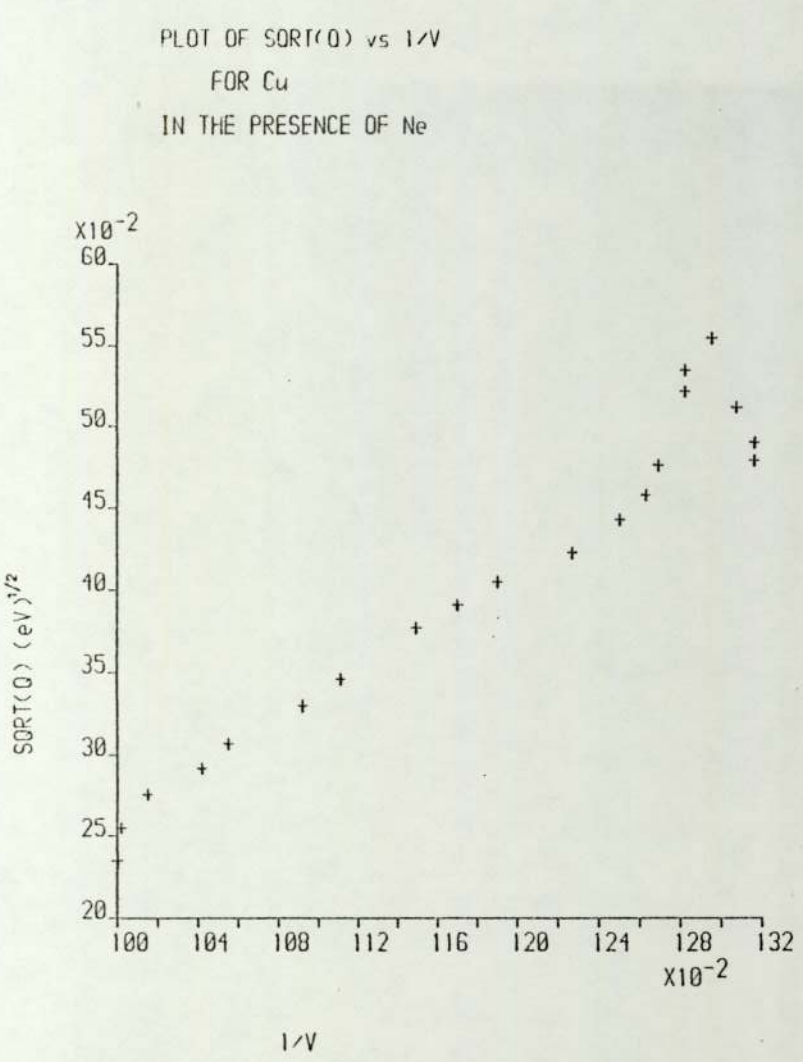

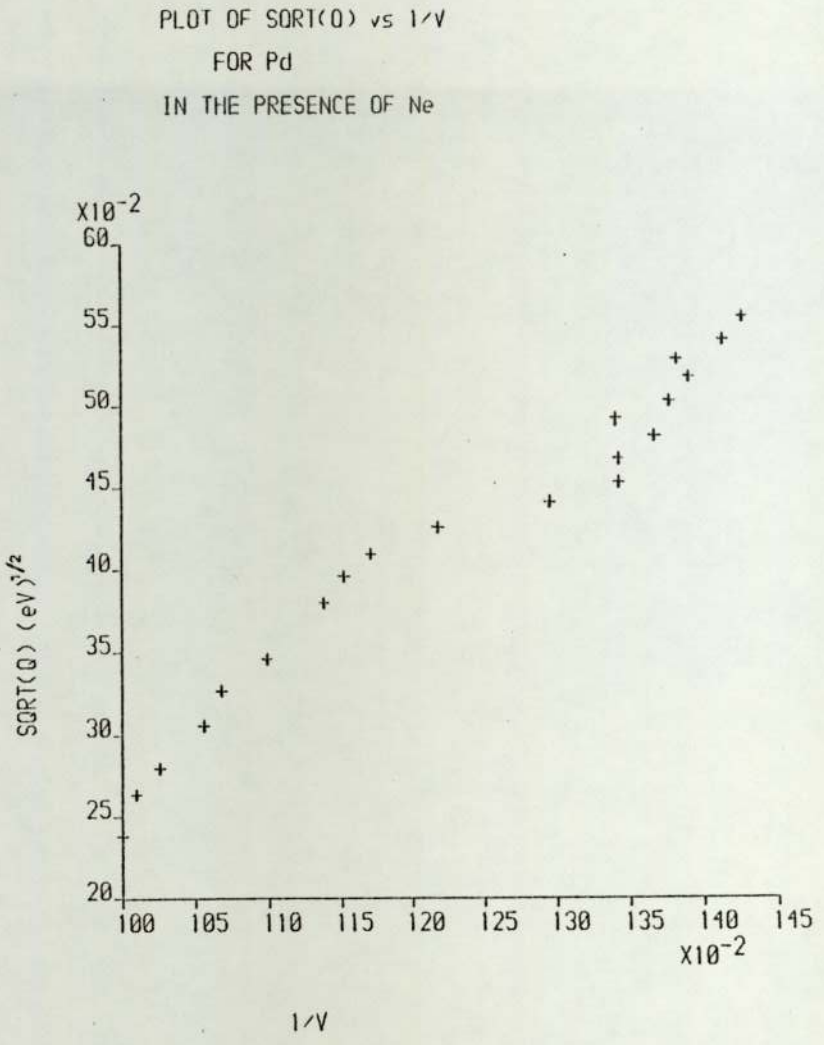

Fig. (7.14) The "other" Wada et al. results (Cu and Pd).

Fig. (7.15) The "other" Wada et al. results (Fe and Ni).

here, it seems inappropriate to carry out a more detailed analysis of the new Wada et al. results.

7.8 SUMMARY AND CONCLUSIONS

7.8.1 Summary of the Results

The main work in this chapter has been the employment of three different forms for the atomic bonding well. The crossing point of the atomic and ionic curves - for a charge-hopping mechanism - has been determined numerically, and $Q^{\frac{1}{2}}$ vs 1/F plots have been produced for W, Mo and Rh. This investigation was stimulated after Kellogg's (1981a) T-F results - taken over a range of temperatures higher than those of Wada et al. (1980) - showed a turn-over phenomenon at high temperatures. This initially suggested a breakdown of the parabolic approximation introduced in Chapter 4; - hence the use of more realistic forms for the atomic bonding well, namely a Morse potential and a Universal bonding curve . We may summarise our investigations as follows:

(1) Both the Morse and Universal bonding well confirmed the existence of a linear region in the $Q^{\frac{1}{2}}$ vs 1/F plots for all of W, Mo and Rh. Turn-over occurred at sufficiently high values of 1/F, but was different in kind from that observed by Kellogg.

(2) Simultaneously, Kellogg (1984) published new results for W where direct Q-F measurements, as well as T-F

measurements were made. The Q-F results, when replotted in the form $Q^{\frac{1}{2}}$ vs 1/F showed a straight line (in agreement with our earlier predictions) but the $T^{\frac{1}{2}}$ vs 1/F plots turned over.

(3) The same type of behaviour has also been observed in the case of Rh when the Ernst (1979) Q-F results were compared with Kellogg's T-F results.

(4) From his Q-F measurements, Kellogg also found an apparent field-dependence in the pre-exponential factor. This finding provides us with a ready explanation of the turn-over behaviour of the T-F plots. However, the very large deviation observed at the lowest field ($A=3\times10^{16}s^{-1}$ as opposed to $4\times10^{11}s^{-1}$ at the highest field - see Table (7.4)) is very surprising. We cannot think at present of any physical origin behind this effect. Possibly some experimental artefact (or the occurrence of surface diffusion) may be partly involved, and it would be helpful to have more experiments on this matter.

(5) Generally, our results showed that all three bonding well shapes behaved in a broadly similar manner.

(6) The $Q^{\frac{1}{2}}$ vs 1/F plots for Fe, Ni, Cu and Pd were basically compatible with our results on W, Mo and Rh.

We will come back, in Chapter 8, to discuss the results of this chapter in a broader context; however, the next section

draws some conclusions about the T-F and Q-F type experiments.

7.8.2 Some Comments on the T-F and Q-F Measurements

Throughout this thesis many T-F and Q-F measurements have been used, and it is useful to make some comparisons on their relative importance. Three different experimental techniques are usually involved:

(1) Straightforward Field-Ion Microscopy (FIM) experiments of the type used by Wada et al.

(2) Pulsed Laser Atom Probe (PLAP) techniques as used by Kellogg.

(3) More sophisticated experiments employing a retarding potential analyser as well as an ion counting system, of the type carried out by Ernst.

Experiments of type (1) above are carried out simply using direct visual observation. Techniques (2) and (3) involve more complicated apparatus and lengthier procedures, and are more laborious to perform.

Also the determination of activation energy Q is based on Arrhenius plots, so it is less direct than measurements of T and F. However, obtaining a theoretical relationship between Q and F involves fewer theoretical assumptions than a relationship between T and F, so it is useful to test the Q-F relationship directly, which can be done using

data provided from the counting facilities used, for example, by Ernst, Kellogg and Block et al.

In general, the more complex the experiments, the more information can be extracted. Thus in the experiments of the Berlin group (Ernst, Block and co-workers), where activation energy and appearance energy are measured jointly, additional information can be derived between binding energy and field, and about a relationship between x^p and F.

This latter type of experiment should be extended to more materials, because they provide most information.

CHAPTER 8

CONCLUSIONS, REVIEW OF RESULTS AND IDEAS FOR FUTURE WORK

This thesis has mainly been concerned with application of the theory of metal field evaporation to the analysis of experimental data, in particular that derived from the experiments of Tsong (1978b), Wada et al. (1980), Ernst (1979) and Kellogg (1981a, 1984). New formulae for the field dependence of activation energy and the temperature dependence of evaporation field were successfully applied to Tungsten, Molybdenum and Rhodium by assuming a charge-hopping evaporation mechanism. And we have shown how surface atomic parameters, such as the F^2-energy term coefficient c_α, bonding distance a, vibrational force-constant κ and frequency ν, can be estimated from field evaporation experiments involving measurements of activation and appearance energies as a function of field and temperature.

The aim of this chapter is to discuss further our earlier conclusions. We start first by summarising the main achievements arising in this work in Section 8.1. Section 8.2 re-examines the charge-draining mechanism, Section 8.3 tries to find an answer to why our model works, whilst Section 8.4 is a discussion of the discrepancies observed from the different plots. In Section 8.5 interpretations are given to the meaning of the various surface atomic parameters, in the context of charge-hopping and charge-draining. Finally, Section 8.6 suggests some future work.

8.1 MAIN ACHIEVEMENTS: SUMMARY

8.1.1 On The Image-Hump Formalisms

The simple image-hump formalisms for discussing the Müller mechanism have been re-investigated. In general, they have been found to be inconsistent with experimental data on evaporation flux field-sensitivities for most of the six refractory metals used (W, Mo, Ru, Hf, Ir and Pt), although in some cases no conclusions could be achieved. Incompatibilities between image-hump formalisms and experimental data have also been found by Biswas and Forbes (1982), Biswas (unpublished work), Ernst (1979) and Kellogg (1984). Investigation of Gomer-type mechanisms seemed a better route to follow.

8.1.2 Derivation of a c_α Value

By assuming an F^2-form for the field-dependent binding energy increase $\Delta\Lambda$, a value for the coefficient c_α has been estimated for Rh, namely: 1.05 ± 0.3 $meV^{-2}nm^2$. This was achieved by analysis of Ernst's (1979) data, based on the field-dependence of activation and appearance energies. We found that a zkT-type correction was necessary, with $z=10.5\pm3$. One implication of the derived c_α value was that the "F^2-energy term correction" in the activation energy formula, equation (4.5), was not insignificant.

It is worth noting that the analysis carried out on the coefficient c_α is independent of the assumed mechanism

of escape. We have also seen that c_α seems to have two origins: orbital polarization and partial ionization. This last point is very relevant to the question of whether the escape process is best described as a charge-hopping or charge-draining mechanism.

8.1.3 Basic Assumptions

The principal assumption in this work has been the use of a curve-intersection formalism for the field evaporation process, together with certain assumptions about the form of potential energy terms. The important assumptions of our model have been reviewed in Chapter 3. They include: a linear form for the electrostatic ion potential energy, on the grounds of historical reasons and the lack of well-developed charged surface models that take into account the various local field variations; the assumption of the validity of the classical image-potential at distances relevant to metal field evaporation; the use of flat surface models, so that field evaporation takes place in a perpendicular path; and - in part of the work - the use of a parabolic bonding well shape.

However, as suggested by Waugh et al., the evaporating atom may move sideways prior to evaporation. This indicates that the ion potential energy should perhaps be written in a two-dimensional form. Our supposition has in effect been that evaporation can be treated as if taking place in a straight path and that a curve-intersection formalism can be used as a first approximation. We return to this shortly.

8.1.4 Adopted Formulae

In our model, the following assumptions lead to basic mathematical formulae:

- The pre-evaporating atom is moving in a bonding well that is parabolic around its bottom, so that the activation energy Q is given by:

$$Q = \tfrac{1}{2}K\,(x^p - a)^2$$

- For values of x^p around the bonding distance a, the activation energy values are small and as a first approximation can be neglected in the determination of a relationship between x^p and F (Appendix A), namely:

$$x^p \simeq a\,F^e/F$$

These equations lead to the Q-F formula:

$$Q^{\frac{1}{2}} \simeq \Omega\,(F^e/F - 1)$$

- Through the emission equation:

$$Q = kT\,\ell n\,\left(\frac{n_{hr}A}{J^o}\right)$$

the T-F formula has been given by:

$$T^{\frac{1}{2}} = \theta^{\frac{1}{2}}\,(F^e/F - 1)$$

as long as the product $n_{hr}A$ does not vary significantly with field.

Thus it can be seen that our model involves independent assumptions/predictions of linear relationships between x^p

and 1/F, x^p and $Q^{\frac{1}{2}}$ and Q and T, and these lead to further predicted relationships between $Q^{\frac{1}{2}}$ and 1/F and $T^{\frac{1}{2}}$ and 1/F. These relationships can be arranged hierarchically, thus:

1) $x^p \propto 1/F$

2) $x^p \propto Q^{\frac{1}{2}}$, and hence from (1): $Q^{\frac{1}{2}} \propto 1/F$

3) $Q \propto T$, and hence from (2) : $T^{\frac{1}{2}} \propto 1/F$.

8.1.5 Application to Experimental Data

Ernst has derived values of x^p from his experiments, assuming electrostatic potential linearity and the classical image-potential form (Chapter 6). When these x^p are plotted against the independently known values of F, a straight line relationship is obtained, as shown in Fig.(8.1). This result at least demonstrates that Ernst's procedure and assumption (1) above are self-consistent.

Linearity between $Q^{\frac{1}{2}}$ and 1/F was originally predicted analytically by Forbes, on the basis of assumption (1) and a presumed parabolic shape for the bonding well. In this work numerical methods were used and a more realistic alternative, namely a Morse potential form, was used for the bonding well and compared with the parabolic case. Both cases contained a linear region but diverged at low field values. Basically, both bonding well shapes behaved in the same manner, except that divergence from linearity occurred at different levels. Towards the end of the project, a Universal bonding well form was used: the resulting $Q^{\frac{1}{2}}$ vs 1/F plots again showed a similar behaviour

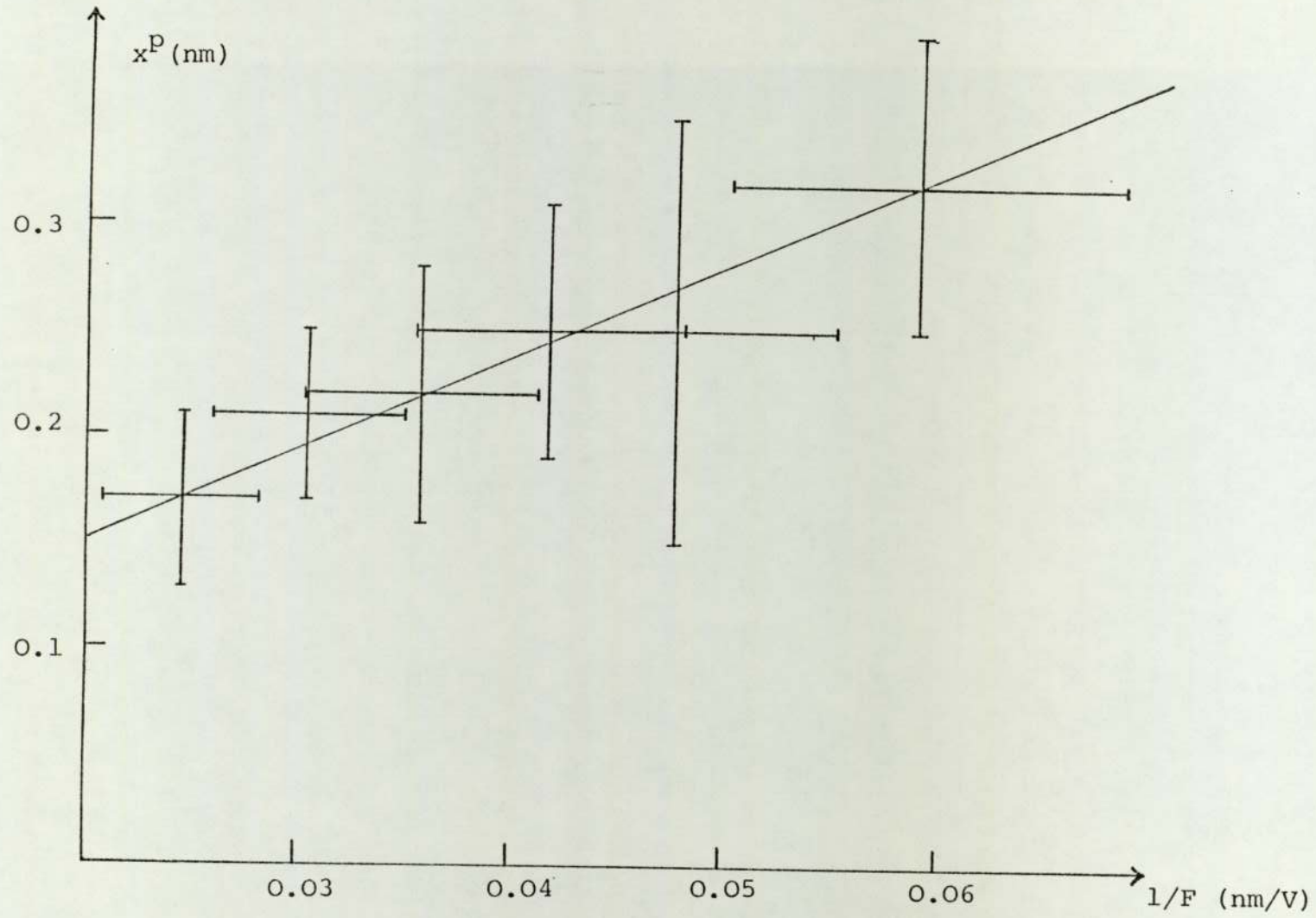

Fig. (8.1) A plot of x^p vs 1/F using Ernst's (1979) data, for Rh.

to the parabola and Morse cases. This shows that the general form of the results is independent of whether a parabola, Morse or Universal form is assumed for the bonding well shape.

Experimentally, the predicted linearities between x^p and $Q^{\frac{1}{2}}$, and $Q^{\frac{1}{2}}$ and 1/F, have been verified in the case of Rh over a wide range of fields and corresponding temperatures (100 to 600 K). The $Q^{\frac{1}{2}}$ vs 1/F linearity prediction has also been confirmed in the case of W (see section 7.5.1).

Recently, a further confirmation of linearities between x^p and $Q^{\frac{1}{2}}$, and $Q^{\frac{1}{2}}$ and 1/F have been found by Block et al. (private communication), in the case of Ag. We show in Fig. (8.2) the derived experimental x^p vs $Q^{\frac{1}{2}}$ and $Q^{\frac{1}{2}}$ vs 1/F plots.

Reasonable linearities in the $T^{\frac{1}{2}}$ vs 1/F plots have been found over a limited range of fields and corresponding temperatures, for a number of materials, including W, Mo, Rh and Cu, Ni, Fe, Pd (in the presence of Ne). Linearity was best evidenced in the W and Mo results, but there was no significant linearity in the Ga results (Chapter 4). Thus there seems to be some indication that the predicted relationship between $T^{\frac{1}{2}}$ vs 1/F is best demonstrated in the case of the highly field-resistant materials.

In many cases deviations from linearity in the $T^{\frac{1}{2}}$ vs 1/F plots were found at high fields, at low fields, or both,

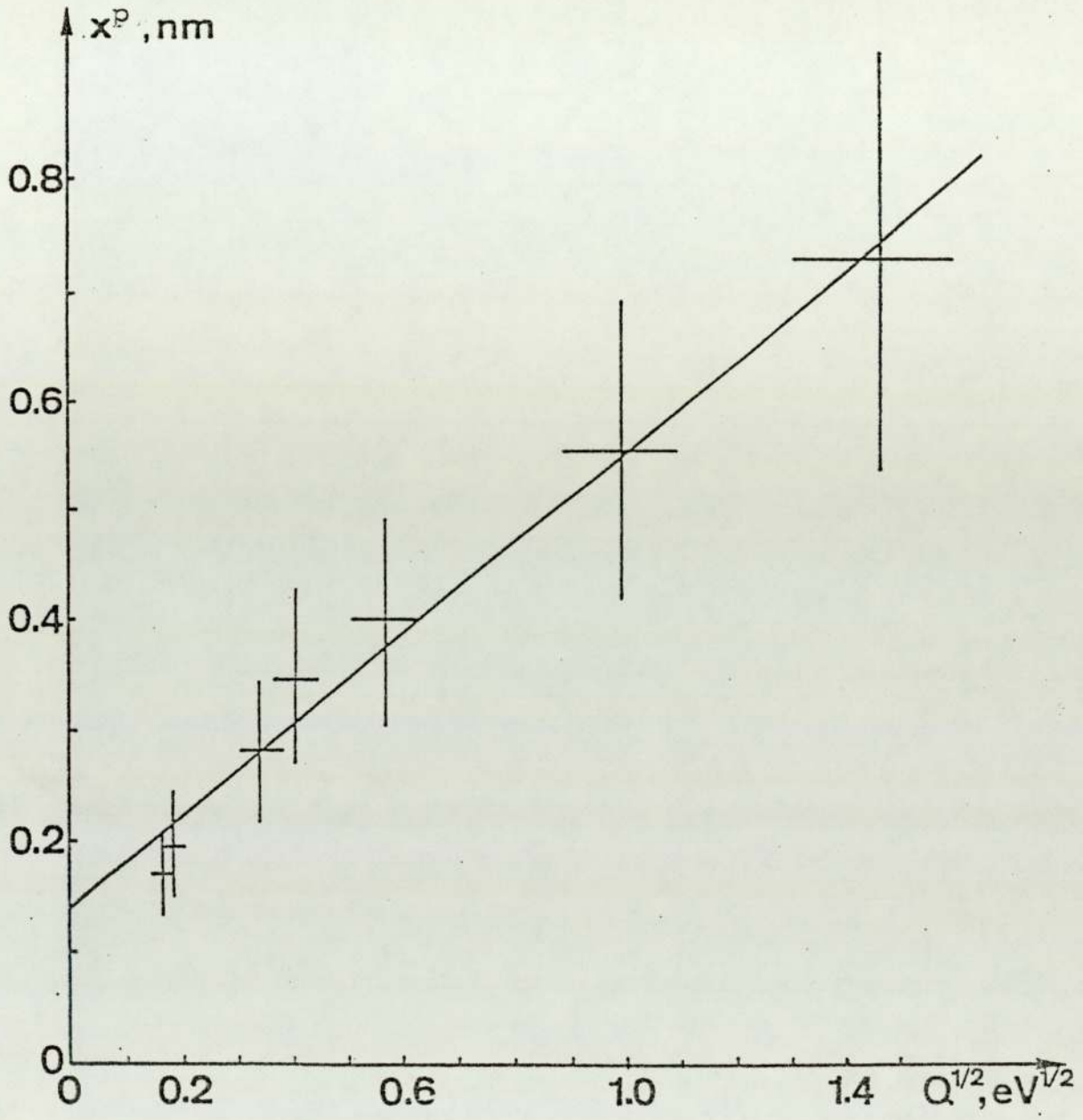

Fig. (8.2a) A plot of x^p vs $Q^{\frac{1}{2}}$ for Ag.

(Block et al.:private communication)

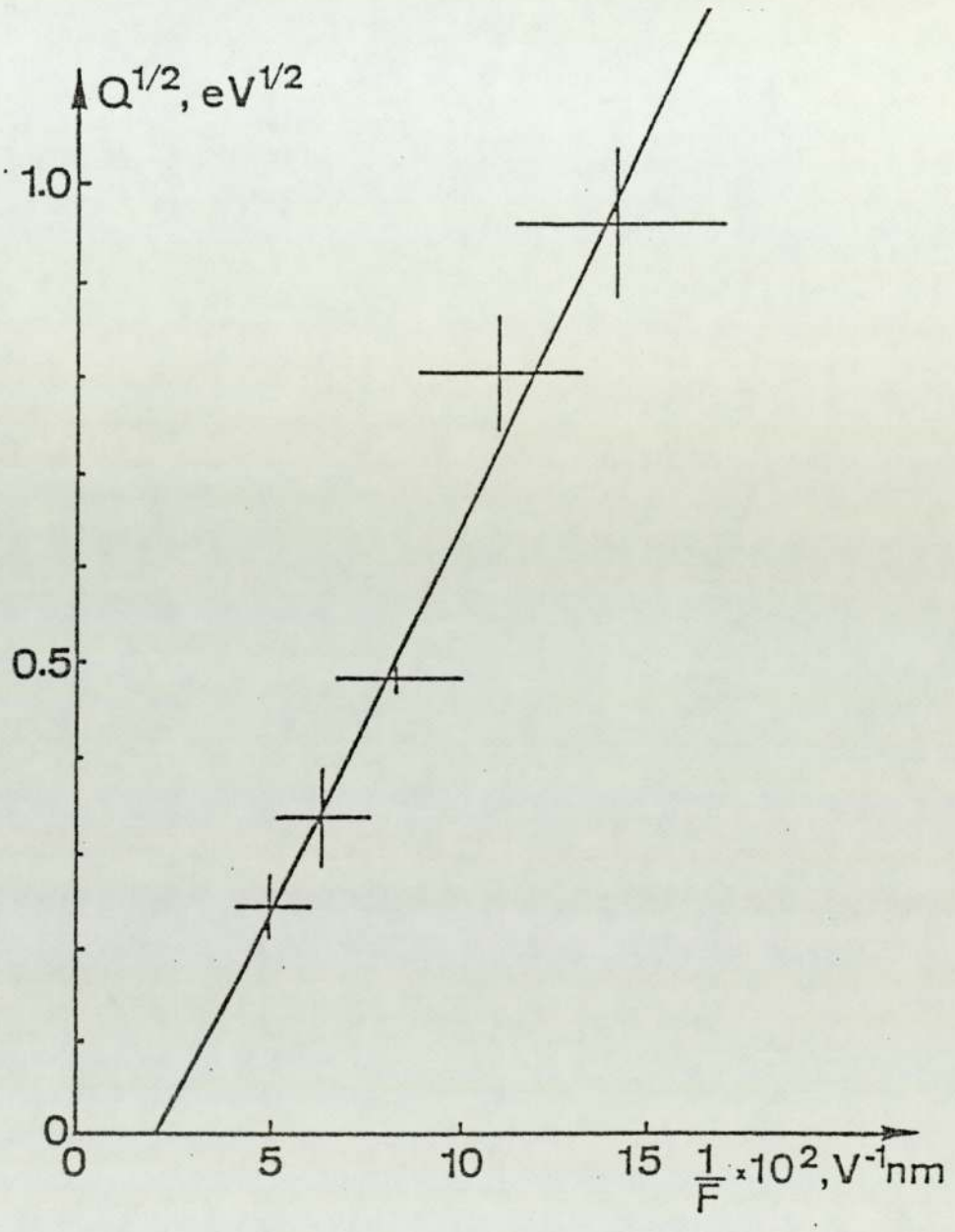

Fig. (8.2b) A plot of $Q^{\frac{1}{2}}$ vs 1/F for Ag.

(Block et al.: private communication)

as summarised in Table (8.1). On the other hand, for W and Rh, the $Q^{\frac{1}{2}}$ vs 1/F plots were linear over a range of low fields where the $T^{\frac{1}{2}}$ vs 1/F plots had deviated.

The discrepancies observed in connection with the T-F plots at low and high fields respectively, and the interpretation of the Q-F plots will be discussed in a later section.

Perhaps the most important point to be noticed is that linearities predicted by the curve-intersection formalism (and other assumptions) were present in the experiments. This is somewhat surprising, because the curve-intersection formalism is based on the charge-hopping mechanism, whereas there is every reason to suppose that charge-draining is the mechanism that operates. Hence, the next step must be to explore whether the mathematical relationships discussed in section 8.1.4 may still be valid in the theory of charge-draining. In this context, we return to reconsider the charge-draining mechanism.

8.2 ANOTHER LOOK AT THE CHARGE DRAINING MECHANISM

We must begin by pointing out that Fig. (3.7), which is the diagram most commonly used to discuss charge-draining is probably not strictly applicable to field evaporation under normal circumstances. This is because it really corresponds to a situation where, well to the left of the crossing point (i.e. close to the metal), the broadened energy level of the top electron in the surface

TABLE (8.1)

	high fields	medium fields	low fields
$T^{\frac{1}{2}}$ vs 1/F		observed linearity	
W (Wada et al.)	No	Yes	
Mo (Wada et al.)	No	Yes	
W (Kellogg)		Yes	No
Mo (Kellogg)		Yes	No
Rh (Kellogg)		Yes	No
$Q^{\frac{1}{2}}$ vs 1/F		observed linearity	
W (Kellogg)		Yes	Yes
Rh (Ernst)		Yes	Yes
Ag (Block)		Yes	Yes

Observed linearities of the various experimental $T^{\frac{1}{2}}$ vs 1/F and $Q^{\frac{1}{2}}$ vs 1/F plots at high fields, medium fields and low fields.

particle is completely below the Fermi level, so the particle is neutral. This is the situation envisaged in the "localised bonding" case described in Müller and Tsong (1969), originally discussed by Gomer and Swanson (1963).

In the case of metallic adsorption in the presence of a field, where the surface atom is presumed to be partially ionic, the broadened energy level is not completely filled at the bonding point. Consequently, it is probably better to draw the potential-energy diagram as in Fig. (8.3).

Here the top most curve, marked "F=O", is that corresponding to a neutral atom in zero-field. The intermediate curve, marked "U_o", corresponds to a neutral atom in the presence of a field. The inmost part of this curve is, however, hypothetical. And due to the presence of the field, the lowest curve, marked "U_α", corresponds to the equilibrium-state partially-charged object.

Hence in field evaporation, an atom should first conform to the curve U_α. As it starts moving away from the surface, charge drains out of it and, (at fields high enough for field evaporation to occur) it goes over the activation energy hump in a partially-charged state. Eventually, ionization is completed via further charge-draining and movement away from the surface. The resulting particle is an ion with a well defined charge

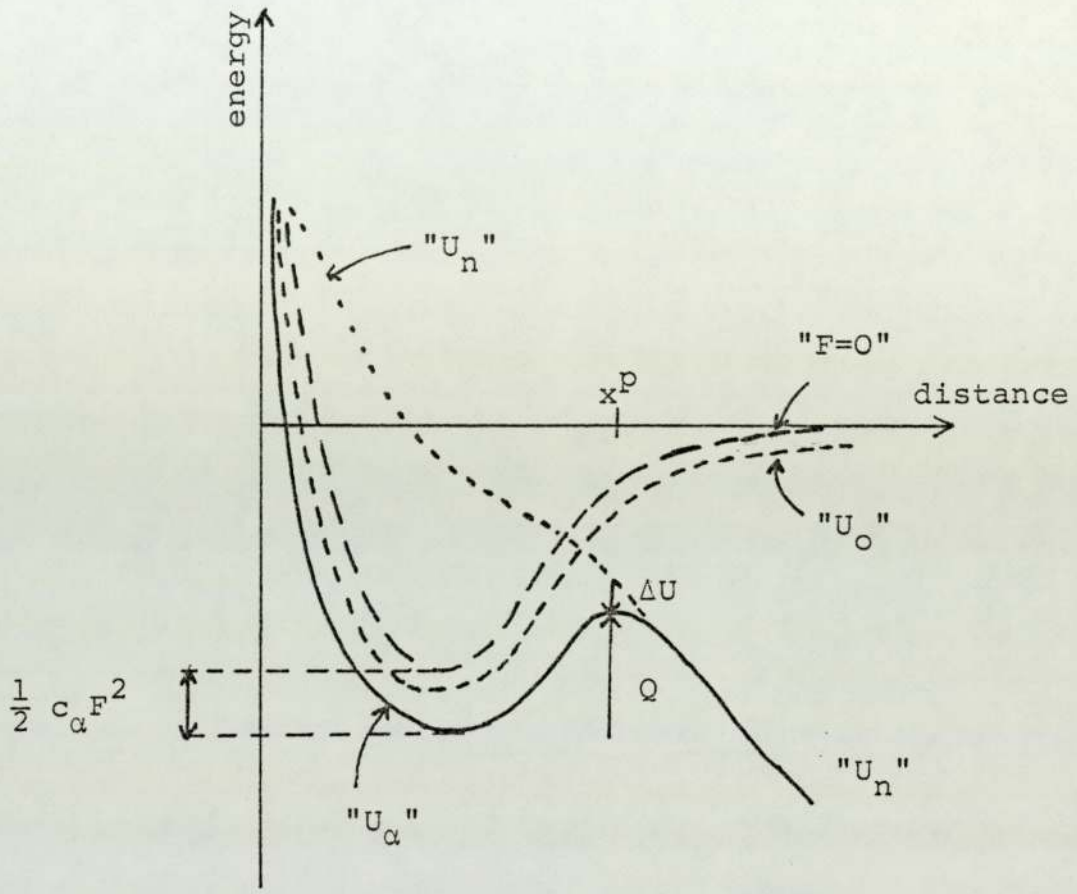

Fig. (8.3) The new bonding curve picture of charge-draining.

(ne) and follows the standard ionic potential energy curve, marked "U_n" in Fig. (8.3). Since well defined analytical forms exist for the different components that contribute to the ion potential energy, this "pure n-fold ionic curve" can be continued in towards the surface. This is shown as the dashed portion of the curve marked U_n on the diagram.

This whole picture, however, ceases to be valid if the activation energy hump is so far from the emitter surface that it is physically implausible that the evaporating entity can be partially charged, and in this case the mechanism is presumably charge-hopping. However, at the high fields characteristic of conventional field evaporation, the atom-surface distance is relatively small and charge-draining is presumed to be the escape mechanism.

In Fig. (8.3) it is the energy difference between the well-bottom levels of the "F=0" and "U_α" curves that is given by $\frac{1}{2} c_\alpha F^2$. Also, since the position x^p of the top of the hump is well defined (in the diagram) the difference ΔU between the level of the top of the hump and the value of the pure n-fold ionic potential at this position ($U_n(x^p)$) is also well defined in principle, although currently impossible to calculate. However, it is no longer easy to see how ΔU can be written meaningfully as $-\Gamma/2-\Delta\varepsilon$, as it was with the localised bonding picture of charge-draining (see Chapter 3).

It is also clear that the activation energy Q in Fig. (8.3) is well defined (although currently impossible to calculate accurately), and that it is possible in principle to express Q as a function of x^p, thus $Q=Q(x^p)$. (x^p is of course a function of external field F.)

8.3 WHY DOES OUR MODEL WORK?

8.3.1 The Charge-Draining Problem

In spite of its limitations and simplicity, our model has proved its usefulness. Hence, we may ask the question: why does it work adequately (at least for the more field-resistant materials) over a certain field range? One part of the answer must presumably be that the relationships $x^p \propto 1/F$ and $Q^{\frac{1}{2}} \propto x$ are inherent in the charge-draining mechanism as well as in the charge-hopping mechanism. We look at these in turn.

For the charge-hopping mechanism, the $x^p \propto 1/F$ relationship was derived as explained from the diagram shown in Appendix A, and reproduced in Fig.(8.4a). The corresponding diagram for the charge-draining case is shown in Fig. (8.4b). In both cases the bottom of the well (at any given field strength) is taken as the energy-zero level.

In the charge-hopping case the activation energy Q(C.H) is ignored in comparison with the height h^e. Clearly an equivalent approximation can be made in the charge-draining case about Q(C.D), so in this case too we expect $x^p \propto 1/F$, approximately.

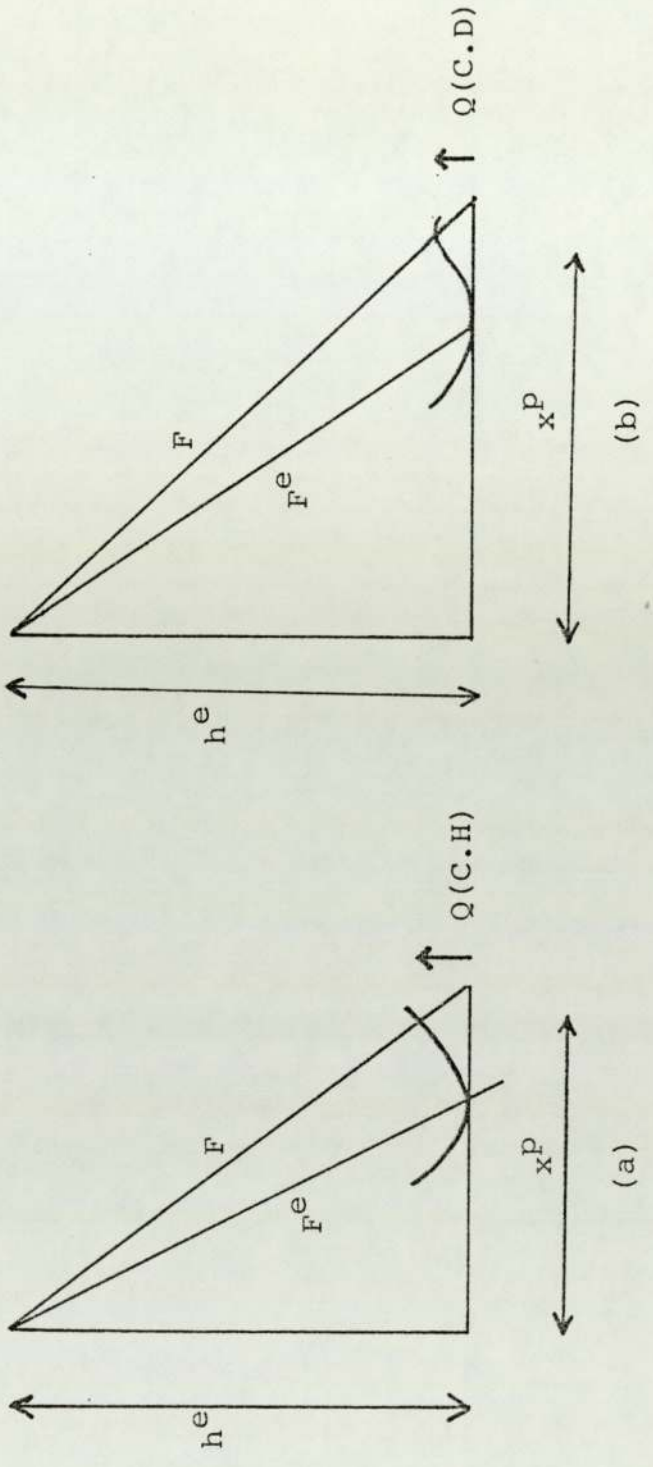

Fig. (8.4) Illustration of the x^p vs 1/F relationship.

(a) diagram from which the relationship between x^p and 1/F has been derived, for a charge-hopping mechanism.

(b) application to the charge-draining mechanism.

(Note that in the charge-draining case the position of the bottom of the well may be field dependent and shifts outwards, but this does not affect the relationship under discussion.)

As regards the second linearity relationship, we have seen that Q(C.D) can be expressed as a function of x^p, and it is obvious that Q(C.D) must increase as F decreases and the position of the hump moves out. Whilst it is difficult to reliably predict how Q(C.D) varies as a function of x^p, a variation of the form $Q^{\frac{1}{2}} \propto x^p$ (as deduced from experiments) is plausible. It is thus also plausible that $Q^{\frac{1}{2}} \propto 1/F$, approximately.

8.3.2 The Surface Structure Problem

Another surprising result comes from the work of Ernst who, assuming electrostatic potential linearity and a straight evaporation path, as mentioned earlier, derived experimental x^p values that vary linearly with the reciprocal of the measured fields, as shown in Fig. (8.1). This finding is not obviously compatible with the Waugh et al. suggestion of a two-stage path discussed in Chapter 3.

One may think of two possible explanations. First, if the evaporating entity does really move sideways, then this movement must occur over a very short distance, but ionization takes place on the straight portion of the path. Thus this possibility would certainly not affect

one of the assumptions of our model. Second, the Waugh et al. interpretation of their results might have been wrong. An apparent movement sideways could be due to some other reason, for example space-charge effects.

8.4 DISCUSSION: THE HIGH AND LOW FIELD ANOMALIES

We now examine the possible reasons behind the observed deviations in the T-F plots in the high and low-field regions, and the absence of these in the Q-F plots.

8.4.1 The High-Field Case

Under these conditions, the activation energy is low (i.e. low temperature) and ionization occurs close to the surface.

The observed deviations in the T-F plots (Chapter 4) could be due to the pre-dominance of ion-tunnelling, as already mentioned in Chapter 4. The deviation temperatures were 50 K for W and 35 K for Mo and are within the range of recent calculations of critical temperatures T^c. Another possibility is that one or other of the assumptions $x^p \propto 1/F$ or $Q^{\frac{1}{2}} \propto x^p$ ceases to be valid close to the surface. In the first case, failure of the relationship $x^p \propto 1/F$ could be due to the breakdown of the "straight path/constant field" model. In the second case, failure of the assumption $Q^{\frac{1}{2}} \propto x^p$ might be due to the fact that the top of the activation energy hump in charge-draining

gets closer to the bottom of the bonding well. These factors would also affect the x^p vs $Q^{\frac{1}{2}}$ and $Q^{\frac{1}{2}}$ vs 1/F plots, but no data points were available in the high fields range.

Independent evidence that ion-tunnelling effects are operative in the high fields range can, however, be found in the work of Menand and Kingham (1983; submitted for publication) and Menand et al. (1984).

Menand and Kingham first suggested the possibility of ion-tunnelling for Boron field-desorbed from FeB and CoB metallic glasses at T=78 K and T = 20 - 30 K respectively, during a study on the isotopic variations in field evaporation charge-state of B ions. Their suggestion was supported in a subsequent investigation where the desorption rate of B ions was found to be almost independent of temperature, below 140 K. Further evidence for tunnelling was provided by the relative abundance of $^{10}B^{2+}$ and $^{11}B^{2+}$ isotopes as the temperature was varied. The critical temperature predicted for Boron by Menand and Kingham (1983) is in the range 140-200 K; this is compatible with the experimental findings, and tends to confirm the adequacy of the theory used to predict critical temperatures.

In our case (certainly for W and Mo) we may conclude that in the high-fields situation, ion-tunnelling is probably an important factor. But a possible failure of either of the x^p vs 1/F or $Q^{\frac{1}{2}}$ vs x^p relationship should also be considered.

8.4.2 The Low-Field Case

In this case, the activation energy is high (i.e. high temperature) and ionization occurs further away from the surface.

The corresponding deviations in the $T^{\frac{1}{2}}$ vs 1/F plots (Chapter 7) may have several origins. It was first thought that the major reason was due to break-down of the parabolic approximation (i.e. a bonding well shape effect). Then, other possibilities were considered, for example, the desorption of the Helium used as an imaging-gas, or the onset of surface diffusion, at high temperatures. Hence, the bonding well shape effect stimulated the work on the Morse potential (Chapter 7).

However, several points deserve notice. First, the imaging-gas was not present in Kellogg's experiments for example. Second, the Morse potential (and Universal form) cases behaved similarly to the parabolic case. But the most remarkable result comes directly from the experimental $Q^{\frac{1}{2}}$ vs 1/F plots for both Rh and W, which fitted consistently our model prediction (i.e. no deviation was observed in the low-field regime where the $T^{\frac{1}{2}}$ vs 1/F plots do deviate). This prediction has now been supported further by the recent $Q^{\frac{1}{2}}$ vs 1/F plot for Ag, provided by Block et al. (see Fig. (8.2)).

If the bonding well shape effect were the main cause for the observed deviations in the $T^{\frac{1}{2}}$ vs 1/F plots, it

would also have appeared as deviations in the experimental $Q^{\frac{1}{2}}$ vs 1/F plots. But we now have evidence that these deviations do not show for three materials. So the deviations in the $T^{\frac{1}{2}}$ vs 1/F plots must have another cause.

In this context, Kellogg (1984) discovered experimentally (in the case of Tungsten) an apparent field-dependence in what he called the "frequency prefactor". In more specific terms, this should be interpreted as an apparent field-dependence in the product $n_{hr}A$. A field-dependence in $n_{hr}A$ would lead to a breakdown of the assumption that $Q \propto T$ (for a constant flux). This would provide an explanation of the different $Q^{\frac{1}{2}}$ vs 1/F and $T^{\frac{1}{2}}$ vs 1/F behaviours observed in the case of W, and probably in the case of Rh and Ag too. The physical cause of the field-dependence in $n_{hr}A$ is not at present clear, even though one can speculate theoretically about its possibility, due for example to bonding well shape effects. At somewhat lower fields (i.e. at higher temperatures), outside the range of the experimental $Q^{\frac{1}{2}}$ vs 1/F plots, we should presumably expect effects due to bonding well shape as discussed in Chapter 4 and/or surface diffusion, and effects due to the field-dependence in $n_{hr}A$, to occur. In this case, the interpretation of the experimental results, in that field range, might be found difficult.

8.5 EXTRACTION OF SURFACE ATOMIC PARAMETERS

In the context of a charge-hopping mechanism and using the x-Q and Q-F plots, values of bonding distance, force-constant and vibration frequency have been derived for Rh. These are: $a = 0.13 \pm 0.03$ nm, $\kappa = 80(-36/+57)$ eV/nm^2 and $\nu = 1.4\ (-0.3/+0.5) \times 10^{12}$ Hz. These results were based on weighted linear regressions of the x-Q and Q-F plots. In the analysis, it was found important to estimate and include a zkT-type correction. The work-function was also an important factor. Its choice had a significant effect on the values found for a and κ. The value derived for κ was physically reasonable in size, but the value of a was less than the neutral Rh atom radius. This last result was interpreted to suggest that surface atomic structure must be considered in field evaporation theory. Values found for the zero-Q evaporation field F^e were significantly higher than reported experimental fields, for all three materials (W, Mo, Rh), but some justification for this has been given.

The above parameters F^e, a and κ have of course been derived in the context of a model that assumes the charge-hopping mechanism and a constant field/straight path. We now re-examine these parameters in the context of a charge-draining mechanism, but still using the constant field/straight path model. In this case it is assumed that the position of the bottom of the bonding well moves outwards slightly, as the field is increased and the bound

atom become more ionic. Thus the bonding distance at the point where Q=0 (which is denoted by a^e) is expected to be greater than the zero-field bonding distance (which is denoted by a^o).

In the case of charge-hopping, extrapolating the experimental x^p vs $Q^{\frac{1}{2}}$ plot should yield a value for the zero-field bonding distance a^o, since the assumptions are made that $Q^{\frac{1}{2}} \propto x^p$ all the way down to the bottom of the well, and that the position of the well bottom is independent of field.

But if the charge-draining mechanism is operating, the bonding distance is moved out slightly from its zero-field value, as the field is increased. If a linear extrapolation back to the x^p axis can be used, the deduced value would be a^e, and would correspond to the point of inflexion when the activation energy hump has just disappeared, since Q=0 in this case. For Rh, this value has been found to be 0.13 nm. The corresponding zero-field value a^o would be less than this, so the bonding site would be even closer to the electrical surface than assumed in Chapter 6, and the considerations of section 6.11 would be reinforced.

However, it is not certain that a linear extrapolation would be fully valid. At the highest fields, the top of the activation energy hump gets closer to the surface, the bottom region of the bonding well changes rapidly with field, and the assumption $Q^{\frac{1}{2}} \propto x^p$ might break down. But

it seems likely that any deviation might be relatively small, perhaps as shown in Fig. (8.5), so the extrapolated value a* (shown in the figure) is probably close to a^e.

For the charge-draining mechanism, the parameter F^e is still defined by Q(C.D)=0. If a linear extrapolation of the experimental $Q^{\frac{1}{2}}$ vs 1/F plot can be used, it would yield a value for F^e. However, as in the case of the x^p vs $Q^{\frac{1}{2}}$ plot, if the linear extrapolation is not valid, there would be a small divergence between the real and extrapolated values for F^e.

The extrapolated F^e is, of course, still higher than experimental field values, but the consistency argument presented in section 6.10 still holds because it actually employs consistent values of a^e and F^e derived from Ernst's results.

With the charge-draining mechanism, the slope of the x^p vs $Q^{\frac{1}{2}}$ can no longer be directly interpreted as a force-constant, that is a parameter associated with a bonding well shape. However, we can imagine that the level and position of the top of the hump must to some extent reflect the shape of the zero-field bonding well. Then it is not surprising that the measured slope has a value close to that of the force-constant expected for a well where the vibration frequency is about 1×10^{12} Hz.

For the charge-draining mechanism but with a sideways movement, the interpretation of the extrapolated parameters

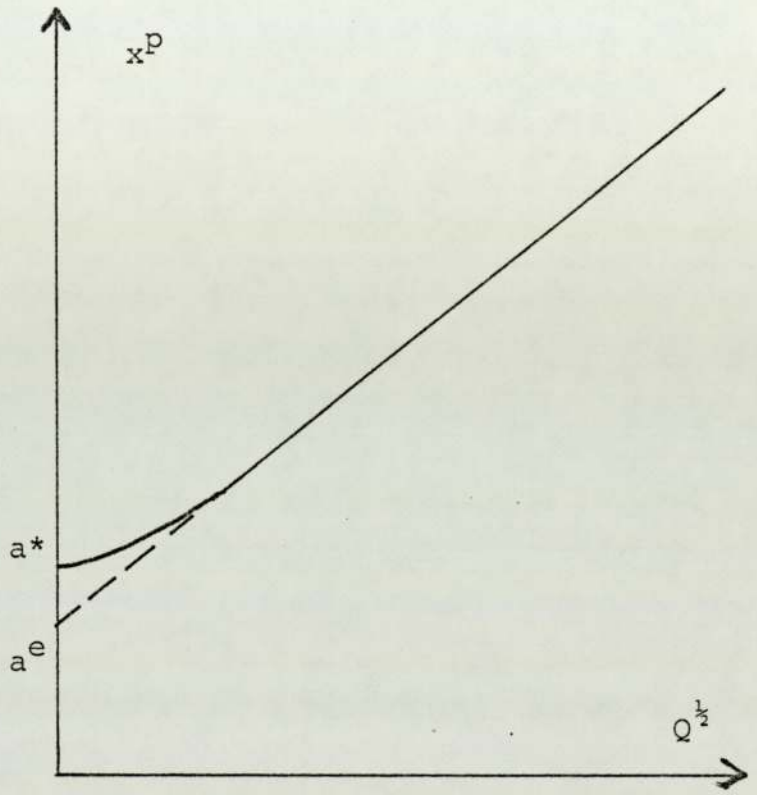

Fig. (8.5) A possible variation of the x^p vs $Q^{\frac{1}{2}}$ relationship at high fields.

a^e : bonding distance assuming a linear extrapolation

a^* : bonding distance in the case where $Q^{\frac{1}{2}} \propto x^p$ breaks down.

is more speculative. From the x^p vs $Q^{\frac{1}{2}}$ plot, only the parameter a^e can be deduced; we cannot directly associate this with the bonding site. As regards F^e, the argument presented above still seems to apply, i.e. there may be a small divergence between the extrapolated and real values. The parameter derived from the slope of the x^p vs $Q^{\frac{1}{2}}$ plot presumably relates to the shape of the part of the bonding well that lies along the section of the path where ionization occurs. It seems unwise to speculate further, because in this sideways movement case, Ernst's experiments really ought to be analysed in terms of a structured surface model.

8.6 SOME SUGGESTIONS FOR FUTURE WORK

From the analysis in this thesis, it is clear that more experimental and theoretical work would be useful in a number of areas. In order to improve our understanding of the theory of field evaporation, we certainly need progress in the following topics. First, a better view on the behaviour of charged surfaces. In particular, we need surface models that are able to predict local field and potential variations, taking into account the local atomic (geometrical) and electronic structures. It would, for example, be useful to re-analyse Ernst's Rhodium data on the basis of a well developed surface model. Second, the charge-draining mechanism needs a better theoretical basis. In this context, we may suggest two main approaches that deserve to be explored:

(1) The use of semi-empirical potential energy terms to give a better picture of ion-surface interactions. This has recently been attempted by Kingham (1985), although his particular treatment seems unsatisfactory because it predicts that the evaporating entity will have an integral charge in its as-bound state, and that the field evaporation process involves an integral change in the charge-state.

(2) Another more sophisticated approach would involve chemisorption-based calculations, but with electrostatic potential terms included self-consistently. Possible techniques include a tight-binding method (for example a development of Kingham's cluster calculations) or some modification of the Universal bonding curve approach to take account of the partial ionization of the pre-evaporating entity. However, calculations of this type seem likely to prove very difficult.

On the experimental side, the immediate requirement is for:

(1) More measurements on the temperature dependence of evaporation field, and the field dependence of activation energy and appearance energy, of the type first carried out by Ernst. These should include a wider range of materials and (if possible) use a wider range of fields.

(2) Confirmation of the apparent field-dependence of the

pre-exponential product $n_{hr}A$, in the case of W, and similar investigations for a wider range of materials. Possible theoretical reasons for the field-dependence in $n_{hr}A$ must also be explored.

For the time being, however, our model can be seen as a good first approximation towards a better understanding of the theory of field evaporation.

APPENDICES

APPENDIX A

NEW ACTIVATION ENERGY FORMULA:

From Chapter 1, the virial of an ion at a distance x from the emitter's electrical surface, in an external field F, is:

$$W_n(x,F)=(\Lambda^F+H_n-n\phi^E)-neFx-\frac{n^2e^2}{16\pi\varepsilon_o x}+\frac{G}{x^t}-\frac{1}{2}c_nF^2 \qquad (A1)$$

where the parameters have meanings as described in Chapter 1. The activation energy is then given by equation (1.14), i.e.:

$$Q_n=W_n(x^p,F)=(\Lambda^F+H_n-n\phi^E)-neFx^p-\frac{n^2e^2}{16\pi\varepsilon_o x^p}+\frac{G}{(x^p)^t}-\frac{1}{2}c_nF^2 \qquad (A2)$$

If we use $\eta_n(x,F)$ to represent the "purely chemical" ion-surface interaction, approximated here by the image-potential, repulsion and F^2-energy terms, then:

$$\eta_n(x,F)=-\frac{n^2e^2}{16\pi\varepsilon_o x}+\frac{G}{x^t}-\frac{1}{2}c_nF^2 \qquad (A3)$$

and

$$Q_n=(\Lambda^F+H_n-n\phi^E)-neFx^p+\eta_n(x^p,F) \qquad (A4)$$

which can be put in the form:

$$neFx^p=(\Lambda^F+H_n-n\phi^E)+\eta_n(x^p,F)-Q_n\equiv h(x^p,F)-Q_n \qquad (A5)$$

where

$$h(x^p,F)=(\Lambda^F+H_n-n\phi^E)+\eta_n(x^p,F) \qquad (A6)$$

$h(x^p,F)$ as defined by Equation (A6) is a slowly varying parameter called the "pivot height" (Forbes: 1982d) and has the dimensions of energy. At the zero-Q evaporation field F^e, $x^p=a$ and $Q_n=0$, so that equation (A5) becomes:

$$neFa = (\Lambda^{F^e} + H_n - n\phi^E) + \eta_n(a,F^e) = h^e \qquad (A7)$$

h^e is a constant defined by Equation (A7) and is called "standard pivot height". The relationship between h^e, a and F^e can be illustrated graphically as follows:

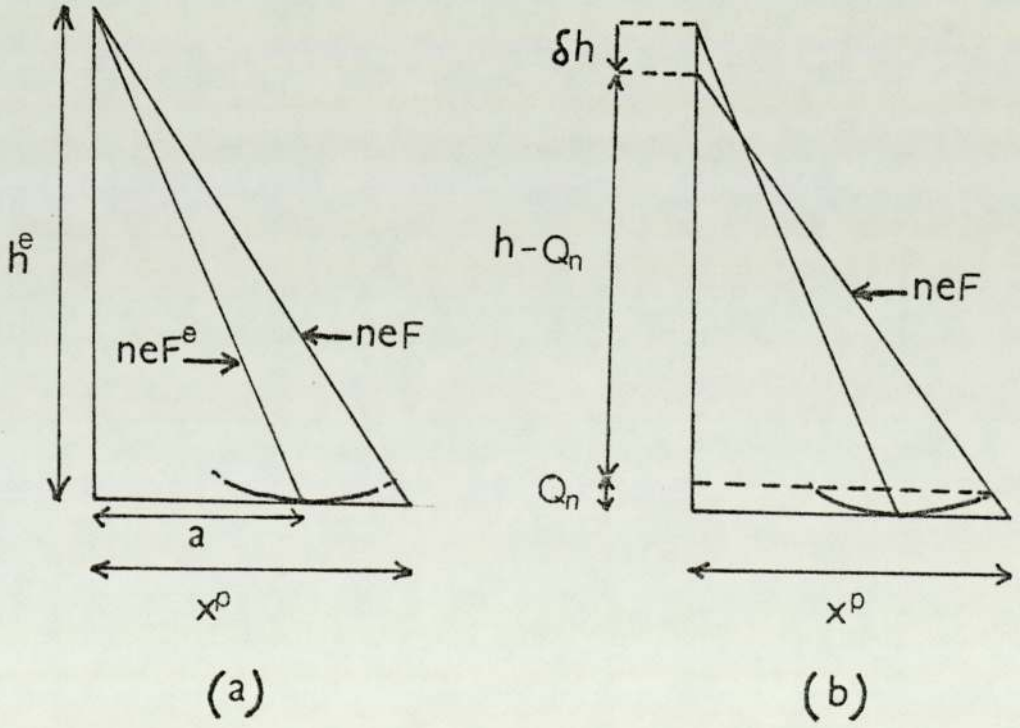

The x-axis is placed at the level of the bottom of the potential well, and the y-axis is placed to coincide with the metal's electrical surface: the third side of

the triangle is drawn through a "pivot" on the y-axis at an energy level h^e (Fig. (a) above).

For F slightly less than F^e, the third side - neF - would cut the x-axis at x^p greater than a. For values of x^p not very far from the bottom of the well, Q_n is small. Assuming that the variation of h is also small enough to be neglected, we have:

$$h(x^p,F) \simeq h^e \tag{A8}$$

and in a first approximation equation (A5) becomes:

$$neFx^p = h(x^p,F) - Q_n \simeq h^e \tag{A9}$$

This last point is illustrated in Fig. (b), where the third side is swinging about the pivot on the y-axis and intercepting the x-axis at x^p. From Equations (A7) and (A9), it follows that:

$$x^p \simeq h^e/neF = a\ F^e/F \tag{A10}$$

At this point it is necessary to introduce some specific assumption about the shape of the bonding well. As a first approximation valid near the well bottom, Forbes (1982d), took the well to be parabolic. The atomic potential energy relative to the bottom of the well, V(x,F) is then given by:

$$V(x,F) = \frac{1}{2}\kappa(x-a)^2 \tag{A11}$$

where κ is a force-constant. Any field-dependence appears in the value of κ.

Bearing in mind the subsidiary condition in equation (1.22), (and using x^p interchangeably with x^{cr}), the activation energy is:

$$Q(F) = V(x^p,F) = \frac{1}{2} \kappa (x^p-a)^2 \qquad \text{(A12)}$$

Substituting x^p from equation (A10) into equation (A12) we obtain:

$$Q_n \simeq \frac{1}{2} \kappa \left(\frac{h^e}{neF} - a\right)^2 = \frac{1}{2} \kappa a^2 (F^e/F - 1)^2 \qquad \text{(A13)}$$

or

$$Q_n = \Omega (F^e/F - 1)^2$$

where

$$\Omega = \frac{1}{2} \kappa a^2 \qquad \text{(A14)}$$

This is a Q-formula explicit in F for the charge-hopping mechanism.

Equation (A13) is a first approximation. A better approximation can be obtained by adding higher-order terms to h^e when Taylor-expanding $h(x^p,F)$ in Equation (A9) while continuing to neglect Q_n. Thus:

$$h(x^p,F) \simeq h^e + \left[\left(\frac{d\Lambda}{dF}\right) + \left(\frac{\partial \eta_n}{\partial F}\right)\right]_{a,F^e} (F-F^e) + (x^p-a) \left.\frac{\partial \eta_n}{\partial x^p}\right|_{a,F^e} + \ldots \qquad \text{(A15)}$$

since it is known that

$$\left.\frac{\partial \Lambda}{\partial x^p}\right|_{a,F^e} \equiv 0$$

Using

$$\eta_n' = \left.\frac{\partial \eta_n}{\partial x^p}\right|_{a,F^e} \tag{A16}$$

and

$$\pi^e = \left[\left(\frac{d\Lambda}{dF}\right) + \frac{\partial \eta_n}{\partial F}\right]_{a,F^e} \tag{A17}$$

we write Equation (A15) in the simpler form:

$$h(x^p,F) \simeq h^e + \pi^e(F-F^e) + \eta_n'(x^p-a) \tag{A18}$$

Then, substituting into Equation (A 9.), we obtain:

$$x^p \simeq \frac{h^e}{neF} + \frac{\pi^e}{neF}(F-F^e) + \frac{\eta_n'}{neF}(x^p-a) \tag{A19}$$

and an expression for (x^p-a) is easily derived:

$$(x^p-a) \simeq \left[\left(\frac{h^e}{neF} - a\right) + \frac{\pi^e}{ne}\left(1 - \frac{F^e}{F}\right)\right]\left[1 - \frac{\eta'}{neF}\right]^{-1} \tag{A20}$$

knowing that $h^e = neF^e a$, we have:

$$(x^p-a) \simeq \left[a\left(\frac{F^e}{F} - 1\right) - \frac{\pi^e}{ne}\left(\frac{F^e}{F} - 1\right)\right]\left[1 - \frac{\eta'}{neF}\right]^{-1} \tag{A21}$$

Hence,

$$(x^p-a)^2 \simeq \left[(a- \frac{\pi^e}{ne})(\frac{F^e}{F} - 1)\right]^2 \left[1- \frac{\eta'}{neF}\right]^{-2} \quad \text{(A22)}$$

A new expression for Q is then given by:

$$Q_n \simeq \frac{1}{2}\kappa(a- \frac{\pi^e}{ne})^2 (1- \frac{\eta'}{neF})^{-2} (\frac{F^e}{F} -1)^2 \quad \text{(A23)}$$

An explicit expression for π^e can be obtained by using the conventional F^2 expression in Equation (A17), thus:

$$\pi^e = (c_\alpha - c_n)F^e \quad \text{(A24)}$$

APPENDIX B

B.1 INTRODUCTION

The chemical bonding of an atom (the "adsorbate") to a surface (the "substrate") is termed chemisorption. Chemisorption involves electron sharing or exchange between adsorbate and substrate, as opposed to physisorption which involves only the Van de Waals interactions.

In general, adsorption include alkali metals, Hydrogen, Oxygen, Nitrogen, small organic and inorganic molecules and other metals, whilst the main substrates are the transition and noble metals. Our interest here is, of course, the chemisorption of transition and noble metals on their own substrates, and particularly the chemisorption of kink-site atoms on field-ion emitters.

As indicated in Chapter 1, surface atoms at the kink site positions can be seen as chemically bound to the surface, with binding energy Λ°. Various experimental methods exist for estimating Λ° (commonly known as the heat of sublimation). They range from the early thermodynamic approaches, to field desorption techniques (e.g. Plummer and Rhodin: 1968).

The general form of the bonding potential vs. distance relationship is well known. It might in principle be derived from chemisorption-type calculations, as a function of substrate-adsorbate distance. But this would be tedious

(unless the "Universal binding-energy function" has solved the problem!), and has rarely been attempted. Hence, simple classical models (e.g. Lennard-Jones, Morse, Buckingham potentials) are still in use.

The aim of this Appendix is to briefly describe some of the theoretical methods that are used in chemisorption calculations, in particular the one-electron approximations to an N-body problem (see Muscat and Newns: 1978), and the electron-level broadening approach first put forward by Gurney (1935). We then indicate how this may be relevant to field evaporation theory by citing the work of a few authors.

B.2 N-ELECTRON THEORY

The chemisorption energy ΔE (= Λ^{o} at the bonding point) can be simply defined as the difference between the energy E^{∞} of the separated substrate and adsorbate, and the energy E of the adsorbed system:

$$\Delta E = E^{\infty} - E \qquad (B.1)$$

In this discussion, it is assumed that interaction between the adsorbate ion and the substrate may be neglected, and hence E is taken as the energy of the electron system.

Chemisorption is thus regarded as the theory of a system consisting of a large number N (assumed even) of electrons. The system is described, in the Born-Oppenheimer approximations, by its electronic wavefunction $\Psi(r_1,\ldots r_n)$

where r_n is the coordinate of the n^{th} electron. The Schrödinger equation for the system is then solved using different approximations, which are mentioned in the following discussion.

In the Hartree approximation, the wavefunction Ψ, assuming spin degeneracy, is given by the product:

$$\Psi(r_1,\ldots r_n) = \prod_{n=1}^{N/2} \psi_{n\uparrow}(r_{2n-1})\psi_{n\downarrow}(r_{2n}) \qquad (B.2)$$

where $\psi_{n\uparrow\downarrow}(r_{2n})$ are one-electron wavefunctions.

The corresponding one-electron Hamiltonian is given by:

$$H = -\frac{\hbar^2}{2m}\nabla^2 + V(\vec{r}) \qquad (B.3)$$

where

$$V(\vec{r}) = V_I(\vec{r}) + V_H(\vec{r}) \qquad (B.4)$$

$V_I(\vec{r})$ is the potential of the ion cores and $V_H(\vec{r})$ is the electrostatic potential at $\vec{r}$ due to the other electrons. The corresponding Schrödinger equation is then:

$$H(\vec{r})\psi_n(\vec{r}) = \varepsilon_n \psi_n(\vec{r}) \qquad (B.5)$$

Its solution shows the existence of a band of electron energy levels. The energy levels are occupied up to the level $\varepsilon_{N/2} = \varepsilon_F$ i.e. the Fermi level. The total energy E of the system will be:

$$E = 2\,\Sigma\varepsilon_n - \frac{e^2}{2}\int d^3\vec{r}\int d^3\vec{r}'\,\frac{\rho(\vec{r})\rho(\vec{r}')}{|\vec{r}-\vec{r}'|} \qquad (B.6)$$

where $\rho(\vec{r})$ and $\rho(\vec{r}')$ are electron densities at $\vec{r}$ and $\vec{r}'$. This is the general solution, where the second term (total Coulomb energy) is subtracted since it is already included in the ε_n.

In solving the Schrödinger equation, the potential $V(\vec{r})$ considers interactions between electrons and potential due to the ion cores. However, since there are instantaneous correlations between electrons, known as exchange and correlation, other treatments (within a Hartree-like formalism) exist that take into account these effects.

(1) The Local Density Functional (LDF) (Hohenberg and Kohn: 1964; Kohn and Sham: 1965; Lang: 1973) and the X_α theory (Slater and Johnson: 1972) where an extra term μ_{xc}, for exchange and correlation, is added to $V(\vec{r})$ in equation (B.4) giving:

$$V(\vec{r}) = V_I(\vec{r}) + V_H(\vec{r}) + \mu_{xc}[\rho(\vec{r})] = V_I(\vec{r}) + V_{LDF} \qquad (B.7)$$

This extra term is a function of the local electron density at $\vec{r}$, and gives rise to an extra term in equation (B.6).

(2) The Hartree-Fock (HF) theory (e.g. A. Messiah: 1962) is more complex. It takes into account exchange but not correlation and again an extra term is added to both $V(\vec{r})$ and E.

These then, are the main approaches associated with what we call one-electron approximations to the N-body problem. To evaluate the electron density $\rho(\vec{r})$, it is necessary to solve the Schrödinger equation for the eigenfunction ψ_n. Sometimes, in chemisorption theory, this is done by employing some form of LCAO (Linear Combination of Atomic Orbitals) technique, where ψ_n is expanded as:

$$\psi_n = \sum_{i,\alpha} c_{n,i\alpha} \psi_{i\alpha} \qquad (B.8)$$

where $\psi_{i\alpha}$ is the α^{th} atomic orbital on the i^{th} atom, and $c_{n,i\alpha}$ is a coefficient. This approach has, for example, been used in a cluster calculation appropriate to field evaporation (Kingham: 1982c), in which the substrate is represented by a finite number of atoms.

With the LDF approach, the ion cores are replaced by the smeared out positively charged background ("Jellium") and binding potential curves for a number of chemisorption situations have been calculated (Smith et al.: 1973, 1975; Kahn and Ying: 1976).

B.2.1 Universal Bonding Curve

Recently, it has been discovered that various bonding situations on metals (e.g. Ferrante et al.: 1983) can be 'scaled' to fit onto a single "Universal bonding curve". This scaling depends on two parameters: the equilibrium binding energy and the scaling length (see Chapter 7). The

scaling length for a metal surface has been found to be dependent on elastic constants and surface energies (Rose et al.: 1983). Hence, it is possible to obtain specific bonding curves from elastic constant and surface energy measurements. A method based on a Universal bonding curve is applied to Tungsten data in Chapter 7.

B.3 THE GURNEY MODEL

A somewhat different approach to single-atom chemisorption was proposed by Gurney (1935). This has provided the basis of the so-called "Anderson model" in chemisorption, and of the discussion of Gomer and Swanson (1963) about field desorption, and we briefly examine it. It was originally proposed for the case of an alkali atom A adsorbed on a transition metal M.

Using Fig. (B.1), as the atom A approaches the surface of the metal M, two important effects are presumed to occur. First, the valence level in the atom, ε_a (measured relative to the metal's Fermi level) is shifted by an amount $\Delta\varepsilon$ to $\varepsilon'_a = \varepsilon_a + \Delta\varepsilon$. The second effect concerns the (squared) amplitude of the wavefunction $|\psi|^2$ at small A to M separations; at small separations the valence electron is pictured as resonating between the metal and the adatom. The probability of finding the electron around ε'_a has appreciable magnitude. This is pictured as a broadened level of half-width Γ, centred at ε'_a, where all levels belong to the system atom-metal.

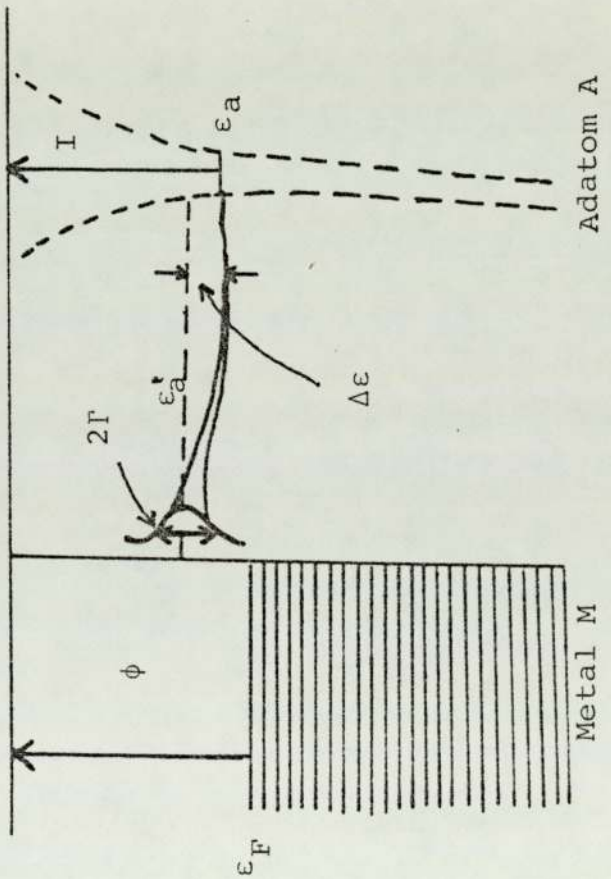

Fig. (B.1) Illustration of the Gurney model of single-atom chemisorption.

The character of adsorbate-transition metal bonding is then found to be dependent on the level ε_a' (also called the virtual level), i.e. its location relative to the Fermi level in the metal. Four situations are envisaged:

(a) if the virtual level ε_a' is well below the bottom of the metal band, the adsorbate remains neutral and the bonding is said to be "localised".

(b) if the virtual level falls within the metal band, then the adsorption is "metallic" i.e. the adsorbate acts like a surface metal atom.

(c) if the virtual level lies in the vicinity of the Fermi level, it will be only partially occupied, and the bonding is considered as semi-ionic (or semi-metallic).

(d) if the virtual level lies completely above the Fermi level, the ionization is total and the bonding is ionic.

As we shall see, there is a certain sense in which, in the charge-draining mechanism, an evaporating atom goes progressively through situations (b), (c) and (d) as it moves away from the surface.

This is a qualitative picture of single atom chemisorption, formulated by Gurney when he attempted to explain work-function changes due to adsorption, though it

has subsequently been used for calculations of alkali-on-transition metal binding energies (see Muscat and Newns: 1978; Roberts and McKee: 1978).

B.4 APPLICATION TO FIELD DESORPTION AND FIELD EVAPORATION

The Gurney approach of adsorption has been used by Gomer and Swanson (1963) in their discussion of field desorption, and subsequently by Kingham (1982b). The effect of the electric field was pictured as lifting the level ε_a' as the adsorbate-atom nucleus moved away from the surface. In the case where situation (b) above applies in the absence of the field, Gomer and Swanson assumed that as the evaporating atom moved away from the surface, "electrons would drain out of it until the pure ion is obtained". This means that they considered field evaporation to be a "charge-draining process" (see Chapter 3). A basically similar view was adopted by Kingham (1982b).

On the other hand, only a few people have attempted to carry out detailed chemisorption-type calculations related to field evaporation. We may cite the following:

(1) Kingham (1982c), who carried out cluster calculations based on a tight-binding approach, has clearly demonstrated the theoretical possibility of charge-draining. However, it is not clear how the electrostatic term has been incorporated. Beside this, the distances were measured from the plane of the

surface nuclei rather than the plane of an electrical surface in front of the nuclei.

(2) Kahn and Ying (1976) calculated, using a Local Density Functional approach, the binding energy of an alkali ion to a Jellium model in the presence of a field, and have also calculated the field at which the "Schottky hump" disappeared.

(3) McMullen, Perdew and Rose (1982) carried out an LDF-based calculation aimed at describing the field evaporation of a whole flat metal layer. Their calculated evaporation fields were higher (by a factor of 2) than observed evaporation fields. In their calculations no charge-state change was involved during field evaporation, so it is clear that their escape mechanism is not a Gomer-type mechanism, and it seems probable that their method is not directly relevant to conventional metal tip field evaporation.

APPENDIX C

Existing treatments of field evaporation and metal surface models in general are based on the "Jellium surface model" (e.g. Tsong and Müller: 1969; Kittel: 1966). In this model the positive nuclear charges are smeared together to form a positively charged background whilst the electron cloud spreads out above it to form a negatively charged layer. This double layer model was useful in calculating work-functions and their differences as between different faces (Smoluchowski: 1941; Lang and Kohn: 1971, for Tungsten).

At a charged surface, however, many workers discussed a metal's electrical surface in terms of "field penetration", where the electrostatic energy of an electron is given by $eF(y+\delta)$, y being the distance measured from the electron edge and δ a parameter shown in Fig. (C.1).

Estimations and interpretations of δ have been given by various authors over the years, in conjunction with field adsorption, field evaporation and field-ionization studies. Gomer and Swanson (1963) first introduced δ in their theory of field desorption. Müller (1969) estimated δ as 0.05 nm for He on W, and

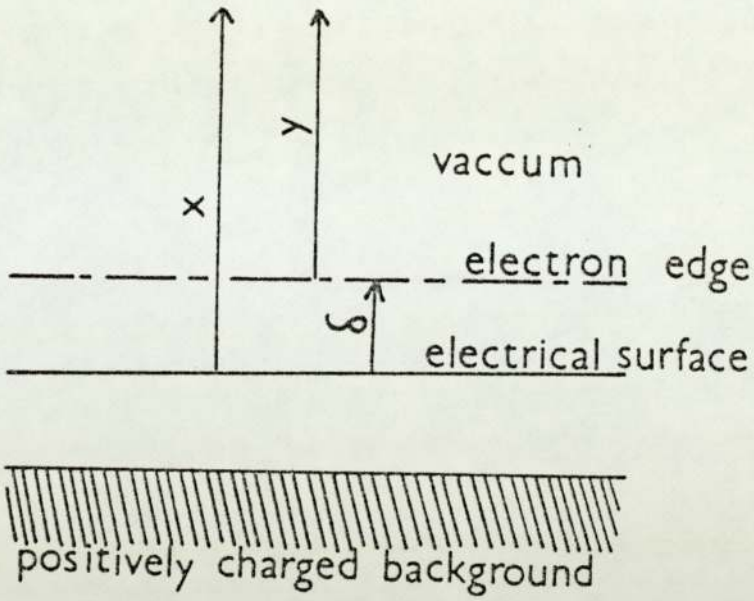

(A)

Fig. (C.1) : The "Jellium-type" surface model and the electrical surface.

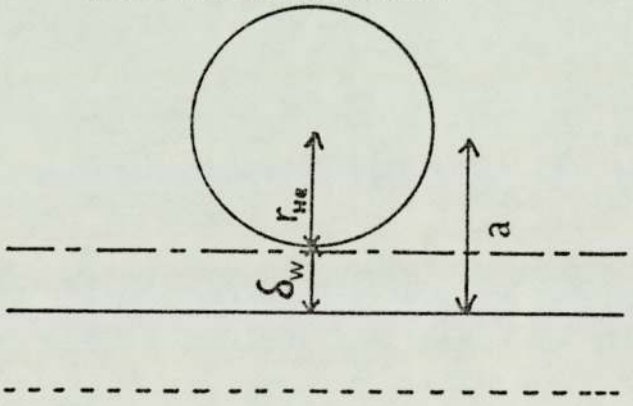

(B)

δ_W varies from 40→60 pm for the He on W (110) and He on W(111).

Tsong and Müller (1969) described its effects in terms of work-function variations, whilst Theophilou and Modinos (1972) interpreted δ as a field dependent quantity which can be either positive or negative. However, there seem to be inconsistencies in all these treatments (Forbes, private communication).

Perhaps the most important theoretical work comes from Lang and Kohn (1973) on metal surface theory. Using a Jellium-type model, they calculated the profiles of the charges induced in a metal surface by the application of a uniform electric field, or by the presence of an external point charge. The thickness of the induced charge distributions is shown to increase with the bulk electron densities and the position of its centre of mass is found to be between the edge of the Jellium positive charge background and the edge of the electron cloud (their calculated distances from the Jellium edge to the centre of mass range from 0.06 to 0.08 nm). At large distances from the plane passing through the indicated centre of mass, Lang and Kohn showed that the electrostatic potential energy of say an ion, is proportional to distance from that plane, and the correlation potential energy is given by the classical image-potential, with distance measured from the plane. Finally, they also determined the distance of the edge of the electron distribution from that

plane, to be approximately 0.04 nm for Tungsten. Lang and Kohn called this plane the "effective metal surface", but it will be called the "electrical surface" here, and any distance x is measured from it.

The idea of an electrical surface is particularly useful in the study of field-adsorbed neutral imaging-gas atoms. For example, in the experiments of Culbertson et al. (1979) on the behaviour of the field-adsorption on W, Hydrogen was used as auxiliary gas. The field-adsorbed He atoms were excited by the impact of electrons released during free-space ionization of H_2 and energy distributions measurements showed two distinct He peaks: the first was due to normal free-space ionization and the second one was due to the field-adsorbed He atoms. They went on to determine the position of the adsorbate with respect to the image plane, on the (011), (112) and (111) planes of W. It exceeded the neutral-atom radius of He by distances varying from 0.042 nm on the (011) face to 0.058 nm on the (111) face. These figures are compatible with the range expected (in the case of W) from the Lang and Kohn theory (this example is also illustrated in Fig. (C.1)). We can look on these experiments as constituting an experimental determination of the position of the electrical surface.

In conclusion, it should be emphasised that the main objection to the continuing use of Jellium-type model, is that it ignores the atomic structure of a real surface. In this context, Forbes and Wafi (1980) introduced a structured model of a real surface in the case of field-adsorption of He on the (111) face of Tungsten and used it to predict the S.I polarisability b_w of Tungsten (Chapter 5 discusses various definitions of polarisabilities). This model is introduced in Chapter 3.

APPENDIX D

DERIVATION OF PARTIAL-ENERGIES COEFFICIENTS

The Arrhenius equation for the evaporation rate-constant is given by:

$$k_{hr} = A \exp(-Q/kT) \tag{D.1}$$

Another way of writing it is:

$$[k_{hr}/s^{-1}] = \exp\{M(F)/kT\} \tag{D.2}$$

where

$$M(F) = kT\ell n\{A\} - Q(F) \tag{D.3}$$

Consider now the case where $F=F^{o}$, the field at which the evaporation flux J^{o} has some fixed value (10^{-2} layers/s in Tsong's experiments).

Hence,

$$J^{o} = n^{o}_{hr} \cdot k^{o}_{hr} \tag{D.4}$$

and

$$\ell n(J/J^{o}) = \ell n(n_{hr}/n^{o}_{hr}) + \ell n(k_{hr}/k^{o}_{hr}) \tag{D.5}$$

Also

$$M(F^{o}) = kT\ell n\{A\} - Q(F^{o}) \tag{D.6}$$

In the above equations, k is the Boltzmann constant, T the evaporation temperature.

Each of the logarithmic terms in equation (D.5) is zero at $F=F^{o}$.

The rate-constant term can be Taylor-expanded about $F=F^{o}$, as follows. From equation (D.2):

$$\ell n(k_{hr}/k_{hr}^{o}) = [M(F)-M(F^{o})]/kT \qquad (D.7)$$

Taylor-expanding M in terms of F, about $F=F^{o}$, one obtains:

$$M(F) = M(F^{o}) + (F-F^{o}) \left.\frac{dM}{dF}\right|_{F=F^{o}} + \frac{1}{2}(F-F^{o})^{2} \left.\frac{d^{2}M}{dF^{2}}\right|_{F=F^{o}} + \ldots \qquad (D.8)$$

Equation (D.7) becomes:

$$\ell n(k_{hr}/k_{hr}^{o}) = \frac{(F-F^{o})}{kT} \left.\frac{dM}{dF}\right|_{F=F^{o}} + \frac{1}{2}\frac{(F-F^{o})^{2}}{kT} \left.\frac{d^{2}M}{dF^{2}}\right|_{F=F^{o}} + \ldots \qquad (D.9)$$

At this stage, a variable g is introduced by:

$$g = (F-F^{o})/F^{o} \qquad (D.10)$$

Equation (D.9) can then be put in the form:

$$\ell n(k_{hr}/k_{hr}^{o}) = F^{o}\frac{g}{kT} \left.\frac{dM}{dF}\right|_{F^{o}} + \frac{1}{2}(F^{o})^{2}\frac{g^{2}}{kT} \left.\frac{d^{2}M}{dF^{2}}\right|_{F^{o}} + \ldots \qquad (D.11)$$

or

$$\ell n(k_{hr}/k_{hr}^{o}) = (\frac{\mu_{1}}{kT})g + \frac{1}{2}(\frac{\mu_{2}}{kT})g^{2} + \ldots \qquad (D.12)$$

where

$$\mu_{1} = F^{o} \left.\frac{dM}{dF}\right|_{F^{o}} \simeq - F^{o} \left.\frac{dQ}{dF}\right|_{F^{o}} \qquad (D.13a)$$

$$\mu_2 = (F^o)^2 \frac{d^2M}{dF^2}\bigg|_{F^o} \simeq -(F^o)^2 \frac{d^2Q}{dF^2}\bigg|_{F^o} \qquad \text{(D.13b)}$$

The same treatment, when applied to $\ell n(J/J^o)$ and $\ell n(n_{hr}/n_{hr}^o)$ respectively, leads to:

$$\ell n(J/J^o) = (\frac{\lambda_1}{kT})g + \frac{1}{2}(\frac{\lambda_2}{kT})g^2 + \ldots \qquad \text{(D.14)}$$

$$\ell n(n_{hr}/n_{hr}^o) = (\frac{\nu_1}{kT})g + \frac{1}{2}(\frac{\nu_2}{kT})g^2 + \ldots \qquad \text{(D.15)}$$

where

$$\lambda_1 = F^o\left[\partial \ell n(J/J^o)/\partial F\right]\Big|_{F^o} \qquad \text{(D.16)}$$

$$\nu_1 = F^o\left[\partial \ell n(n_{hr}/n_{hr}^o)/\partial F\right]\Big|_{F^o} \qquad \text{(D.17)}$$

and the higher-order derivatives are defined analogously.

Hence, it can be shown that:

$$\lambda_1 = \mu_1 + \nu_1 \quad \text{and} \quad \lambda_2 = \mu_2 + \nu_2 \qquad \text{(D.18)}$$

In field evaporation, Tsong and other workers (for example, Brandon: 1963) assumed that the field-dependence of the amount of material evaporated is negligible, and therefore $\nu_1 \simeq \nu_2 \simeq 0$. This implies that:

$$\mu_1 \simeq \lambda_1 \quad ; \quad \mu_2 \simeq \lambda_2 \qquad \text{(D.19)}$$

REFERENCES

REFERENCES

Aitken, K. L., and Mair, G. L. R.: Emission characteristics of a liquid caesium ion source, J. Phys. D, 13 (1980), 2165-73.

Alison Flood, E.: The solid-gas interface, Vol. 1, E. Arnold (publishers) Ltd., London, 1966

Andrén, H. O., Henjered, A. and Kingham, D. R.: On the charge state of Tungsten ions in the pulsed-field atom probe, Surface. Sci., 138, (1984), 227.

Basset, D. W.: In surfaces and defect properties of solids, Eds. M. W. Roberts and J. M. Thomas, Vol. 2, p.34, The Chemical Society, London, 1973.

Birdseye, P. J.: Ph.D. Thesis, University of Oxford, 1972.

Biswas, R. K. and Forbes, R. G.: Theoretical arguments against the Müller-Schottky mechanism of field evaporation, J. Phys. D.: Appl. Phys., 15 (1982), 1323-38.

Brandon, D. G.: 1963 The resolution of atomic structure, recent advances in the theory and development of the field-ion microscope, Brit. J. Appl. Phys., 14, (1963), 474.

1964 The structure of field evaporated surfaces, Surface Sci., 3, (1964), 1-18.

1965 The analysis of field evaporation data from field-ion microscope experiments, Brit. J. Appl. Phys., 16 (1965), 683.

1966a The field evaporation of dilute alloys, Surface Sci., 5 (1966), 137.

1966b On field evaporation, Phil. Mag., 14 (1966), 803.

Brenner, S. S. and McKinney, : On the ionization state of field evaporated atoms as measured in the FIM atom probe, Appl. Phys. Letters, 13 (1968), 29.

Carlsson, A. E., Gelatt, C. D. and Ehrenreich, H.: An ab initio pair potential applied to metals, Phil. Mag.

A., Vol. 41, No. 2, (1980), 241.

Chambers, R. S., Ehrlich, G. and Vesely, M.: in 17th FES, Yale University (1970).

Chambers, R. S.: Ph.D. Thesis, University of Illinois at Urbana-Champaign, (1975).

Chan, C. M., Thiel, P. A., Yates, J. T. and Weinberg, W. H.: The geometrical and vibrational properties of the Rh(111) surface, Surface Sci., 76 (1978), 296.

Cleaver, J. R. A., Heard, P. J. and Ahmed, H.: Scanning ion beam lithography for submicron structure fabrication, Proc. SPIE: Electron beam, x-ray, and Ion beam Techniques for Submicron Lithographies II, P.D. Blais (Ed.) 393, (1983), 129-36.

Culbertson, R. J., Sakurai, T. and Robertson, G. H.: Field ionization of surface adsorbates, Phys. Rev., B19, (1979), 4427.

Domke, M., Hummel, E. and Block, J. H.: Temperature effects on appearance potentials of gas phase field ions, Surface Sci., 78 (1978), 307.

Ehrlich, G. and Kirk, C. F.: Binding and field desorption of individual Tungsten atoms, J. Chem. Phys. 48, (1968), 1465.

Ernst, N.: Experimental investigation of field evaporation of singly and doubly-charged Rhodium, Surface Sci. 87 (1979), 469-82.

Ernst, N. and Block, J. H.: Comparison of Debye temperature for Rhodium surface atoms determined during field evaporation and low energy electron diffraction, Surface Sci., 91 (1980), L27-L31.

Ernst, N. and Jentsch, T. H.: Post-field-ionization of singly charged Rhodium: an experimental and theoretical study, Phys. Rev., B24 (1982), 6234-41.

Ferrante, J. F., Smith, J. R. and Rose, J. H.: Diatomic molecules and metallic adhesion, cohesion and chemisorption: a single binding energy relation, Phys. Rev. Letters, Vol. 50, No. 18, (1983), 1385.

Forbes, R. G.: 1974, An alternative theoretical approach to field evaporation rate sensitivities, Surface Sci., 46 (1974), 577-601.

Forbes, R. G.: 1976 A generalised theory of standard field ion appearance energies, Surface Sci., 61, (1976), 221-240.

1977a Proc. 7th Intern. Vac. Congr. and 3rd Intern. Conf. Solid Surfaces (Vienna, 1977), 387.

1977b Basic field-desorption theory (unpublished report).

1977c Atomic polarizability values in the SI system, Surface Sci., 64 (1977), 367-71.

1978a Negative work-function correction at a positively-charged surface, J. Phys. D: Appl. Phys., 11, (1978), L161.

1978b Field evaporation theory: the atomic-jug formalism, Surface Sci., 70, (1978), 239-54.

1980a Derivation of surface atom polarizability from field-ion energy deficits, Appl. Phys. Letters, 36, (1980), 739.

1980b Wave-mechanical theory of field ionization and field ion energy distributions, Progr. Surf. Sci., 10, (1980), 249-285.

1981 Charge-hopping and charge-draining: two mechanisms of field desorption, Surface Sci., 102, (1981), 255.

1982a Electrothermodynamic cycles applied to ionic potentials and to field evaporation, J. Phys. D.: Appl. Phys., 15, (1982), 1301-22.

1982b A new formula for predicting low-temperature evaporation field, Appl. Phys. Letters, 40, (1982), 277.

1982c Towards a criterion for the a-priori prediction of field evaporation mechanism, J. Phys. D.: Appl. Phys., 15, (1982), L99-104.

Forbes, R. G.: 1982d New activation energy formulae for charge-exchange type mechanisms of field evaporation, Surface Sci., 116 (1982), L195-201.

1982e An evaporation field formula including the repulsive ion-surface interaction, J. Phys. D.: Appl. Phys., 15, (1982), L75-77.

Forbes, R. G., and Wafi, M. K.: An array model for the field adsorption of helium on tungsten (111), Surface Sci., 93, (1980), 192.

Forbes, R. G., Biswas, R. K. and Chibane, K.: A re-analysis of published field sensitivity data, Surface Sci, 114, (1982), 498-514.

Goldenfeld, I. V., Korostyshevsky, I. Z. and Mischadchuk, B. G.: Analysis of field-ion energies in a mass spectrometer, Intern. J. Mass Spectrom. Ion Phys., 13, (1974), 297.

Gomer, R.: Field desorption, J. Chem. Phys., 31, (1959), 341.

Gomer, R. and Swanson, L. W.: Theory of field desorption, J. Chem. Phys., 38, (1963), 1613.

Gurney, R. W.: Theory of electrical double layers in adsorbed films, Phys. Rev., Vol. 47, (1935), 479.

Haydock, R., Heine, V. and Kelly, M. J.: Electronic structure based on the local atomic environment for tight-binding bands, J. Phys. C, 5 (1972), 2845.

Haydock, R., Heine, V. and Kelly, M J.: Electronic structure based on the local atomic environment for tight-binding bands: II, J. Phys. C, 8, (1975), 2591.

Haydock, R. and Kingham, D. R.: Post-ionization of field evaporated ions, Phys. Rev. Letters, 44 (1980), 1520-23

Hohenberg, P. and Kohn, W.: Inhomogeneous electron gas, Phys. Rev. B, 136 (1964), 864.

Hummel, E., Domke, M. and Block, J. H.: Appearance potentials of field desorbed silver ions, Z. Naturforsch, 34a, (1978), 307.

Kahn, L. M. and Ying, S.C.: A model for alkali chemisorption, Surface Sci., 59, (1976), 333.

Kellogg, G. L.: 1981a Determining the field emitter temperature during Laser irradiation in the pulsed Laser atom probe, J. Appl. Phys., 52, (1981), 5320-28.

1981b Experimental evidence for multiple post-ionization of field evaporated ions, Phys. Rev. B, 24 (1981), 1848.

1982 Measurement of the charge state distribution of field evaporated ions: evidence for post-ionization, Surface Sci., 120, (1982), 319.

1984 Measurement of activation energies for field evaporation of tungsten ions as a function of electric field, Phys. Rev. B, 29, (1984), 4304-12.

Kingham, D. R.: 1981 Ph.D. Thesis, Cambridge University (1981).

1982a The post-ionization of field evaporated ions: a theoretical explanation of multiple charge states, Surface Sci., 116, (1982), 273-301.

1982b A new view of field evaporation, Vacuum, Vol. 32, No. 8, (1982), 471-476.

1982c The mechanism of charge transfer during field evaporation, Proc. of the 29th IFES, Göteborg, Sweden, 1982.

1985 A simple theoretical model of field evaporation, 32nd IFES, Wheeling, West Virginia, 1985.

Kittel, C.: Introduction to solid state physics, 3rd Edition, John Wiley and Sons Inc., New York, 1966.

Knor, Z.: Surface and defect properties of solids, Vol. 6 (1977), p. 139.

Kohn, W. and Sham, L. J.: Self-consistent equations including exchange and correlation effects, Phys. Rev. A, 140 (1965), 1133.

Konishi, M., Wada, M. and Nishikawa, O.: Polarisabilities and binding energies of Ga and W and

post-field-ionization of Ga, Surface Sci., 107, (1981), 63-74.

Landau, L. D and Lifshitz, E. M.: Quantum Mechanics, Pergamon, Oxford, 1958.

Lang, N. D.: The density-functional formalism and the electronic structure of metal surfaces, Solid St. Phys., 28, (1973), 225.

Lang, N. D. and Kohn, W.: Theory of metal surfaces: work-function, Phys. Rev. B, 3, (1971), 1215.

Lang, N. D. and Kohn, W.: Theory of metal surfaces: induced surface charge and image-potential, Phys. Rev., 7, (1973), 3541B.

Langmuir, I.: The vapor pressure of metallic Tungsten, Phys. Rev., 2, (1913), 329.

McKinstry, D.: An examination of field evaporation theory, Surface Sci., 39, (1972), 37.

McMullen, E. R., Perdew, J. P. and Rose, J. H.: Effects of an intense electric field on metal surface geometry, Solid Stat. Communic., Vol. 44, No. 6, (1982), 945-949.

Menand, A. and Kingham, D. R.: Isotopic variations in field evaporation charge-state of Boron ions, J. Phys. D.: Appl. Phys., 17 (1984), 203-208.

Menand, A., Martin, C. and Sarrau, J. M.: Field evaporation charge-state of Boron ions: a temperature effect study, Journal de Physique, Colloque C9, Supplement au No. 12, Tome 45, (1984).

Messiah, A.: in: Quantum Mechanics, Vol. 2, North-Holland, Amsterdam (1962).

Miller, T. M. and Bederson, B.: in: Advances in atomic and molecular physics, 13, (Academic Press, London, 1977).

Müller, E. W., 1941 Tearing off adsorbed ions by high electric field strengths, Naturwissenschaften 29, (1941), 533.

1951 The field ion microscope (German), Z. Phys., 131, (1951), 136.

1956 Field desorption, Phys. Rev., 102, (1956), 618.

Müller, E. W. 1960 Field-ionization and field-ion microscopy, Adv. Electr. and Electron Phys., 13, (1960), 83.

1964 The effect of polarization, field stress and gas impact on the topography of field-evaporated surfaces, Surface Sci., 2, (1964), 484.

Müller, E. W., Panitz, J. A. and McLane, S. B.: The atom-probe field-ion microscope, Rev. Sci. Inst., 39, (1968), 83.

Müller, E. W. and Tsong, T. T.: Field-ion microscopy: principles and applications, (Elsevier: New York 1969).

Müller, E. W. and Krishnaswamy, S. V.: High ionic charges on field evaporating 5d transition metals, Phys. Rev. Letters, 37 (1976), 1011.

Muscat, J. P. and Newns, D. M., Chemisorption on metals, Progr. Surf. Sci., 9, No. 1, (1978), 1-43.

Nakamura, S. and Kuroda, T.: On field evaporation end forms of a bcc metal surface observed by a field-ion microscope, Surface Sci., 17, (1969), 436.

Oppenheimer, J. R.: Three notes on the quantum theory of Aperiodic effects, Phys. Rev., 31, (1928), 67.

Patel: M.Sc. Thesis, University of Aston in Birmingham (1974).

Pierce, D. T. and Spicer, W. E.: Photoemission studies of Rhodium, Phys. Rev., B, 5, (1972), 2125.

Plummer, E. W. and Rhodin, T.N.: Atomic binding of transition metals on clean single crystal Tungsten surfaces, J. Chem. Phys., 49, No. 8, (1968), 3479-96.

Prutton, M.: in: Surface Physics, 2nd Edition, Clarendon Press, Oxford, 1983.

Riviere, J. C.: Solid state science, Vol. 1, Ed. M. Green, (Dekker, New York, 1969), 179.

Roberts, M. W. and McKee, C.S.: in: Chemistry of the metal-gas interface, Clarendon Press, Oxford, 1978.

Rose, J. H., Ferrante, J. F. and Smith, J. R.: Universal binding energy curves for metals and bi-metallic interfaces, Phys. Rev. Letters, 47, No. 9, (1981), 675.

Rose, J. H., Smith, J. R. and Ferrante, J. F.: Universal features of bonding in metals, Phys. Rev. B28, No. 4 (1983), 1835-45.

Sakurai, T. and Müller, E. W., Field calibration using the energy distribution of field-ionization, Phys. Rev. Letters, 30, No. 12, (1973), 532.

Slater, J. C. and Johnson, K. H., Self-consistent field $X\alpha$ cluster method for polyatomic molecules and solids, Phys. Rev. B, 5, (1972), 844.

Smith, J. R., Ying, S. C. and Kohn, W., Charge densities and binding energies in Hydrogen chemisorption, Phys. Rev. Letters, 30, No. 13, (1973), 610.

Smith, J. R., Ying, S. C. and Kohn, W.: Density-functional theory of chemisorption on metal surfaces, Phys. Rev. B, 11, (1975), 1483.

Smoluchowski, R., Anisotropy of the electronic work-function of metals, Phys. Rev., 60, (1941), 661.

Taylor, D. M., Ph.D. Thesis, Cambridge University (1970).

Theophilou, A. K. and Modinos, A.: Metallic field effect and its consequences in field emission, field ionization and capacitance of a capacitor, Phys. Rev. B, 6, (1972), 801.

Tsong, T. T.: 1968 Surface states and field ion image formation, Surface Sci, 10, (1968), 102.

1971 Measurement of the polarisabilities and field evaporation rates of individual Tungsten atoms, J. Chem. Phys., 54 (1971), 4205.

1978a Field ion image formation, Surface Sci., 70, (1978), 211.

1978b Measurement of the field evaporationg rate of several transition metals, J. Phys. F. (Metal Phys.), 8, (1978), 1349.

1980 Quantitative investigations of atomic processes on metal surfaces at atomic resolution, Progr. Surf. Sci., 10, (1980), 165-248.

Tsong, T. T. and Müller, E. W., Effects of static field penetration and atomic polarizability on the capacity of a capacitor, field evaporation, and field ionization processes, Phys. Rev., 181, (1969), 530.

Tsong, T. T. and Müller, E. W.: Field evaporation rates of Tungsten, Phys. Stat. Sol., (a), 1, (1970), 513.

Tsong, T. T. and Müller, E. W.: Field adsorption of inert-gas atoms. J. Chem. Phys., 55, (1971), 2884.

Tsong, T. T. and Walko, R. J.: Measurements of the polarizability of Tungsten adatoms on Tungsten (110) planes, Phys. Stat. Sol. (a), 12, (1972), 11.

Tsong, T. T. and Kellogg, G. L.: Direct observation of the directional walk of single adatoms and the adatom polarizability, Phys. Rev. B, 12, (1975), 1343.

Vesely, M. and Ehrlich, G.: Field evaporation: model and experiments, Surface Sci. 34, (1973), 547.

Wada, M., Konishi, M. and Nishikawa, O.: Binding states of Ga and Sn on W and Mo: structures, evaporation field and its temperature dependence, Surface Sci., 100, (1980), 439.

Wada, M., Uemori, R. and Nishikawa, O: Effect of Hydrogen on the evaporation field of metals, Surface Sci., 134, (1983), 17.

Wafi, M. K.: Ph.D Thesis, The University of Aston in Birmingham, (1981).

Waugh, A. R., Boyes, E. D. and Southon, M. J.: Investigations of field evaporation with a field desorption microscope, Surface Sci., 61, (1976), 109-142.

Ying, S. C.:in: Theory of Chemisorption, Ed. J. R. Smith, (Springer, Berlin, 1980).